The Geomicrobiology of Cementitious Radioactive Waste

A thesis submitted to The University of Manchester for the degree of Doctor of Philosophy in the Faculty of Engineering and Physical Sciences

2014

Adam John Williamson

School of Earth, Atmospheric and Environmental Sciences

Table of Contents

Table of Contents 2
List of Figures 8
List of Tables 13
Abbreviations 16
Abstract 18
Declaration 19
Copyright Statement 20
Acknowledgments 21
The Author 22

1. Introduction and Thesis Content 23
1.1. Project relevance 24
1.1. Research objectives 25
1.2. Thesis structure 25
1.3. Paper status and collaborator contributions 27
1.4. References 28

2. A Review of Neutral and Alkaline Biogeochemistry, Relevant to Radioactive Waste Disposal 30
2.1. The nuclear legacy 31
2.1.1. The nuclear fuel cycle 31
2.1.2. Radioactive waste legacy 32
2.1.3. Geological disposal 33
2.1.4. Natural analogues 34
2.2. Background to the elements in this study 35
2.3. Stable element biogeochemistry 36
2.3.1. Iron biogeochemistry 37
2.3.2. Metal reduction mechanisms 39
2.4. Alkaline biogeochemistry 43
2.4.1. Physiology 43
2.4.2. Environments 44

2.4.3. Phylogenetic diversity and metal reduction 45
2.5. Radionuclide biogeochemistry 47
2.5.1. Uranium biogeochemistry 47
2.5.2. Technetium biogeochemistry 49
2.5.3. Neptunium biogeochemistry 50
2.6. Summary and site overview 51
2.6.1. Summary 51
2.6.2. Overview of the Buxton site 51
2.7. References 53

3. Materials and Methods 66
3.1. Geochemical analyses 67
3.1.1. pH 67
3.1.2. Eh (the reduction potential) 67
3.2. Spectrophotometry (UV-Vis) 67
3.2.1. Determination of Fe(II): the ferrozine method 69
3.2.2. Determination of U(VI): the bromo-PADAP method 69
3.3. Ion chromatography (IC) 70
3.4. Inductively coupled plasma (ICP) 72
3.4.1. Inductively coupled plasma-atomic emission spectroscopy (ICP-AES) 72
3.4.2. Inductively coupled plasma-mass spectroscopy (ICP-MS) 72
3.5. Electron microscopy 73
3.5.1. Transmission electron microscopy (TEM) 73
3.5.2. Select area electron diffraction (SAED) 74
3.5.3. Energy dispersive X-ray spectroscopy (EDX) 75
3.6. X-ray techniques 75
3.6.1. X-ray absorption spectroscopy (XAS) 75
3.6.2. X-ray magnetic circular dichroism (XMCD) 81
3.6.3. X-ray fluorescence (XRF) 82
3.6.4. X-ray diffraction (XRD) 84
3.7. Microbiological techniques 85
3.7.1. Polymerase chain reaction (PCR) 85
3.7.2. 16S rRNA gene based clone libraries 86

3.7.3. Ribosomal intergenic spacer analysis (RISA) 87
3.7.4. 16S amplicon pyrosequencing and data analysis 87
3.7.5. Microcosm experiments 88
3.8. Radiological techniques 89
3.8.1. Liquid scintillation counting (LSC) 89
3.8.2. Determination of pertechnetate: the TPAC method 90
3.8.3. Gamma camera imaging 90
3.9. Radiation safety 91
3.9.1. Protocols 91
3.9.2. Radioactive characteristics of ^{238}U, ^{99}Tc, ^{99m}Tc and ^{237}Np 91
3.10. References 93

4. Microbial Reduction of Fe(III) under Alkaline Conditions Relevant to Geological Disposal 97
Abstract 3320
Introduction 3320
Materials and methods 3321
Microcosm experiments 3321
Geochemical analyses 3321
Mineralogical characterization X-ray (powder) diffraction 3321
X-ray absorption spectroscopy (XAS) and X-ray magnetic circular dichroism (XMCD) 3321
Ribosomal intergenic spacer analysis (RISA) 3322
Amplification, cloning, and sequencing of 16S rRNA gene sequences 3322
Nucleotide sequence accession numbers 3322
Results and discussion 3322
Fe(III) reduction 3322
Mineralogical characterization. (i) XRD 3323
Mineralogical characterization. (ii) TEM/SAED 3323
Mineralogical characterization. (iii) XAS/XMCD 3323
Microbial communities associated with Fe(III) reduction 3324
Conclusions 3325
Acknowledgments 3325

References **3325**

Supporting Information **98**

References **101**

5. Microbial Reduction of U(VI) under Alkaline Conditions; Implications for Radioactive Waste Geodisposal **102**

5.1. Abstract **104**

5.2. Introduction **104**

5.3. Materials and methods **106**

5.3.1. Sediment collection and storage 106

5.3.2.Uranium bioreduction microcosm experiments 106

5.3.3. Uranium reoxidation experiments 107

5.3.4. Geochemical analyses 107

5.3.5. Uranium L_{III}-edge XAS analysis 107

5.3.6. 16S rRNA gene amplicon pyrosequencing and data analysis 108

5.4. Results and discussion **108**

5.4.1. Sediment bioreduction experiments 108

5.4.2. Uranium fate during bioreduction – *no added Fe(III)* 109

5.4.3. Uranium fate during bioreduction – *with added Fe(III)* 110

5.4.4. Reoxidation experiments 111

5.4.5. Bacterial diversity assessed by 16S rRNA gene amplicon pyrosequencing 113

5.5. Significance **114**

5.6. Supporting information available **114**

5.7. Acknowledgments **115**

5.8. References **115**

5.9. Supporting information **123**

5.9.1. Sediment and surface water characteristics 123

5.9.2. Linear combination fitting analysis 123

5.9.3. XAS modelling 123

5.9.4. Design of tagged fusion primers and PCR amplifications 124

5.10. References **132**

6. Biogeochemical Cycling of ^{99}Tc in Alkaline Sediments 134
6.1. Abstract 136
6.2. Introduction 136
6.3. Materials and methods 138
6.3.1. Sample collection 138
6.3.2. Bioreduction microcosm construction 138
6.3.3. Reoxidation experiments 139
6.3.4. Geochemical analyses 139
6.3.5. X-ray absorption spectroscopy (XAS) 139
6.3.6. 16S rRNA gene amplicon pyrosequencing and data analysis 140
6.3.7. Geochemical modelling 141
6.3.8. Gamma imaging of ^{99m}Tc associated activity 142
6.4. Results and discussion 142
6.4.1. Sediment and surface water characteristics 142
6.4.2. Biogeochemistry in sediment microcosms 142
6.4.3. Technetium fate during bioreduction – *no added Fe(III)* systems 143
6.4.4. Technetium fate during bioreduction – w*ith added Fe(III)* systems 146
6.4.5. Air reoxidation experiments 148
6.4.6. Nitrate reoxidation experiments 149
6.4.7. Bacterial diversity assessed by 16S rRNA gene amplicon pyrosequencing 149
6.5. Conclusions and geochemical significance 151
6.6. Acknowledgments 152
6.7. Supporting information 152
6.7. References 158

7. Microbial Reduction of Np(V) under Alkaline Conditions 163
7.1. Abstract 165
7.2. Introduction 165
7.3. Materials and methods 166
7.3.1. Safety 166
7.3.2. Sample collection 166
7.3.3. Bioreduction microcosm construction 167

7.3.4. Geochemical analyses-low level experiments 167
7.3.5. X-ray absorption spectroscopy (XAS)-high level experiments 168
7.4. Results and discussion 169
7.4.1. Sediment and surface water characteristics 169
7.4.2. Biogeochemistry in sediment microcosms 169
7.4.3. Neptunium fate during bioreduction- *no added Fe(III)* systems 171
7.4.4. Neptunium fate during bioreduction- *with added Fe(III)* systems 173
7.5. Conclusions and geochemical significance 175
7.6. Acknowledgments 175
7.7. References 175

8. Summary, Conclusions and Future Directions 177
8.1. Summary and conclusions 178
8.2. Future directions 180
8.3. References 183

Appendix: Conference presentations 186
A.1. Oral presentations 187
A.2. Poster presentations 187

Word Count: 58,240

List of Figures

1. Introduction and Thesis Content 23

2. A Review of Neutral and Alkaline Biogeochemistry, Relevant to Radioactive Waste Disposal 30

Figure 1 – The principal operations in the nuclear fuel cycle, adapted from (Eisenbud & Gesell 1997) 31

Figure 2 – Generic radioactive waste disposal scenario 33

Figure 3 – Eh-pH stability fields for iron, hematite, magnetite and siderite in water at 25 °C, 1 atm total pressure and total dissolved carbonate activity of $10^{-1.35}$. Adapted from (Mills et al. 1987) 38

Figure 4 – Gram-negative and Gram-positive bacteria (note, pili and flagellum are not found in all bacteria) 39

Figure 5 – Proposed mechanism of electron shuttling of Fe(III) by AQDS, coupled to acetate oxidation via the semiquinone moiety 41

Figure 6 – Flavin redox chemistry. The R group varies depending on the compound (R=mononucleotide (FMN), adenine dinucleotide (FAD) and ribose (riboflavin)) 42

Figure 7 – Simplified schematic representation of cytoplasmic pH regulation, adapted from (Horikoshi 2011). (A) Respiratory electron transport chain; (B) ATPase pathway; (C) ΔpH and $\Delta\psi$-dependence Na^+/H^+ antiporters; (D) amino acid and oligopeptide/Na^+ symporters 44

Figure 8 – The Buxton site (Google Earth 2014). (1) The waste margin sampling location; (2) hyperalkaline spring; (3) the lime kiln waste deposits (described as “Rises” in OS maps from 1924) and (4) the former Hoffman kiln site (Derbyshire County Council) 52

3. Materials and Methods 66

Figure 1 – Simplified schematic of a spectrophotometer 68

Figure 2 – Structure of ferrozine. The ferroin group is highlighted in red 69

Figure 3 – Periodic table showing elements that can be detected by ICP-AES, with their working detection limits, adapted from (Gill 1997) 72

Figure 4 – Periodic table showing elements that can be detected by ICP-MS, with their working detection limits, adapted from (Gill 1997) 73

Figure 5 – Schematic of a TEM, adapted from (Williams & Carter. 1996) 73

Figure 6 – TEM image of magnetite and its corresponding SAED (taken from Chapter 4) 75

Figure 7 – EDX spectra taken on nanocrystalline magnetite (taken from Chapter 4) ... 75

Figure 8 – An X-ray interacting with an absorbing atom 77

Figure 9 – Simple beam schematic, adapted from (Denecke 2006; Charnock. 1995).... 77

Figure 10 – Uranium L_{III} edge XAS spectrum (taken from Chapter 5) with the origin of EXAFS oscillations from constructive and destructive interference of neighbouring atoms (A and B) with outgoing photoelectron (e^-)..... 78

Figure 11 – Fe $L_{II,III}$ edge XAS and XMCD (taken from Chapter 4) 82

Figure 12 – Periodic table showing elements that can be detected by XRF, with their working detection limits, adapted from (Gill, 1997) 83

Figure 13 – Bragg diffraction, adapted from (Williams & Carter, 1996) 84

Figure 14 – The polymerase chain reaction and the clone library procedure 86

Figure 15 – RISA (taken from Chapter 4) 87

Figure 16 – Energy transfer in LSC 90

4. Microbial Reduction of Fe(III) under Alkaline Conditions Relevant to Geological Disposal 97

Figure 1 – 0.5 N HCl extractable Fe(II) concentration (Fe(II); ▫) and reduction potential (Eh; ▪) in microcosms containing Buxton sediments supplemented with 120 mM ferrihydrite incubated under a range of biogeochemical regimes as defined in Materials and Methods: oxic control (a); anoxic, no electron donor (b); anoxic, electron donor (c); anoxic AQDS (d); anoxic riboflavin (e); and anoxic Elliot lake humic acid (ELHA) (f) 3322

Figure 2 – XRD analysis of microcosms containing Buxton sediments incubated under a range of biogeochemical regimes*:* unamended Buxton sediment (a); Buxton sediment with ferrihydrite amendment (b); oxic control (c); anoxic, no electron donor (d); anoxic, electron donor (e); anoxic AQDS (f); anoxic riboflavin (g); and anoxic ELHA (h). Arrows are used to indicate the broad shoulder feature characteristic of magnetite in samples d-h. The XRD of magnetite has also been given for reference (top) 3323

Figure 3 – High resolution TEM images of ferrihydrite prepared from anhydrous $FeCl_3$ (a); calcite within the Buxton sediment (b); Biogenic magnetite (c) in the anoxic electron donor systems after 28 days incubation, with its corresponding select area electron diffraction (SAED) pattern (d) and its energy dispersive X-ray analysis (e) on an individual crystallite. The SAED pattern has been overlaid with the standard pattern of magnetite confirming its identity (53) 3324

Figure 4 – X-ray absorption spectra (XAS) and X-ray magnetic circular dichroism (XMCD) analyses of microcosms containing Buxton sediments incubated under a range of biogeochemical regimes: ferrihydrite amended oxic sediment (line a); an anoxic, electron donor system after a 28 day incubation (line b); and an anoxic *AQDS* system after a 28 day incubation (line c). Arrows indicate shoulder features characteristic of an Fe(III) rich compound and the 3 main theoretical components of magnetite have been indicated on the XMCD spectrum (Fits). The intensities of the first three peaks at the L_3

edge XMCD are related to the relative amounts of Fe(III) d^6 Oh (negative); Fe(III) d^5 Td (positive); and (iii) Fe(III) d^5 Oh (negative) present in the sample (43, 54) 3324

Figure 5 – 16S rRNA gene clone libraries of (a) raw, non-incubated Buxton sediment; (b) sediment pellet taken from a progressive 28 day anoxic incubation (*anoxic electron donor* system) and (c) sediment pellet taken following a 7th progressive enrichment in defined medium containing 10 mM sodium lactate, 1 g L^{-1} yeast extract and 50 mM ferrihydrite 3324

Supplementary information

Figure S1 – Ion chromatographic analysis of organic acids of supernatant samples taken from the electron donor amended system over the 28 day incubation period 99

Figure S2 – 0.5 N HCl extractable Fe(II) concentration (Fe(II); ▫) and reduction potential (Eh; ▪) in microcosms containing Buxton sediments supplemented with 120 mM ferrihydrite incubated without electron shuttle (left) and with Aldrich humic acid (AHA) (right) 99

Figure S3 – Fe(II) and Fe(III) cation occupancies in O_h and T_d sites were determined using by fitting XMCD spectra to atomic multiplet calculations (1, 2, 3) for incubations with electron donor (lactate) but without electron shuttle and incubations with electron donor (lactate) and electron shuttle (AQDS). Samples are compared to the cation occupancy of biogenic magnetite of similar particle size produced under optimum conditions. The dashed line indicates stoichiometric magnetite with a cation site occupancy of (1:1:1 $Fe(II)O_h$:$Fe(III)T_d$:$Fe(III)O_h$) 100

Figure S4 – Ribosomal Intergenic Spacer Analysis of raw, non-incubated Buxton sediment (Raw), following a 28 day incubation (t28) and consecutive enrichments in defined medium with 50 mM ferrihydrite as a source of electron acceptor (R-1 to R-7) 100

4. Microbial Reduction of U(VI) under Alkaline Conditions; Implications for Radioactive Waste Disposal 102

Figure 1 – Biocycling of U in Buxton sediments showing 0.5 N HCl extractable Fe(II) concentration (mM) (●) and total $U_{(aq)}$ (expressed as % of the added U(VI)) (○). Systems: (A) no added Fe(III) reduction with air reoxidation from 210 days; (B) with added Fe(III) reduction and air reoxidation from 210 days; (C) no added Fe(III) reduction + AQDS; (D) with added Fe(III) reduction + AQDS; (E) with added Fe(III) reduction and nitrate reoxidation from 210 days; (F) with added Fe(III) reduction and air reoxidation from 210 days. Error bars are 1σ of triplicate results (where not shown, errors are within the size of the symbol). Dashed lines indicate the start of reoxidation experiments; red for air and green for nitrate treatments (nitrate reoxidations were run as single experiments) 120

Figure 2 – k^3 weighted ^{238}U $L_{(III)}$ edge EXAFS spectra (left) and Fourier transform (right) for bioreduction systems at experimental end-points: (A) no added Fe(III) oxic sediment; (B) no added Fe(III) reduction; (C) no added Fe(III) + AQDS reduction; (D) with added Fe(III) reduction; (E) with added Fe(III) reduction + AQDS; (F) no added

Fe(III) and subsequent nitrate reoxidation; and (G) with added Fe(III) and subsequent nitrate reoxidation. Black lines are the experimental data and red lines are the best-fit models (SI Table 3) 121

Figure 3 – Bacterial phylogenetic diversity at the Phylum level for (A) bulk unamended sediment; (B) no added Fe(III) reduction; (C) with added Fe(III) reduction; (D) no added Fe(III) and subsequent nitrate reoxidation (E) with added Fe(III) and subsequent nitrate reoxidation. Only the phyla with more than 1% of the total number of reads are shown. Abundance at the class level is shown for Firmicutes (blue hues) and Proteobacteria (green hues) 122

Supplementary information

SI Figure 1 – U $L_{(III)}$-edge normalised XANES spectra for all sediment bioreducing treatments with schoepite (U(VI)) and uraninite (U(IV)) reference spectra 125

SI Figure S2 – U $L_{(III)}$-edge normalised XANES spectra for nitrate reoxidised sediments, no added Fe(III) and with added Fe(III) with schoepite (U(VI)) and uraninite (U(IV)) reference spectra 126

SI Figure S3 – Rarefaction curves showing the number of observed operational taxonomic units (OTUs) at 97 % ID similarity per sample, after 16S rRNA gene amplicon pyrosequencing 126

4. Biogeochemical Cycling of ^{99}Tc in Alkaline Sediments 134

Figure 1 – Redox cycling on Fe and technetium in high pH sediments showing 0.5 N HCl extractable Fe(II) concentration (●) and % Tc(VII) in solution (O) in progressive anoxia experiments with: (A) no added Fe(III); (B) with added Fe(III), and pre-reduced sediments with no added Fe(III) (C+E), and with added Fe(III) (D+F). Error bars are 1σ of triplicate results (where not shown, errors are within the size of the symbol). Dashed lines indicate the start of reoxidation experiments; red for air and green for nitrate (reoxidation were run as single experiments) 143

Figure 2 – Start and end point γ-camera images for microcosm experiments with no added Fe(III), with added Fe(III) and biomagnetite (reducing control). Images were taken approximately 5 min after injection of ~ 20 pM ^{99m}Tc (0) or following 26 h incubation 144

Figure 3 – ^{99}Tc K edge XANES stack plot of all bioreducing, sterile and reoxidation treatments with $Tc(VII)O_4^-$ and $Tc(IV)O_2$ reference spectra (Hess et al. 2004) 146

Figure 4 – k^3 weighted ^{99}Tc K edge EXAFS spectra (left) and Fourier transform (right) for progressive anoxia experiments; (A) no added Fe(III); (B) with added Fe(III), and pre-reduced experiments with (C) no added Fe(III); (D) with added Fe(III) and (E) air reoxidised pre-reduced sediments with added Fe(III). The Fourier Transform is plotted with a phase correction calculated from the first shell of oxygen backscatterers. Black lines are the experimental data and red lines are the best-fit models (SI Table 2). 148

Figure 5 – Bacterial phylogenetic diversity at the Phylum level for (A) bulk unamended sediment; low level Tc bioreduction experiments (B) no added Fe(III); (C) with added

Fe(III) and high level Tc bioreduction experiments (D) no added Fe(III); (E) with added Fe(III). Only the phyla with more than 1% of the total number of reads are shown. Abundance at the class level is shown for Firmicutes (blue hues) and Proteobacteria (green hues) 151

Supplementary information

SI Figure 1 – Ion chromatographic analysis of organic acids and inorganic anions in supernatant samples taken from the progressive anoxia systems with no added Fe(III) (A+B) and with added Fe(III) (C+D) over a 28 day incubation period 152

SI Figure 2 – Rarefaction curves showing the number of observed operational taxonomic units (OTUs) at 97 % ID similarity per sample, after 16S rRNA gene amplicon pyrosequencing 153

6. Microbial Reduction of Np(V) under Alkaline Conditions 163

Figure 1 – Bioreduction of Buxton sediments with no added Fe(III) (●) and with added Fe(III) (O) showing (A) pH; (B) % Np in solution; (C) NO_3^-; (D) NO_2^-; (E) 0.5 N HCl extractable sediment Fe as Fe(II) (%) and (F) SO_4^{2-}. Dashed lines in A and B represent pre-reduced controls. Error bars are 1 σ of triplicate results (where not shown, errors are within the symbol size) 170

Figure 2 – Ion chromatographic analysis of organic acids in supernatant samples taken from the progressive anoxia systems with (A) no added Fe(III) and (B) with added Fe(III) over the 28 day incubation period 170

Figure 3 – ^{237}Np L_{III} edge XANES stack plot of all oxic, bioreducing systems and pre-reduced sediments incubated at 5 °C with $Np(V)O_2^+$ and $Np(IV)O_2$ reference spectra. Values in brackets are estimated Np(IV):Np(V) ratio determined by linear combination modelling between Np(IV) and Np(V) standards (Rossberg et al. 2014; Hennig 2007) 173

Figure 4 – k^3 weighted ^{237}Np L_{III} edge EXAFS spectra (left) and Fourier transform (right) for (A) oxic sediments with no added Fe(III) and progressive anoxia experiments with (B) no added Fe(III) and (C) with added Fe(III). The Fourier Transform is plotted with a phase correction calculated from the first shell of oxygen backscatterers. Black lines are the experimental data and red lines are the best-fit models (Table 2) 174

7. Summary, Conclusion and Future Directions 177

Appendix. Conferences and Presentations 186

List of Tables

1. Introduction and Thesis Content……..... 23

2. A Review of Neutral and Alkaline Biogeochemistry, Relevant to Radioactive Waste Disposal..... 30

Table 1 – Properties of UK low, intermediate and high level radioactive wastes with corresponding volume and activity at 01-04-13 (NDA 2014) 32

Table 2 – Energy yields of terminal electron accepting processes at pH 7 (Konhauser 2009) 37

Table 3 – Alkaliphilic organisms known to reduce Fe(III). Optimum salinity, temperature and pH for growth are given in parentheses 46

Table 4 – Buxton Harpur Hill surface water major anions and cations 52

3. Materials and Methods..... 66

Table 1 – Specifications for the IC systems used in this thesis 71

Table 2 – Concentrations and corresponding ALIs of U, Tc and Np used in experiments in this study 92

4. Microbial Reduction of Fe(III) under Alkaline Conditions Relevant to Geological Disposal 97

5. Microbial Reduction of U(VI) under Alkaline Conditions; Implications for Radioactive Waste Disposal 102

Supplementary Information

SI Table 1 – Buxton Harpur Hill lime workings surface water major anions and cations. Note, on equilibration of surface waters with sediment and electron donor, SO_4^{2-} concentration at t=0 was 7.12 ppm 127

SI Table 2 – Linear combination fitting percentage estimates (± ~ 20 %) for U XANES modelling with U(VI) bearing oxic end member with added Fe(III) and U(IV) bearing reduced with added Fe(III) + AQDS end member spectra. N/A indicates not applicable as the sample was used as an end member spectrum for linear combination modelling 127

SI Table 3 – EXAFS fitting results from bioreduction microcosm experiments: no added Fe(III), no added Fe(III) + AQDS, with added Fe(III), with added Fe(III) + AQDS; and subsequent nitrate reoxidation experiments: no added Fe(III) and with added Fe(III). N is coordination number, r is interatomic distance (Å) and σ^2 is Debye Waller factor ($Å^2$). Errors on are r ± 0.02 Å (first shell), 0.05 Å (outer shells) and $2\sigma^2$ are ± 25 %; N ± 25 %. R (least squares residual) is a measure of the overall goodness of fit 128

SI Table 4 – Number of pyrosequencing reads obtained for (A) bulk unamended sediment; (B) no added Fe(III) reduction 210 days; (C) with added Fe(III) reduction 210 days; (D) no added Fe(III) and subsequent nitrate reoxidation 14 days and (E) with added Fe(III) and subsequent nitrate reoxidation 14 days, number of reads after denoising and removal of short and chimeric sequences, and the number of observed operational taxonomic units (OTUs) at 97 % ID similarity.. 129

SI Table 5 – Phylogenetic affiliations of the most abundant bacterial OTUs identified in samples from (A) bulk unamended sediment, (B) no added Fe(III) reduction 210 days, (C) with added Fe(III) reduction 210 days, (D) no added Fe(III) and subsequent nitrate reoxidation 14 days and (E) with added Fe(III) and subsequent nitrate reoxidation 14 days.. 130

6. Biogeochemical Cycling of ^{99}Tc in Alkaline Sediments 134

Supplementary information

SI Table 1 – Buxton Harpur Hill lime workings surface water major anions and cations 153

SI Table 2 – EXAFS fitting results from progressive anoxia experiments: (A) no added Fe(III); (B) with added Fe(III); pre-reduced sediments with (C) no added Fe(III); (D) with added Fe(III) and (E) air reoxidised pre reduced sediments with added Fe(III). CN denotes coordination number, r is interatomic distance (Å) and σ^2 is Debye Waller factor (Å^2). ΔE_0 represents the shift in energy from the calculated Fermi level (eV) and $S0^2$ denotes the amplitude factor which was constrained between 0.85 and 1.05. R is the goodness of the fit and χ_v^2 is the reduced χ^2 value. Numbers in parentheses are the standard deviation on the last decimal place. 154

SI Table 3 – Number of pyrosequencing reads obtained for (A) bulk unamended sediment; the low Tc experiments (B) no added Fe(III) reduction 28 days; (C) with added Fe(III) reduction 28 days; and the high Tc experiments (D) no added Fe(III) reduction 56 days and (E) with added Fe(III) reduction 56 days, number of reads after denoising and removal of short and chimeric sequences, and the number of observed operational taxonomic units (OTUs) at 97 % ID similarity 155

SI Table 4 – Phylogenetic affiliations of the most abundant bacterial OTUs identified in samples from (A) bulk unamended sediment; the low Tc experiments (B) no added Fe(III) reduction 28 days; (C) with added Fe(III) reduction 28 days; and the high Tc experiments (D) no added Fe(III) reduction 56 days and (E) with added Fe(III) reduction 56 days 156

6. Microbial Reduction of Np(V) under Alkaline Conditions 163

Table 1 – Buxton Harpur Hill lime workings surface water major anions and cations 169

Table 2 – EXAFS fitting results from oxic with added Fe(III) sediments and progressive anoxia experiments: no added Fe and with added Fe. CN denotes coordination number, r is interatomic distance (Å) and σ^2 is Debye Waller factor ($Å^2$). ΔE_0 represents the shift in energy from the calculated Fermi level. $S0^2$ denotes the amplitude factor which was constrained between 0.85 and 1.05 in reduced samples and set to 1 in the oxic sample. R is the goodness of the fit and χ_v^2 is the reduced χ^2 value. Numbers in parentheses are the standard deviation on the last decimal place 174

Summary, Conclusion and Future Directions 177

Appendix. Conferences and Presentations 186

Abbreviation	Term
AHA	Aldrich humic acid
ALI	Annual limit of intake
ALS	Advanced lightsource
AHQDS	Anthrahydroquinone-2,6-disulfonate
AQDS	Anthraquinone-2,6-disulfonate
ADP	Adenosine diphosphate
ATP	Adenosine triphosphate
ATPase	Adenosine triphosphatase
bp	Base pairs
CCD	Charge-coupled device
CDZ	Chemically disturbed zone
C-S-H	Calcium-silicate-hydrate
DNA	Deoxyribonucleic acid
DU	Depleted uranium
EBS	Engineered barrier system
EDTA	Ethylenediaminetetraacetic acid
EDX	Energy-dispersive X-ray spectroscopy
ELHA	Elliot Lake humic acid
EXAFS	Extended X-ray absorption fine structure
FAD	Flavin adenine dinucleotide
FMN	Flavin mononucleotide
GDF	Geological disposal facility
HLW	High level waste
IAEA	International Atomic Energy Agency
IC	Ion chromatography
ICP-AES	Inductively coupled plasma-atomic emission spectroscopy
ICP-MS	Inductively coupled plasma-mass spectroscopy
ILW	Intermediate level waste
ISA	Isosaccharinic acid
LB	Luria-Bertani
LEMAS	Leeds Electron Microscopy and Spectroscopy Centre
LLW	Low level waste
LSC	Liquid scintillation counting
NAD	Nicotinamide adenine dinucleotide
NADH	Nicotinamide adenine dinucleotide (reduced form)
NERC	National Environmental Research Council
NTA	Nitrilotriacetic acid
OM	Organic matter
OSA	Octane sulfonic acid
OTU	Operational taxonomic unit

PCR	Polymerase chain reaction
PPi	Inorganic pyrophosphate
RCF	Relative centrifugal force
RDP	Ribosomal Database Project
RISA	Ribosomal intergenic spacer analysis
RNA	Ribonucleic acid
SAED	Select area electron diffraction
SEAES	School of Earth, Atmospheric and Environmental Science
SIS	Spectral index of sample
TAE	Tris base, acetic acid and EDTA
TEA	Terminal electron acceptor
TEM	Transmission electron microscopy
TPAC	Tetraphenylarsonium chloride
VFA	Volatile fatty acid
WDXRF	Wavelength dispersive system
XANES	X-ray absorption near edge structure
XAS	X-ray absorption spectroscopy
XMCD	X-ray magnetic circular dichroism
XRD	X-ray diffraction
XRF	X-ray fluorescence

Abstract

The University of Manchester

Adam John Williamson

Doctor of Philosophy (PhD)

The Geomicrobiology of Cementitious Radioactive Waste

2014

It is government policy that the UK's intermediate level radioactive wastes (ILW) will be disposed of in a deep geological disposal facility (GDF), where cementitious materials will be ubiquitous. After ILW disposal, groundwater ingress through the engineered facility is expected, forming a hyperalkaline plume from the cementitious materials into the surrounding host rock. This will form a persistent, high pH, "chemically disturbed zone" over timescales of 10^5 - 10^6 years, that will evolve from pH >13 to pH 10 over time. In the deep subsurface, microbial processes, particularly metal reduction may immobilise redox active radioactive contaminants in the waste, yet these reactions remain poorly characterised under these extreme conditions. In this project, microbiologically-mediated Fe(III) reduction was explored under alkaline conditions in sediment from a lime workings site in Buxton, UK, as an analogue for an ILW impacted subsurface environment. In addition, the impact of these processes on radionuclide (U, Tc and Np) behaviour was considered. Microcosms were set up using sediments taken from the site, adjusted to pH 10, augmented with electron donor (organic acids with yeast extract) and Fe(III), U(VI), Tc(VII) or Np(V) as electron acceptors. Biogeochemical processes were monitored using geochemistry, microbial ecology and X-ray absorption spectroscopy (XAS) techniques.

A cascade of microbial reduction processes occurred at pH 10 – 10.5 in all microbially active systems. In Fe(III) enriched systems, the dominant post-reduction mineral phase was magnetite and the rate and extent of Fe(III) reduction was increased in the presence of extracellular (AQDS, Aldrich humic acid) and endogenous (riboflavin) electron shuttles. In U(VI) supplemented sediment systems, partial U(VI) reduction occurred to a non-uraninite phase, which was susceptible to reoxidation by air (O_2) and nitrate. By contrast, in Fe(III)-augmented microcosms, more complete U removal to solids was noted, with uraninite identified as the end product, which was also reoxidised by air (O_2) and nitrate. In these experiments there was, however, evidence to suggest that uranium was associated with the reoxidised Fe(III) mineral. In Tc supplemented microcosm experiments, complete Tc(VII) reduction occurred in systems with and without added Fe(III). In the microcosms with no added Fe(III) however, only partial Tc removal from solution occurred, despite evidence for complete reduction, suggesting that soluble or colloidal Tc(IV) may be present. Moderate Tc reoxidation occurred with air (O_2) in both systems with and without added Fe(III) however no Tc remobilisation occurred during reoxidation with added nitrate. XAS on Fe(III) enriched sediments that had been microbially reduced and then re-oxidised by air, indicated that Tc may be associated with the reoxidised Fe mineral phase in these experiments. In the Np experiments, significant Np(V) sorption to sediments with and without added Fe(III) occurred initially, followed by Np(V) bioreduction to Np(IV). In all experiments, microbial (16S rRNA gene) profiling suggested a role for novel Gram-positive bacteria in Fe(III) and radionuclide reduction. These results highlight the significance of microorganisms on radionuclide biogeochemistry at high pH and have implications for the safe disposal of intermediate level nuclear wastes.

Declaration

No portion of the work referred to in the thesis has been submitted in support of an application for another degree or qualification of this or any other university or other institute of learning.

Copyright Statement

Acknowledgments

First and foremost I would like to thank my supervisors Jon Lloyd and Kath Morris, for giving me the opportunity to work on this project and for their guidance, patience and mentoring over the course of my studies. The last 4 years have seen a near 1:1 ratio of break-through to broken body parts, with 4 research papers prepared vs 1 broken stomach, 1 sprained ankle and 2 broken arms. For this I would like to thank SEAES football, Strength in Numbers CC, the Chill Factor[e] and the Manchester Royal Infirmary for both helping me through and holding me back.

For their invaluable help over the last 4 years I thank Chris Boothman and Thanos Rizoulis (microbial ecology), Gareth Law and Pieter Bots (radiochemistry) and Sam Shaw (mineralogy). A very big thank you to Al Bewsher (IC) and Paul Lythgoe (ICP/XRF) for their countless hours of work on the barrage of putrid samples I sent their way. I would also like to acknowledge John Waters for XRD, Mike Ward at Leeds for TEM, Joe Small at NNL for geochemical modelling, Heather Williams at MRI for gamma imaging, Fred Mosselmans and Steve Parry at Diamond, Jörg Rothe and Kathy Dardenne at ANKA, and John Charnock for his unprecedented EXCURV ability. I would also like to thank Tim Marshall for XAS data acquisition and modelling, and for making beam time night shifts bearable; our endless cocktail of Diamond strength coffee infused with 80's power ballads caused only mild hysteria, with mirages of glazed tender baby back ribs fading into lukewarm spare rib pot noodles.

I would like to thank my friends, past and present in the department, Ashley Brown, James Byrne, Richard Kimber and Nicholas Masters-Waage and my office mates Clare, Fabiola, Humood, Lorenzo and Nicola, for putting up with my odd ways and our impromptu songs, Halloween films and decorating my desk while I was in hibernation/ writing this thesis. Special thanks go to Aime White and also to Alex Budds, Andrew Edwards, Robert Soltysiak, Kate Tucker and Tom Wilkinson for many memorable moments along the way. Finally I would like to thank my family for their continued support throughout my academic career.

I acknowledge the financial support from the National Environment Research Council (NERC) for providing the funding for this project.

The Author

The Author graduated from The University of Manchester in 2010 with an undergraduate master's degree in Chemistry (MChem). The author then joined the Geomicrobiology group in the School of Earth Atmospheric and Environmental Sciences where he has conducted the research reported in this thesis for the duration of the project.

1

Introduction and Thesis Content

1. Introduction and Thesis Content

1.1. Project relevance

UK civil and military nuclear programmes over the last 60+ years have led to the generation of substantial amounts of radioactive wastes, while any new reactors that are built will add to the waste legacy over the next century. In the UK, Government policy is that these materials will be disposed of in a deep geological disposal facility (GDF) and this work focusses on the generic intermediate level waste (ILW) disposal concept, where cementitious materials will be used in waste packaging, engineering and/or backfill (DEFRA 2008; Morris et al. 2011). After ILW disposal, groundwater ingress through the engineered facility is expected, resulting in a hyperalkaline plume from the cementitious materials into the surrounding host rock. This will form a persistent, high pH, chemically disturbed zone (CDZ) where biogeochemical (pH, Eh, organic/inorganic metal/metalloid concentration) gradients will develop in the host rock and evolve over a wide range of spatial and temporal scales (10^5 - 10^6 years), from pH >13 to pH 10 over time (Marty et al. 2010).

The presence of electron donors (alkaline degradation products of cellulose in the ILW wasteforms, H_2 from the radiolysis of water and the anaerobic corrosion of stainless steel (Glaus & Van Loon 2008; Libert et al. 2011) and electron acceptors (nitrate, steel corrosion products (iron minerals), sulphate and radionuclides) with the increased recognition that extremophilic microbes can tolerate these harsh environments (Burke et al. 2012; Rizoulis et al. 2012), mean that improving our understanding of geomicrobiological processes in the CDZ is critical to understanding the fate of radionuclides in and around a GDF. Microorganisms in the deep subsurface have the potential to affect metal solubility during anaerobic respiratory processes (Anderson et al. 2011; Behrends et al. 2012), and under ambient conditions microbes have been shown to have a significant effect on metal and radionuclide speciation (Lloyd 2003; Law et al. 2010; Newsome et al. 2014). Overall, due to the steep biogeochemical gradients and the uncertainty of radionuclide behaviour expected in the CDZ, this work represents an essential, yet poorly understood component which will need to be considered during the performance assessment of a GDF.

The work presented in this thesis is therefore focussed on the biogeochemistry of iron and radionuclides (^{238}U, ^{99}Tc and ^{237}Np) at pH 10 using alkaline impacted sediments from the vicinity of a legacy lime working in Buxton, UK. Here, groundwater has

penetrated through lime kiln wastes, creating hyperalkaline calcium rich (~pH 12) plume which has filled the valley, impacted the surrounding geology and allowed indigenous microbial populations to develop over several decades. These sediments are therefore broadly representative of an evolved CDZ of a GDF.

1.2. Research objectives

The work outlined in this study aims to explore microbial redox processes under alkaline conditions and their impact on iron and radionuclide geochemistry. This will help develop a greater understanding of the potential for microbial processes in the CDZ of a GDF and give an insight into the fate of radionuclides in these high pH systems. The following aims and objectives were formulated and tested using a range of geochemical, mineralogical, electron microscopy, microbiological and spectroscopic techniques:

1. Identify the bioavailability of ferrihydrite to an indigenous sediment microbial community using batch microcosm experiments with and without added electron donor (lactate and yeast extract), with appropriate aerobic controls.
2. Determine the impact of redox mediators (such as humic substances and endogenous flavins) on microbial Fe(III) reduction under alkaline conditions using the same batch experimental setup.
3. Characterise the post reduction mineral phases produced in these Fe(III) enriched sediment systems using mineralogical techniques (XRD, TEM, SAED, EDX, XAS, XMCD).
4. Determine the fate of priority long lived radionuclides (U, Tc and Np) in batch sediment microcosm experiments under alkaline conditions with and without added Fe(III) as ferrihydrite.
5. Characterise the end-member radionuclide speciation and coordination environment using synchrotron techniques (XAS).
6. Assess the stability of radionuclides (U and Tc) to oxidative perturbations with air and nitrate under alkaline conditions.
7. Use microbiological techniques to characterise the microbial communities in all of these systems.

1.3. Thesis structure

This thesis consists of a detailed background into the relevant literature, a chapter describing the methodologies used, followed by 4 research papers that have been

prepared for publication to address the aims and objectives above. These are followed by a summary and finally a section describing future work.

Chapter 2 gives an introduction into the UK nuclear waste legacy, geological disposal, neutral and alkaline stable element geomicrobiology and radionuclide biogeochemistry (U, Tc and Np).

Chapter 3 covers all of the methods used in this thesis and outlines the theory behind each technique.

Chapter 4 contains the paper "Microbial reduction of Fe(III) under alkaline conditions relevant to geological disposal", published in Applied Environmental Microbiology in June 2013. This work investigates the potential for microbial redox processes in pH 10 Fe(III) enriched Buxton sediments, as Fe(III) reduction has the potential to play a defining role in controlling radionuclide biogeochemistry in and around a GDF for cementitious ILW. The impact of redox mediators (AQDS, riboflavin and soluble and insoluble humic acids) were also explored. A microcosm approach was taken in conjunction with mineralogical (XRD, TEM, SAED, EDX, XAS, XMCD) and microbiological (RISA and clone libraries) techniques.

Chapter 5 comprises of the paper "Microbial reduction of U(VI) under alkaline conditions; implications for radioactive waste geodisposal". This paper investigates the redox cycling of uranium under alkaline conditions using Buxton sediments with and without added Fe(III) as ferrihydrite. A key focus of this, and later chapters on Tc(VII) and Np(V) reduction, is the potential coupling between these priority radionuclides and the biogeochemistry of Fe. Select systems were augmented with AQDS (as a humic analogue and extracellular redox mediator) to further explore U(VI) reduction mechanisms. Synchrotron techniques were used to characterise the speciation and coordination environment of oxic, reduced (biotic and sterile) and reoxidised end member spectra.

Chapter 6 consists of the paper "Biogeochemical cycling of ^{99}Tc in alkaline sediments". This paper explores the fate of Tc(VII) in progressive anoxia and pre-reduced sediment microcosm experiments with and without added Fe(III) as ferrihydrite and the stability of these minerals to air and nitrate reoxidation. A combination of geochemical (UV/vis, LSC) and mineralogical (XAS), in conjunction with ^{99m}Tc γ-imaging experiments and geochemical modelling, were used to characterise technetium transformations in these high pH systems.

Chapter 7 is entitled “Microbial reduction of Np(V) under alkaline conditions”. This paper investigates neptunium biogeochemistry under alkaline conditions using progressive anoxia and pre-reduced batch sediment microcosm experiments with and without added Fe(III). Synchrotron techniques were used to characterise the speciation and coordination environment of all oxic and reduced (biotic and sterile) end member spectra.

Chapter 8 contains a summary of the work presented in this thesis and suggests future directions that may be followed from this work.

The appendix comprise of a list of oral and poster conference presentations.

1.4. Paper status and collaborator contributions

The submission status of the publications and the contributions of the listed authors are as follows:

Chapter 4: Microbial reduction of Fe(III) under alkaline conditions relevant to geological disposal, submitted in October 2012 to Applied Environmental Microbiology and published in June 2013.

A. J. Williamson- principal author, microcosm experiments and associated geochemical (UV-vis, IC) and mineralogical (XRD, TEM, SAED, EDX) analysis; *K. Morris*- extensive manuscript review; *S. Shaw*- TEM data acquisition; *J. M. Byrne*- XAS/XMCD data collection and analysis; *C. Boothman*- RISA and clone libraries; *J. R. Lloyd*- conceptual guidance and extensive manuscript review.

Chapter 5: Microbial reduction of U(VI) under alkaline conditions; implications for radioactive waste disposal, submitted in April 2014 to Environmental Science and Technology and currently in review.

A. J. Williamson- principal author, microcosm experiments and associated geochemical (UV-vis, IC, ICP-MS) and mineralogical (XAS) collection and analysis; *K. Morris*- conceptual guidance and extensive manuscript review; *J. Charnock*- XAS modelling guidance; *G. T. W. Law*- XAS data collection, modelling guidance and manuscript review; *A Rizoulis*- pyrosequencing; *J. R. Lloyd*- conceptual guidance and extensive manuscript review.

Chapter 6: Biogeochemical cycling of ^{99}Tc in alkaline sediments (Currently in preparation for submission to Environmental Science and Technology).

A. J. Williamson- principal author, microcosm experiments and associated geochemical (UV-vis, IC, LSC) and mineralogical (XAS) collection and analysis; *J. R. Lloyd*- conceptual guidance and extensive manuscript review; *C. Boothman*- pyrosequencing; *G. T. W. Law*- XAS data collection; *J. S. Small*- geochemical modelling; *H. A. Williams*- ^{99m}Tc gamma imaging experiments; *K. Morris*- conceptual guidance and extensive manuscript review.

Chapter 7: Microbial reduction of Np(V) under alkaline conditions (Currently in preparation for submission to Mineralogical Magazine (special edition for IGDTP 2014 conference)).

A. J. Williamson- principal author, microcosm experiments and associated geochemical (UV-vis, IC, ICP) and mineralogical (XAS) collection and analysis; *K. Morris*- conceptual guidance and extensive manuscript review; and XAS modelling guidance; *G. T. W. Law*- Np(V) and XAS preparation; *J. R. Lloyd*- conceptual guidance and extensive manuscript review.

1.5. References

Anderson, C., Johnsson, A., Moll, H. & Pedersen, K., 2011. Radionuclide geomicrobiology of the deep biosphere. *Geomicrobiology Journal*, 28 (5-6), 540–561.

Behrends, T., Krawczyk-Bärsch, E. & Arnold, T., 2012. Implementation of microbial processes in the performance assessment of spent nuclear fuel repositories. *Applied Geochemistry*, 27 (2), 453–462.

Burke, I.T., Mortimer, R.J.G., Palaniyandi, S., Whittleston, R.A., Lockwood, C.L., Ashley, D.J. & Stewart, D.I., 2012. Biogeochemical reduction processes in a hyper-alkaline leachate affected soil profile. *Geomicrobiology Journal*, 29 (9), 769–779.

Department for Environment Fisheries and Rural Affairs (DEFRA) & Department for Business Enterprise and Regulatory Reform (BERR) Devolved Welsh Administration for Wales and Northern Ireland, 2008. Managing Radioactive Waste Safely: A Framework for Implementing Geological Disposal, p.100.

Glaus, M.A. & Van Loon, L.R., 2008. Degradation of cellulose under alkaline conditions: new insights from a 12 years degradation study. *Environmental Science & Technology*, 42 (8), 2906–2911.

Law, G.T.W., Geissler, A., Lloyd, J.R., Livens, F.R., Boothman, C., Begg, J.D.C., Denecke, M.A., Rothe, J., Dardenne, K., Burke, I.T., Charnock, J.M. & Morris, K., 2010. Geomicrobiological redox cycling of the transuranic element neptunium. *Environmental Science & Technology*, 44 (23), 8924–8929.

Libert, M., Bildstein, O., Esnault, L., Jullien, M. & Sellier, R., 2011. Molecular hydrogen: an abundant energy source for bacterial activity in nuclear waste repositories. *Physics and Chemistry of the Earth, Parts A/B/C*, 36 (17–18), 1616–1623.

Lloyd, J.R., 2003. Microbial reduction of metals and radionuclides. *FEMS Microbiology Reviews*, 27 (2-3), 411–425.

Marty, N.C.M., Fritz, B., Clément, A. & Michau, N., 2010. Modelling the long term alteration of the engineered bentonite barrier in an underground radioactive waste repository. *Applied Clay Science*, 47 (1–2), 82–90.

Morris, K., Law, G.T.W. & Bryan, N.D., 2011. Chapter 6: Geodisposal of Higher Activity Wastes. In R. Harrison, ed, *Issues in Environmental Science and Technology*. Royal Society of Chemistry, pp. 129–151.

Newsome, L., Morris, K. & Lloyd, J.R., 2014. The biogeochemistry and bioremediation of uranium and other priority radionuclides. *Chemical Geology*, 363 (0), 164–184.

Rizoulis, A., Steele, H.M., Morris, K. & Lloyd, J.R., 2012. The potential impact of anaerobic microbial metabolism during the geological disposal of intermediate-level waste. *Mineralogical Magazine*, 76 (8), 3261–3270.

2

A Review of Neutral and Alkaline Biogeochemistry, Relevant to Radioactive Waste Disposal

2. A Review of Neutral and Alkaline Biogeochemistry, Relevant to Radioactive Waste Disposal

This chapter provides an introduction into the UK radioactive waste legacy and the current policy for the disposal of these wastes. This will be followed by a review of iron and radionuclide (^{238}U, ^{99}Tc and ^{237}Np) biogeochemistry. The chapter will conclude with a short overview of the field site used in this study.

2.1. The nuclear legacy

2.1.1. The nuclear fuel cycle

Following the discovery of nuclear fission in 1938, the UK nuclear weapon program started in April 1940, leading to the formation of the Atomic Energy Research Establishment in 1946 (Bayliss & Langley 2003). The International Atomic Energy Agency (IAEA) was established by the United Nations in 1957 to ensure the peaceful use of nuclear energy worldwide and is responsible for safety guideline development at each stage of the nuclear fuel cycle (Figure 1). As of 2014, in the UK there are 9 nuclear power stations in operation and ~ 15 that are undergoing decommissioning. This activity has led to significant quantities of radioactive wastes.

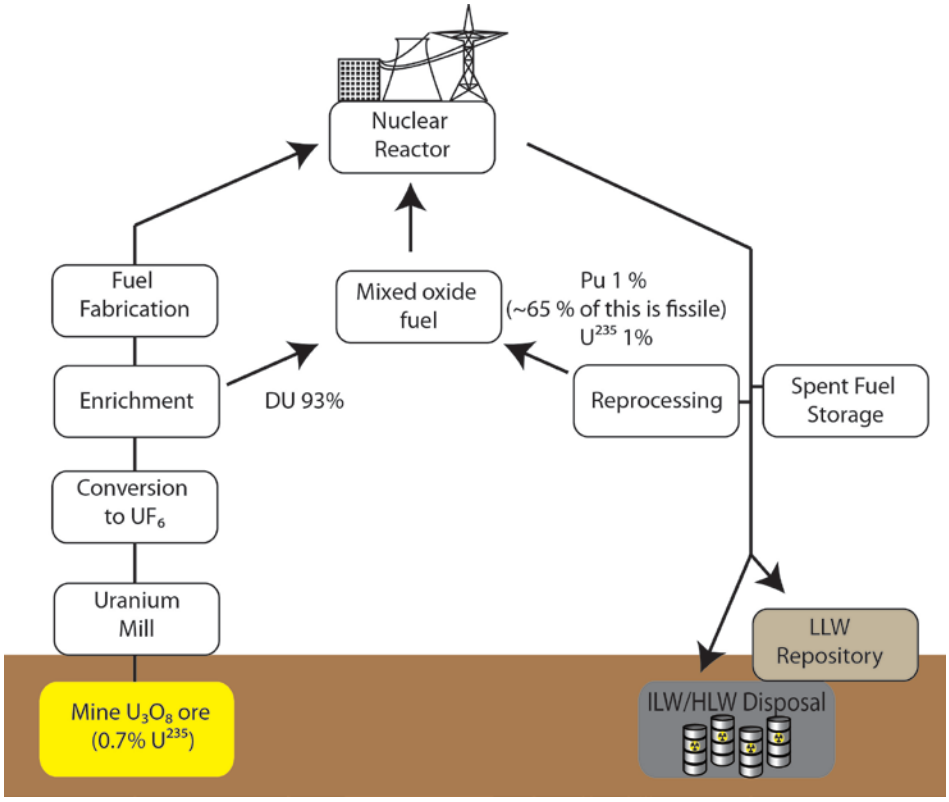

Figure 1: The principal operations in the nuclear fuel cycle, adapted from (Eisenbud & Gesell 1997).

2.1.2. Radioactive waste legacy

Defined by the IAEA, radioactive waste is “any material that contains or is contaminated by radionuclides or radioactivity levels greater than the exempted quantities established by the component authorities and for which no use is foreseen” (Jankowitsch 1990). As a result of a number of civil and defence programmes, the UK has generated significant quantities of radioactive wastes from operations and decommissioning, which can be classified as low (LLW), intermediate (ILW) and high level wastes (HLW) (Table 1).

Table 1: Properties of UK low, intermediate and high level radioactive wastes with corresponding volume and activity at 01-04-13 (NDA 2014).

	LLW	**ILW**	**HLW**
Radioactive content and handling	Activity < 4 GBq T^{-1} (α)/ 12 GBq T^{-1} (β,γ), do not require specialist shielding during handling or transport operations. Primarily short-lived radioisotopes	Activity > LLW but do not require special disposal procedures	Activity > LLW which require heavy shielding to account for significant heat generation from radioactivity
Total volume (m^3) (by 01-04-2014)	1,370,000 (+ 2,840,000 very LLW)	287,000	1020
Radioactivity (TBq) (by 01-04-2013)	57	3,900,000	78,000,000
Number of packages required	57,370	216,000	7,200
% by volume	93.6	6.4	<0.1
% of radioactivity	<0.0001	4.64	95.4
Composition	Operations-paper, plastic, clothing, wood and metals. Decommissioning- rubble, soil, plant, contaminated equipment	A heterogeneous wasteform, including metals, fuel cladding, sludges and flocs, organics (cellulose), concrete and cement	Spent nuclear fuel and highly radioactive reprocessing liquors
Current storage	Generally stored on site, with the majority (~50 %) stored at Drigg Low Level Waste Repository (LLWR) Cumbria	Generally on site, with the majority at Sellafield (~25 %), AWE, Berkeley, Harwell, Hinkley Point A and B, Hunterston A and Trawsfynydd	At Sellafield- vitrified waste is stored in stainless steel tanks fitted with cooling coils
Future disposal routes	LLWR at the Dounreay site in Caithness (20 % currently stored here awaiting disposal)	ILW GDF	HLW GDF

Reprocessing activities (e.g. at Hanford, USA and Sellafield UK) have significantly contributed to the world’s radioactive waste legacy, generating a highly radioactive heterogeneous mix of uranium, transuranic and fission products in addition to stable element and organic contaminants which poses a significant radiological hazard

(Renshaw et al. 2007). Legacy mining and ore processing, particularly during the Cold War in central Europe (Wismut in East Germany and Czech Republic) USA, Canada, Australia and Russia have generated the largest waste by volume, resulting in millions of tonnes of deposits rich in uranium decay products such as radium and radon gas. Heap leaching of lower grade ores worldwide and *in situ* leaching methods, predominantly used in Kazakhstan and the USA have also generated large volumes of surface and subsurface contamination (World Nuclear Association).

2.1.3. Geological disposal

In the UK, it is Government policy that high and intermediate level radioactive waste will be disposed of in a deep geological disposal facility, and this position is echoed in many other countries (Morris et al. 2011). A geological disposal facility (GDF) is a deep underground (200-1000 m depth) bespoke engineered facility for the disposal of radioactive wastes. It is a multi-barrier concept, where the combination of natural and engineered barriers aims to prevent harmful quantities of radioactive material from reaching the biosphere (Figure 2). The work presented in this study focusses on the generic ILW disposal system, where cementitious materials will be used. For example, in many geodisposal concepts, ILW will be grouted in steel drums and cement will be used for engineering or backfill purposes (Morris et al. 2011; Wieland et al. 2013).

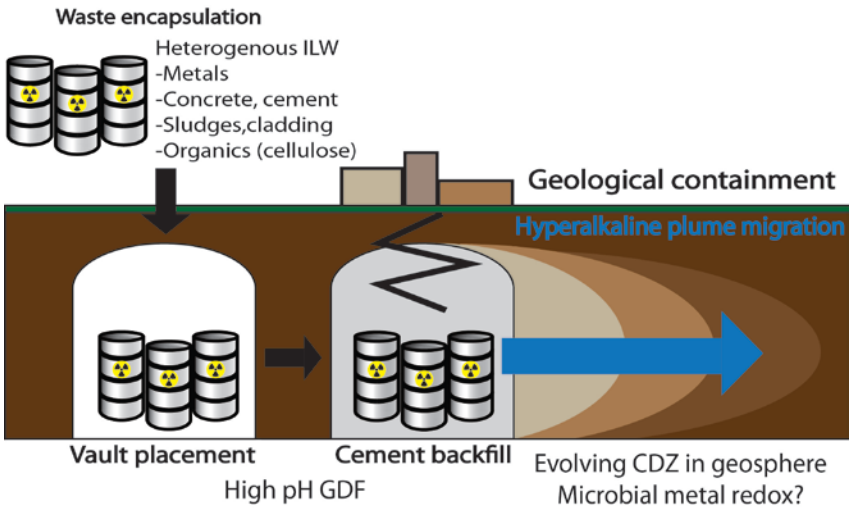

Figure 2: Generic radioactive waste disposal scenario.

In order to meet the applicable safety regulations and requirements, a safety case needs to demonstrate evidence to support the GDF during operations and post closure (DEFRA 2008). Currently, a generic safety case is being prepared to cover a range of possible disposal environments (higher/lower strength or evaporite host rock) and materials (Engineered Barrier System (EBS)) and is in an early stage of development.

The current UK disposal concept involves backfill with Nirex Reference Vault Backfill, a mix of Portland cement and excess hydrated lime (Nirex 2003). Initially, groundwater in contact with the cement will lead to KOH and NaOH dissolution, forming a highly alkaline leachate of pH ~ 13. These alkaline pore waters will migrate from the facility and react with host rock minerals, creating a chemically disturbed zone (CDZ). Silicate dissolution will lead to the formation of poorly ordered calcium silicate hydrate (C-S-H) phases and will affect physical (e.g. porosity and permeability) and chemical (e.g. adsorption capacity and reactive surfaces) properties of the host rock. After 10^5 years, buffering will be maintained by $Ca(OH)_2$ at ~ pH 12.5. Over geological timescales, $Ca(OH)_2$ will be consumed and in combination with C-S-H dissolution, the pH will fall to ~ 10. The pH will return to perturbed groundwater levels as CSH phases are consumed. The time taken for these processes to occur will be dependent on host rock composition and GDF infrastructure (e.g. cement type). This evolving CDZ will be characterised by extreme biogeochemical gradients which will occur over a wide range of spatial and temporal scales. Therefore, biogeochemical processes within the CDZ have the potential to significantly influence radionuclide transport.

2.1.4. Natural analogues

Natural waters with high $Ca(OH)_2$ concentrations may be used as an analogue for when groundwater interacts with a cementitious GDF. These are known as natural analogues and this offers an opportunity to study interactions with mineral surfaces, solubility and speciation of radionuclides, the nature and stability of colloids and the nature and viability of microbially mediated processes (wasteform breakdown and near field radionuclide mobilisation). These interactions can also be monitored at the interface between high pH and neutral waters, similar to the CDZ and hence have become an integral part of the safety case design for a geological disposal facility (Miller et al. 2000).

Groundwater interaction with naturally occurring cement materials in Maquarin, Jordan has formed hyperalkaline leachates which follow the order $NaOH>KOH>>Ca(OH)_2$ and can be accurately modelled by groundwater cement degradation models. Combined with the other elements of interest (Na, Ca, Si, K, Fe) to the safety assessment of a repository make this a realistic analogue of a cementitious repository (Khoury et al. 1992). The hyperalkaline (pH 10-12) groundwaters (from Allas, Chrisovrysi and Parsata Springs) over the majority of the 30 sites that comprise the Cyprus natural analogue project are a product of serpentisation of the ophiolites (Alexander et al. 2012). The

work conducted here has identified hyperalkaline fluid reactions with naturally occurring, GDF representative materials such as bentonite and analogous clay-rich sediments (Alexander et al. 2012).

As well as natural geological and geochemical systems, archaeological systems and anthropogenic contaminated sites may also have the potential to provide useful data. Archaeological sites include roman settlements, where corrosion of metallic/cementitious materials, degradation of glasses, long term evolution of cementitious materials, decay and breakdown of organic materials, and chemical interactions with surrounding rocks may all provide quantitative (e.g. corrosion rates) data if the artefacts are deemed to be relevant to a repository material (Jones et al. 1998). Anthropogenically contaminated environments can arise from cement manufacture [$Ca(OH)_2$] (section 2.6.2), mining operations, paper and pulp production [Na(OH)] and food processing effluents (Jones et al. 1998).

2.2. Background to the elements in this study

Typically Fe(III) is the most abundant electron acceptor in soils and sediments, which hold one to several g Kg^{-1} of Fe(III) (Cornell & Schwertmann 2003) and therefore will be a significant component of the wider GDF environment. Additionally, anaerobic steel corrosion may provide bioavailable Fe(III) for microbial Fe(III) reduction, coupled to organic material within the ILW wasteform. Products of microbial Fe(III) reduction may have a potential control on radionuclide solubility (Lloyd 2003 and refs therein).

Civilian and military nuclear programmes over the last 50+ years have led to a substantial legacy of radioactive wastes which contain uranium as the most significant radionuclide by mass. Natural occurring uranium is primarily comprised of ^{238}U (99.27 %, $t_{1/2}$ 4.47 x 10^9 y) and ^{235}U (0.72 %, $t_{1/2}$ 7.04 x 10^8 y), which decay by α-emission. ^{235}U is the only naturally occurring fissile isotope, whereas ^{238}U is transmuted to the fissile ^{239}Pu within a nuclear reactor. Uranium poses a significant environmental hazard primarily due to its heavy metal toxicity which can cause acute renal damage, amongst other severe medical disorders (Bryan & Siegel 2003).

Nuclear fission generates a vast number of long lived radionuclides, primarily ^{135}Cs (6.9 %, $t_{1/2}$ 2.3 x 10^6 y), ^{99}Tc (6.13 %, $t_{1/2}$ 2.1 x 10^5 y), ^{93}Zr (5.5 %, $t_{1/2}$ 1.53 x 10^6 y) which will be present in high, intermediate and low level wastes. Approximately 1 kg of ^{99}Tc is produced per tonne of enriched ^{235}U and ~ 15 % of this is partitioned to ILW (NDA 2014). Additionally, a number of accidental and approved release of TcO_4^- to the

environment has led to widespread contamination in surface and groundwater and their associated sediments (Icenhower et al. 2010 and refs therein). ^{99}Tc is redox active β-emitter (E_{max} 0.29 MeV) and particularly problematic in oxic environments due to its very mobile pertechnetate (Tc(VII)) species and is readily accumulated by plants (as a sulphate analogue), animals and marine biota (Icenhower et al. 2010).

^{237}Np ($t_{1/2}$ 2.14 x 10^6 y) is a transuranic alpha emitter with high radiotoxicity and ~ 70 % of the UK radioactive waste inventory is partitioned to the intermediate level waste fraction (NDA 2014). It is primarily formed through ^{236}U neutron capture and β decay (Equation 2.1).

$$^{235}_{92}\mathrm{U} \xrightarrow[n]{} {}^{236}_{92}\mathrm{U_m} \xrightarrow[\gamma\,(120\,ns)]{} {}^{236}_{92}\mathrm{U} \xrightarrow[n]{} {}^{237}_{92}\mathrm{U} \xrightarrow[\beta^-\,(6.75\,d)]{} {}^{237}_{93}\mathrm{Np} \qquad (2.1)$$

As the granddaughter decay product of ^{241}Pu ($t_{1/2}$ 14.4 y) and daughter of ^{241}Am ($t_{1/2}$ 433 y), it will become the dominant radionuclide in the $10^{4\text{-}7}$ years and within the expected lifetime of a geological disposal facility (Lloyd & Renshaw 2005) (Equation 2.2).

$$^{238}_{92}\mathrm{U} \xrightarrow[transmutation]{} {}^{239}_{94}\mathrm{Pu} \xrightarrow[2(n,\gamma)]{} {}^{241}_{94}\mathrm{Pu} \xrightarrow[\beta^-(14.35\,y)]{} {}^{241}_{95}\mathrm{Am} \xrightarrow[\alpha\,(432.2\,y)]{} {}^{237}_{93}\mathrm{Np} \quad (2.2)$$

It exists predominantly as Np(V) in oxic environments, which has the lowest affinity for surfaces of all the transuranic elements (Kaszuba & Runde 1999). If ingested, neptunium primarily deposits in the liver and bones, which may cause radiation carcinogenesis (Taylor 1989).

2.3. Stable element biogeochemistry

Microorganisms play a key part in geochemical and mineralogical transformations in ambient environments, through the use of organic and inorganic substrates in respiration (Gadd 2010). In oxic environments, microorganisms couple oxygen (the terminal electron acceptor, TEA) respiration to the oxidation of an electron donor. Oxidation of an electron donor to CO_2 in the citric acid cycle reduces NAD^+ (nicotinamide adenine dinucleotide) to NADH. A downward electron flow is generated as NADH delivers an electron to the electron transfer proteins and extrudes its H ion through the inner plasma membrane into the periplasmic space (in Gram-negative bacteria) or into the cell wall region (in Gram-positive bacteria). This generates a proton gradient and is balanced by adenosine triphosphatase (ATPase), a facilitative protein, which allows protons to diffuse back into the cell. This proton motive force generates the energy required for the oxidative phosphorylation of adenosine triphosphate (ATP) from adenosine diphosphate

(ADP) (Brock 1999). The electron transfer proteins pass the e^- towards the terminal reductase on the cell surface, which transfers the e^- to the TEA.

Anaerobic microbial respiration proceeds by a cascade of TEAs corresponding to their respective energy yields (Gibbs free energy, ΔG_0) (Table 2) (Brock 1999). More electropositive oxidants (O_2 and NO_3^{2-}) are consumed in near surface, oxic environments whereas poorer oxidants (Mn(IV), Fe(III), SO_4^{2-} and CO_2) are reduced in anoxic environments at depth (Reeburgh & Henrichs 1987).

Table 2: Energy yields of terminal electron accepting processes at pH 7 (Konhauser 2009).

Terminal Electron Accepting Process	**ΔG kJ mol^{-1} CH_3COO^-**
$CH_3COO^- + 2O_2 \rightarrow H_2O + 2CO_2 + OH^-$	-854
$CH_3COO^- + 1.6NO_3^- \rightarrow 2CO_2 + 0.8N_2 + 2.6OH^- + 0.2H_2O$	-801
$CH_3COO^- + 4MnO_2 + 3H_2O \rightarrow 4Mn_2^+ + 2HCO_3^- + 7OH^-$	-558
$CH_3COO^- + 8Fe(OH)_3 \rightarrow 8Fe_2^+ + 2HCO_3^- + 15OH^- + 5H_2O$	-337
$CH_3COO^- + SO_4^{2-} \rightarrow HS^- + 2HCO_3^-$	-48
$CH_3COO^- + H_2O \rightarrow CH_4 + HCO_3^-$	-31

2.3.1. Iron biogeochemistry

Chemical weathering of igneous and metamorphic rocks, such as olivine and pyroxene, leads to the mobilisation of iron in the environment, which predominantly exist in 0,+2 and +3 oxidation states. In oxygen rich environments, ferric (Fe^{3+}) complexes form strong insoluble oxide and hydroxide complexes at circumneutral pH. Under anoxic conditions, ferrous (Fe^{2+}) dominates, typically as lone species in most aqueous environments, but can form insoluble salts in high carbonate (siderite, $FeCO_3$), sulphide (pyrite, FeS_2) and orthophosphate (vivianite, $Fe_3(PO_4)_2.8H_2O$) environments (Langmuir 1997). There are sixteen known oxides and oxyhydroxides of iron with varying stoichiometric composition of Fe, O and H and crystallinity, depending upon formation conditions.

Ferrihydrite (hydrous ferric oxide) is a fine grain amorphous metastable iron mineral and is predominantly found on the coatings of rock fragments in subsurface environments or as suspended material in groundwater (Cornell & Schwertmann 2003). It is formed via rapid hydrolysis of Fe(III) or oxidation of Fe(II) and exhibits a high surface area (~100 m g^{-1}). Ostwald ripening/structural aggregation of ferrihydrite can form more thermodynamically and kinetically stable crystalline minerals such as goethite (α-FeOOH) or haematite (Fe_2O_3) which has given rise to their abundance in natural environments (Johnston & Lewis 1983; Schwertmann et al. 1998; Banfield et al. 2000). Higher temperatures (> 80 °C), circumneutral pH ranges (pH 7-8), lower

humidity (< 40 %) and older sediments favour the stability of haematite (Schwertmann & Murad 1983; Torrent et al. 1982).

At neutral pH Fe(III) reduction is widely mediated by dissimilatory iron-reducing bacteria (Nevin & Lovley 2000). Dissimilatory metal reduction is a microbial respiratory process which involves the reduction of an extracellular metallic TEA, solely coupled to ATP generation. On the other hand, assimilatory Fe(III) reduction generates soluble Fe(II) which is incorporated into cellular proteins (Schröder et al. 2003). Dissimilatory Fe(III) reduction coupled to electron donors such as H_2 and/or simple fermentation products, organic matter (OM) or more complex substrate such as pyruvate, toluene, amino acids and sugars (Lovley et al. 2004 and refs therein) have been observed. This aspect of the energy conservation process contributes to the oxidation of 65% of OM in nature in some environments (Canfield & Raiswell 1998).

Amorphous iron oxide phases such as ferrihydrite are the preferred substrates for reduction by Fe(III)-reducing bacteria due to their poor morphology and crystallinity and large surface area (Schwertmann & Murad 1983; Lovley et al. 1987; Cutting et al. 2009). Microbial Fe(III) reduction of hematite is thought to follow the abiotic reductive dissolution of a thin surface layer of material that contains bioavailable Fe(III), followed by mass transport of Fe(II) from the dissolving mineral surface (Hansel et al. 2003). Fe(III) reduction in goethite is thought to proceed by layer by layer etching of the surface. Lower Fe(II) fluxes have been shown to favour goethite formation, whilst higher concentrations of Fe(II) favour magnetite formation (Nico et al. 2009). Additionally, magnetite has been shown to be stabilised at lower Eh and higher pH in reducing iron-carbonate-water systems (Figure 3) (Mills et al. 1987).

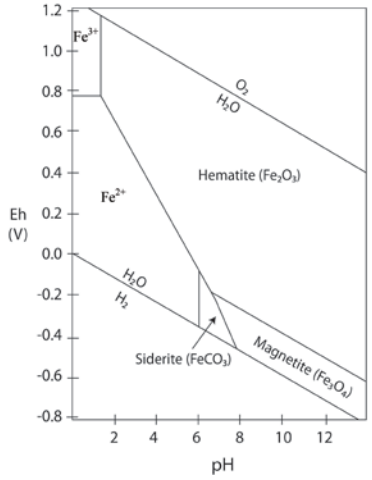

Figure 3: Eh-pH stability fields for iron, hematite, magnetite and siderite in water at 25 °C, 1 atm total pressure and total dissolved carbonate activity of $10^{-1.35}$. Adapted from (Mills et al. 1987).

Biomineralisation is the collective term for microbially mediated mineral formation, where microbially produced ligands complex with metals, leading to extracellular precipitation (Newsome et al. 2014). Sulphide, phosphate and silicates, and in response to localised alkaline conditions carbonates and hydroxides are all ligands capable of Fe complexation, forming e.g. pyrite, vivianite, odinite, siderite/ankerite or goethite respectively (Newsome et al. 2014 and refs therein). Redox cycling can also lead to the precipitation of multi-valent iron minerals such as magnetite (Fe_3O_4); a black ferromagnetic mineral of nanoparticle size with magnetite with a cation site occupancy of (1:1:1 $Fe(II)O_h$:$Fe(III)T_d$:$Fe(III)O_h$) (Pattrick et al. 2002). Magnetite has commercial uses in the bioremediation of toxic metal contaminated wastes (Lovley 1995) and in various cancer treatment methods (Kawashita et al. 2005).

2.3.2. Metal reduction mechanisms

A wide variety of microorganisms have been found capable of dissimilatory metal reduction. These comprise of Gram-negative and Gram-positive species, classified by the ability of their cell wall/outer membrane structure to retain crystal violet-iodine (CV-I) complex after ethanol treatment (Gram 1884) (Figure 4).

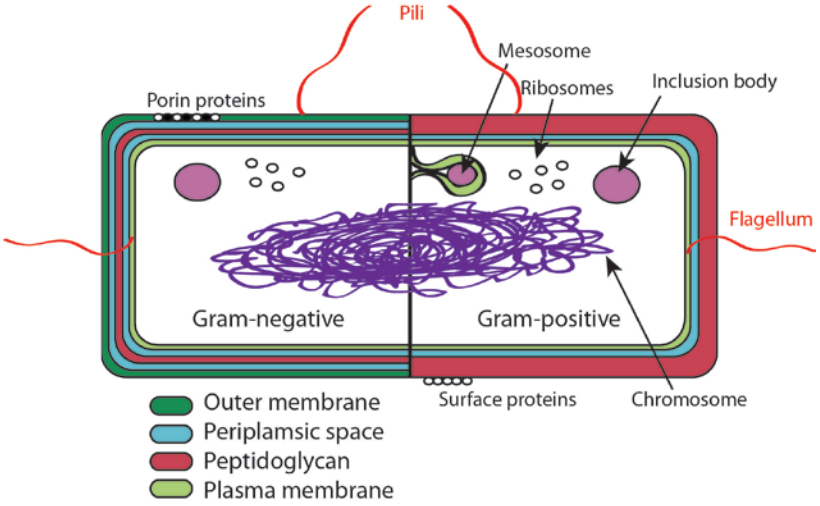

Figure 4: Gram-negative and Gram-positive bacteria (note, pili and flagellum are not found in all bacteria).

Geobacter sp (Lovley et al. 1987; Lovley et al. 1993) and *Shewanella* sp, (Myers & Nealson 1988; Caccavo Jr. et al. 1992; Nealson et al. 1992) are well studied model Gram-negative Fe(III)-reducing bacteria. Several Fe(III) reduction mechanisms have been proposed in these organisms, including direct cell contact, indirect transfer through chelators/ humic substances/flavins and more recently, electron transfer via nanowires (Lloyd 2003; Reguera et al. 2005). A number of Gram-positive bacteria have also been

found capable of dissimilatory Fe(III) reduction, primarily comprising of Firmicutes *Clostridia* (Dobbin et al. 1999) and *Bacilli* (Boone et al. 1995), however, the mechanisms by which these processes occur are poorly understood.

i) Direct contact

Unlike soluble electron accepting species such as O_2 or NO_3^-, Fe(III) is highly insoluble in most terrestrial environments, so cannot diffuse into the cell where it is reduced (Lovley et al. 2004). In order for electron transfer to occur between microbe and metal, the microbe needs direct contact onto the surface of the mineral. In Gram-negative bacteria, electron transfer occurs at 3 key locations; from the inner membrane quinone pool to the periplasm, across the periplasmic space and across the outer membrane to extracellular acceptors. Cytochromes are electron transfer proteins that have iron containing pophyrin rings (heme) capable of shifting between Fe(II) and Fe(III) states. Each type of cytochrome has a variable functional or different site within the electron transport chain.

Direct electron transfer by Gram-positive bacteria was not thought to be able to occur due to the lack an outer membrane, thicker cell wall (10-80 nm) and glycoprotein S-layer (Figure 4). However, evidence of direct contact dependent Fe(III) reduction has been reported in *Thermincola potens* strain JR (Wrighton et al. 2011; Carlson et al. 2012). The peptidoglycan layer of the cell wall of Gram-positive organisms have an affinity for proteins, which may allow non-covalent packing of hexaheme cytochromes (Desvaux et al. 2006; Carlson et al. 2012). Alternatively, non-peptide teichoic acids traverse the cell wall and may reversibly bind metals so may be involved in electron shuttling across the cell (Ehrlich 2008). *Carboxydothermus ferrireducens* was also found to be able to utilise electron shuttles (AQDS) and siderophores (DFO) (section 2.3.2 (ii)) as complementary mechanisms to promote direct solid phase Fe(III) reduction in Gram-positive microrganisms (Gavrilov et al. 2012).

ii) Indirect contact-chelators

As iron oxides are insoluble in most natural environments, many microbes rely on iron chelators for Fe(III) assimilation. Siderophores are low molecular iron chelators secreted by organisms which promote metal dissolution (Drechsel & Jung 1998) and many aerobic microorganisms are able to produce catecholate, carboxylate or hydroxomate siderophores which form strong complexes with Fe(III) (Gadd 2010). Nitrilotriacetic acid (NTA) and ethylenediaminetetraacetic acid (EDTA) are often used

in wastewater treatment, including nuclear facility operations, to complex metals. Fe(III)-NTA complexes undergo microbial reduction more readily than ferrihydrite, goethite and hematite (Lovley & Woodward 1996). These chelated complexes are able to enter the periplasm prior to reduction, increasing its bioavailability for microbe delivery to the electron transport chain (Dobbin et al. 1996).

iii) Indirect contact- exogenous electron shuttles

Fe(III)-reducing bacteria can overcome the problem of mineral insolubility by using organic compounds such as dissolved humic substances to shuttle electrons to mineral phases not in direct contact with the cell. Humic substances are high molecular weight, heterogeneous organic material, ubiquitous in terrestrial and aquatic environments, produced by biodegradation of dead OM such as lignin (Stevenson 1994). Humic acids are di/tribasic and contain chelating ligands such as carboxyl (COOH) and phenolate (C_6H_5OH) groups, capable of metal (Mg^{2+}, Ca^{2+}, Fe^{2+} and Fe^{3+}) ion complexation, which may increase their bioavailability (Stevenson 1994).

Experiments with 2,6-anthraquinone disulphonate (AQDS) identified that humic redox chemistry is primarily driven by the quinone/hydroquinone couple (Curtis & Reinhard 1994). In experiments with *Geobacter metallireducens*, enhanced Fe(III) reduction occurred in the presence of humic acids by electron shuttling, which alleviates the need for direct contact between the microbe cell and Fe(III) oxides (Lovley et al. 1996). Quinone reduction to hydroquinone was found to proceed via an organic radical intermediate semiquinone state (Scott et al. 1998) (Figure 5).

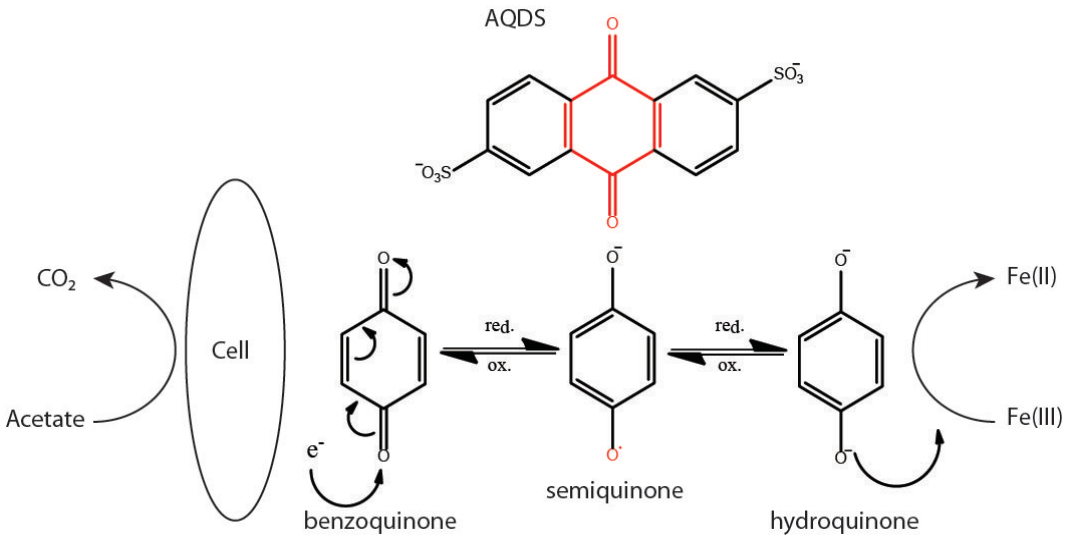

Figure 5: Proposed mechanism of electron shuttling of Fe(III) by AQDS, coupled to acetate oxidation via the semiquinone moiety.

Model compounds such as AQDS are now widely used as a humic analogue, due to the difficulty of handling highly complex and poorly characterised humic substances (Lovley et al. 1996; Lovley et al. 2004) and several microorganisms including *Geobacter metallireducens* and *Shewanella alga* have been shown to use reduced form of AQDS, anthrahydroquinone disulphonate (AHQDS) as an electron donor for Fe(III) reduction (Lovley et al. 1999). As humic acids are highly resistant to microbial biodegradation, and are not consumed during metal reduction, low concentrations (< 100 µM) of these compounds can significantly increase the rate of Fe(III) reduction in both amorphous and more crystalline iron oxides, hydroxides and oxyhydroxysulphates, especially akaganeite and schwertmannite (Cutting et al. 2009). Humic substances in the environment are primarily in the solid phase however (Stevenson 1994) and recent work has demonstrated the ability of *Geobacter* and *Shewanella* to also use these solid state humic substances as electron shuttles (Roden et al. 2010).

iv) Indirect contact- endogenous electron shuttles

These shuttles were first demonstrated by *Shewanella putrefaciens*, which was found to excrete a small non-proteinaceous quinone-type compound under anaerobic conditions which were involved in extracellular electron transfer to insoluble ferric oxides (Newman & Kolter 2000). The isoalloxazine (flavin) group is capable of Fe chelation and found to be responsible for redox shuttling (Figure 6) (Marsili et al. 2008). A range of *Shewanella* species are now known to be capable of secreting and utilising these compounds, which have been characterised as flavin mononucleotide (FMN) and riboflavin (von Canstein et al. 2008). Flavin adenine dinucleotide (FAD) was only found within the cell in strains of *Shewenalla* but secreted by the majority of the *Pseudomonas* and *Escherichia* strains (von Canstein et al. 2008).

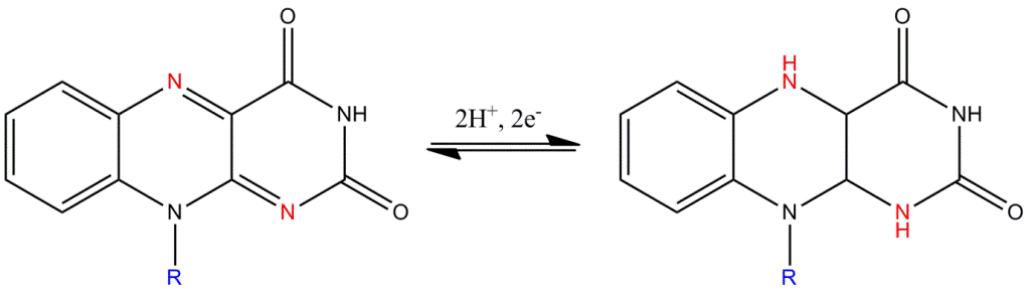

Figure 6: Flavin redox chemistry. The R group varies depending on the compound (R=mononucleotide (FMN), adenine dinucleotide (FAD) and ribose (riboflavin)).

v) Indirect contact- nanowires

It was hypothesised that *Geobacter metallireducens* had the potential to scavenge, detect and move towards solid oxidised Fe(III) phases (chemotaxis) using their cellular appendages, (Childers et al. 2002). This was later contested in a study with *pilT* (required for twitching and motility) deficient *Geobacter sulfurreducens* which showed no effect on the rate or extent of Fe(II) reduction (Reguera et al. 2005). It was also found that the *pilA* deficient strain could no longer reduce insoluble Fe(III) oxides suggesting that the conductive pili were serving as biological nanowires and involved in electron transfer (Reguera et al. 2005). The OmcS cytochrome thought to be involved in electron transfer was not packed close enough within the pili to facilitate electron hopping, so it has been suggested that pili exhibit metallic like electron conductive properties (Lovley 2012). Nanowire production by *Shewanella oneidensis* strain MR-1 was observed in response to low electron acceptor concentrations (Gorby et al. 2006), possibly mediated by pilus bound membrane vesicles (Gorby et al. 2008), but have not been characterised further. The role of nanowires in electron transfer in these model organisms remains highly contested.

2.4. Alkaline biogeochemistry

Microbes that require an alkaline pH of 9 or above for growth, are known as alkaliphiles (Grant et al. 1990). Strict alkaliphiles either cannot grow, or grow slowly at circumneutral pH environments, whereas facultative alkaliphiles are able to survive at high pH, but can grow at neutral pH. Additionally, haloalkaliphiles require both a high pH and high salinity (up to 33% wt/vol NaCl).

2.4.1. Physiology

The internal pH of the majority of alkaliphiles is typically 8 (Horikoshi 1999) and cytoplasmic pH regulation in high pH environments involves two regulatory barriers, the cell wall and plasma membrane. The peptidoglycan cell wall comprise of acidic polymers (e.g. glutamic acid and phosphoric acid in *Baccilus* spp.) that carry a negative charge, which repel OH^- and adsorb Na^+ and H_3O^+,protecting the plasma membrane, which is unstable at high pH (> 8.5) (Aono & Horikoshi 1983). At high pH, H^+ concentrations are low and Na^+ concentrations are high, providing a low proton motive force (-50 mV) at pH 10 which is not sufficient for growth in alkaline environments (Horikoshi 2006). Sodium plays an important role in growth, sporulation, germination and flagellar motility (Horikoshi 2006). Additionally, Na^+ replaces H^+ generating a

sodium motive force which drives substrate into the cell (Na^+/H^+ antiporter system). The plasma membrane maintains pH homeostasis by Na^+/H^+ antiporter, $Na^{+/}$amino acid symporter systems and ATP driven H^+ expulsion (Figure 7) (Horikoshi 1999; Horikoshi 2011).

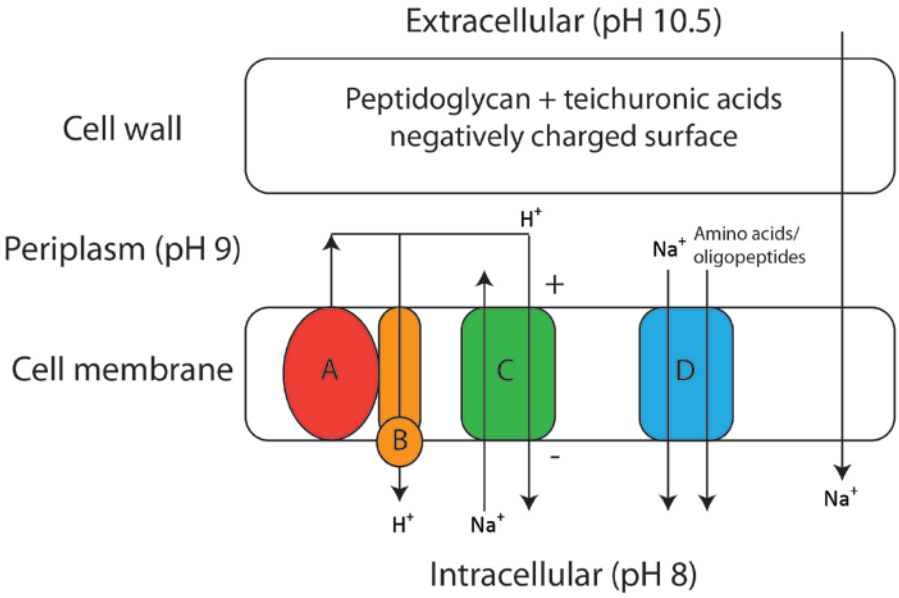

Figure 7: Simplified schematic representation of cytoplasmic pH regulation, adapted from (Horikoshi 2011). (A) Respiratory electron transport chain; (B) ATPase pathway; (C) ΔpH and Δψ-dependence Na^+/H^+ antiporters; (D) amino acid and oligopeptide/Na^+ symporters.

2.4.2. Environments

The most stable naturally occurring alkaline environments are formed by geological, climatic and geographical conditions. Alkaline environments which are low in Ca^{2+} are also known as soda lakes or deserts and are formed by the evaporation of sodium carbonate rich waters (Jones et al. 1998). Due to the low abundance of Mg^{2+} and Ca^{2+} in these systems, the lakes can become enriched with CO_3^{2-} and Cl^-, which give rise to hypersaline soda lakes. Lake Magadi (Kenya) and Wadi Natrun (Egypt) (Grant et al. 1990) are the most stable, highly alkaline environments known on Earth with site water pH levels recorded between pH 10.5 and 12.

High Ca^{2+} environments arise from the serpentinization of primary silicate minerals olivine and pyroxene by CO_2 charged surface waters, which release Ca^{2+} (which precipitates as $CaCO_3$) and OH^- into solution. As carbonate depletes, a $Ca(OH)_2$ brine equilibrates and maintains hyper alkaline environment (> pH 11). Natural hyperalkaline Ca^{2+} rich groundwater have been located in California, Oman, Yugoslavia, Cyprus and

Jordan (Grant et al. 1990) (section 2.1.4). Commercial processes such as cement manufacture and chromite ore processing residue can also generate alkaline wastes which leach into the aqueous environment (Whittleston et al. 2011; Burke et al. 2012).

2.4.3. Phylogenetic diversity and metal reduction

Microbial communities have been found to live at a pH of 12.9 in the soda lakes of Maqarin, Jordan (Pedersen et al. 2004), however, microbial growth was slow and low cell counts suggested microbial activity will be low during the hyperalkaline phase of cementitious repositories. Recent work however has shown evidence for microbially mediated NO_3^{2-} and Fe(III) reduction up to pH 12.3 in the organic rich soil beneath the calcite precipitate layer of the alkaline impacted sediments from a legacy lime workings in Buxton, also used in this study (Burke et al. 2012). Other workers using sediments from this site explored the biochemical limits for microbial redox processes using microcosm studies in combination with free energy calculations and showed that biogeochemical processes were occurring up to pH 12, but the rate and extent of reduction decreased with increasing alkalinity (Rizoulis et al. 2012). Although a vast number of studies have focussed on alkaliphilic microorganisms over the last 20 years, there is a paucity of studies which explore microbially mediated metal reduction under alkaline conditions. A list of alkaliphilic microorganisms capable of Fe(III) reduction are given in Table 3.

Recent work has shown that an alkaliphilic enrichment culture from a hyperalkaline chromite ore processing residue site dominated by Gram-positive *Tissierella*, *Clostridium* and *Alkaliphilus* sp. is capable of Fe(III) reduction at pH 9.2 (Whittleston et al. 2011). Further experiments suggested that the consortium secreted a flavin species (most likely riboflavin) to facilitate solid Fe(III) reduction at pH 9-11 (Fuller et al. 2014). Currently, radionuclide biogeochemistry under alkaline conditions is poorly understood and only one study has explored Tc(VII) reduction at pH 10, with haloalkaliphilic strains of *Halomonas* suggested to form soluble Tc(IV) carbonate complexes (Khijniak et al. 2003). No studies to date however have focussed on radionuclide biogeochemistry with sediment consortia.

Table 3: Alkaliphilic organisms known to reduce Fe(III). Optimum salinity, temperature and pH for growth are given in parentheses.

Organism	Source	Electron donors oxidised with Fe(III)	Fe forms reduced	Fe reduction product	Other electron acceptors	NaCl content (g l^{-1})	Growth temp (°C)	Growth pH range	Reference
Alkaliphilus metalliredigens	Leachate ponds at the U.S. Borax Company in Boron, California	Lactate, acetate, glucose, lactate, pyruvate (10 mM) and H_2 (20%)	Fe(III) citrate, Fe(EDTA)	Vivianite biomineralisation	Co(III)-EDTA, Cr(VI), $UO_2CO_3^{2-}$, $Mn(IV)O_2$	0-80 (20)	4-45 (35)	7.5-11 (9.5)	(Ye et al. 2004; Roh et al. 2007)
Anaerobaranca californiensis	Hot spring sediments, Paoha Island on Mono Lake, California, USA	Peptone and casamino acids preferred, slow growth on fructose, sucrose, maltose, starch, glycogen, cellobiose, glycerol and pyruvate	HFO, Fe(III) citrate	5-7 % HFO reduced and were black and magnetic (but not further characterised)	Se(IV), polysulfide and thiosulfate	0-60 (5-25)	45-70 (58)	8.6-10.4 (9-9.5)	(Gorlenko et al. 2004)
Anaerobranca gottschalkii	Hot inlet of Lake Bogoria, Kenya	Peptone and casamino acids preferred, slow growth on fructose, sucrose, maltose, starch, glycogen, cellobiose, glycerol and pyruvate	Fe(III) citrate	Not reported	Se(IV), polysulfide and thiosulfate	0-40	30-65 (50-55)	6-10.5 (9.5)	(Gorlenko et al. 2004) (isolated by (Prowe & Antranikian 2001))
Anaerobranca horikoshii	Hot spring at Old Faithful Hotel, Yellowstone National Park, USA	Peptone and casamino acids preferred, slow growth on fructose, sucrose, maltose, starch, glycogen, cellobiose, glycerol and pyruvate	Fe(III) citrate	Not reported	Se(IV), polysulfide and thiosulfate	Not reported	30-66 (57)	6.5-10.3 (8.5)	(Gorlenko et al. 2004)
Alkaliphilus peptidofermentans	Soda lake Verkhnee Beloe (Buryatia, Russia)	Peptide fermentation products (primarily acetate and formate)	HFO, Fe(III)-EDTA but not Fe(III) citrate	Siderite (Chistyakova 2003)	AQDS, fumarate, crotonate and $S_2O_3^{2-}$ (did not reduce Mn(IV)	0-50 (20)	6-40 (35)	7.5-9.7 (9.1)	(T. Zhilina et al. 2009)
Bacillus arseniciselenatis **(strain E1H0)**	Mono Lake, California	Lactate	Fe(III)-NTA	Not reported	Se(VI), As(V), fumarate, nitrate	20-120 (60)	Not reported	(8.5-10)	(Switzer Blum et al. 1998; Zavarzina et al. 2009)
Bacillus **strain SFB**	Flat sediments of Soap Lake, Washington	Hexose sugars, glucose and fructose to lactate, acetate and formate	Fe(III)-citrate, Fe(III)-NTA, Fe(III)-pyrophosphate	Solid phase Fe(II), not identified	$Mn(IV)O_2$	0, but tolerant up to 15 %	23-40 (30)	8.5-11 (9)	(Pollock et al. 2007)
Geoalkalibacter ferrihydriticus	Bottom sediments of Lake Khadyn in Tuva, Russia	Acetate with HFO and Fe(III)-EDTA. Pyruvate, oxolate, ethanol, tryptone, arginine, serine, propionate and lactate with Fe(III)-EDTA only	Fe(III)-EDTA, HFO	Siderite or magnetite, depending on growth medium	S^0, $Mn(IV)O_2$	0-3 g L-1 but tolerant up to 50 g L-1	18-39 (35)	7.8-10 (8.6)	(Zavarzina et al. 2006; Chistyakova 2010)
Halomonas SL1	Mono Lake, California, USA	Acetate	Fe(III)-citrate	20 % reduced, not further characterised	Cr(VI), Tc(VII)	Not reported	Not reported	pH 10	(Khijniak et al. 2003; VanEngelen et al. 2008)
Natronincola ferrireducens	Soda Lake Khadyn (Tyva, Russia)	Histidine, peptone	Fe(III)-EDTA, HFO	Iron sesquioxides and magnetite	Fumarate, crotonate, AQDS, Mn(IV)	0-60	Not reported	7.5-10.2 (8.4-8.8)	(T. N. Zhilina et al. 2009)
Natronincola peptidovorans	Soda Lake Verkhnee Beloe (Buryatia, Russia)	Pyruvate, peptone	HFO	Iron sesquioxides and magnetite	AQDS, Mn(IV)	0-70	Not reported	7.5-10.2 (8.4-8.8)	(T. N. Zhilina et al. 2009)

2.5. Radionuclide Biogeochemistry

2.5.1. Uranium biogeochemistry

Uranium exhibits complicated geochemistry and its behaviour is controlled by a combination of complexation, precipitation, redox and adsorption processes. Under oxic conditions soluble uranyl $[UO_2]^{2+}$ species U(VI) dominate but can form a range of insoluble complexes with OH^- and PO_4^{3-} (Langmuir 1997). Uranyl adsorbs strongly onto iron oxides, forming direct mononuclear bidentate inner sphere complexes with ferrihydrite and lepidocrocite (Waite et al. 1994; Dodge et al. 2002). Sorption has been found to decrease in the presence of carbonate (Clark et al. 1995; Zheng et al. 2003) and humic/fulvic acids, especially in combination with Ca^{2+} and/or to a lesser extent, Mg^{2+} (Duff & Amrhein 1996). Iron oxide transformations through dissolution-precipitation reactions coupled to ternary $Ca\text{-}UO_2\text{-}CO_3$ complexes are thought to promote U(VI) incorporation into iron oxides (Stewart et al. 2009). U(VI) incorporation into hematite (Duff et al. 2002; Ilton et al. 2012; Marshall et al. 2014), goethite (Nico et al. 2009; Boland et al. 2011), magnetite (Nico et al. 2009) and a range of iron oxides associated with corroded steel surfaces (Dodge et al. 2002) have all been observed. Additionally, one study has shown the stability of these uranium complexes to oxidative remobilisation (Nico et al. 2009).

Under anoxic conditions, uranium exists as insoluble U(IV) precipitates, predominantly as uraninite (UO_2). U(III) phases are readily oxidised whereas U(V) disproportionates to U(VI) and U(IV). Several studies however have reported metastable U(V) complexes (Docrat et al. 1999; Kerisit et al. 2011; Behrends et al. 2012), where the surrounding carbonate ligands may create electrostatic repulsion, which may hinder the reaction between two U(V) atoms by increasing the activation energy (Kubicki et al. 2009). *Geobacter metallireducens* and *Shewanella putrefaciens* were the first microorganisms found capable of dissimilatory U(VI) reduction coupled to acetate (Equation 2.3) or hydrogen oxidation, forming uraninite (Lovley et al. 1991; Gorby & Lovley 1992). A wide range of prokaryotes are now known to be capable of dissimilatory U(VI) reduction (Williams et al. 2013).

$$CH_3COO^- + 4U(VI) + 4H_2O \rightarrow 4U(IV) + 2HCO_3^- + 9H^+ \quad \Delta G = -447 \text{ kJ mol}^{-1} \qquad (2.3)$$

More recent studies have also suggested that ‘non-uraninite’ U(IV) bioreduction end products can also form in pure culture experiments, and also natural and engineered sediment systems (Bernier-Latmani et al. 2010; Veeramani et al. 2011; Alessi et al. 2012; Bargar et al. 2013; Cerrato et al. 2013). The non-uraninite is thought to be

polymeric and coordinated to carboxyl and/or phosphoryl groups on biomass (Williams et al. 2013).

Although U(VI) and Fe(III) exhibit similar redox potentials, heavy metal toxicity caused by oxidative stress (Hu et al. 2005) limits the number of microorganisms that are capable of dissimilatory U(VI) reduction. Additionally, calcium and carbonate form soluble Ca-U(VI)-CO_3 complexes which have been reported to be less bioavailable for respiration (Clark et al. 1995; Morris 2002; Brooks et al. 2003; Stewart et al. 2010). The mechanisms of U(VI) reduction are not yet resolved but it has been postulated that direct U(VI) reduction occurs by a one electron transfer to form U(V), which disproportionates (Renshaw et al. 2005). Although c-type cytochromes are thought to play a role in U(VI) reduction in *Geobacter* and *Shewanella* species, the proteins which are essential to U(VI) reduction remain unknown and it is likely that multiple electron pathways exist. U(VI) reduction by extracellular protein nanowires (pili) remain highly contested (Cologgi et al. 2011; Orellana et al. 2013).

AQDS has been reported to enhance U(VI) reduction in pure culture and sediment consortia studies (Fredrickson et al. 2000; Ray et al. 2011), potentially through facilitating electron transfer to U(VI) sorbed in enzymatically inaccessible states (Jeon et al. 2004), but was not observed *in situ* (Finneran et al. 2002). Whilst humic acids have been shown to enhance U(VI) reduction by complexing Ca^{2+} and Ni^{2+} in lab scale studies and *in situ*, they also form soluble U(IV) complexes, increasing its susceptibility to oxidative remobilisation (Gu et al. 2005). Additionally, studies with natural OM have shown little effect on U(VI) reduction (Chen et al. 2003). FMN has been shown to enhance U(VI) bioreduction by *Shewanella* species suggesting flavins may also act as an electron transfer mediator (Suzuki et al. 2010). Abiotic U(VI) reduction by Fe(II) in magnetite (Singer et al. 2012a; Singer et al. 2012b) and Fe(II) loaded onto haematite (Zeng & Giammar 2011) and goethite suspensions (Fredrickson et al. 2000) have all been reported. A recent study however has shown that elevated carbonate concentrations inhibit Fe(II)-mediated U(VI) reduction (Fox et al. 2013).

Uranium immobilisation can also occur through biosorption, where basic carboxylic, phosphoric, phosphodiester, amino and hydroxyl groups on bacterial surfaces (Schultze-Lam et al. 1996) can bind with H^+ or metal cations such as UO_2^{2+}. Biosorption depends on several factors, such as groundwater pH, temperature, actinide speciation, (e.g. oxidation state, complexation and aggregation) and bacterial type. Uranium biosorption has been observed in a variety of microorganisms including Gram-negative

Pseudomonas species (Bencheikh-Latmani & Leckie 2003) and Gram-positive Firmicutes such as *Bacillus* species (Merroun et al. 2005). Additionally, bioaccumulation, and biomineralisation with phosphate have been shown to immobilise U(VI) (Macaskie et al. 2000; Suzuki & Banfield 2004; Choudhary & Sar 2011).

Several workers have assessed the stability of U(IV) to reoxidation. Reoxidation by air (O_2) has been shown to reoxidise both fresh (Moon et al. 2007; Law et al. 2011) and aged uraninite (Komlos et al. 2008; Moon et al. 2009) as well as U(IV) associated with iron oxides (Stewart et al. 2009). Additionally, non-uraninite formed in sediments (Sharp et al. 2011) and pure culture (Fletcher et al. 2010) have been shown to be more susceptible to reoxidation, however, recent work has shown little difference with uraninite (Cerrato et al. 2013). Rapid U(VI) reoxidation *in situ* has also been observed, with significant reoxidative remobilisation occurring within minutes (Komlos et al. 2008). Nitrate is a common environmental contaminant and will be present in the nuclear waste of many nations (Jacquot et al. 1997; Albrecht 2013) and workers have shown that products of denitrification (nitrite) can serve as efficient U(IV) oxidisers (Senko et al. 2002; Beller 2005; Moon et al. 2009). A recent study however has shown evidence for U(IV) stability towards nitrate reoxidation in sediments, despite essentially complete Fe(II) reoxidation (Law et al. 2011).

2.5.2. Technetium biogeochemistry

Technetium is an artificial transition metal that can exist in the -I to VII oxidation states, but predominantly occurs as Tc(IV) or Tc(VII) in the environment. In oxic environments, technetium exists as the pertechnetate anion, $[TcO_4]^-$ which is electrostatically repelled by surfaces and this poor attenuation leads to its high mobility, presenting a significant environmental hazard. Moreover, concern regarding its behaviour in the environment is heightened by its uptake by plants and bioaccumulation in animals and marine biota such as lobsters for example (Bennett & Willey 2003; Howard & Beresford 2009; Hunt et al. 2013). Under reducing conditions, insoluble crystalline Tc(IV)O_2 (Lloyd et al. 2000a; Wildung et al. 2004), amorphous polymeric chains of $TcO_2.nH_2O$ (Lukens et al. 2002; Peretyazhko et al. 2008; Peretyazhko et al. 2012;) or Tc(IV) sorbed to sediments (Fredrickson et al. 2004; Burke et al. 2010; Lear et al. 2010) dominate in most natural environments. A recent study has also shown evidence for technetium incorporation into corroded steel surfaces (Heald et al. 2012). Tc(IV) solubility has been reported to increase with high carbonate (Wildung et al. 2000; Zachara et al. 2007), chloride, (Hess et al. 2004) and humic content in waters

(Sekine et al. 1993; Geraedts et al. 2002; Maes et al. 2004; Wildung et al. 2004; Boggs et al. 2011).

Under ambient conditions, microbial reduction of Tc(VII) has been reported by direct enzymatic pathways in strains of *Shewanella* and *Geobacter*, mediated by hydrogenase enzymes (Lloyd et al. 1997; Wildung et al. 2000). Indirect reduction of Tc(VII) by magnetite has also been shown (Lloyd et al. 2000a) and sediment associated Fe(II) (Wildung et al. 2004; Jaisi et al. 2009; Bishop et al. 2011) and Fe(II) bearing minerals in sediments (Wildung et al. 2004; Burke et al. 2005; Begg et al. 2007; Morris et al. 2008; McBeth et al. 2007; Bishop et al. 2011; Geissler et al. 2011; McBeth et al. 2011). The Fe(II) concentration, speciation and coordination environment of the Fe(II) have all been found to influence the rate of Tc(VII) reduction (Fredrickson et al. 2004; Fredrickson et al. 2009; Jaisi et al. 2009). Abiotic coupling of Fe(II) to Tc(VII) is thought to be at a 3:1 ratio, forming TcO_2 (Equation 2.4) or $TcO_2.2H_2O$ (Equation 2.5) (Icenhower et al. 2010).

$$3Fe^{2+}(aq) + TcO_4^-(aq) + 4H^+ \rightarrow TcO_2(s) + 2H_2O + 3Fe^{3+}(aq) \qquad (2.4)$$

$$TcO_4 + 3Fe^{2+} + 9H_2O \rightarrow TcO_2.2H_2O(s) + 3Fe(OH)_3(s) + 5H^+ \qquad (2.5)$$

Several studies have focussed on the stability of Tc(IV) to reoxidation in the presence of air or nitrate. Workers have shown Tc(IV) to be resistant to air reoxidation, with residual technetium thought to be protected (armoured) by structural incorporation into the reoxidised Fe mineral (Morris et al. 2008; Fredrickson et al. 2009; Heald et al. 2012). Technetium has been widely reported to be recalcitrant to reoxidation by nitrate (Burke et al. 2005; Begg et al. 2007; McBeth et al. 2007; Morris et al. 2008; Geissler et al. 2011; McBeth 2011).

2.5.3. Neptunium biogeochemistry

Neptunium is a transuranic element which displays valency between (III) and (VII), but only (IV) to (VI) are stable in the environment. In oxic environments, pentavalent ($Np(V)O_2^+$) species dominate which have a low affinity for surfaces (Kaszuba & Runde 1999). Under reducing conditions, Np(IV) complexes form and are scavenged by surfaces (Kaszuba & Runde 1999). Microbial reduction of Np(V) has been reported by direct enzymatic pathways in strains of *Desulfovibrio vulgaris* (Banaszak et al. 1999), and *Shewanella putrefaciens* (Lloyd et al. 2000b; Icopini et al. 2007), but not by *Geobacter sulfurreducens*, despite being thermodynamically favourable (Renshaw et al. 2005). Reductive coprecipitation with phosphate in *Citrobacter* sp. has also been

reported (Lloyd et al. 2000b). Np(V) reduction by sediment consortia has been observed and thought to occur during early metal (Mn(IV)) reduction (Rittmann et al. 2002; Law et al. 2010). Microbially reduced Np(IV) in these systems exhibited resistance to reoxidation by both air and nitrate (< 20 % remobilised after 40 days) forming a mixed (IV)/(V) phase (Law et al. 2010). Abiotic reduction of Np(V) by sulphide has been reported at neutral pH, with the rate increasing with alkalinity (pH > 10.5) (Nash 1986). Biosorptive processes are also thought to be a significant route of Np(V) immobilisation in the environment and significant (85 %) Np(V) sorption to *Pseudomonas fluorescens* (Songkasiri et al. 2002) and *Shewanella alga* (Deo et al. 2010) under neutral aerobic conditions has been reported, but decreasing with alkalinity and ionic strength (Gorman-Lewis et al. 2013).

2.6. Summary and site overview

2.6.1. Summary

It is policy in the UK that intermediate level radioactive waste will be disposed of by geological disposal. Microbially-mediated metal reduction can influence the migration of radionuclides in the surface and a number of studies have been conducted at circumneutral pH over the last 20 years; however little work to date has studied metal reduction by indigenous microbial communities in alkaline impacted sediments. Little is known about the development of the CDZ which will form post closure of the GDF and the influence on radionuclide transport, so characterising the biogeochemistry and associated mineralogical transformations of redox active metals in these systems will have clear implications for the safety case of a GDF. In this study, model sediments from a legacy lime workings in Buxton, UK have been used. This is an alkaline impacted environment, where microbial populations will have had the potential to equilibrate with the high pH sediment over decades. The site therefore offers a source of microbiologically active materials to study geochemical and mineralogical processes which may occur during the evolution of a cementitious ILW disposal facility.

2.6.2. Overview of the Buxton site

Buxton lies in Derbyshire, UK, on Lower Carboniferous limestone and Upper Carboniferous shale, sandstone and gritstone. Built in 1872, the Hoffman Kiln at Harpur Hill was one of several burning kilns built at this site. Operations ended in 1944, and the kiln chimney was demolished in 1951, followed by the bottom part of the kiln in April 1980. Limestone-roasting produces significant quantities of CaO-rich lime kiln wastes, which were deposited to the west of the kiln. A spoil heap, approximately 200 m long

and 50 m wide was deposited across the valley in location 3 (Figure 8), blocking the path of the stream. Drainage continued to develop and flow beneath the spoil heap, forming a hyperalkaline spring saturated in Ca, Na and K hydroxides, filling the valley with hyperalkaline leachate (pH 11.5-13.5). These Ca^{2+} rich waters have subsequently reacted with atmospheric CO_2, forming calcium carbonate precipitates (Burke et al. 2012).

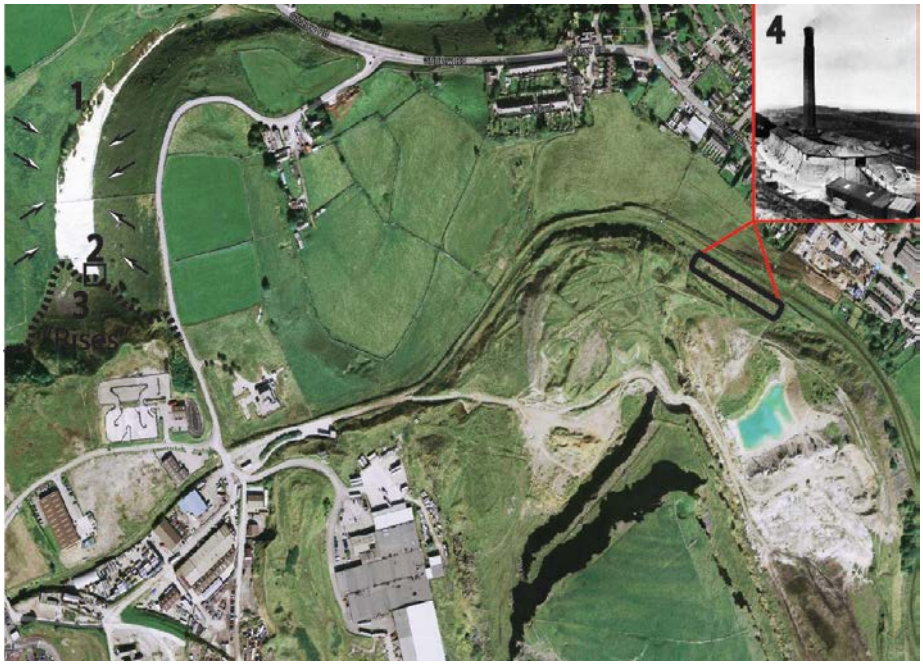

Figure 8: The Buxton site (Google Earth 2014). (1) The waste margin sampling location; (2) hyperalkaline spring; (3) the lime kiln waste deposits (described as “Rises” in OS maps from 1924) and (4) the former Hoffman kiln site (Derbyshire County Council).

Near surface (~10 cm depth) sediments from the waste margin sampling location (Figure 8) are dominated by calcite, with minor quartz and ankerite. The elemental composition is dominated by Ca (51.2 wt %), with significant concentrations of Si (1.1 wt %), Al (0.5 wt %) and Fe (0.17 wt %). The pH of surface waters across the site ranges from pH 10-13 and are dominated by Ca^{2+}, Na^{+} and K^{+} (Table 4).

Table 4: Buxton Harpur Hill surface water major anions and cations.

Cations	**Na^{+}**	**Ca^{2+}**	**Si^{4+}**	**K^{+}**	**Sr^{2+}**	**Ba^{2+}**
Concentration (mg L^{-1})	38.7	270	10.4	58.2	1.0	0.6

Anions	**Cl^{-}**	**NO_3^{-}**	**NO_2^{-}**	**SO_4^{2-}**	**PO_4^{3-}**
Concentration (mg L^{-1})	60.5	31.9	0.2	3.6	0.27

2.7. References

Albrecht, A., 2013. Les réactions redox dans les barrières ouvragées en béton, leur catalyse microbienne et l'impact sur la spéciation des radionucléides: Introduction et état de l'art. *Revue Générale Nucléaire*, 4, 70–83.

Alessi, D.S., Uster, B., Veeramani, H., Suvorova, E.I., Lezama-Pacheco, J.S., Stubbs, J.E., Bargar, J.R. & Bernier-Latmani, R., 2012. Quantitative separation of monomeric U(IV) from UO_2 in products of U(VI) reduction. *Environmental Science & Technology*, 46 (11), 6150–6157.

Alexander, W.R., Milodowski, A. E., Pitty, a. F., Hardie, S.M.L., Kemp, S.J., Korkeakoski, P., Rigas, M., Rushton, J.C., Sellin, P. & Tweed, C.J., 2012. Reaction of bentonite in low-alkali cement leachates: an overview of the Cyprus Natural Analogue Project (CNAP). *Mineralogical Magazine*, 76 (8), 3019–3022.

Aono, R. & Horikoshi, K., 1983. Chemical composition of cell walls of alkaliphilic strains of *Bacillus*. *Journal of General Microbiology*, 129 (4), 1083–1087.

Banaszak, J.E., Rittmann, B.E. & Reed, D.T., 1999. Reduction and precipitation of neptunium(V) by sulfate-reducing bacteria. In *Migration 1999*. Lake Tahoe, NV, 26 September-01 October 1999, pp. 1-11.

Banfield, J.F., Welch, S.A., Zhang, H., Ebert, T.T. & Penn, R.L., 2000. Aggregation-based crystal growth and microstructure development in natural iron oxyhydroxide biomineralization products. *Science*, 289 (5480), 751–754.

Bargar, J.R., Williams, K.H., Campbell, K.M., Long, P.E., Stubbs, J.E., Suvorova, E.I., Lezama-Pacheco, J.S., Alessi, D.S., Stylo, M., Webb, S.M., Davis, J.A., Giammar, D.E., Blue, L.Y. & Bernier-Latmani, R., 2013. Uranium redox transition pathways in acetate-amended sediments. *Proceedings of the National Academy of Sciences of the United States of America*, 110 (12), 4506–4511.

Bayliss, C. & Langley, K., 2003. *Nuclear Decommissioning, Waste Management, and Environmental Site Remediation*. Oxford: Butterworth-Heinemann, p. 330.

Begg, J.D.C., Burke, I.T. & Morris, K., 2007. The behaviour of technetium during microbial reduction in amended soils from Dounreay, UK. *Science of The Total Environment*, 373 (1), 297–304.

Behrends, T., Krawczyk-Bärsch, E. & Arnold, T., 2012. Implementation of microbial processes in the performance assessment of spent nuclear fuel repositories. *Applied Geochemistry*, 27 (2), 453–462.

Beller, H.R., 2005. Anaerobic, nitrate-dependent oxidation of U(IV) oxide minerals by the chemolithoautotrophic bacterium *Thiobacillus denitrificans*. *Applied and Environmental Microbiology*, 71 (4), 2170–4.

Bencheikh-Latmani, R. & Leckie, J.O., 2003. Association of uranyl with the cell wall of *Pseudomonas fluorescens* inhibits metabolism. *Geochimica et Cosmochimica Acta*, 67 (21), 4057–4066.

Bennett, R. & Willey, N., 2003. Soil availability, plant uptake and soil to plant transfer of ^{99}Tc- a review. *Journal of Environmental Radioactivity*, 65 (2), 215-231.

Bernier-Latmani, R., Veeramani, H., Vecchia, E.D., Junier, P., Lezama-Pacheco, J.S., Suvorova, E.I., Sharp, J.O., Wigginton, N.S. & Bargar, J.R., 2010. Non-uraninite products of microbial U(VI) reduction. *Environmental Science & Technology*, 44 (24), 9456–9462.

Bishop, M.E., Dong, H., Kukkadapu, R.K., Liu, C. & Edelmann, R.E., 2011. Bioreduction of Fe-bearing clay minerals and their reactivity toward pertechnetate (Tc-99). *Geochimica et Cosmochimica Acta*, 75 (18), 5229–5246.

Boggs, M.A., Minton, T., Dong, W., Lomasney, S., Islam, M.R., Gu, B. & Wall, N.A., 2011. Interactions of Tc(IV) with humic substances. *Environmental Science & Technology*, 45 (7), 2718–2724.

Boland, D.D., Collins, R.N., Payne, T.E. & Waite, T.D., 2011. Effect of amorphous Fe(III) oxide transformation on the Fe(II)-mediated reduction of U(VI). *Environmental Science & Technology*, 45 (4), 1327–1333.

Boone, D.R., Liu, Y., Zhao, Z.-J., Balkwill, D.L., Drake, G.R., Stevens, T.O. & Aldrich, H.C., 1995. *Bacillus infernus* sp. nov., an Fe(III)- and Mn(IV)-reducing anaerobe from the deep terrestrial subsurface. *International Journal of Systematic Bacteriology*, 45 (3), 441–448.

Brock, T.D., Madigan M.T., Martinko J.M. & Parker, J., 1999. *Biology of Microorganisms*. 7th ed. Englewood Cliffs: Prentice-Hall, p. 909.

Brookins, D., 1988. *Eh-pH Diagrams for Geochemistry*. New York: Springer-Verlag, p. 176.

Brooks, S.C., Fredrickson, J.K., Carroll, S.L., Kennedy, D.W., Zachara, J.M., Plymale, A.E., Kelly, S.D., Kemner, K.M. & Fendorf, S., 2003. Inhibition of bacterial U(VI) reduction by calcium. *Environmental Science & Technology*, 37 (9), 1850–1858.

Bryan, C.R. & Siegel, M.D., 2003. Environmental geochemistry of radioactive contamination, in *Environmental Geochemistry*. Oxford: Elsevier, pp. 205-263

Burke, I.T., Boothman, C., Lloyd, J.R., Mortimer, R.J.G., Livens, F.R. & Morris, K., 2005. Effects of progressive anoxia on the solubility of technetium in sediments. *Environmental Science & Technology*, 39 (11), 4109–4116.

Burke, I.T., Livens, F.R., Lloyd, J.R., Brown, A.P., Law, G.T.W., McBeth, J.M., Ellis, B.L., Lawson, R.S. & Morris, K., 2010. The fate of technetium in reduced estuarine sediments: combining direct and indirect analyses. *Applied Geochemistry*, 25 (2), 233–241.

Burke, I.T., Mortimer, R.J.G., Palaniyandi, S., Whittleston, R.A., Lockwood, C.L., Ashley, D.J. & Stewart, D.I., 2012. Biogeochemical reduction processes in a hyper-alkaline leachate affected soil profile. *Geomicrobiology Journal*, 29 (9), 769–779.

Caccavo Jr., F., Blakemore, R.P. & Lovley, D.R., 1992. A hydrogen-oxidizing, Fe(III)-reducing microorganism from the Great Bay Estuary, New Hampshire. *Applied and Environmental Microbiology*, 58 (10), 3211–3216.

Canfield, D.E. & Raiswell, R., 1998. Sources of iron for pyrite formation in marine sediments. *American Journal of Science*, 298 (3), 219–245.

von Canstein, H., Ogawa, J., Shimizu, S. & Lloyd, J.R., 2008. Secretion of flavins by *Shewanella* species and their role in extracellular electron transfer. *Applied and Environmental Microbiology*, 74 (3), 615–623.

Carlson, H.K., Iavarone, A.T., Gorur, A., Yeo, B.S., Tran, R., Melnyk, R.A., Mathies, R.A., Auer, M. & Coates, J.D., 2012. Surface multiheme c-type cytochromes from *Thermincola potens* and implications for respiratory metal reduction by Gram-positive bacteria. *Proceedings of the National Academy of Sciences of the United States of America*, 109 (5), 1702–1707.

Cerrato, J.M., Ashner, M.N., Alessi, D.S., Lezama-Pacheco, J.S., Bernier-Latmani, R., Bargar, J.R. & Giammar, D.E., 2013. Relative reactivity of biogenic and chemogenic uraninite and biogenic noncrystalline U(IV). *Environmental Science & Technology*, 47 (17), 9756–63.

Chen, J., Gu, B., Royer, R.A. & Burgos, W.D., 2003. The roles of natural organic matter in chemical and microbial reduction of ferric iron. *The Science of The Total Environment*, 307 (1-3), 167–178.

Childers, S.E., Ciufo, S. & Lovley, D.R., 2002. *Geobacter metallireducens* accesses insoluble Fe(III) oxide by chemotaxis. *Nature*, 416 (6882), 767–769.

Chistyakova, 2010. Reduction of amorphous Fe(III)-hydroxide by binary microbial culture, a Mossbauer study. *Hyperfine Interactions*, 197 (1-3), 325-330.

Choudhary, S. & Sar, P., 2011. Uranium biomineralization by a metal resistant *Pseudomonas aeruginosa* strain isolated from contaminated mine waste. *Journal of Hazardous Materials*, 186 (1), 336–343.

Clark, D.L., Hobart, D.E. & Neu, M.P., 1995. Actinide carbonte complexes and their importance in actinide environmental chemistry. *Chemical Reviews*, 95 (1), 25–48.

Cologgi, D.L., Lampa-Pastirk, S., Speers, A.M., Kelly, S.D. & Reguera, G., 2011. Extracellular reduction of uranium via *Geobacter* conductive pili as a protective cellular mechanism. *Proceedings of the National Academy of Sciences of the United States of America*, 108 (37), 15248–15252.

Cornell, R.M. & Schwertmann, U., 2003. *The iron oxides: structure, properties, reactions, occurrences and uses*. 2nd ed. Weinheim: Wiley-VCH, p. 646.

Curtis, G.P. & Reinhard, M., 1994. Reductive dehalogenation of hexachloroethane, carbon tetrachloride, and bromoform by anthrahydroquinone disulfonate and humic acid. *Environmental Science & Technology*, 28 (13), 2393–401.

Cutting, R.S., Coker, V.S., Fellowes, J.W., Lloyd, J.R. & Vaughan, D.J., 2009. Mineralogical and morphological constraints on the reduction of Fe(III) minerals by *Geobacter sulfurreducen*s. *Geochimica et Cosmochimica Acta*, 73 (14), 4004–4022.

Derbyshire County Council. *Picture the past*. Available at http://www.picturethepast.org.uk [Accessed June 03, 2014].

Department for Environment Fisheries and Rural Affairs (DEFRA) & Department for Business Enterprise and Regulatory Reform (BERR) Devolved Welsh Administration for Wales and Northern Ireland, 2008. Managing Radioactive Waste Safely: A Framework for Implementing Geological Disposal, p.100.

Desvaux, M., Dumas, E., Chafsey, I. & Hebraud, M., 2006. Protein cell surface display in Gram-positive bacteria: from single protein to macromolecular protein structure. *FEMS Microbiology Letters*, 256 (1), 1–15.

Dobbin, P.S., Burmeister, L.M.R., Heath, S.L., Powell, A.K., McEwan, A.G. & Richardson, D.J., 1996. The influence of chelating agents upon the dissimilatory reduction of Fe(III) by *Shewanella putrefaciens*. Part 2. Oxo-and hydroxo-bridged polynuclear Fe(III) complexes. *BioMetals*, 9 (3), 291–301.

Dobbin, P.S., Carter, J.P., San Juan, C. G-S., Hobe, M., Powell, A.K. & Richardson, D.J., 1999. Dissimilatory Fe(III) reduction by *Clostridium beijerinckii* isolated from freshwater sediment using Fe(III) maltol enrichment. *FEMS Microbiology Letters*, 176 (1), 131–138.

Docrat, T.I., Mosselmans, J.F.W., Charnock, J.M., Whiteley, M.W., Collison, D., Livens, F.R., Jones, C. & Edmiston, M.J., 1999. X-ray absorption spectroscopy of tricarbonatodioxouranate(V), $[UO_2(CO_3)_3]^{5-}$, in aqueous solution. *Inorganic Chemistry*, 38 (8), 1879–1882.

Dodge, C.J., Francis, A.J., Gillow, J.B., Halada, G.P., Eng, C. & Clayton, C.R., 2002. Association of uranium with iron oxides typically formed on corroding steel surfaces. *Environmental Science & Technology*, 36 (16), 3504–3511.

Drechsel, H. & Jung, G., 1998. Peptide siderophores. *Journal of Peptide Science*, 4 (3), 147–181.

Duff, M.C. & Amrhein, C., 1996. Uranium(VI) adsorption on goethite and soil in carbonate solutions. *Soil Science Society of America Journal*, 60 (5), 1393-1400.

Duff, M.C., Coughlin, J.U. & Hunter, D.B., 2002. Uranium co-precipitation with iron oxide minerals. *Geochimica et Cosmochimica Acta*, 66 (20), 3533–3547.

Ehrlich, H.L., 2008. Are Gram-positive bacteria capable of electron transfer across their cell wall without an externally available electron shuttle? *Geobiology*, 6 (3), 220–224.

Eisenbud, M. & Gesell, T., 1997. *Environmental Radioactivity from Natural, Industrial & Military Sources: From Natural, Industrial and Military Sources*. 4th ed. New York: Academic Press. p. 684.

Finneran, K.T., 2002. Potential for bioremediation of uranium-contaminated aquifers with microbial U(VI) reduction. *Soil & Sediment Contamination*, 11 (3), 339.

Fletcher, K.E., Boyanov, M.I., Thomas, S.H., Wu, Q., Kemner, K.M. & Löffler, F.E., 2010. U(VI) reduction to mononuclear U(IV) by *Desulfitobacterium* species. *Environmental Science & Technology*, 44 (12), 4705–4709.

Fox, P.M., Davis, J.A., Kukkadapu, R., Singer, D.M., Bargar, J. & Williams, K.H., 2014. Abiotic U(VI) Reduction by sorbed Fe(II) on natural sediments. *Geochimica et Cosmochimica Acta*, 117, 266-282.

Fredrickson, J.K., Zachara, J.M., Kennedy, D.W., Duff, M.C., Gorby, Y.A., Li, S.W. & Krupka, K.M., 2000. Reduction of U(VI) in goethite (α-FeOOH) suspensions by a dissimilatory metal-reducing bacterium. *Geochimica et Cosmochimica Acta*, 64 (18), 3085–3098.

Fredrickson, J.K., Zachara, J.M., Kennedy, D.W., Kukkadapu, R.K., McKinley, J.P., Heald, S.M., Liu, C. & Plymale, A.E., 2004. Reduction of TcO_4^- by sediment-associated biogenic Fe(II). *Geochimica et Cosmochimica Acta*, 68 (15), 3171–3187.

Fredrickson, J.K., Zachara, J.M., Plymale, A.E., Heald, S.M., McKinley, J.P., Kennedy, D.W., Liu, C. & Nachimuthu, P., 2009. Oxidative dissolution potential of biogenic and abiogenic TcO_2 in subsurface sediments. *Geochimica et Cosmochimica Acta*, 73 (8), 2299–2313.

Fuller, S.J., McMillan, D.G.G., Renz, M.B., Schmidt, M., Burke, I.T. & Stewart, D.I., 2014. Extracellular electron transport mediated Fe(III) reduction by a community of alkaliphilic bacteria that use flavins as electron shuttles. *Applied and Environmental Microbiology*, 80 (1), 128-137

Gadd, G.M., 2010. Metals, minerals and microbes: geomicrobiology and bioremediation. *Microbiology*, 156 (3), 609–643.

Gavrilov, S.N., Lloyd, J.R., Kostrikina, N.A. & Slobodkin, A.I., 2012. Fe(III) oxide reduction by a Gram-positive thermophile: physiological mechanisms for dissimilatory

reduction of poorly crystalline Fe(III) oxide by a thermophilic Gram-positive bacterium *Carboxydothermus ferrireducens*. *Geomicrobiology Journal*, 29 (9), 804–819.

Geissler, A., Law, G.T.W., Boothman, C., Morris, K., Burke, I.T., Livens, F.R. & Lloyd, J.R., 2011. Microbial communities associated with the oxidation of iron and technetium in bioreduced sediments. *Geomicrobiology Journal*, 28 (5-6), 507–518.

Geraedts, K., Bruggeman, C., Maes, A., Van Loon., L.R., Rossberg, A. & Reich, T., 2002. Evidence for the existence of Tc(IV)-humic substance species by X-ray absorption near-edge spectroscopy. *Radiochimica Acta,* 90 (12), 879-884.

Google Earth 7.1.3. 2014. Hoffman kiln at Harpur Hill 53°14'6.00"N, 1°54'17.57"W. Available at http://www.google.com/earth/index [Accessed June 03 2014].

Gorby, Y., McLean, J., Korenevsky, A., Rosso, K., El-Naggar, M.Y. & Beveridge, T.J., 2008. Redox-reactive membrane vesicles produced by *Shewanella*. *Geobiology*, 6 (3), 232–241.

Gorby, Y.A. et al., 2006. Electrically conductive bacterial nanowires produced by *Shewanella oneidensis* strain MR-1 and other microorganisms. *Proceedings of the National Academy of Sciences of the United States of America*, 103 (30), 11358–11363.

Gorby, Y.A. & Lovley, D.R., 1992. Enzymic uranium precipitation. *Environmental Science & Technology*, 26 (1), 205–207.

Gorlenko, V., Tsapin, A., Namsaraev, Z., Teal, T., Tourova, T., Engler, D., Mielke, R. & Nealson, K., 2004. *Anaerobranca californiensis* sp. nov., an anaerobic, alkalithermophilic, fermentative bacterium isolated from a hot spring on Mono Lake. *International Journal of Systematic and Evolutionary Microbiology*, 54 (3), 739–743.

Gorman-Lewis, D., Jensen, M.P., Harrold, Z.R. & Hertel, M.R., 2013. Complexation of neptunium(V) with *Bacillus subtilis* endospore surfaces and their exudates. *Chemical Geology*, 341, 75–83.

Grant, W.D., Mwatha, W.E. & Jones, B.E., 1990. Alkaliphiles: ecology, diversity and applications. *FEMS Microbiology Letters*, 75 (2-3), 255–269.

Gu, B., Yan, H., Zhou, P., Watson, D.B., Park, M. & Istok, J., 2005. Natural humics impact uranium bioreduction and oxidation. *Environmental Science & Technology*, 39 (14), 5268–5275.

Hansel, C.M., Benner, S.G., Neiss, J., Dohnalkova, A., Kukkadapu, R.K. & Fendorf, S., 2003. Secondary mineralization pathways induced by dissimilatory iron reduction of ferrihydrite under advective flow. *Geochimica et Cosmochimica Acta*, 67 (16), 2977–2992.

Heald, S.M., Krupka, K.M. & Brown, C.F., 2012. Incorporation of pertechnetate and perrhenate into corroded steel surfaces studied by X-ray absorption fine structure spectroscopy. *Radiochimica Acta International Journal for Chemical Aspects of Nuclear Science and Technology*, 100 (4), 243–253.

Hess, N.J., Xia, Y., Rai, D. & Conradson, S.D., 2004. Thermodynamic model for the solubility of $TcO_2 \cdot xH_2O$ (am) in the Aqueous Tc (IV)–Na^+–Cl^-–H^+–OH^-–H_2O system. *Journal of Solution Chemistry*, 33 (2), 199–226.

Horikoshi, K., 1999. Alkaliphiles: some applications of their products for biotechnology. *Microbiology and Molecular Biology Reviews*, 63 (4), 735–750.

Horikoshi, K., 2006. *Alkaliphiles-genetic properties and application of enzymes*. Berlin: Springer-Verlag, p. 270.

Horikoshi, K., Antranikan, G., Bull, A.T., Robb, F.T., Stetter, K.O., 2011. *Extremophiles Handbook.* Japan: Springer-Verlag, p. 240.

Howard, B. & Beresford, N., 2009. Radionuclide transfer to animal products: revised recommended transfer coefficient values. *Journal of Environmental Radioactivity*, 100 (3), 263-273.

Hu, P., Brodie, E.L., Suzuki, Y., McAdams, H.H. & Andersen, G.L., 2005. Whole-genome transcriptional analysis of heavy metal stresses in *Caulobacter crescentus*. *Journal of Bacteriology*, 187 (24), 8437–49.

Hunt, J., Leonard, K. & Hughes, L., 2013. Artificial radionuclides in the Irish Sea from Sellafield: remobilisation revisited. *Journal of Radiological Protection : Official Journal of the Society for Radiological Protection*, 33 (2), 261–79.

Icenhower, J.P., Qafoku, N.P., Zachara, J.M. & Martin, W.J., 2010. The biogeochemistry of technetium: A review of the behavior of an artificial element in the natural environment. *American Journal of Science*, 310 (8), 721–752.

Icopini, G.A., Boukhalfa, H. & Neu, M.P., 2007. Biological reduction of Np(V) and Np(V) citrate by metal-reducing bacteria. *Environmental Science & Technology*, 41 (8), 2764–2769.

Ilton, E.S., Pacheco, J.S.L., Bargar, J.R., Shi, Z., Liu, J., Kovarik, L., Engelhard, M.H. & Felmy, A.R., 2012. Reduction of U(VI) incorporated in the structure of hematite. *Environmental Science & Technology*, 46 (17), 9428–9436.

Istok, J.D., Senko, J.M., Krumholz, L.R., Watson, D., Bogle, M.A., Peacock, A., Chang, Y.J. & White, D.C., 2004. *In situ* bioreduction of technetium and uranium in a nitrate-contaminated aquifer. *Environmental Science & Technology*, 38 (2), 468–475.

Jacquot, F., Libert, M.F., Romero, M.A. & Besnainou, B., 1997. *In vitro* evaluation of microbial effects on bitumen waste form. In J. H. Wolfram, R.D. Rogers and L.G. Gazso, eds. *Microbial Degradation Processes in Radioactive Waste Repository and in Nuclear Fuel Storage Area*s. Netherlands: Springer, pp. 275–283.

Jaisi, D.P., Dong, H., Plymale, A.E., Fredrickson, J.K., Zachara, J.M., Heald, S. & Liu, C., 2009. Reduction and long-term immobilization of technetium by Fe(II) associated with clay mineral nontronite. *Chemical Geology*, 264 (1-4), 127–138.

Jankowitsch, O., 1990. A Code of Practice on the International Transboundary Movement of Radioactive Waste, *IAEA Bulletin*, 32 (4) 28-31.

Jeon, B.-H., Kelly, S.D., Kemner, K.M., Barnett, M.O., Burgos, W.D., Dempsey, B.A. & Roden, E.E., 2004. Microbial reduction of U(VI) at the solid-water interface. *Environmental Science & Technology*, 38 (21), 5649–5655.

Johnston, J.H. & Lewis, D.G., 1983. A detailed study of the transformation of ferrihydrite to hematite in an aqueous medium at 92°C. *Geochimica et Cosmochimica Acta*, 47 (11), 1823–1831.

Jones, B.E., Grant, W.D., Duckworth, A.W. & Owenson, G.G., 1998. Microbial diversity of soda lakes. *Extremophiles*, 2 (3), 191–200.

Kaszuba, J.P. & Runde, W.H., 1999. The aqueous geochemistry of neptunium: dynamic control of soluble concentrations with applications to nuclear waste disposal. *Environmental Science & Technology*, 33 (24), 4427–4433.

Kawashita, M., Tanaka, M., Kokubo, T., Inoue, Y., Yao, T., Hamada, S. & Shinjo, T., 2005. Preparation of ferrimagnetic magnetite microspheres for in situ hyperthermic treatment of cancer. *Biomaterials*, 26 (15), 2231–2238.

Kerisit, S., Felmy, A.R. & Ilton, E.S., 2011. Atomistic simulations of uranium incorporation into iron (hydr)oxides. *Environmental Science & Technology*, 45 (7), 2770–2776.

Khijniak, T. V, Medvedeva-Lyalikova, N.N. & Simonoff, M., 2003. Reduction of pertechnetate by haloalkaliphilic strains of *Halomonas*. *FEMS Microbiology Ecology*, 44 (1), 109–15.

Khoury, H.N., Salameh, E., Clark, I.D., Fritz, P., Bajjali, W., Milodowski, A.E., Cave, M.R. & Alexander, W.R., 1992. A natural analogue of high pH cement pore waters from the Maqarin area of northern Jordan. I: introduction to the site. *Journal of Geochemical Exploration*, 46 (1), 117–132.

Komlos, J., Peacock, A., Kukkadapu, R.K. & Jaffé, P.R., 2008. Long-term dynamics of uranium reduction/reoxidation under low sulfate conditions. *Geochimica et Cosmochimica Acta*, 72 (15), 3603–3615.

Konhauser, K.O., 2009. *Introduction to Geomicrobiology*. Oxford: Blackwell Publishing, p. 425.

Kubicki, J.D., Halada, G.P., Jha, P. & Phillips, B.L., 2009. Quantum mechanical calculation of aqueuous uranium complexes: carbonate, phosphate, organic and biomolecular species. *Chemistry Central Journal*, 3, 1-29.

Langmuir, D., 1997. *Aqueous Environmental Geochemistry*. New Jersey: Prentice Hall, p. 600.

Law, G.T.W., Geissler, A., Burke, I.T., Livens, F.R., Lloyd, J.R., McBeth, J.M. & Morris, K., 2011. Uranium redox cycling in sediment and biomineral systems. *Geomicrobiology Journal*, 28 (5-6), 497–506.

Law, G.T.W., Geissler, A., Lloyd, J.R., Livens, F.R., Boothman, C., Begg, J.D.C., Denecke, M.A., Rothe, J., Dardenne, K., Burke, I.T., Charnock, J.M. & Morris, K., 2010. Geomicrobiological redox cycling of the transuranic element neptunium. *Environmental Science & Technology*, 44 (23), 8924–8929.

Lear, G., McBeth, J.M., Boothman, C., Gunning, D.J., Ellis, B.L., Lawson, R.S., Morris, K., Burke, I.T., Bryan, N.D., Brown, A.P., Livens, F.R. & Lloyd, J.R., 2010. Probing the biogeochemical behavior of technetium using a novel nuclear imaging approach. *Environmental Science & Technology*, 44 (1), 156–62.

Lloyd, J.R., 2003. Microbial reduction of metals and radionuclides. *FEMS Microbiology Reviews*, 27 (2-3), 411–425.

Lloyd, J.R., Cole, J. & Macaskie, L., 1997. Reduction and removal of heptavalent technetium from solution by *Escherichia coli*. *Journal of Bacteriology*, 179 (6), 2014–2021.

Lloyd, J.R. & Macaskie, L.E., 1996. A novel phosphorimager-based technique for monitoring the microbial reduction of technetium. *Applied and Environmental Microbiology*, 62 (2), 578–582.

Lloyd, J.R. & Renshaw, J., 2005. Microbial transformations of radionuclides: fundamental mechanisms and biogeochemical implications. In A. Siegal & R. K. O. Siegal, eds. *Metal Ions in Biological Systems*. New York: M. Dekker, pp. 205–240.

Lloyd, J.R., Sole, V.A., Van Praagh, C.V.G. & Lovley, D.R., 2000a. Direct and Fe(II)-mediated reduction of technetium by Fe(III)-reducing bacteria. *Applied and Environmental Microbiology*, 66 (9), 3743–3749.

Lloyd, J.R., Yong, P. & Macaskie, L.E., 2000b. Biological reduction and removal of Np(V) by two microorganisms. *Environmental Science & Technology*, 34 (7), 1297–1301.

Lovley, D.R., 1995. Bioremediation of organic and metal contaminants with dissimilatory metal reduction. *Journal of Industrial Microbiology & Biotechnology*, 14 (2), 85–93.

Lovley, D.R., 1991. Dissimilatory Fe(III) and Mn(IV) reduction. *Microbiological Reviews*, 55 (2), 259–87.

Lovley, D.R., 2012. Electromicrobiology. *Annual Review of Microbiology*, 66 (1), 391-409.

Lovley, D.R., Coates, J.D., Blunt-Harris, E.L., Phillips, E.J.P. & Woodward, J.C., 1996. Humic substances as electron acceptors for microbial respiration. *Nature*, 382 (6590), 445–448.

Lovley, D.R., Fraga, J.L., Coates, J.D. & Blunt-Harris, E.L., 1999. Humics as an electron donor for anaerobic respiration. *Environmental Microbiology*, 1 (1), 89–98.

Lovley, D.R., Giovannoni, S.J., White, D.C., Champine, J.E., Phillips, E.J.P., Gorby, Y.A. & Goodwin, S., 1993. *Geobacter metallireducens*; gen. nov. sp. nov., a microorganism capable of coupling the complete oxidation of organic compounds to the reduction of iron and other metals. *Archives of Microbiology*, 159 (4), 336–344.

Lovley, D.R., Holmes, D.E., Nevin, K.P. & Poole, 2004. Dissimilatory Fe(III) and Mn(IV) reduction. In R. K. Poole, ed, *Advances in Microbial Physiology Vol. 49*. London: Elsevier Academic, pp. 219–286.

Lovley, D.R., Phillips, E.J.P., Gorby, Y.A. & Landa, E.R., 1991. Microbial reduction of uranium. *Nature*, 350 (6317), 413–416.

Lovley, D.R., Stolz, J.F., Nord, G.L. & Phillips, E.J.P., 1987. Anaerobic production of magnetite by a dissimilatory iron-reducing microorganism. *Nature*, 330 (6145), 252–254.

Lovley, D.R. & Woodward, J.C., 1996. Mechanisms for chelator stimulation of microbial Fe(III)-oxide reduction. *Chemical Geology*, 132 (1-4), 19–24.

Lukens, W.W., Bucher, J.I., Edelstein, N.M. & Shuh, D.K., 2002. Products of pertechnetate radiolysis in highly alkaline solution: structure of $TcO_2.xH_2O$. *Environmental Science & Technology*, 36 (5), 1124–9.

Macaskie, L.E., Bonthrone, K.M., Yong, P. & Goddard, D.T., 2000. Enzymically mediated bioprecipitation of uranium by a *Citrobacter* sp.: a concerted role for exocellular lipopolysaccharide and associated phosphatase in biomineral formation. *Microbiology*, 146 (8), 1855–1867.

Maes A., Geraedts, K, Bruggeman, C, , Vancluysen J., Rossberg, A Reich & T, 2004. Evidence for the interaction of technetium colloids with humic substances by X-ray absorption spectroscopy. *Envrionmental Science & Technology*, 38 (7), 2044-2051.

Marshall, T.A., Morris, K., Law, G.T.W., Livens, F.R., Mosselmans, J.F.W., Bots, P. & Shaw, S., 2014. Incorporation of uranium into hematite during crystallization from ferrihydrite. *Environmental Science & Technology*, 48 (7), 3724–3731.

Marsili, E., Baron, D.B., Shikhare, I.D., Coursolle, D., Gralnick, J.A. & Bond, D.R., 2008. *Shewanella* secretes flavins that mediate extracellular electron transfer. *Proceedings of the National Academy of Sciences of Sciences of the United States of America*, 105 (10), 3968–3973.

McBeth, J.M., Lear, G., Lloyd, J.R., Livens, F.R., Morris, K. & Burke, I.T., 2007. Technetium reduction and reoxidation in aquifer sediments. *Geomicrobiology Journal*, 24 (3-4), 189–197.

McBeth, J.M., Lloyd, J.R., Law, G. T. W., Livens, F. R., Burke, I. T., & Morris, K., 2011. Redox interactions of technetium with iron-bearing minerals. *Mineralogical Magazine*, 75 (4), 2419–2430.

Merroun, M.L., Raff, J., Rossberg, A., Hennig, C., Reich, T. & Selenska-Pobell, S., 2005. Complexation of uranium by cells and S-layer sheets of *Bacillus sphaericus* JG-A12. *Applied and Environmental Microbiology*, 71 (9), 5532–43.

Miller, W., Alexander, R. & Chapman, N., 2000. *Geological Disposal of Radioactive Wastes and Natural Analogues.* Oxford: Pergamon, p. 328.

Mills, A.L., Bell, P.E. & Herman, J.S., 1987. Biogeochemical conditions favoring magnetite formation during anaerobic iron reduction. *Applied and Environmental Microbiology*, 53 (11), 2610–2616.

Moon, H.S., Komlos, J. & Jaffé, P.R., 2009. Biogenic U(IV) oxidation by dissolved oxygen and nitrate in sediment after prolonged U(VI)/Fe(III)/SO_4^{2-} reduction. *Journal of Contaminant Hydrology*, 105 (1–2), 18–27.

Moon, H.S., Komlos, J. & Jaffé, P.R., 2007. Uranium reoxidation in previously bioreduced sediment by dissolved oxygen and nitrate. *Environmental Science & Technology*, 41 (13), 4587–4592.

Morris, D.E., 2002. Redox energetics and kinetics of uranyl coordination complexes in aqueous solution. *Inorganic Chemistry*, 41 (13), 3542–3547.

Morris, K., Law, G.T.W. & Bryan, N.D., 2011. Chapter 6: Geodisposal of Higher Activity Wastes. In R. Harrison, ed, *Issues in Environmental Science and Technology*. Royal Society of Chemistry, pp. 129–151.

Morris, K., Livens, F.R., Charnock, J.M., Burke, I.T., McBeth, J.M., Begg, J.D.C., Boothman, C. & Lloyd, J.R., 2008. An X-ray absorption study of the fate of technetium in reduced and reoxidised sediments and mineral phases. *Applied Geochemistry*, 23 (4), 603–617.

Myers, C.R. & Nealson, K.H., 1988. Bacterial manganese reduction and growth with manganese oxide as the sole electron acceptor. *Science*, 240 (4857), 1319–1321.

NDA, 2014. *The 2013 UK Radioactive Waste and Materials Inventory: Waste Quantities from all Sources*, NDA, Cumbria, p. 17.

Nealson, K, H., Myers & C, R., 1992. Microbial reduction of manganese and iron: new approaches to carbon cycling. *Applied and Environmental Microbiology.*, 58 (2), 439-443.

Nevin, K.P. & Lovley, D.R., 2000. Potential for nonenzymatic reduction of Fe(III) via electron shuttling in subsurface sediments. *Environmental Science & Technology*, 34 (12), 2472–2478.

Newman, D.K. & Kolter, R., 2000. A role for excreted quinones in extracellular electron transfer. *Nature*, 405 (6782), 94–97.

Newsome, L., Morris, K. & Lloyd, J.R., 2014. The biogeochemistry and bioremediation of uranium and other priority radionuclides. *Chemical Geology*, 363 (0), 164–184.

Nico, P.S., Stewart, B.D. & Fendorf, S., 2009. Incorporation of oxidized uranium into Fe (hydr)oxides during Fe(II) catalyzed remineralization. *Environmental Science & Technology*, 43 (19), 7391–7396.

Nirex, 2003. *Generic Post-closure Performance Assessment*, *Nirex Report*, Didcot, Oxforshire, p. 153.

Orellana, R., Leavitt, J.J., Comolli, L.R., Csencsits, R., Janot, N., Flanagan, K.A., Gray, A.S., Leang, C., Izallalen, M., Mester, T. & Lovley, D.R., 2013. U(VI) reduction by diverse outer surface c-type cytochromes of *Geobacter sulfurreducens*. *Applied and Environmental Microbiology*, 79 (20), 6369–74.

Pattrick, R.A.D., Van Der Laan, G., Henderson, C.M.B., Kuiper, P., Dudzik, E. & Vaughan, D.J., 2002. Cation site occupancy in spinel ferrites studied by X-ray magnetic circular dichroism: developing a method for mineralogists. *European Journal of Mineralogy*, 14 (6), 1095–1102.

Pedersen, K., Nilsson, E., Arlinger, J., Hallbeck, L. & O'Neill, A., 2004. Distribution, diversity and activity of microorganisms in the hyper-alkaline spring waters of Maqarin in Jordan. *Extremophiles*, 8 (2), 151–164.

Peretyazhko, T., Zachara, J.M., Heald, S.M., Jeon, B.-H., Kukkadapu, R.K., Liu, C., Moore, D. & Resch, C.T., 2008. Heterogeneous reduction of Tc(VII) by Fe(II) at the solid–water interface. *Geochimica et Cosmochimica Acta*, 72 (6), 1521–1539.

Peretyazhko, T.S., Zachara, J.M., Kukkadapu, R.K., Heald, S.M., Kutnyakov, I. V, Resch, C.T., Arey, B.W., Wang, C.M., Kovarik, L., Phillips, J.L. & Moore, D.A., 2012. Pertechnetate (TcO_4^-) reduction by reactive ferrous iron forms in naturally anoxic, redox transition zone sediments from the Hanford Site, USA. *Geochimica et Cosmochimica Acta*, 92 (0), 48–66.

Pollock, J., Weber, K., Lack, J., Achenbach, L., Mormile, M. & Coates, J., 2007. Alkaline iron(III) reduction by a novel alkaliphilic, halotolerant, *Bacillus* sp. isolated from salt flat sediments of Soap Lake. *Applied Microbiology and Biotechnology*, 77 (4), 927–934.

Prowe, S.G. & Antranikian, G., 2001. *Anaerobranca gottschalkii* sp. nov., a novel thermoalkaliphilic bacterium that grows anaerobically at high pH and temperature. *International Journal of Systematic and Evolutionary Microbiology*, 51 (Pt 2), 457–65.

Ray, A.E., Bargar, J.R., Sivaswamy, V., Dohnalkova, A.C., Fujita, Y., Peyton, B.M. & Magnuson, T.S., 2011. Evidence for multiple modes of uranium immobilization by an anaerobic bacterium. *Geochimica et Cosmochimica Acta*, 75 (10), 2684–2695.

Reeburgh, W.S. & Henrichs, S.M., 1987. Anaerobic mineralization of marine sediment organic-matter - rates and the role of anaerobic processes in the oceanic carbon economy. *Geomicrobiology Journal*, 5 (3-4), 191–237.

Reguera, G., McCarthy, K.D., Mehta, T., Nicoll, J.S., Tuominen, M.T. & Lovley, D.R., 2005. Extracellular electron transfer via microbial nanowires. *Nature*, 435 (7045), 1098–1101.

Renshaw, J.C., Butchins, L.J.C., Livens, F.R., May, I., Charnock, J.M. & Lloyd, J.R., 2005. Bioreduction of uranium: environmental implications of a pentavalent intermediate. *Environmental Science & Technology*, 39(15), 5657–60.

Renshaw, J.C., Lloyd, J.R. & Livens, F.R., 2007. Microbial interactions with actinides and long-lived fission products. *Comptes Rendus Chimie*, 10, 1067–1077.

Rittmann, B.E., Banaszak, J.E. & Reed, D.T., 2002. Reduction of Np(V) and precipitation of Np(IV) by an anaerobic microbial consortium. *Biodegradation*, 13 (5), 329–342.

Rizoulis, A., Steele, H.M., Morris, K. & Lloyd, J.R., 2012. The potential impact of anaerobic microbial metabolism during the geological disposal of intermediate-level waste. *Mineralogical Magazine*, 76 (8), 3261–3270.

Roden, E.E., Kappler, A., Bauer, I., Jiang, J., Paul, A., Stoesser, R., Konishi, H. & Xu, H., 2010. Extracellular electron transfer through microbial reduction of solid-phase humic substances. *Nature Geoscience*, 3 (6), 417–421.

Roh, Y., Chon, C.-M. & Moon, J.-W., 2007. Metal reduction and biomineralization by an alkaliphilic metal-reducing bacterium, *Alkaliphilus metalliredigens* (QYMF). *Geosciences Journal*, 11 (4), 415–423.

Schröder, I., Johnson, E. & De Vries, S., 2003. Microbial ferric iron reductases. *FEMS Microbiology Reviews*, 27 (2-3), 427–447.

Schultze-Lam, S., Fortin, D., Davis, B.S. & Beveridge, T.J., 1996. Mineralization of bacterial surfaces. *Chemical Geology*, 132 (1–4), 171–181.

Schwertmann, U., Friedl, J. & Stanjek, H., 1998. From Fe(III) ions to ferrihydrite and then to hematite. *Journal of Colloid and Interface Science*, 209 (1), 215–223.

Schwertmann, U. & Murad, E., 1983. Effect of pH on the formation of goethite and hematite from ferrihydrite. *Clays and Clay Minerals*, 31 (4), 277–284.

Scott, D.T., McKnight, D.M., Blunt-Harris, E.L., Kolesar, S.E. & Lovley, D.R., 1998. Quinone moieties act as electron acceptors in the reduction of humic substances by humics-reducing microorganisms. *Environmental Science & Technology*, 32 (19), 2984–2989.

Sekine, T., Watanabe, A., Yoshihara, K. & Kim, J., 1993. Complexation of technetium with humic acid. *Radiochimica Acta*, 63, 87-90.

Senko, J.M., Istok, J.D., Suflita, J.M. & Krumholz, L.R., 2002. In-situ evidence for uranium immobilization and remobilization. *Environmental Science & Technology*, 36 (7), 1491–1496.

Sharp, J.O., Lezama-Pacheco, J.S., Schofield, E.J., Junier, P., Ulrich, K.-U., Chinni, S., Veeramani, H., Margot-Roquier, C., Webb, S.M., Tebo, B.M., Giammar, D.E., Bargar, J.R. & Bernier-Latmani, R., 2011. Uranium speciation and stability after reductive immobilization in aquifer sediments. *Geochimica et Cosmochimica Acta*, 75 (21), 6497–6510.

Singer, D.M., Chatman, S.M., Ilton, E.S., Rosso, K.M., Banfield, J.F. & Waychunas, G.A., 2012a. Identification of simultaneous U(VI) sorption complexes and U(IV) nanoprecipitates on the magnetite (111) surface. *Environmental Science & Technology*, 46 (7), 3811–3820.

Singer, D.M., Chatman, S.M., Ilton, E.S., Rosso, K.M., Banfield, J.F. & Waychunas, G.A., 2012b. U (VI) sorption and reduction kinetics on the magnetite (111) surface. *Environmental Science & Technology*, 46 (7), 3821–3830.

Songkasiri, W., Reed, D.T. & Rittmann, B.E., 2002. Bio-sorption of neptunium (V) by *Pseudomonas fluorescens*. *Radiochimica Acta*, 90 (9/11), 785–789.

Stevenson, F.J., 1994. *Humus Chemistry: Genesis, Composition, Reactions*. Sussex: John Wiley & Sons, p. 496.

Stewart, B.D., Mayes, M.A. & Fendorf, S., 2010. Impact of Uranyl− calcium− carbonato complexes on uranium(VI) adsorption to synthetic and natural sediments. *Environmental Science & Technology*, 44 (3), 928–934.

Stewart, B.D., Nico, P.S. & Fendorf, S., 2009. Stability of uranium incorporated into Fe (hydr)oxides under fluctuating redox conditions. *Environmental Science & Technology*, 43 (13), 4922–7.

Suzuki, Y. & Banfield, J., 2004. Resistance to, and accumulation of, uranium by bacteria from a uranium-contaminated site. *Geomicrobiology Journal*, 21 (2) 113-121.

Suzuki, Y., Kitatsuji, Y., Ohnuki, T. & Tsujimura, S., 2010. Flavin mononucleotide mediated electron pathway for microbial U(VI) reduction. *Physical Chemistry Chemical Physics*, 12 (34),10081–10087.

Switzer Blum, J., Burns Bindi, A., Buzzelli, J., Stolz, J.F. & Oremland, R.S., 1998. *Bacillus arsenicoselenatis*, sp. nov., and *Bacillus selenitireducens*, sp. nov.: two haloalkaliphiles from Mono Lake, California that respire oxyanions of selenium and arsenic. *Archives of Microbiology*, 171 (1), 19–30.

Taylor, D.M., 1989. The biodistribution and toxicity of plutonium, americium and neptunium. *Science of The Total Environment*, 83 (3), 217–225.

Torrent, J., Guzman, R. & Parra, M.A., 1982. Influence of relative humidity on the crystallization of Fe(III) oxides from ferrihydrite. *Clays and Clay Minerals*, 30 (5), 337–340.

VanEngelen, M.R., Peyton, B.M., Mormile, M.R. & Pinkart, H.C., 2008. Fe(III), Cr(VI), and Fe(III) mediated Cr(VI) reduction in alkaline media using a *Halomonas* isolate from Soap Lake, Washington. *Biodegradation*, 19 (6), 841–50.

Veeramani, H., Alessi, D.S., Suvorova, E.I., Lezama-Pacheco, J.S., Stubbs, J.E., Sharp, J.O., Dippon, U., Kappler, A., Bargar, J.R. & Bernier-Latmani, R., 2011. Products of abiotic U(VI) reduction by biogenic magnetite and vivianite. *Geochimica et Cosmochimica Acta*, 75 (9), 2512–2528.

Waite, T.D., Davis, J.A., Payne, T.E., Waychunas, G.A. & Xu, N., 1994. Uranium(VI) adsorption to ferrihydrite: application of a surface complexation model. *Geochimica et Cosmochimica Acta*, 58 (24), 5465–5478.

Whittleston, R.A., Stewart, D.I., Mortimer, R.J.G., Tilt, Z.C., Brown, A.P., Geraki, K. & Burke, I.T., 2011. Chromate reduction in Fe(II)-containing soil affected by hyperalkaline leachate from chromite ore processing residue. *Journal of Hazardous Materials*, 194 (0), 15–23.

Wieland, E., Dähn, R., Gaona, X., Macé, N. & Tits, J., 2013. Micro- and Macroscopic Investigations of Actinide Binding in Cementitious Materials. In F. Bart, C. Cau-di-Coumes, F. Frizon and S. Lorente, eds, *Cement-Based Materials for Nuclear Waste Storage*. New York: Springer, pp. 93–101.

Wildung, R.E., Gorby, Y.A., Krupka, K.M., Hess, N.J., Li, S.W., Plymale, A.E., McKinley, J.P. & Fredrickson, J.K., 2000. Effect of electron donor and solution chemistry on products of dissimilatory reduction of technetium by *Shewanella putrefaciens*. *Applied and Envionmental Microbiology*, 66 (6), 2451-2460.

Wildung, R.E., Li, S.W., Murray, C.J., Krupka, K.M., Xie, Y., Hess, N.J. & Roden, E.E., 2004. Technetium reduction in sediments of a shallow aquifer exhibiting dissimilatory iron reduction potential. *FEMS Microbiology Ecology*, 49 (1), 151–162.

Williams, K.H., Bargar, J.R., Lloyd, J.R. & Lovley, D.R., 2013. Bioremediation of uranium-contaminated groundwater: a systems approach to subsurface biogeochemistry. *Current Opinion in Biotechnology*, 24 (3), 489–497.

World Nuclear Association. Available at: http://www.world-nuclear.org [Accessed May 22, 2014].

Wrighton, K.C., Thrash, J.C., Melnyk, R. a, Bigi, J.P., Byrne-Bailey, K.G., Remis, J.P., Schichnes, D., Auer, M., Chang, C.J. & Coates, J.D., 2011. Evidence for direct electron transfer by a Gram-positive bacterium isolated from a microbial fuel cell. *Applied and Environmental Microbiology*, 77 (21), 7633–9.

Ye, Q., Roh, Y., Carroll, S.L., Blair, B., Zhou, J., Zhang, C.L. & Fields, M.W., 2004. Alkaline anaerobic respiration: isolation and characterization of a novel alkaliphilic and metal-reducing bacterium. *Applied and Environmental Microbiology*, 70 (9), 5595–5602.

Zachara, J.M., Heald, S.M., Jeon, B.-H., Kukkadapu, R.K., Liu, C., McKinley, J.P., Dohnalkova, A.C. & Moore, D.A., 2007. Reduction of pertechnetate [Tc(VII)] by aqueous Fe(II) and the nature of solid phase redox products. *Geochimica et Cosmochimica Acta*, 71 (9), 2137–2157.

Zavarzina, D., Kolganova, T., Boulygina, E., Kostrikina, N., Tourova, T. & Zavarzin, G., 2006. *Geoalkalibacter ferrihydriticus* gen. nov. sp. nov., the first alkaliphilic representative of the family *Geobacteraceae*, isolated from a soda lake. *Microbiology*, 75 (6), 673–682.

Zavarzina, D.G., Tourova, T.P., Kolganova, T. V., Boulygina, E.S. & Zhilina, T.N., 2009. Description of *Anaerobacillus alkalilacustre* gen. nov., sp. nov.—Strictly anaerobic diazotrophic bacillus isolated from soda lake and transfer of *Bacillus arseniciselenatis*, *Bacillus macyae*, and *Bacillus alkalidiazotrophicus* to *Anaerobacillus* as the new combinations *A. arseniciselenatis* comb. nov., *A. macyae* comb. nov., and *A. alkalidiazotrphicus* comb. nov.. *Microbiology*, 78 (6), 723–731.

Zeng, H. & Giammar, D., 2011. U(VI) reduction by Fe(II) on hematite nanoparticles. *Journal of Nanoparticle Research*, 13 (9), 3741–3754.

Zheng, Z., Tokunaga, T.K. & Wan, J., 2003. Influence of calcium carbonate on U(VI) sorption to soils. *Environmental Science & Technology*, 37 (24), 5603–5608.

Zhilina, T., Zavarzina, D., Kolganova, T., Lysenko, A. & Tourova, T., 2009. *Alkaliphilus peptidofermentans*; sp. nov., a new alkaliphilic bacterial soda lake isolate capable of peptide fermentation and Fe(III) reduction. *Microbiology*, 78 (4), 445–454.

Zhilina, T.N., Zavarzina, D.G., Osipov, G.A., Kostrikina, N.A. & Tourova, T.P., 2009. *Natronincola ferrireducens* sp. nov., and *Natronincola peptidovorans* sp. nov., new anaerobic alkaliphilic peptolytic iron-reducing bacteria isolated from soda lakes. *Microbiology*, 78 (4), 455–467.

3

Materials and Methods

3. Materials and Methods

A series of geochemical, mineralogical, microbiological and radiological techniques have been used to characterise biogeochemical processes in the experiments in this project. This chapter will focus on the theoretical aspects of each technique, whereas experimental details are given in Chapters 4-7.

3.1. Geochemical analyses

3.1.1. pH

The pH scale is a measure of acidity or basicity of a solution. It is the negative logarithm of the solvated hydronium ion (Equation 3.1).

$$pH = -\log_{10}[H^+] \qquad (3.1)$$

The microcosms in the experiments in the study were established at pH 10.5, however microbial activity in all anoxic (especially electron donor amended) incubations lead to the production of organic acids which acidified the sample. To combat this, in selected experiments, manual injections of 2 M NaOH held the pH at 10.

3.1.2. E_h (the reduction potential)

A measure of the tendency of a chemical species to gain (become reduced) or lose (become oxidised) electrons or hydrogen. A solution with a low reduction potential suggests that one species is gaining electrons from a reducing agent (which in turn becomes oxidised). Several factors can limit its interpretation, including temperature, pH, the presence of multiple redox couples and inert redox couples. Due to these set-backs it is a useful qualitative analytical tool to monitor changes in a reaction rather than quantitative absolute data values.

3.2. Spectrophotometry (UV-vis)

If a monochromatic wave of light of initial intensity (I_0) is shone through an aqueous sample, a portion will pass through (I) and the ratio I/I_0 is known as the transmittance (T). The remainder will be attained (absorbed, A) by the sample (Figure 1; Equation 3.2)

$$A = \log_{10} 1/T \qquad (3.2)$$

The amount of absorption will depend on the concentration of the absorbing species (c, mol l^{-1}), the path length (b, cm) through the sample (i.e. the width of the cuvette the sample is in) and a measure of how strongly the chemical species absorbs light (the

molar absorptivity (extinction) coefficient, ε (l mol^{-1} cm^{-1})). The relationship between the light absorbed, the thickness of the sample and the concentration of the sample is generally linear and is based upon the Beer-Lambert Law (Figure 1; Equation 3.3).

$$A=\varepsilon bc \qquad (3.3)$$

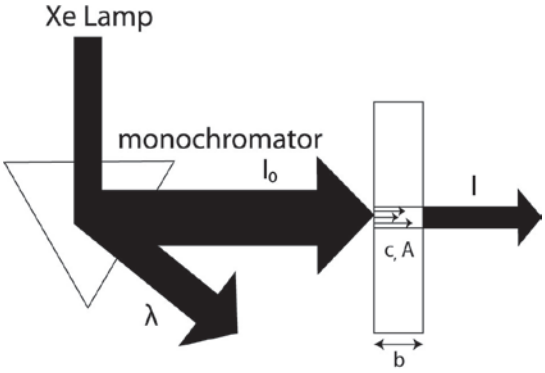

Figure 1: Simplified schematic of a spectrophotometer.

This linear relationship has been shown to break down with increasing concentration and through instrument performance limitations (primarily stray (unwanted) light from the diffraction gratings of the monochromator). If samples exceed the upper absorbance limit of the spectrophotometer, they can be serially diluted, or a shorter path length cell can be used. Linearity can also be affected occasionally by fluorescence, pH (which can shift the absorption wavelength of some chromophores) and sample turbidity (Upstone, 2000).

Cuvettes are often glass (transmit light > 320 nm) or quartz (transmits light well below 190 nm, which is the usual low level wavelength limit for most photospectrometers). Alternatively, many manufacturers produce disposable cuvettes, which are generally used in laboratories and have been used for all the experiments in this thesis. UV-vis spectroscopy was also used to check the Np spike purity prior to addition into microcosm experiments. Quartz vials were used for this as these cells have a wider wavelength range, a higher optical performance and more accurate cell path length (Upstone 2000). UV-vis spectroscopy was obtained on a Jenway 6715 spectrometer at the selected wavelength for the species to be determined and the measured absorbance for each sample were compared to matrix matched calibration standards of known concentrations and typically, calibration regressions had $R^2 > 0.99$. The path length is defined as the cuvette width which typically is 1 cm (and was consistent throughout this project). The following colorimetric assays have been used in this study:

3.2.1. Determination of Fe(II): the ferrozine method

Ferrozine is a disodium salt of 3-(2-pyridyl)-5,6-bis(4-phenysulfonic acid)-1,2,4-triazine and forms a stable soluble magenta complex with ferrous iron (complete complexation occurs between pH 4 and 9). Fe(II) complexes with the bidentate ligand –N=C-C=N-, known as the ferroin group (Figure 2) and absorbs visible light at 562 nm with ε of 27,900. The Beer-Lambert Law is obeyed to approximately 4 mg L^{-1} of Fe (Stookey 1970).

Figure 2: Structure of ferrozine. The ferroin group is highlighted in red.

In order to determine Fe(II) concentration in sediments, a 1 hour extraction of 20 µl slurried sample into 980 µl 0.5 N HCl is required, as this was deemed a valid approximation of the bioavailable fraction of iron to microorganisms (Lovley & Phillips 1987). The digest was centrifuged at a relative centrifugal force (RCF) of 12, 500 *g* for 5 minutes and then 50 µl of the supernatant was added to 2.45 ml ferrozine solution (ferrozine (1 g L^{-1}) and HEPES buffer (11.96 g L^{-1}) adjusted to pH 7) and mixed thoroughly, before measuring absorbance at 562 nm (for concentrations between 1 mM and 50 mM). In order to determine Fe(II) concentration for no added ferrihydrite systems in this study, 200 ul of sample or standard was added to 2.3 ml of ferrozine and adjusted to pH 4-9 with 2 M NaOH.

To determine the total bioavailable Fe(III) fraction, typically 20 µl slurried sample and 40 µl of 6.25 N hydroxylamine hydrochloride (a strong reducing agent) was digested into 940 µl of 0.5 N HCl for 1 hour. The same method as Fe(II) determination was then used. Additionally, a total iron digest was achieved using aqua regia (1:3 ratio of conc HNO_3: conc HCl), but Fe (aq) concentrations here was measured using ICP-AES (section 3.4.1.).

3.2.2. Determination of U(VI): the bromo-PADAP method

Bromo-PADAP (2-(5-bromo-2-pyridylazo)-5-diethylaminophenol) was derived from PADAP as a sensitive and species specific method for U(VI) determination. When a U(VI) containing sample is mixed with a Bromo-PADAP ethanolic solution (0.5 g L^{-1}),

the uranyl-bromo-PADAP complex that forms in the organic phase has an ε of 74,000 at 578 nm. In the presence of a mixed complexing solution (containing 1,2-cyclohexylenedinitrilio) tetraacetic acid (CyDTA) (26.3 g L^{-1}), sulphosalicyclic acid (65 g L^{-1}) and 0.5 g NaF (5 g L^{-1})), only Cr(III), V(V) and PO_4^{3-} interfere significantly (e.g. 1 g of phosphate causes only a ~ 7 % error) (Johnson & Florence 1971). The solution is buffered to 7.85 (for optimum absorption) using a solution of triethanolamine (149 g L^{-1}), adjusted to pH 7.85 using 9.2 M $HClO_4$ (Johnson & Florence 1971; Wielinga et al. 2000)

3.3. Ion chromatography (IC)

IC is a commonly used technique which involves the separation and quantification of ions (analytes) based on their charge in solution at ppm concentrations. Its popularity has arisen from its efficiency (cost and time) and accuracy (less interferences) over other geochemical methods such as colorimetric assays. There are two forces acting upon an analyte on the IC column, the ability of the mobile phase (known as the eluent) to take the analyte through the column and the ability of the stationary phase (the column) to sorb the analytes (Small 1989). The speed in which an ion passes through the column depends on its size and charge, i.e. stronger interactions with the stationary phase slow elution. Several factors influence the selectivity of the column, including the support material and the chemical structure of the ion exchange group. The selectivity is thus due to the interaction of the column and the ion properties, charge (monovalent/multivalent), hydrated radii and the ability of the ion to contribute or disrupt the hydrogen bonding of the surrounding water (SeQuant 2007).

Guard columns are used to protect the column from dissolved metal contaminants, particulates or biomass. A suppressor removes background conductivity from the mobile phase before the eluent and analyte ions reach the detector and increase the analyte ion signal. As the eluent passes through the detector, different ions give separate peaks and using matched matrix standards, these peaks can be quantified. Ion exclusion chromatography allows fine separation of the organics in the system, but cannot separate inorganic anions. During ion exchange, all of the anionic analytes are attracted to the column and then washed off sequentially by the eluent.

Eluents can be aqueous, water containing only or a strong electrolyte. The ionic strength, pH, temperature, flow rate and choice of buffer salt of the eluent all affect anion retention on the separation column. The choice of eluent is dependent on elution strength, separation efficiency and the resolution of the analytes of interest (Dionex

1998). Organic solvents (e.g. methanol or acetonitrile) can provide important selective control during ion exchange separations but can only be used in conjunction with an organic solvent compatible column. As they are non-conductive they do not interact with the conductivity detection.

Carbonate eluents are traditionally used for anion separation as it allow the proportions of monovalent (HCO_3^-) and divalent (CO_3^{2-}) ions to be adjusted to optimise retention time and selectivity between monovalent and multivalent anions (SeQuant 2007). It is supressed to carbonic acid, hence some background conductivity is observed. Hydroxide eluents are advantageous as it is neutralised in the suppressor to water and hence gives very low background conductivity. A CO_2 trap is used to protect the eluent from CO_2 absorption, which can increase background conductivity (SeQuant 2007). For cation exchange, dilute strong acids, (e.g. 1 mM HNO_3) are the best eluents. They are often mixed with organic solvents and are good eluents for monovalent and divalent cations (e.g. octane sulfonic acid (OSA)).

Conductivity detection is the most commonly used mode of detection in IC and was employed by all the IC systems used in this thesis. Conductivity detection is best for anions (e.g. chloride, nitrate, phosphate and sulphate) and cations (e.g. sodium and potassium) of strong acids and bases, with pKa < 6. Most transition metal cations are not detected as they either hydrolyse in water to form anions or precipitate in the suppressor (Dionex 1998).

Table 1: Specifications for the IC systems used in this thesis.

Chapter	**4** (Organic acids)	**4** (Anion/cation)	**5-7**
Technique	Ion exclusion	Ion exchange	Capillary ion exchange
System	DIONEX D120	BioLC	DIONEX ICS5000
Sample loading onto sample loop	50 µl by an AS auto sampler	50 µl by an AS auto sampler	0.4 µl by an AS-AP auto sampler
Guard column	ICE-AS1	IonPAC AS11-HC guard column	AS11-HC capillary (0.4 um)
Column	none	IonPAC AS11-HC	IonPAC AS11-HC capillary (0.4 um)
Eluent	Isocratic with 1 mM OSA	NaOH gradient (created by a quaternary pump)	KOH gradient (1-40 mM, electronically generated)
Flow rate (ml min^{-1})	0.5	1	0.015
Suppressed conductivity	100 mM TBAOH	AS-RS electronic suppressor	AS-RS electronic suppressor
Detection limit	~100 ppb	~100 ppb	~10 ppb
Reference	(Dionex 1998)	(Dionex 2006)	(Dionex 2012)

The advantage of using the Dionex ICS5000 system is that it runs with higher precision (detection limit of ~10 ppb) and allows inorganic anions and organic acids concentration to be determined in a single run. Additionally, due to low sample injections (0.4 µl), negligible waste is created, making it suitable for radioactive samples. For all experiments, samples were centrifuged at a RCF of 12, 500 g in a microcentrifuge for 5 minutes to separate biomass and sample particulates and then diluted to the correct limits of detection for analytes (typically 0.5 mg L^{-1} for organic acids and 0.05 mg L^{-1} for nitrate, nitrite and sulfate) into IC vials. For radionuclide experiments, samples were diluted below 0.4 Bq ml^{-1}) prior to analysis for radiological safety considerations.

3.4. Inductively coupled plasma (ICP)

3.4.1. Inductively coupled plasma-atomic emission spectroscopy (ICP-AES)

ICP-AES is an analytical technique for trace metal concentration determination (Figure 3). In this thesis, a Perkin Elmer Optima 5300 dual view ICP-AES was used. The dissolved sample is delivered to a nebuliser by a periplasmic pump where it is converted into an aerosol and is passed through to the argon ICP torch, which creates an intense electromagnetic field which creates high T (7000 K) plasma (Jarvis et al. 1992; Gill 1997). The sample aerosols pass through the plasma, where the analyte atoms are energised and emit photons of energy characteristic to that element. The echelle grating resolves the incident light into its component wavelengths and these are diffracted accurately onto specific pixels on a charged coupled device (CCD). The CCD multipliers are mounted behind secondary (exit) slits and aligned to measure specific wavelengths (spectral lines for each element).

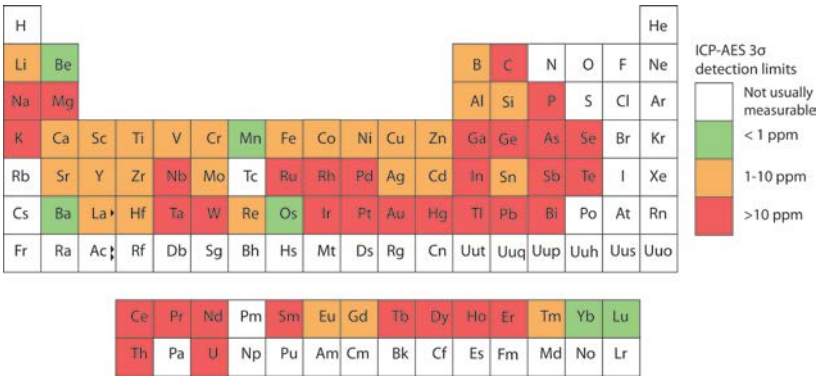

Figure 3: Periodic table showing elements that can be detected by ICP-AES, with their working detection limits, adapted from (Gill 1997).

3.4.2. Inductively coupled plasma- mass spectroscopy (ICP-MS)

One of the great advantages of ICP-MS is the extremely low detection limits for a wide range of elements (most at the ppt level) (Figure 4). In this thesis, an Agilent 7500cx ICP-MS was used. Unlike AES, ICP-MS must operate under high vacuum so that ions are free to move without colliding with air molecules (Gill 1997). It has a differentially pumped interface region which transmits the supersonic jet of ions from the atmospheric pressure plasma into the mass spectrometer (Jarvis et al. 1992; Gill 1997). Two conical nickel apertures are used, the sampling cone and the skimmer, which allow ions to pass into the MS but deflect away a majority of uncharged molecules and atoms (Gill 1997). A collision cell is placed in the ion beam path and prevents light reaching the ion detector and thus removes background interferences, giving a higher resolution.

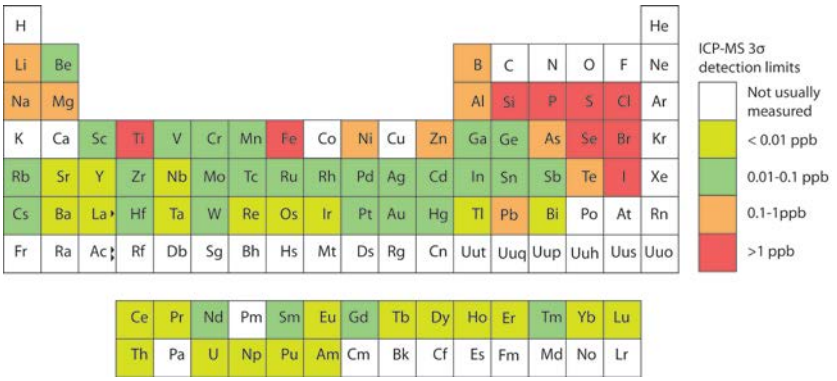

Figure 4: Periodic table showing elements that can be detected by ICP-MS, with their working detection limits, adapted from (Gill 1997).

3.5. Electron microscopy

3.5.1. Transmission electron microscopy (TEM)

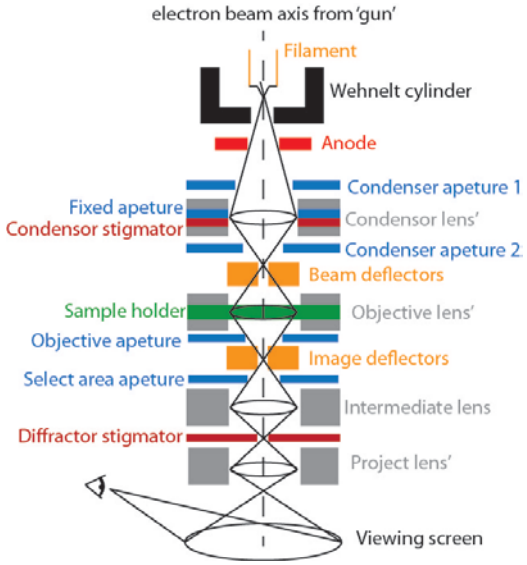

Figure 5: Schematic of a TEM, adapted from (Williams & Carter 1996).

TEM was carried out using a Philips CM 200 electron microscope at the Leeds Electron Microscopy and Spectroscopy (LEMAS) Centre, University of Leeds, UK. The microscope was equipped with a field emission gun, which emits electrons up to 200 kV into the vacuum which is subsequently manipulated by electromagnets, creating a distribution of magnetic flux and forms a magnetic lens. Electrostatic fields can cause the electrons to be deflected through a constant angle. Apertures are placed in the TEM to remove diffracted electrons and the objective aperture is important for image contrast (Figure 5). These diffracted electrons contribute to dark areas on the image, The absorption and transmission of electrons through the sample give rise to the contrast in the sample image, which is magnified and focussed onto the Gatan imaging filter (GIF200) with a 1k x 1k CCD camera mounted below the viewing chamber, with energy resolution of 0.9 eV and 1 nm spatial resolution. As electrons have a small de Broglie wavelength we can obtain a much higher resolution than a light microscope. This extreme magnification is useful for the identification of nanoparticles such as magnetite, however, it is difficult to determine the surrounding environment and therefore this technique is more useful in conjunction with other mineralogical analyses. TEM imaging has no depth sensitivity and the data is averaged through the thickness of the specimen (projection-limitation) and the thinning process for sample preparation (usually require ~ 50 nm) can cause structural and chemical changes (Williams & Carter 1996). Due to high acceleration voltages, TEM may also cause electron beam damage to the specimen of interest, particularly polymers, most organics, and a number of minerals (Williams & Carter 1996).

3.5.2. Select area electron diffraction (SAED)

Adjusting the intermediate lens and removing the objective aperture (which allows the electron beam to pass through) so that the back focal plane of the lens (rather than the imaging plane) is placed on the imaging apparatus allows a diffraction pattern to be generated on a small area. Introducing the selected area aperture limits electron diffraction to the sample area only (Figure 5+6). SAED occurs due to electron beam diffraction by crystal lattice planes, similar to X-ray diffraction (XRD) (section 3.6.4.) and can give structural characteristics of samples up to 1 μm. A single wavelength of electrons can see many diffracted beams, whereas in XRD, the crystal has to be rotated to see all the beams (Williams & Carter 1996). Dots indicate crystalline material and rings suggest the material is polycrystalline or an amorphous solid (Williams & Carter 1996).

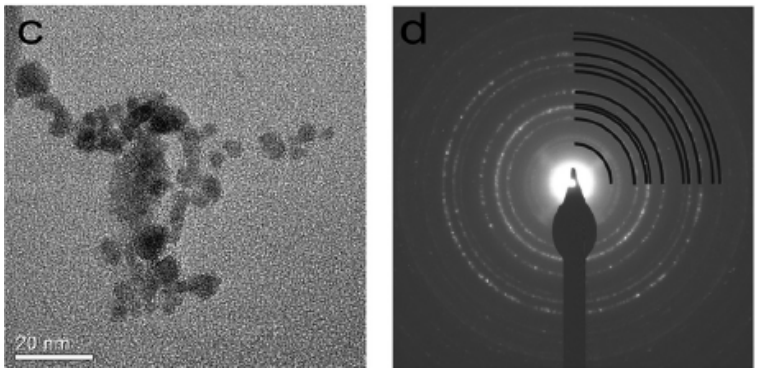

Figure 6: TEM image of magnetite and its corresponding SAED (taken from Chapter 4).

3.5.3. Energy dispersive X-ray spectroscopy (EDX)

The TEM was also equipped with an EDX detector (Oxford instruments, ISIS software). EDX is an analytical technique to determine elemental composition of a sample. The incident electron beam excites ground state electrons of elements to an excited state. When the electron relaxes to the ground state it releases an X-ray photon with a wavelength characteristic of that element, forming an EDX spectrum (Figure 7).

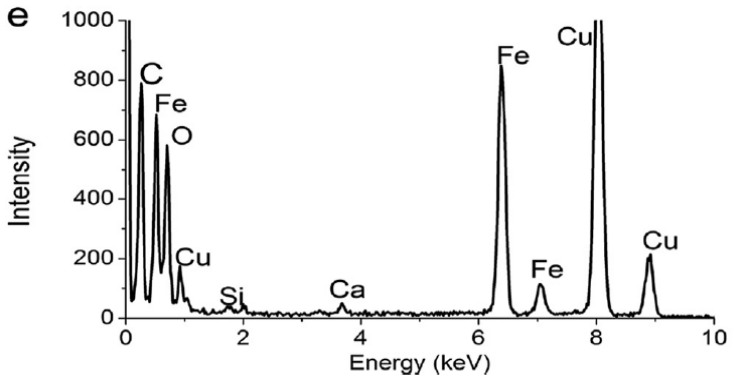

Figure 7: EDX spectra taken on nanocrystalline magnetite (taken from Chapter 4).

3.6. X-ray techniques

3.6.1. X-ray absorption spectroscopy (XAS)

XAS is a technique used in mineralogical and biological systems to identify the oxidation state and coordination of a target element. In this study, XAS was used to characterise Fe, U, Tc and Np in oxic, reduced and reoxidised samples on the magnetic spectroscopy beamline 4.0.2 at the Advanced Light Source (ALS), Lawrence Berkeley National Laboratory, Berkeley, CA, USA (Fe), Diamond Light Source B18, UK (U and Tc) (Dent et al. 2009) and the INE-Beamline at ANKA, Germany (Np) (Rothe et al. 2012). Here, an overview of the theory behind XAS is given; the specific sample

preparation and data analysis for these experiments are given in the corresponding research papers.

XAS is a largely non-destructive and non-invasive technique and is advantageous over other mineralogical techniques such as XRD as it allows analysis on both crystalline and amorphous solids and solutions. Other advantages include fast data collection (beneficial for *in situ* chemical processes), the ability for data collection at extreme temperatures and pressure and the fact that only small sample volumes and relatively low concentrations of analyte are needed (Newville 2004). As the detector takes an average environment around the element of interest however, mixed phases can be challenging to interpret, as it only provides averaged interatomic distances and cannot distinguish between backscattering atoms with similar atomic number. Interatomic distances are accurate to ± 0.02 Å and coordination numbers to ± 25 % for inner coordination shells, with larger errors for outer shells or very noisy data.

When an X-ray (an electromagnetic wave (λ 0.01 to 10 nm (0.1 to 100 KeV)) hits matter, some is transmitted through and a fraction is absorbed. A portion of X-rays are also scattered back by Compton scatter (scatter with a loss of energy) or Raleigh scatter (scatter without a loss of energy). The amount of scatter depends on thickness, density and composition of the material and the energy of the X-ray.

X-ray absorption is reported as the absorption coefficient (μ) which gives the probability that an X-ray will be absorbed (Equation 3.5), based on the Beer-Lambert Law (Equation 3.4). I_0 represents the incident X-ray intensity and I is the intensity transmittted through the sample of thickness (t). The absorption coefficient is dependent on the sample density (ρ), the atomic number (Z), the atomic mass (A) and the X-ray energy (E).

$$I = I_0 e^{-\mu t} \qquad (3.4)$$

$$\mu(E) \approx \frac{\rho Z^4}{AE^3} \qquad (3.5)$$

If the incident X-ray is of lower energy than the electron binding energy, the electron is excited into a higher energy state but does not leave the atom. When the incident X-ray energy is larger than the binding energy, the electron is ejected as a photoelectron with kinetic energy (the difference between the incident X-ray and the binding energy of the electron, $E\text{-}E_0$) as a spherical sine wave (where $\lambda \sim 1/(E\text{-}E_0)^{1/2}$), leaving a core hole (Figure 8). This is observed as a sharp increase in absorption, known as the absorption edge, and corresponds to the absorbing atoms characteristic ionisation energy (E_0: the

energy at which the X-ray energy overcomes the binding energy of a core electron) of a 1s (where n=1 represents the K edge, e.g. Tc) or 2p (where n=2 represents the $L_{(III)}$ edge for e.g. U, Np) electron. Outer electrons can drop into the core hole, with the emission of a fluorescent X-ray with characteristic energy (Figure 8).

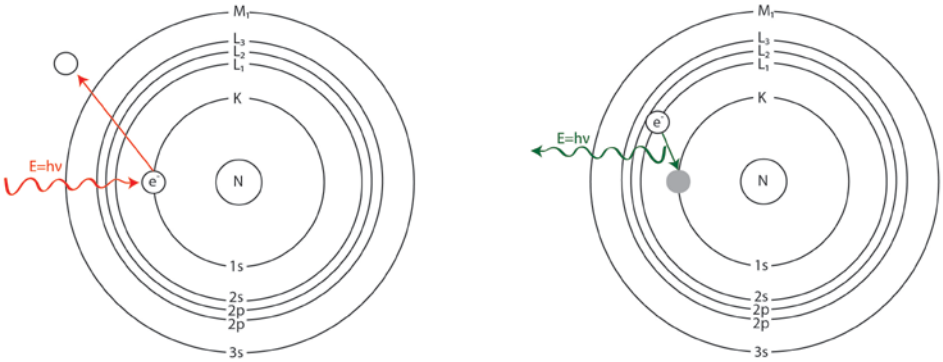

Figure 8**:** An X-ray interacting with an absorbing atom.

XAS can be collected in transmission or fluorescence, usually depending on the nature of the sample (priamrily due to the concentration of the central scatterer of interest). In this study, all samples were collected in fluorescence mode, apart from the schoepite (U(VI)) and pertechnetate (Tc(VII)) standards, which were collected in transmission mode.

To record a transmission spectrum, the photon intensity is measured at a specfic energy in front of (I_0 (X-ray intensity)) and behind (I_1 (tranmission intensity)) the sample, which can be converted to $\mu(E)$ (Figure 9; Equation 3.6) (Denecke 2006). A reference channel is placed upstream and the absorption is also measured simultaneously for energy calibration (For the reference absorption, $I_0 = I_1$ and $I_1=I_2$). In this study, the K edge of Y (E_0 of 17.038 keV) was used for actinide L_{III} edges U and Np.

$$\mu(E) = \ln[\frac{I_0(E)}{I_1(E)}] \qquad (3.6)$$

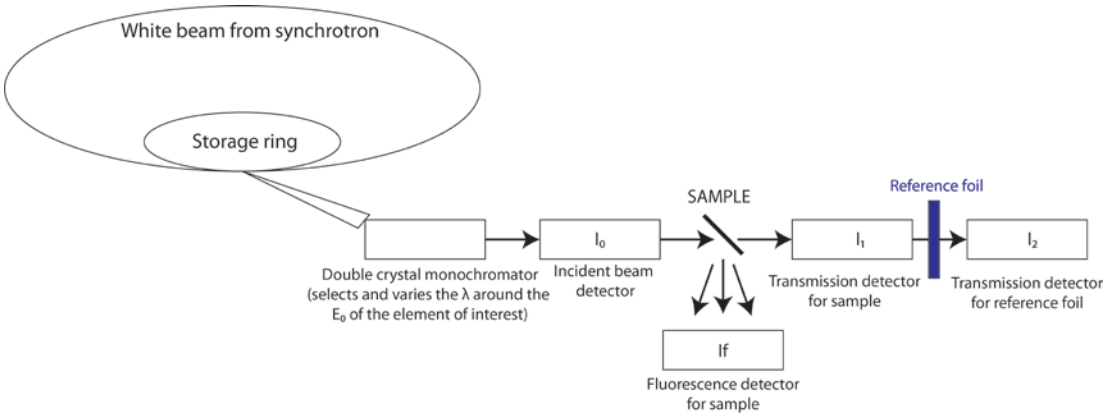

Figure 9: Simple beam schematic, adapted from (Denecke 2006; Charnock 1995).

In fluorescence mode, the sample is rotated 45 ° to the incident beam direction to minimise elastic and Compton scattering radiation noise on the detector. It is used on dilute samples (actinide concentration generally <1 %) which are totally absorbing or impermeable for X-rays, such as sediment samples. The advantage of this technique is that it is surface specific, however, it is less useful for aqueous or wet samples.

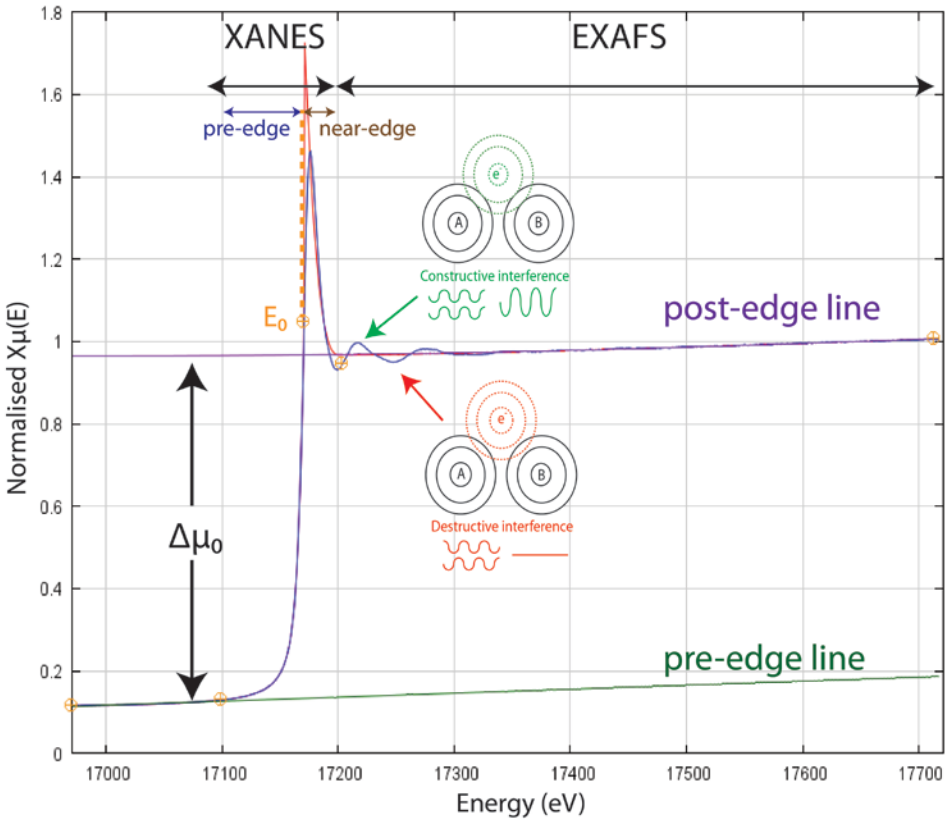

Figure 10: Uranium L_{III} edge XAS spectrum (taken from Chapter 5) with the origin of EXAFS oscillations from constructive and destructive interference of neighbouring atoms (A and B) with outgoing photoelectron (e^-).

The X-ray near edge structure (XANES) region can be divided into 2 parts, the pre-edge and the near-edge region (Figure 10). The pre-edge is below the absorption edge (at E below E_0) and involve transitions from core level to the lowest partially unoccupied level (e.g. 1s to 3d in Fe, or 4d in Tc) (Newville 2004). L edge actinides such as U and Np however show no pre-edge structure (Newville 2004). A common application of XANES is to determine the valence state by the shift in edge position (Newville 2004). The peak intensity is sensitive to oxidation state and site symmetry and the edge position changes with the charge on the absorbing atom, i.e. energy increases with positive charge. The structure in the near-edge region (at E_0 50-100 eV above the edge) is produced by ionisation of a core electron to a delocalised energy band, or complete

ejection of the electron from the structure. The interference of electron waves produce the edge structure and this is effected by site geometry and neighbouring atoms. Fingerprinting technique can be used to compare unknown with model compounds and linear combination fitting of XANES to standard compounds can provide quantitative and phase specific information, which allows the approximate proportion of each standard in the sample to be determined.

The extended X-ray fine structure (EXAFS) spectra are at the high energy end of the absorption edge (up to 1000 eV past the edge) (Figure 10). The outgoing photoelectron is emitted as a spherical wave; if the absorbing atom is isolated then the wave will escape freely and no EXAFS structure will be observed. If the atom is incorporated in matter however, it can be elastically scattered by neighbouring atoms. EXAFS interferences can be constructive (lead to a maxima in the EXAFS oscillations) or destructive interference (lead to a minima) (Figure 10). In highly symmetrical coordination environments, the electron wave can interact with several scatterers, which give multiple scatterer effects. The EXAFS is the summation of several of these sine waves from *n* coordination shells.

To isolate the EXAFS oscillations, the energy axis is converted to photoelectron (wave) vector (k) values, which is proportional to the square of the difference between the X-ray energy and E_0 (Equation 3.7) (Denecke 2006). m_e is the mass of an electron and $\hbar = h/2\pi$ (where h is the Planck's constant). The difference between the incident X-ray energy (E) and the energy of the most prominent feature in the XANES (commonly known as the white line, E_0) is the kinetic energy of the emitted photelectron (E_{kin}).

$$k = \sqrt{\frac{2m_e(E-E_0)}{\hbar^2}} \qquad (3.7)$$

The next step in EXAFS data reduction is the background subtraction of pre-edge (to remove instrumental background and absoprtion from other edges) and post-edge (which represents the photoelectron from an isolated atom (which has no structure) and approximates $\mu_0(E)$) regions (Figure 10). The threshold energy (E_0) is identified as the maximum derivative of $\mu(E)$. The data is then normalised between 0 and 1, to represent the absorption of one X-ray. This allows the EXAFS fine structure function (X(E)) to be expressed as the change in the absorption coefficient (μ) by scattering on neighbouring atoms (Equation 3.8). $\mu(E)$ is the measured absorption coefficient, $\mu_0(E)$ is a smooth background function representing the absorption of an isolated atom and $\Delta\mu_0$ is the measured jump in the absorption at the threshold energy E_0.

$$\chi(E) = \frac{\mu(E)-\mu_0(E)}{\Delta\mu_0(E)} \qquad (3.8)$$

The EXAFS ($\chi(k)$) is comprised of oscillations as a function of the photoelectron wave number, proportional to the amplitude of the scattered photoelectron at the absorbing atom and decays quickly with k. To emphasise the oscillations, $\chi(k)$is usually multiplied by a power of k (k^2 or k^3). By fitting the experimental data to the EXAFS equation (Equation 3.9), the coordination structure of the absorbing atom can be obtained (Denecke 2006).

$$\chi(k) = \frac{S_0^2}{k} l^{-1} \sum_{j=1}^{n} N_j \left|f_j(k,\pi)\right| \frac{e^{-2R_j/\lambda(k)}}{R_j^2} e^{-2k^2\sigma^2} \times \sin\left[2kR_j + \Phi_j(k,R)\right] \quad (3.9)$$

The sum in the EXAFS equation is over each coordination shell j, up to the nth cordination shell and generally up to distances of 5 Å. S_0^2 is the amplitude reduction factor, l is the angular momentum quantum number, and $\frac{e^{-2R_j/\lambda(k)}}{R_j^2}$ accounts for the energy loss of a photoelectron (where λ = mean free path of photoelectron) with distance from the central scatterrer atom (inelastic scattering).There are 5 terms in the EXAFS equation that are unknown. The amplitude of the EXAFS is proportional to N_j, which is the number of scattering atoms of element at distance R_j from the target atom (coordination number). $\left|f_j(k,\pi)\right|$ is the amplitude of backscattering by atom j. $e^{-2k^2\sigma^2}$ is the Debye-Waller factor term, which is the dampening factor on the outgoing sine wave and σ^2 is the Debye-Waller factor, a measure of the oscillation of the absorber-scatterer distance around the mean value for a pair of atoms. The two forces which affect σ^2 are dynamic disorder (mean distance and atomic vibrations by thermal motion) and static disorder (due to differences in absorber-scatter distance in a single shell of interest- scatterers in the same shell with the same R would result in low σ^2, however as more scatterers vary in difference in that shell, σ^2 increases). The Debye-Waller factor can therefore be improved by cooling the sample with a cryostat (however static disorder still exists). The phase term $\left[2kR_j + \Phi_j(k,R)\right]$ represents the wave nature of the photoelectron and accounts for phase shifts that occur during scattering. As $\Phi_j(k,R)$ and f(k) are dependent on the backscatterer we can identify elements which comprise a coordination shell. It is only possible to differentiate between atoms which significantly differ in atomic number however and Z+1 atoms (e.g. C and N) cannot be distinguished.

Performing a Fourier transform from the wave (k) space to the real (R) spaces gives a 1D radial distribution function showing shells of scatterers (i.e. groups of scatterers at

similar distance) around the absorber atom. The Fourier transform peaks appear at distances shorted than the real value due to the Φ(k,R) phase shift (which is typically ~ 0.5 Å shorter). The functions f(k) and the phase shift Φ(k,R) can be theoretically calculated by the FEFF code (named after the $f_{eff}(k)$ notation for the effective curved wave scattering amplitude). In this study, EXCURV98 (Binsted 1998) was used for U experiments and ARTEMIS (Ravel & Newville 2005) was used in Tc and Np experiments to calculate f(k) and Φ(k,R) and by refining parameters in the model (n, r and σ^2) as well as E_f (Fermi energy, an energy correction factor). These software packages allow the user to build a theoretical model of distribution of scatterers around the central atom to to minimise the least squares residual, giving the best fit to the experimental data X(k).

The EXAFS least squared residual gives a meaningful indication of the quality of the fit to the EXAFS data in k-space. Combining this with the standard deviation during averaging of experimental spectra (σ_i) allows the R factor to be defined, where χ_i^{exp} is the experimental EXAFS and χ_i^{th} is the theoretical model (Equation 3.10).

$$R\ factor = \sum_i^N \frac{1}{\sigma_i}\left(\left|\chi_i^{exp}(k) - \chi_i^{th}(k)\right|\right) x\ 100\% \qquad (3.10)$$

An absolute index of goodness of fit is given by the reduced chi squared (ε_v^2) function (Equation 3.11) (Binsted et al. 1992). To calculate this, the number of independent points (N_{ind}) (Equation 3.12) and number of parameters (N_{pars}) need to be quantified to determine the number of degrees of freedom (N_{ind}-N_{pars}) (Binsted et al. 1992). N represents the number of data points, K_{min} and K_{max} is the data range being fitted and r_{min} and r_{max} indicate the range in the r-space actually being fitted (not just where the structure is apparent). A refinement that gives $N_{ind}/N_{par} < 1$ cannot be justified as it suggests that less than one observation accounts for each parameter.

$$\varepsilon_v^2 = \frac{1}{(N_{ind}-N_{par})}\left(\frac{N_{ind}}{N}\right)\sum_i^N \frac{1}{\sigma_i^2}\left(\chi_i^{exp}(k_i) - \chi_i^{th}(k_i)\right)^2 \quad (3.11)$$

$$N_{ind} = \frac{2(r_{max}-r_{min})(k_{max}-k_{min})}{\pi} \qquad (3.12)$$

In this thesis, shells of backscattering atoms were only accepted if there was a > 5 % decrease in the R factor and a significant reduction in ε_v^2.

3.6.2. X-ray magnetic circular dichroism (XMCD)

In this study, XMCD was used to identify the presence and properties of magnetite produced in sediment microcosms. The XMCD is derived from XAS at the Fe $L_{II/III}$

edge. At the $L_{II,III}$ edge, 2p electrons (L) are excited into (partially) localised unoccupied 3d (M) states. Fe $L_{II,III}$ edge XAS data were collected in magnetic fields set to parallel and antiparallel to the helicity vector of the X-rays (± 0.6 T), which is set along the beam direction. XMCD is the difference between the two XAS profiles. The measured Fe $L_{II/III}$ XMCD was used to obtain the Fe cation site occupancies in the spinel structure of magnetite using QFit (Coker et al. 2006).

XMCD provides information regarding the local electronic and magnetic structure of the absorbing atoms in the material (Pattrick et al. 2002). The magnetic properties of magnetite is derived from the Fe^{2+} O_h magnetic contribution after the two sub lattices, T_d and O_h Fe(III), which have anti-parallel magnetic moments, cancel. The XMCD spectrum of magnetite consists of 3 main components, characteristic of magnetite: Fe(II) O_h (d^6), Fe(III) T_d (d^5) and Fe(III) O_h (d^6). The sign of the magnetic dichroism for each component is given by the direction of its magnetic moment: O_h sites are arranged ferromagnetically and T_d sites are antiferromagnetically to these (Figure 11). Fe(II) ions are shifted to the left of this spectrum due to Coulomb interactions of core valence electrons (van der Laan and Thole, 1991). The XMCD spectrum changes, depending upon magnetisation, site location and valence state (number of *d* electrons).

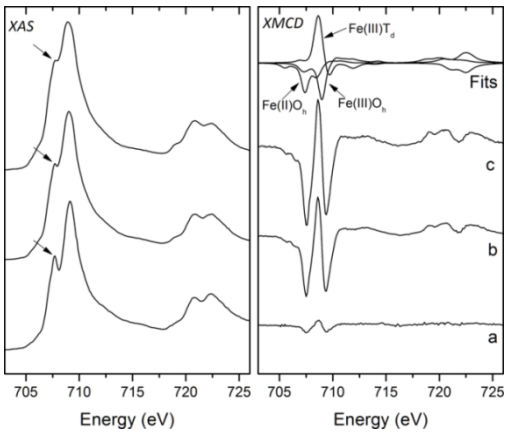

Figure 11: Fe $L_{II,III}$ edge XAS and XMCD (taken from Chapter 4).

Atomic multiplet calculations were calculated using QFit (Coker et al. 2006) and were fitted to the XMCD to quantify the site occupancies of Fe cations with the crystalline material (i.e. Fe(II) and Fe(III) in octahedral (O_h) and tetrahedral coordination (T_d)) (van der Laan & Thole 1991; van der Laan & Kirkman 1992; Thole et al. 1992).

3.6.3. X-ray fluorescence (XRF)

XRF is a near surface, non-destructive method to determine chemical composition of a sample. The principal behind XRF is similar to the photoelectron emission described in

the previous section. XRF on the Buxton sediments used in this thesis was achieved with an Axios Sequential XRF Spectrometer (PANalytical 2014). It is a wavelength dispersive system (WDXRF), which has a high resolution (typically 5-20 eV) and minimal spectral overlaps and can determine Be to U concentration in the range from sub ppm levels to 100 %. Elements with higher atomic numbers have a better detection limit than lighter elements (Figure 12). This is due to the increasing likelihood of auger electron emission, where the excess energy from an electron from a higher atomic orbital relaxing back to fill a lower orbital may be transmitted to a second electron, which in turn can be excited to a higher orbital.

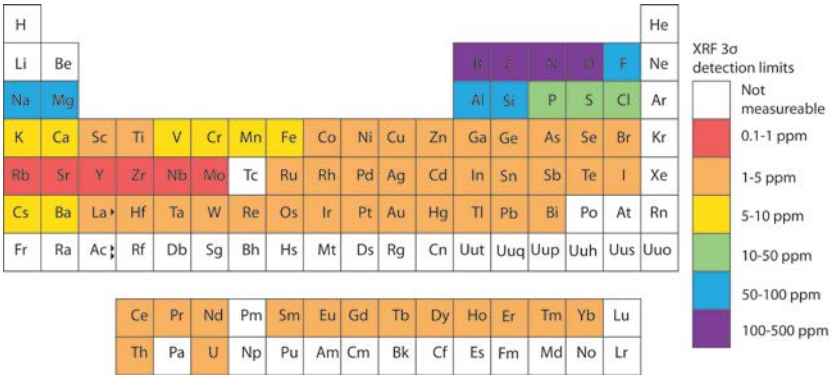

Figure 12: Periodic table showing elements that can be detected by XRF, with their working detection limits, adapted from (Gill 1997).

The WDXRF uses collimators to maintain symmetrical geometry between the sample, the crystal and the detector. All of the elements in the sample are excited simultaneously and a diffraction crystal (which acts like a prism), disperses the different fluorescent wavelengths in different directions (PANalytical 2014). As each element has a characteristic d-spacing, mounting the XRF on a goniometer and moving through an angular range to sequentially measure the intensities of each wavelength can allow the user to determine the quantity of each element present by Bragg's Law ($n\lambda = 2d\sin\theta$). WDXRF uses gas filled detectors and scintillation detectors which produce an electrical pulse when X-ray photons enter the detector. The pulse intensity is proportional to the energy of the incoming photon. The spectrometer sums primary fluorescence (characteristic radiation produced directly by incoming X-rays) and secondary fluorescence (produced in the sample by primary fluorescence of other atoms). Tertiary and further radiation can occur, but are negligible. The pulses are amplified and counted in each height level by a multi-channel analyser. The number of pulses at a certain height gives the intensity of the corresponding energy. The measured energies are plotted as an emission spectrum and peak search and peak match determines the

elements present in the sample (qualitative). After background subtraction, the peak intensity can be measured and converted to element concentration (quantitative) (Gill 1997).

As the spectrometer only analyses the samples surface layer, it must be representative of the whole sample. To achieve this, samples are made into a homogenous circular disc with a radius between 5 and 50 mm and then subsequently placed in a cup which is positioned in the spectrometer.

3.6.4. X-ray diffraction (XRD)

XRD is an analytical technique to determine atomic and molecular structures and identify crystalline components in solids. XRD can be used to identify what mineral phases are present (qualitative) and calculate the percentage of each phase present, particle size and strain (quantitative). It is a non-destructive technique and requires little material (~0.2 g). However, the technique is restricted by a detection limit of 5 % by mass, and inability to quantify elemental composition or identify amorphous materials.

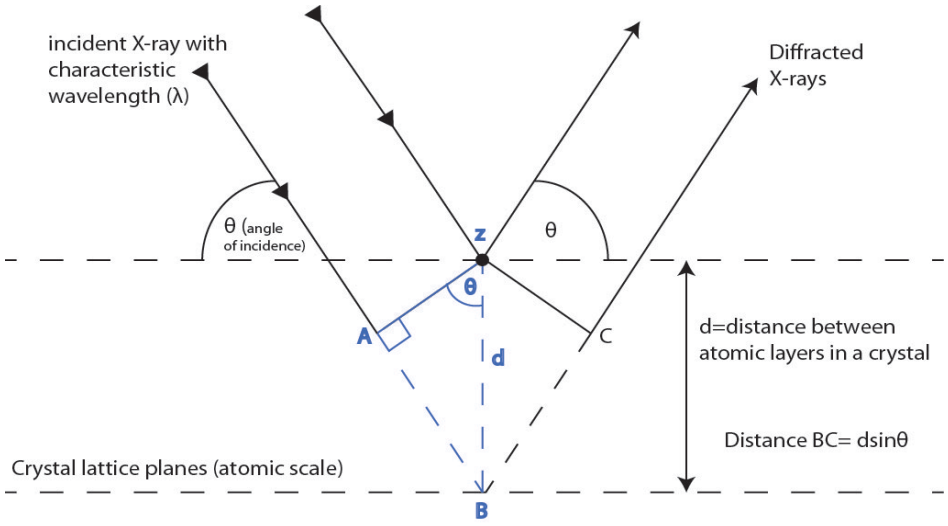

Figure 13: Bragg diffraction, adapted from (Williams & Carter 1996).

The Bragg law assumes that incoming X-rays scatter spectrally from each plane and X-rays scattered from adjacent planes will combine constructively (as constructive waves remain in the same phase) (Figure 13; Equation 3.13). 2dsinθ represents the constructive interference of multiple reflected incidence waves in adjacent planes. n is the order given (a defined integer, usually 1).

$$n\lambda = 2\text{dsin}\theta \qquad (3.13)$$

The Bragg equation can be used to determine the distance between atomic layers in the crystal (d), which can then be used to determine the crystal cell structure (Equation

3.14). α represents the lattice spacing of the cubic crystal and the orientation of crystal lattice planes is determined by its 3 miller indices (*h*, *k* and *l*), which are based on the selection rules and vary for different cubic Bravis lattices

$$d = \frac{a}{\sqrt{h^2}+k^2+l^2} \qquad (3.14)$$

In this thesis, samples were then mounted on a goniometer of a Bruker D8 Advance X-ray diffractometer with a Cu Kα1 source. As the sample rotates it is bombarded/ irradiated with a beam of monochromatic X-rays (collimated to reduce crystal damage) and 2D diffraction patterns were collected at 5° < 2θ < 70° with a 0.02 °C step size. The reflections were converted into a 3D model of electron density by Fourier Transform. Each component of the sample gives a set of diffraction peaks, with intensity proportional to the amount in the sample (LLD ~5 % abundance). Fingerprinting identification of these peaks allows the mineral phase(s) to be characterised, however there is a limit to the number of components that can be detected before the diffraction pattern becomes too complex (Lloyd et al. 2007). Phase percentage compositions can also be calculated against known standards (Lloyd et al. 2007).

3.7. Microbiological techniques

3.7.1. Polymerase chain reaction (PCR)

DNA in a single cell is too dilute to be detected analytically; therefore small sections of the DNA can be replicated (amplified) by several orders of magnitude to create a high enough concentration to be measured analytically. The 16S rRNA gene is used for phylogenetic studies as it is highly conserved between different species of bacteria and archea as it encodes for ribosomes, involved in protein synthesis (Coenye & Vandamme 2003). The 16S rRNA gene also contains 9 hypervariable regions, which allows us to differentiate between different species. Universal primers (small sections of DNA/RNA, generally ~20 base pairs) are used in PCR to amplify conserved regions of DNA.

The PCR process is initiated by heating the sample to 94 °C for 4 minutes and further melting for 30 seconds, which breaks the hydrogen bonds between base pairs of the double helix and splits the DNA into two strands. Primers for the 16S bacterial gene amplification are then added, where forward (8F (position 8 to 27)) and reverse (1492R (position 1510-1492)) primers (Eden et al. 1991) attach to each strand and the primer-DNA strands are cooled and allowed to anneal. The denaturing and annealing cycle leads to the increase in concentration of the 16S gene over the complete genome of the microbial community. Taq polymerase is a thermostable DNA replicating enzyme

isolated from the thermophilic bacterium *Thermus aquaticus* (Eckert & Kunkel 1991). Added alongside a suite of PCR reagents (see Chapters 4-6 for specific details) over a range of temperature cycles can replicate the DNA in the sample during the extension stage at 72°C for 35 cycles over 1 minute and a final extension step at 72°C for 5 minutes (Eden et al. 1991). This creates 2^{35} copies of the gene, which multiplied by the number of genes per species and number of species per environmental sample generates a substantial amount of genetic information.

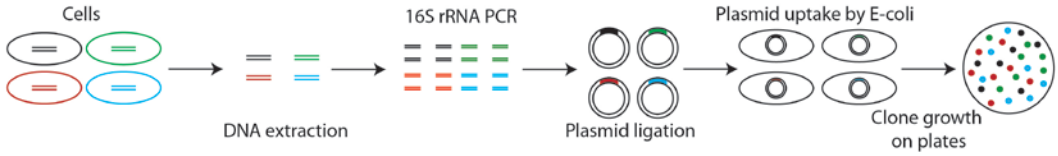

Figure 14: The polymerase chain reaction and the clone library procedure.

3.7.2. 16S rRNA gene based clone libraries

The products of PCR are mixed with plasmids (bacterial vectors) which uptake the genes (ligation stage), activated by the T4 DNA ligase enzyme and incubated at 14 °C. This is performed on agar plates loaded with antibiotics (kanamycin and ampicillin). Plasmid vectors contain genes which code for the aforementioned antibiotic resistance thus preventing non-targeted DNA contamination.

Escherichia coli are a bacterium capable of plasmid uptake and used in the transformation stage of the cloning process (Hanahan 1983). Cooling the cells on ice with divalent cations (Ca or Mg chloride) increases the cell membrane permeability and heat shocking the cells (42 °C for 45 seconds) causes plasmid vector uptake (Hanahan 1983). The cells are then grown in Luria-Bertani (LB) media (supporting *E-coli* growth) for 24 hours and each new cell will contain the DNA strand of interest. The *E-coli* culture is spread onto agar plates loaded with X-gal (a colourless structural analogue of lactose). This is the known as the blue white screening step. Plasmids contain the lacZα gene sequence which is broken when a gene is inserted, thus disrupting the production of α-peptide (β-galactosidase). X-gal can detect the presence of plasmid uptake because it is cleaved by β-galactosidase, which forms bromo-4-chloro-indoxyl, which then spontaneously dimerizes and oxidizes to form a bright blue insoluble pigment 5,5'-dibromo-4,4'-dichloro-indigo. Blue colonies contain a vector with a functional lacZα gene, however colonies which have produced no β-galactosidase, remain white. Under sterile conditions, 96 of the white colonies are picked at random and resuspended in sterile water containing PCR tubes for each microbial gene fragment library. The cells

are lysed in a thermal cycler (run at 100 °C for 5 mins) to extract the DNA. The DNA is then screened using primers (ST1F and ST1R) which target the PCR insertion regions of the plasmid vectors. The resulting PCR products are purified and nucleotide sequences were analysed using Mallard (Ashelford et al. 2006) to check for sequencing anomalies. Operational taxonomic units (OTUs=species) were determined at the 97 % sequence similarity level using Mothur (Schloss et al. 2009) and then analysed against known 16S rRNA gene sequences provided on the Ribosomal Database Project (Cole et al. 2009) to the nearest neighbours. Due to the bias in this process and the number of possible genes in the pot this may not give the best representation of the microbial community present in the sample.

3.7.3. Ribosomal intergenic spacer analysis (RISA)

Often described as a community fingerprinting, it is a commonly used technique to microbial population shifts under different experimental treatments (Borneman & Triplett 1997; Cardinale et al. 2004). Electrophoresis of the PCR products in Tris base, acetic acid and EDTA (TAE) gel, followed by staining with ethidium bromide allows the visualisation of the banding pattern under short-wave UV light. Each band corresponds to a bacterial population, so it can be used as a quantitative method to detect community simplification, for example (Figure 15).

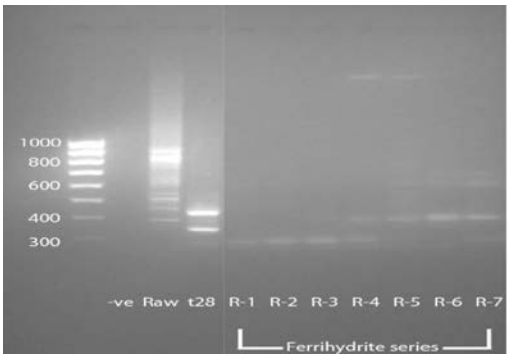

Figure 15: RISA (taken from Chapter 4).

3.7.4. 16S amplicon pyrosequencing and data analysis.

Pyrosequencing is a relatively new sequencing technique that is robust, expedient and has a high throughput (> 200,000 sequences (compared to the 96 sequences of clone libraries) and sequence length can exceed 200 bp) which gains an unprecedented insight into the microbial diversity present in a sample. Simple frequency data can be collected in real time at a high rate (overall reaction from polymerization to light detection takes place within 3–4 seconds at room temperature (Ronaghi 2001). Sample preparation is

also relatively rapid, reagent costs are considerably lower than other methods and can be easily automated (Ronaghi 2001). It is however expensive and short reads give phylogenetic interference (noise), long fusion primers may bring bias and the bioinformatics are cumbersome (Fakruddin et al. 2012).

Pyrosequencing involves the synthesis of a complementary strand alongside a single strand of DNA, one base pair at a time, with one of the 4 deoxynucleoside triphosphates (dNTPs) A, C, G an T nucleotides sequentially added. If a base pair does not match, they are degraded by apyrase, and the reaction starts again with another nucleotide. As a nucleotide is added, inorganic pyrophosphate (PPi) is released and adenosine 5' phosphosulfate (ATP sulfurylase, a recombinant version from the yeast *Saccharomyces cerevisiae* (Karamohamed & Nilsson 1999) and the luciferase is from the American firefly *Photinus pyralis* (Ronaghi 2001) converts PPi to ATP. In a pyrosequencing reaction, typically 1 pmol of DNA in a pyrosequencing reaction yields 6×10^{11} ATP molecules (Ronaghi 2001). ATP fuels luciferase, which oxidises luciferin to oxyluciferin which generates $> 6 \times 10^{9}$ photons at λ 560 nm (Ronaghi 2001), which is detected by a CCD camera. This process allows the sequence of the DNA template to be determined and all the sequences are translated concurrently.

The pyrosequencing reads in this study were analysed using Qiime 1.6.0 release (Caporaso et al. 2010). Low quality reads (mean qual score less than 25) and short sequences (less than 300 bp) were discarded, and both forward and reverse primers were removed from further analysis. Pyrosquencing produces 'noise', which needs to be removed before analysis begins. The main source of noise is when light intensities do not faithfully reflect the homopolymer lengths (Quince & Lanzén 2009). This noise has to be reduced, otherwise the number of OTUs is overestimated. Denoising and chimera detection were removed during OTU picking (at 97% sequence similarity) with usearch in this study. Taxonomic classification of all reads was performed in Qiime using the RDP at 80% confidence threshold (Cole et al. 2009), while the closest GenBank match for the OTUs that contained the highest number of reads (the representative sequence for each OTU was used) was identified by Blastn nucleotide search. In addition, Qiime was used to calculate and compute alpha and beta diversity indices and rarefaction curves. Details on the PCR procedure and pyrosequencing are given in Chapters 5 and 6. The emulsion PCR and the pyrosequencing run were performed at the University of Manchester sequencing facility, using a Roche 454 Life Sciences GS Junior system.

3.7.5. Microcosm experiments

Microcosms are simplified ecosystems that are used to simulate natural biogeochemical processes under controlled conditions. They are often used to monitor biogeochemical transformations by indigenous sediment microbial communities and are advantageous due to their reproducibility over dynamic ecosystems and the ease of variable (e.g. pH, temperature, electron donor/acceptor concentration) control. However, as these are closed systems (which may lead to the accumulation of species and pH alterations) and involve biased sediment to surface water ratios (for lab practicality, e.g. ease of sampling) give an uncharacteristic representation of the environment. In Chapter 4, serial dilutions were performed from the initial microcosm experiment in attempt to enrich the microbial community, by using freshwater minimal media that favours Fe(III)-reducing bacteria (Lovley & Phillips 1988). The media (containing $NaHCO_3$ (2.5 g L^{-1}), NH_4Cl (0.25 g L^{-1}), $NaH_2PO_4.H_2O$ (0.6 g L^{-1}), KCl (0.1 g L^{-1}), and defined vitamin solution (10 ml) (Wolin et al., 1963) and mineral elixir (10 ml) (Coppi et al., 2001)) was adjusted to pH 10 and augmented with 10 mM Na lactate, 1 g L^{-1} yeast extract and 50 mM ferrihydrite.

3.8. Radiological techniques

3.8.1. Liquid scintillation counting (LSC)

This is a useful technique to quantify radioactivity in a sample, particularly dilute α and β (0.05-0.2 MeV) emitters. In this thesis LSC was conducted on samples containing ^{99}Tc using a Tri-Carb 1900 TR Scintillation Counter. In a translucent vial, samples are thoroughly mixed and suspended in a cocktail (Optiphase HiSafe3 Liquid Scintillant, Perkin Elmer), composed of trace amounts fluorescent solute molecules (fluors) suspended in an organic solvent such as toluene. The kinetic energy from β-emission is absorbed by the π cloud of the aromatic ring of an organic solvent molecule (excimer), bringing them to an excited state. As the solvent relaxes back to the ground state, it emits energy as UV light. These electrons are passed between excimers until it is absorbed by the primary fluor (e.g. Butyl PBD ($C_{24}H_{22}N_2O$)), which releases short wavelength photons of light. These are converted to longer wavelengths by secondary fluors (e.g. Dimethyl POPOP ($C_{26}H_{20}N_2O_2$)) and these photons are converted to electrical pulses by the photomultiplier (Figure 16). A spectrum of detected amplitudes is outputted, which can be used to identify the radioisotope present.

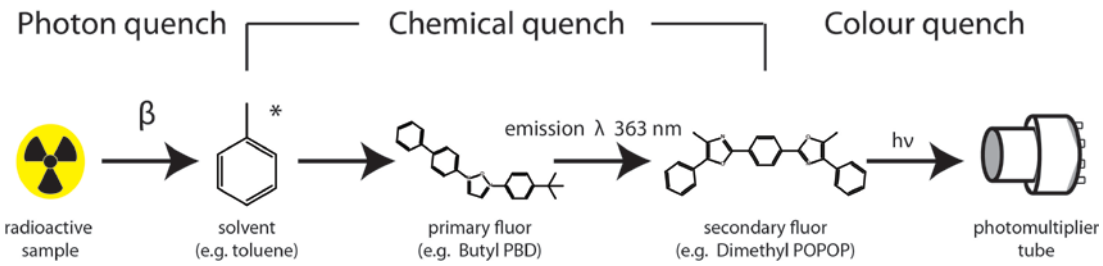

Figure 16: Energy transfer in LSC.

As heat, sun light, static charge and chemical reactions can cause the fluor molecules to become excited, a correction for background must be made. To account for this, a blank with pure water in scintillation cocktail is also placed along with the samples. The background radiation in the laboratory is ~ 30 counts per minute (averaging over 20 blanks). To minimise background radiation a region of interest is selected (~2-300 keV for ^{99}Tc) to maximise the signal to noise ratio. Samples were counted for 10 minutes in two windows; window A (0-300 keV) and window B (0-2000 keV). A higher count number in window B would indicate interference or quenching. There are three types of quench, which all cause counting inefficiency from energy loss. Chemical quenching occurs from poor energy transfer between solvent and fluors, or primary and secondary fluors. Colour quench causes signal suppression, and arises from absorption of energy from coloured samples. Alternatively, scintillation vials may degrade and become coloured. Photon quenching occurs when β-emission is incompletely transferred to the solvent. Quench is measured using a closed source to obtain a spectral index of sample (SIS) reading. The SIS value should not vary more than ± 20 units between samples (including blanks). If the SIS value is > 20 % different, significant quenching is occurring.

3.8.2. Determination of pertechnetate: the TPAC method

Tetraphenylarsonium chloride (TPAC) forms a 2:1 complex with Tc(VII) in chloroform (Singh et al. 1979). LSC on the organic phase can therefore be used to determine species specific TcO_4^- concentration (Tribalat & Beydon 1953; Wildung et al. 2000; Geissler et al. 2011).

3.8.3. Gamma camera imaging

Gamma camera imaging is commonly used to study the function of the human body by mapping the distribution of radiotracers incorporating gamma emitters in the energy range 70-370 keV with a half-life of several hours. A wide range of radiotracers are commercially available for this purpose, including ^{123}I, ^{67}Ga and ^{111}In, but the most commonly used is ^{99m}Tc which is readily and cheaply available from a ^{99}Mo/^{99m}Tc

generator. ^{99m}Tc has a half-life of 6 hours, and decays by gamma (140 keV) emission which can be imaged using a gamma camera based on a solid scintillator crystal detector. Gamma emissions from ^{99m}Tc can be used in the context of biogeochemistry to monitor and semi-quantitatively evaluate real-time transport, and the ability of gamma cameras to acquire a long series of sequential images enables automated data collection and overnight imaging.

A row of samples were placed between the two detectors of a dual-headed gamma camera fitted with lead high resolution parallel hole collimators, to filter out gamma photons which are not perpendicular to the camera detector. Gamma photons hit the sheet of scintillator crystal (NaI(Tl)) which is coupled to a close-packed hexagonal array of photomultiplier tubes, resulting in position signals from which the energy and x, y coordinates of the detected scintillation are computed. In this study, scintillations were collected over a period of 12 hours using a series of 48 sequential 15 minute acquisitions, followed by an additional 15 minute acquisition 16 hours later.

3.9. Radiation safety

The work in this thesis involved the radioactive isotopes ^{238}U, ^{99}Tc, ^{99m}Tc and ^{237}Np. Radioactive isotopes produce ionising radiation which can be hazardous to human health, therefore the correct safety training and practice has to be implemented in a satisfactory radioactive laboratory. A user of these radioactive sources must adhere to the guidelines outlined by their institution (The University of Manchester Health and Safety Service 2010). Users must ensure compliance with the Environmental Permitting Regulations 2010, the Ionising Radiations Regulations 1999 and the Health and Safety at Work act 1974. The possession and use of radioactive sources is subject to statuary controls.

3.9.1. Protocols

Before working with sources of ionising radiation, workers must use the appropriate protective equipment, exercise care in sample manipulations and work within designated radioactive controlled areas. Dosimetric monitors must be worn at all time and be regularly checked to determine the dose a worker has received and a Geiger counter should be used to monitor dedicated work stations before, during and after working with radioactive sources. Personnel must also keep careful and complete records of the use and disposal of radionuclides.

3.9.2. Radioactive Characteristics of ^{238}U, ^{99}Tc, ^{99m}Tc and ^{237}Np

The annual limit of intake (ALI) gives an indication of the radiological hazard association with a particular radionuclide and are available for inhalation and ingestion scenarios (Lloyd et al. 2007). The ALI indicates the maximum amount that a member of public can uptake before their annual dose limit (1 mSv) is reached (Lloyd et al. 2007). This is derived from the committed effective dose per unit intake (Sv Bq^{-1}) (Delacroix et al. 1998). Although ^{238}U and ^{99}Tc pose a significant radiological hazard, they are much less problematic than ^{237}Np (Table 2). Specialist radiochemistry laboratories are needed to handle these long lived radioisotopes, which require safe disposal via designated disposal routes (designated sinks and solid waste bins), specified by the local rules of the lab.

Table 2: Radionuclide (U, Tc and Np) concentration used in low and high level experiments with corresponding multiple of the ALI.

Radionuclide	Half life Mode of decay Energy of decay	Microcosm concentration (μM) **Number of inhalation ALIs** Number of ingestion ALIs	XAS concentration (μM) **Number of inhalation ALIs** Number of ingestion ALIs
^{238}U	4.47 x 10^9 y alpha 4.20 MeV	420 μM **0.0091** 0.0000546	420 μM **0.0091** 0.0000546
^{99}Tc	2.10 x 10^5 y beta 294 KeV	1.6 μM **0.117** 0.0234	898 μM **1.17** 0.234
^{237}Np	2.14 x 10^6 y alpha 4.79 MeV	3.31 μM **12.6** 0.066	414 μM **210** 1.1

Depleted uranium (DU), was used in Chapter 5 and is ~ 60 % the activity of natural uranium (Bleise et al. 2003), hence the chemical (heavy metal (Z 92)) toxicity of uranium is more significant than its radiological hazard. Alpha emission has a penetration range of approximately 4 cm in air and ~ 50 μm in soft tissue thus is unable to penetrate human skin and so uranium only represents an internal radiological hazard (Bleise et al. 2003). Uranium is absorbed into the blood as a soluble U(VI) species and retained in tissue and organs, where it can form complexes with bicarbonate, citrate or proteins (Cooper et al. 1982). During filtration in the kidneys, the uranyl ion can concentrate, leading to acute renal damage (Bryan & Siegel 2003). It is rapidly eliminated from the body (60% in 1h) and is rapidly absorbed from the gastrointestinal tract (Bryan & Siegel 2003).

^{99}Tc and ^{99m}Tc were used in Chapter 6. ^{99}Tc emits β-particles that are easily attenuated by surfaces (typically can only penetrate ~1cm) so do not pose a significant threat unless ingested. The biological half-life of ^{99}Tc is short (~60 hours in humans) and is

rapidly excreted form the body (<1 % retention after 60 days) so due to the low β emission poses little radiological threat to human health (Icenhower et al. 2010). Inhalation of Tc however can result in its accumulation in lung tissue, which has a longer biological excretion half-life and presents a more significant risk, which could lead to lung cancer and related illnesses (Icenhower et al. 2010). Experimental work with ^{99m}Tc was conducted at the Department of Nuclear Medicine, Manchester Royal Infirmary (MRI) by Dr. Heather Williams. ^{99m}Tc pertechnetate was supplied from the hospital radiopharmacy in a syringe, within a tungsten syringe with lead glass window and lead-lined carrying case. This was diluted further in a sample tube within a lead pot and 5 0.3 ml samples of this solution drawn into labelled syringes, working behind a lead body shield, which were transported in the lead-lined carry case. The ^{99m}Tc spike (18-22 MBq at the start of image acquisition) was injected into sample bottles which were kept at least at arm's length from the body for the remainder of the experiment. At the end of the imaging experiments, samples were stored in a secure laboratory at ambient temperature for 7 days to ensure the ^{99m}Tc had decayed to background levels.

^{237}Np undergoes higher energy α-decay (4.79 MeV) than ^{238}U, to Pa, which has a very energetic β-particle ($t_{1/2}$ 26.9 d). It is also a weak γ emitter. If ingested, Np primarily deposits in the liver (complexes with ferritin) and bones, which may potentially induce cancers of bone, lung and liver (Taylor 1989).

3.10. References

Ashelford, K.E., Chuzhanova, N.A., Fry, J.C., Jones, A.J. & Weightman, A.J., 2006. New screening software shows that most recent large 16S rRNA gene clone libraries contain chimeras. *Applied and Environmental Microbiology*, 72 (9), 5734–5741.

Binsted, N., 1998. *EXCURV98: The Manual*, Warrington, UK: CCLRC Daresbury Laboratory, p. 90.

Binsted, N., Strange, R.W. & Hasnain, S.S., 1992. Constrained and restrained refinement in EXAFS data analysis with curved wave theory. *Biochemistry*, 31 (48), 12117–12125.

Bleise, A., Danesi, P.R. & Burkart, W., 2003. Properties, use and health effects of depleted uranium (DU): a general overview. *Journal of Environmental Radioactivity*, 64 (2–3), 93–112.

Borneman, J. & Triplett, E.W., 1997. Molecular microbial diversity in soils from eastern Amazonia: evidence for unusual microorganisms and microbial population shifts associated with deforestation. *Applied and Environmental Microbiology*, 63 (7), 2647–2653.

Bryan, C.R. & Siegel, M.D., 2003. Environmental geochemistry of radioactive contamination In B.S. Lollar, ed, *Environmental Geochemistry*. Oxford: Elsevier, pp. 205-263

Caporaso, J.G., Kuczynski, J., Stombaugh, J., Bittinger, K., Bushman, F.D., Costello, E.K., Fierer, N., Pena, A.G., Goodrich, J.K. & Gordon, J.I., 2010. QIIME allows analysis of high-throughput community sequencing data. *Nature methods*, 7 (5), 335–336.

Cardinale, M., Brusetti, L., Quatrini, P., Borin, S., Puglia, A.M., Rizzi, A., Zanardini, E., Sorlini, C., Corselli, C. & Daffonchio, D., 2004. Comparison of different primer sets for use in automated ribosomal intergenic spacer analysis of complex bacterial communities. *Applied and Environmental Microbiology*, 70 (10), 6147–6156.

Charnock, J.M., 1995. Biological applications of EXAFS spectroscopy. *Radiation Physics and Chemistry*, 45 (3), 385–391.

Coenye, T. & Vandamme, P., 2003. Intragenomic heterogeneity between multiple 16S ribosomal RNA operons in sequenced bacterial genomes. *FEMS Microbiology Letters*, 228 (1), 45–49.

Coker, V.S., Gault, A.G., Pearce, C.I., van der Laan, G., Telling, N.D., Charnock, J.M., Polya, D.A. & Lloyd, J.R., 2006. XAS and XMCD evidence for species-dependent partitioning of arsenic during microbial reduction of ferrihydrite to magnetite. *Environmental Science & Technology*, 40 (24), 7745–7750.

Cole, J.R., Wang, Q., Cardenas, E., Fish, J., Chai, B., Farris, R.J., Kulam-Syed-Mohideen, A.S., McGarrell, D.M., Marsh, T., Garrity, G.M. & Tiedje, J.M., 2009. The Ribosomal Database Project: improved alignments and new tools for rRNA analysis. *Nucleic Acids Research*, 37 (suppl 1), D141–D145.

Cooper, J.R., Stradling, G.N., Smith, H. & Ham, S.E., 1982. The behaviour of uranium-233 oxide and uranyl-233 nitrate in rats. *International Journal of Radiation Biology*, 41 (4), 421–433.

Delacroix, D., Guerre, J.P., Leblanc, P. & Hickman, C., 1998. Radionuclide and radiation protection data handbook. *Radiation Protection Dosimetry*, 76 (1-2), 1–126.

Denecke, M.A., 2006. Actinide speciation using X-ray absorption fine structure spectroscopy. *Coordination Chemistry Reviews*, 250 (7), 730–754.

Dent, A. J.; Cibin, G.; Ramos, S.; Smith, A. D.; Scott, S. M.; Varandas, L.; Pearson, M. R.; Krumpa, N. A.; Jones, C. P.; Robbins, P. E., 2009. B18: A core XAS spectroscopy beamline for Diamond. *Journal of Physics: Conference Series*, 190, 012039.1-012039.4

Dionex, 1998. *DX-120 Ion Chromotograph Operator's Manual*, Sunnyvale, CA: Dionex corporation, p. 131.

Dionex, 2006. *User's Guide: Chromeleon® Operational Qualification and Performance Qualification Software Templates for IC and BioLC Instruments, Rev. 5.1*, Sunnyvale, CA: Dionex Corporation, p. 60.

Dionex, 2012. *DX-ICS-5000$^+$ HPIC System*, Sunnyvale, CA: Dionex Corporation, p. 19.

Eckert, K.A. & Kunkel, T.A., 1991. DNA polymerase fidelity and the polymerase chain reaction. *Genome Research*, 1 (1), 17–24.

Eden, P.A., Schmidt, T.M., Blakemore, R.P. & Pace, N.R., 1991. Phylogenetic analysis of *Aquaspirillum magnetotacticum* using polymerase chain reaction-amplified 16S rRNA-specific DNA. *International Journal of Systematic Bacteriology*, 41 (2), 324–325.

Geissler, A., Law, G.T.W., Boothman, C., Morris, K., Burke, I.T., Livens, F.R. & Lloyd, J.R., 2011. Microbial communities associated with the oxidation of iron and technetium in bioreduced sediments. *Geomicrobiology Journal*, 28 (5-6), 507–518.

Gill, R., 1997. *Modern Analytical Geochemistry: an Introduction to Quantitative Chemical Analysis Techniques for Earth, Environmental and Materials Scientists*, Essex: Addison Wesley Longman, p. 329.

Hanahan, D., 1983. Studies on transformation of *Escherichia coli* with plasmids. *Journal of Molecular Biology*, 166 (4), 557–580.

Icenhower, J.P., Qafoku, N.P., Zachara, J.M. & Martin, W.J., 2010. The biogeochemistry of technetium: A review of the behavior of an artificial element in the natural environment. *American Journal of Science*, 310 (8), 721–752.

Jarvis, K.E., Gray, A.L. & Houk, R.S., 1992. *Handbook of Inductively Coupled Plasma Mass Spectrometry*, London: Blackie and Son Ltd, p. 485.

Johnson, D.A. & Florence, T.M., 1971. Spectrophotometric determination of uranium(VI) with 2-(5-bromo-2-pyridylazo)-5-diethylaminophenol. *Analytica Chimica Acta*, 53 (1), 73–79.

Karamohamed, S. & Nilsson, J., 1999. Production, purification, and luminometric analysis of recombinant *Saccharomyces cerevisiae* MET3 adenosine triphosphate sulfurylase expressed in *Escherichia coli*. *Protein expression and Purification*, 174, 423-436.

van der Laan, G. & Kirkman, I.W., 1992. The 2p absorption spectra of 3d transition metal compounds in tetrahedral and octahedral symmetry. *Journal of Physics: Condensed Matter*, 4 (16), 4189-4204.

van der Laan, G. & Thole, B.T., 1991. Strong magnetic X-ray dichroism in 2p absorption spectra of 3d transition-metal ions. *Physical Review B*, 43 (16), 13401-13413.

Lloyd, J.R., Beveridge, T.J., Morris, K., Polya, D.A., Vaughan, D.J., 2007. Techniques for studying microbial transformations of metals and radionuclides. In C. J. Hurst, R. L. Crawford, J. L. Garland, D. A. Lipson, A. L. Mills & L. D. Stetzenbach, eds, *Manual of Environmental Microbiology*, pp. 1195–1213.

Lovley, D.R. & Phillips, E.J., 1987. Rapid assay for microbially reducible ferric iron in aquatic sediments. *Applied and Environental Microbiology*, 53 (7), 1536–1540.

Lovley, D.R. & Phillips, E.J.P., 1988. Novel mode of microbial energy metabolism: organic carbon oxidation coupled to dissimilatory reduction of iron or manganese. *Applied and Environmental Microbiology*, 54 (6), 1472–1480.

Newville, M., 2004. Fundamentals of XAFS. *Consortium for Advanced Radiation Sources*, University of Chicago, Chicago, p. 43.

PANalytical, 2014. AxiosmAX WDXRF spectrometer. Available at: http://www.panalytical.com/AxiosmAX.htm [Accessed March 22, 2014].

Pattrick, R.A.D., Van Der Laan, G., Henderson, C.M.B., Kuiper, P., Dudzik, E. & Vaughan, D.J., 2002. Cation site occupancy in spinel ferrites studied by X-ray magnetic circular dichroism: developing a method for mineralogists. *European Journal of Mineralogy*, 14 (6), 1095–1102.

Quince, C. & Lanzén, A., 2009. Accurate determination of microbial diversity from 454 pyrosequencing data. *Nature Methods*, 6 (9), 639-641.

Ravel, B. & Newville, M., 2005. ATHENA, ARTEMIS, HEPHAESTUS: data analysis for X-ray absorption spectroscopy using IFEFFIT. *Journal of Synchrotron Radiation*, 12 (4), 537–541.

Ronaghi, M., 2001. Pyrosequencing sheds light on DNA sequencing. *Genome Research*, 11 (1), 3–11.

Rothe, J., Butorin, S., Dardenne, K., Denecke, M.A., Kienzler, B., Löble, M., Metz, V., Seibert, A., Steppert, M., Vitova, T., Walther, C. & Geckeis, H., 2012. The INE-Beamline for actinide science at ANKA. *The Review of Scientific Instruments*, 83 (4), 043105.1–043105.13.

Schloss, P.D., Westcott, S.L., Ryabin, T., Hall, J.R., Hartmann, M., Hollister, E.B., Lesniewski, R.A., Oakley, B.B., Parks, D.H., Robinson, C.J., Sahl, J.W., Stres, B., Thallinger, G.G., Van Horn, D.J. & Weber, C.F., 2009. Introducing mothur: open-source, platform-independent, community-supported software for describing and comparing microbial communities. *Applied and Environmental Microbiology*, 75 (23), 7537–7541.

SeQuant, 2007. *A Practical Guide to Ion Chromatography: An Introduction and Troubleshooting Manual*, Sweden: SeQuant AB, p. 24

Singh, R., Krueger, A. & Lieser, K., 1979. Extraction of technetium from nitric acid by tetraphenyl arsonium chloride. *Radiochim Acta*, 26 (3-4), 197-252.

Small, H., 1989. *Ion Chromatography*, New York: Plenum Press, p. 276.

Stookey, L.L., 1970. Ferrozine-a new spectrophotometric reagent for iron. *Analytical Chemistry*, 42 (7), 779–781.

Taylor, D.M., 1989. The biodistribution and toxicity of plutonium, americium and neptunium. *Science of The Total Environment*, 83 (3), 217–225.

The University of Manchester Health and Safety Service, 2010. Ionising Radiation Safety v3. *University Code of Practice and Guidance, Ionising Radiation Safety*, Manchester, p.13.

Thole, B.T., Carra, P., Sette, F. & van der Laan, G., 1992. X-ray circular dichroism as a probe of orbital magnetization. *Physical Review Letters*, 68 (12), 1943-1946.

Tribalat, S. & Beydon, J., 1953. Isolement du technetium. *Analytica Chimica Acta*, 8 (0), 22–28.

Upstone, S.L., 2000. Ultraviolet/visible light absorption spectrophotometry in clinical chemistry. In R.A. Meyers, ed, *Encyclopedia of Analytical Chemistry*. New York: Ramtech Inc, pp. 1699-1771.

Wielinga, B., Bostick, B., Hansel, C.M., Rosenzweig, R.F. & Fendorf, S., 2000. Inhibition of bacterially promoted uranium reduction: ferric (hydr)oxides as competitive electron acceptors. *Environmental Science & Technology*, 34 (11), 2190–2195.

Wildung, R.E., Gorby, Y.A., Krupka, K.M., Hess, N.J., Li, S.W., Plymale, A.E., McKinley, J.P. & Fredrickson, J.K., 2000. Effect of electron donor and solution chemistry on products of dissimilatory reduction of technetium by *Shewanella putrefaciens*. *Applied and Environmental Microbiology*, 66 (6), 2451-2460.

Williams, D.B. & Carter, C.B., 1996. *Transmission Electron Microscopy*, Boston: Springer, p. 760.

4

Microbial Reduction of Fe(III) under Alkaline Conditions Relevant to Geological Disposal

Paper published, Williamson, A.J., Morris, K., Shaw, S., Bynre, J.M., Boothman, C. and Lloyd, J.R., 2013. Microbial reduction of Fe(III) under alkaline conditions relevant to geological disposal. *Applied and Environmental Microbiology*, 79 (11)**,** 3320-3326.

Applied and Environmental Microbiology

Microbial Reduction of Fe(III) under Alkaline Conditions Relevant to Geological Disposal

Adam J. Williamson, Katherine Morris, Sam Shaw, James M. Byrne, Christopher Boothman and Jonathan R. Lloyd
Appl. Environ. Microbiol. **2013, 79(11):3320. DOI: 10.1128/AEM.03063-12.**
Published Ahead of Print 22 March 2013.

AEM
Journals.ASM.org

Microbial Reduction of Fe(III) under Alkaline Conditions Relevant to Geological Disposal

Adam J. Williamson, Katherine Morris, Sam Shaw, James M. Byrne,* Christopher Boothman, Jonathan R. Lloyd

Research Centre for Radwaste and Decommissioning and Williamson Research Centre for Molecular Environmental Science, School of Earth, Atmospheric, and Environmental Sciences, The University of Manchester, Manchester, United Kingdom

To determine whether biologically mediated Fe(III) reduction is possible under alkaline conditions in systems of relevance to geological disposal of radioactive wastes, a series of microcosm experiments was set up using hyperalkaline sediments (pH ~11.8) surrounding a legacy lime working site in Buxton, United Kingdom. The microcosms were incubated for 28 days and held at pH 10. There was clear evidence for anoxic microbial activity, with consumption of lactate (added as an electron donor) concomitant with the reduction of Fe(III) as ferrihydrite (added as the electron acceptor). The products of microbial Fe(III) reduction were black and magnetic, and a range of analyses, including X-ray diffraction, transmission electron microscopy, X-ray absorption spectroscopy, and X-ray magnetic circular dichroism confirmed the extensive formation of biomagnetite in this system. The addition of soluble exogenous and endogenous electron shuttles such as the humic analogue anthraquinone-2,6-disulfonate and riboflavin increased both the initial rate and the final extent of Fe(III) reduction in comparison to the nonamended experiments. In addition, a soluble humic acid (Aldrich) also increased both the rate and the extent of Fe(III) reduction. These results show that microbial Fe(III) reduction can occur in conditions relevant to a geological disposal facility containing cement-based wasteforms that has evolved into a high pH environment over prolonged periods of time (>100,000 years). The potential impact of such processes on the biogeochemistry of a geological disposal facility is discussed, including possible coupling to the redox conditions and solubility of key radionuclides.

Many nations have now decided that radioactive wastes, including intermediate-level radioactive wastes (ILW) from civil nuclear power programs, will be disposed of in deep geological disposal facilities (GDFs) (1). In the United Kingdom, the current GDF concept comprises ILW encapsulation typically in cementitious grout and steel canisters prior to emplacement in the GDF between 200 and 1,000 m below the surface (1). After the operational lifetime of the facility, the current generic plan for United Kingdom ILW involves backfilling with cementitious materials. Regardless of the backfill material, it is clear that the grout within the ILW waste form and the engineering of any GDF will result in a significant amount of cementitious materials in many different GDF designs. In the current generic United Kingdom model for ILW, with cementitious backfill, it is expected that resaturation will result in the generation of an alkaline plume from reaction with the cementitious materials in the disposal facility. This alkaline plume will evolve with time as the chemical make-up of the repository is altered by reaction with deep groundwater (2). Furthermore, the alkaline fluids will react with the surrounding environment to form a hyperalkaline chemically disturbed zone that persists over tens to hundreds of thousands of years (1).

The repository will be exposed to air during the operational lifetime of several tens of decades. After closure, microbially mediated anoxia is predicted to develop as oxygen is purged from the repository by chemical and presumably biological processes. Indeed, biogeochemical processes are potentially important in geological disposal, but very little work has explored anaerobic redox cycling pathways at high pH. The ILW waste packages are likely to contain elevated levels of organics such as cellulose, which have been found to degrade into a range of electron donating substrates under alkaline conditions (3). Both corrosion of the steel drums and radiolysis of groundwater are expected to liberate hydrogen gas which may also serve as a potent electron donor for anoxic microbial communities (4). In terms of electron accepting processes, the ILW materials will undoubtedly contain Fe(III) from oxic corrosion of wasteforms and iron used in engineering (e.g., rock bolts), and Fe(III) may form a significant part of the geosphere surrounding the disposal facility.

Microbially mediated metal reduction is ubiquitous in both natural and engineered environments (5, 6), and Fe(III) reduction can lead to gross changes in iron speciation, with the precipitation of mixed Fe(II)/Fe(III)-bearing phases such as magnetite and Fe(II) phases such as siderite or vivianite all possible end products. There are a wide variety of prokaryotes that are able to respire Fe(III) at circumneutral pH (6), with the best-studied examples being *Geobacter* (7) and *Shewanella* (8) species, and microorganisms such as these may exist in localized, neutral pH microniches within the pH 13 waste form. However, in the United Kingdom generic ILW system, after closure, resaturation will produce a hyperalkaline leachate where the initial pH is expected to be >13, with pH 10 to 11 conditions expected to occur in the chemically disturbed zone for several tens to hundreds of thousands of years. Clearly, under these high-pH conditions and adequate concentrations of suitable electron donors and electron acceptors, the de-

Received 12 October 2012 **Accepted** 9 March 2013
Published ahead of print 22 March 2013
Address correspondence to Jonathan R. Lloyd, jon.lloyd@manchester.ac.uk.
* Present address: James M. Byrne, Zentrum für Angewandte Geowissenschaften, Geomikrobiologie, Universität Tübingen, Tübingen, Germany.
Supplemental material for this article may be found at http://dx.doi.org/10.1128/AEM.03063-12.

doi:10.1128/AEM.03063-12

velopment of microbial communities within the waste and host rock may be promoted. There is, however, a paucity of information about the extent and type of microbial processes operating under such conditions. Natural hyperalkaline Ca^{2+}-rich groundwaters formed by the serpentization of primary silicate materials olivine and pyroxene, have been studied for their microbial diversity (9). Furthermore, a select range of alkaliphiles capable of Fe(III) reduction have also been isolated from natural (10–13) and anthropogenic (14, 15) sites with pH values from 9.5 to 12.9. However, the impact of these microorganisms on materials and processes related to ILW remain essentially unknown.

Humic substances, both naturally occurring and anthropogenic derivatives from the waste form, may influence the biogeochemistry in radioactive waste disposal through their ability to act as both ligands for radionuclides (16, 17) and as "electron shuttles" for extracellular redox processes such as Fe(III) reduction. In terms of impacts on Fe(III) reduction, shuttling electrons via semiquinone moieties alleviates the need for direct microbe-mineral surface interactions, increasing the rates of Fe(III) reduction (6, 18, 19). In addition, secreted electron shuttles, including flavin compounds such as flavin mononucleotide and riboflavin produced by *Shewanella* sp., have also been shown to accelerate the rate of Fe(III) reduction (20). Microbially mediated Fe(III) reduction also affects the speciation of key long-lived radionuclides such as U (21), Tc (22), and Np (23) under ambient conditions. Reduction can be enzymatic (24, 25) or due to abiotic electron transfer reactions with products of microbial reduction (23, 26), for example, mediated by Fe(II)-bearing minerals (5). Thus, it is critical to understand the potential for microbially mediated biocycling processes under conditions relevant to geological disposal facilities. Here, we explore microbially mediated Fe(III) reduction in a model alkaline system chosen to be of relevance to intermediate level waste disposal. Specifically, we have explored the reduction of Fe(III) oxyhydroxides added to near surface alkaline sediments taken from a legacy lime working site in the Peak District, Derbyshire, United Kingdom, and determined the effect of microbial reduction on iron mineralogy at pH 10 in this system. Overall, our aim was to assess the scope for bioreduction processes by indigenous microbial populations in sediments from an alkaline impacted environment. In turn, this will inform the significance of such anaerobic microbial processes in the safe geological disposal of alkaline, intermediate level wastes.

MATERIALS AND METHODS

Near surface sediment (~20-cm depth) was collected adjacent to legacy lime workings at Harpur Hill Buxton, United Kingdom. Sediment was placed into sterile plastic containers and stored in the dark at 4°C. Sediments were dominated by calcite, quartz, and ankerite. Surface waters were at pH ~11.8 and were dominated by Na^+, K^+, and Ca^{2+} with measurable Sr^{2+} and silicon. For microcosm experiments, ferrihydrite was synthesized using methods outlined by Cornell and Schwertmann (27, 28).

Microcosm experiments. To investigate the impact on indigenous microorganisms on high pH sediments, microcosms were prepared, in triplicate, in sterile serum bottles with Buxton sediment slurried with surface waters (solid solution ratio 1:5). The sediment slurry was then supplemented with excess Fe(III) as ferrihydrite (120 mM) to provide Fe(III) as an electron acceptor for anaerobic growth. This allowed exploration of biogeochemical processes at a pH known to allow microbial reduction to develop in these sediments (2) and under conditions expected to be relevant to deep geological disposal. The following variations were tested: (i) an oxic control, (ii) Buxton sediment slurry at pH 10 groundwater with no added electron donor ("anoxic, no electron donor"), (iii) Buxton sediment slurry at pH 10 with 10 mM sodium lactate and 5 g of yeast extract $liter^{-1}$ (0.5% [wt/vol]; "anoxic, electron donor"), (iv) Buxton sediment slurry at pH 10 with electron donor and 100 μM anthraquinone-2,6-disulfonate (AQDS) ("anoxic AQDS"), (v) Buxton sediment slurry at pH 10 with electron donor and 100 μM riboflavin ("anoxic riboflavin"), (vi) Buxton sediment slurry at pH 10 with electron donor and 2 mg ml^{-1} of a natural source of Elliot Lake humic acid (ELHA; "anoxic ELHA"), and (vii) Buxton sediment slurry at pH 10 with electron donor and 2 mg of Aldrich humic acid ml^{-1} added ("anoxic AHA"). The Elliot soil humic acid was purchased from the International Humic Substances Society (1S102H), and Aldrich humic acid was purchased from Sigma-Aldrich; in both cases the humic acids were used as received. The bottles were sealed with thick butyl rubber stoppers and the headspace was flushed for 5 min with N_2 to create anoxic conditions. The bottles were then incubated at 20°C in the dark. Throughout the incubations, the pH of the microcosms dropped, especially during the first week of incubation, so manual daily pH adjustment of the experiments to pH 10 was achieved with 2 M NaOH. Sample manipulations and analyses were performed under anoxic conditions as appropriate using an aseptic technique.

Geochemical analyses. The pH and the reduction potential (Eh) were measured upon sample withdrawal with a calibrated (pH 7, 10, and 12) Denver Instrument digital meter. Biogenic Fe(II) and total Fe concentrations on sediment slurries were assessed by the ferrozine assay (29). In addition, sediment porewaters were filtered (<0.2-μm pore diameter; Acrodisc) under anaerobic conditions and organic acids, NO_3^-, and SO_4^{2-} were analyzed using a Dionex DX120 ion chromatograph.

Mineralogical characterization X-ray (powder) diffraction. At experimental endpoints, mineral residues were removed from the reduction experiments and dried under anoxic conditions. The dried solid was ground into a fine slurry under anoxic conditions with a few drops of amyl acetate and the sample was then analyzed using a Bruker D8 Advance X-ray diffractometer with a Cu Kα1 source. The data were collected at 5° < 2θ < 70° with a 0.02° step size.

TEM. Transmission electron microscopy (TEM) was carried out using a Philips CM 200 electron microscope at the Leeds Electron Microscopy and Spectroscopy (LEMAS) Centre, University of Leeds, Leeds, United Kingdom. The microscope was equipped with a field emission gun, an energy dispersive X-ray analysis (EDX) detector (Oxford Instruments, ISIS software), and a Gatan imaging filter (GIF200). All images were obtained using an operating beam voltage of 200 kV. In order to confirm the presence of specific mineral phases, selected area electron diffraction (SAED) patterns were acquired using an appropriate diffraction aperture. Prior to introduction in the chamber, aliquots were obtained from each of the anoxic dry powder samples (typically several milligrams) and dispersed in several milliliters of anoxic water using an ultrasonic probe (Misonix; Microson XL) operating at a power of 15 W (root mean square). A droplet of each of the resulting dispersions was placed on a carbon grid (Agar Scientific) and allowed to dry under anoxic conditions before imaging.

X-ray absorption spectroscopy (XAS) and X-ray magnetic circular dichroism (XMCD). XAS spectra at the Fe $L_{2,3}$ edge were collected on the Magnetic Spectroscopy beamline 4.0.2 at the Advanced Light Source, Lawrence Berkeley National Laboratory, Berkeley, CA. Samples were dried and ground in an anaerobic cabinet and mounted onto carbon tape attached to the sample probe. The sample probe was transported to the beamline in a sealed anoxic container and loaded into the sample chamber under a backflow of N_2 to minimize any potential exposure to air. Measurements were made in total electron yield mode using circularly polarized X-rays with an effective probing depth of ca. 3 to 4 nm, with most of the synchrotron energy lost within the first few nm.

XMCD spectra were derived from the difference between two XAS spectra collected under the application of two opposite magnetic fields (±0.6 T), parallel and antiparallel to the beam direction. XMCD spectra are used to obtain information about magnetization, site location, and

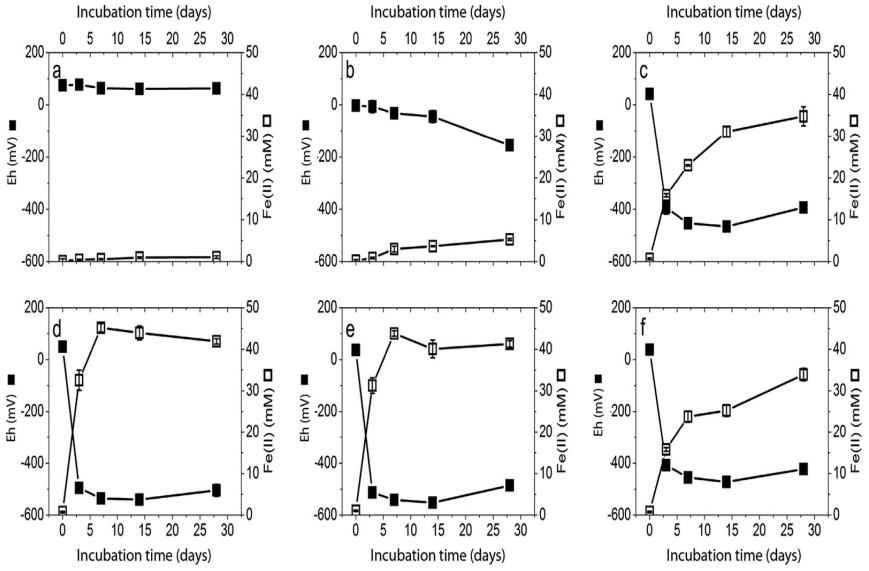

FIG 1 0.5 N HCl extractable Fe(II) concentration (□) and redox potential (Eh) (■) in microcosms containing Buxton sediments supplemented with 120 mM ferrihydrite incubated under a range of biogeochemical regimes as defined in Materials and Methods: oxic control (a); anoxic, no electron donor (b); anoxic, electron donor (c); anoxic AQDS (d); anoxic riboflavin (e); and anoxic Elliot Lake humic acid (ELHA) (f).

valence state (number of d electrons). Atomic multiplet calculations were fitted to the XMCD to quantify the site occupancies of Fe cations with the crystalline material [i.e., Fe(II) and Fe(III) in octahedral (O_h) and tetrahedral (T_d) coordination] (30–32).

Ribosomal intergenic spacer analysis (RISA). DNA was extracted from sediment samples (0.2 g) and microcosm incubations and subsequent enrichment cultures (200 μl) using a PowerSoil DNA isolation kit (PowerSoil DNA isolation kit; MO BIO Laboratories, Inc., Solana Beach, CA). The 16S-23S rRNA intergenic spacer region from the bacterial RNA operon was amplified as described previously using primers ITSF and ITSReub (33). The amplified products were separated by electrophoresis in a Tris-acetate-EDTA agarose gel (1% [wt/vol]). DNA was stained with 4 μl of a 10-mg ml^{-1} ethidium bromide solution and viewed under short-wave UV light. Significant changes in microbial community changes identified by band shifts in the RISA justified further investigation by DNA sequencing of 16S rRNA gene clone libraries.

Amplification, cloning, and sequencing of 16S rRNA gene sequences. A fragment of the 16S rRNA gene, ~1,490 bp, was amplified from samples using the broad-specificity primers 8F (Eden 1991) and 1492R (34) using protocols described previously (22). Briefly, TaKaRa ExTaq polymerase (Millipore UK, Ltd., Watford, United Kingdom) was used to amplify DNA from the sample extract according to previously published protocols and cloned into a vector containing topoisomerase I-charged vector arms (Agilent Technologies, Wokingham, United Kingdom) prior to transformation into *Escherichia coli* competent cells expressing Cre recombinase (Agilent Technologies) (22). White transformants that grew on Luria-Bertani agar containing ampicillin and X-Gal (5-bromo-4-chloro-3-indolyl-β-D-galactopyranoside) were screened for an insert using PCR, using primers that were complementary to the flanking regions of the PCR insertion site of the cloning vector.

The resulting PCR products were purified using an ExoSap protocol, and nucleotide sequences were determined by the dideoxynucleotide method as described previously (22). Sequences (typically 900 bp in length) were analyzed using Mallard (35) to check for the presence of chimeras or sequencing anomalies. Operational taxonomic units (OTU) were determined at a 97% sequence similarity level using Mothur (36). The individual OTU sequences were analyzed using the sequencing database of known 16S rRNA gene sequences provided on the Ribosomal Database Project (37) to identify nearest neighbors.

Nucleotide sequence accession numbers. The 16S rRNA sequence data were submitted to GenBank under accession numbers JX417189 to JX417369.

RESULTS AND DISCUSSION

Fe(III) reduction. A series of sediment based microcosms were set up primarily to determine the rate and extent of Fe(III) reduction in pH 10 sediment microcosms amended with ferrihydrite and to probe the Fe(III)-reducing capability of the sediments and associated microbial communities. Oxidizing conditions, indicated by positive redox potential and the presence of predominantly Fe(III) minerals in 0.5 N HCl extracted sediment slurries, were seen in all treatments before incubation and in oxic controls throughout the time series (Fig. 1a). After anoxic conditions were established (indicated by a drop in Eh), minor nitrate present in the starting systems (14 ± 4 μM without electron donor present and 38 ± 2 μM with electron donor) was removed after 3 days in all experiments. To assess the extent of Fe(III) reduction in these systems, a set of sediment slurries were incubated without added electron donor additions. Fe(III) reduction in these controls occurred, with an increase in 0.5 N HCl extractable Fe(II) after day 3 (Fig. 1b). Furthermore, significant increases in Fe(II) after 28 days were observed, coupled to a drop in Eh to −150 mV (Fig. 1b). These values suggest that these high pH sediments contained indigenous, labile organic material, which supported a low level of microbial reduction of Fe(III).

All anoxic microcosms with added electron donor (Fig. 1c to f) showed enhanced microbial reduction, with clear development of Fe(III)-reducing conditions after 3 days, with Eh values dropping and stabilizing at −400 to −500 mV. Therefore, the addition of lactate and yeast extract clearly stimulated the activity of Fe(III)-reducing microorganisms in these experiments, with lactate completely consumed within the 28 day incubation (see Fig. S1 in the supplemental material). Several organic acids were also produced during the incubation; the carbon balance was nonstoichiometric and presumably complicated by the presence of other carbon

sources in the yeast extract and/or sediment. In these ferrihydrite-augmented systems, the sulfate concentration was low (37 ± 18 μM) in the anoxic, no-electron-donor system and did not drop over the experimental period. Sulfate concentrations were much higher in the electron-donor-amended systems (469 ± 85 μM), presumably from the yeast extract, but showed no appreciable reduction over the incubational period, suggesting that sulfate reduction had not commenced by 28 days, reflected by the high Fe(III) loading for these systems, and intense competition for the added electron donor, exacerbated by the energetically unfavorable sulfate/sulfide couple at high pH (2).

Interestingly, the addition of the electron shuttles AQDS (Fig. 1d) and riboflavin (Fig. 1e) resulted in the lowest reduction potentials of all the systems tested (−540 ± 3 mV and −552 ± 7 mV, respectively, after 14 days), and rapid development of Fe(III) reduction was observed in both systems. Overall, the highest concentrations of 0.5 N HCl extractable Fe(II) were observed in these systems with 45 ± 1 mM and 44 ± 1 mM 0.5 N HCl extractable Fe(II) at 7 days in AQDS- and riboflavin-amended systems, respectively. The levels of 0.5 N HCl extractable Fe(II) in these systems decreased after 14 days and this, coupled to the fact that the Eh remained significantly reducing over the experimental period (−504 ± 23 mV and −486 ± 20 mV, respectively, after 28 days), suggested that Fe(II) was being sequestered into the a newly formed Fe(II)-bearing mineral. Thus, at the high pH of these systems where metal ions, including Fe(III), will be sparingly soluble [e.g., for $Fe(OH)_3$, $\sim 10^{-6}$ mol kg^{-1} (38)], both AQDS and riboflavin enhanced the rate of metal reduction. Presumably, these compounds alleviated the need for direct contact for electron transport between the cell surface and the electron acceptor, thus enhancing the rate of Fe(III) reduction. This suggests that the presence of both natural and anthropogenic electron shuttles, such as humic substances or secreted flavin molecules, respectively, may enhance development of Fe(III)-reducing conditions in the evolved GDF environment.

Interestingly, initial experiments with a natural humic material, Elliot Lake humic, showed no significant increase in the rate of Fe(III)-reduction compared to that noted without the added humic material (Fig. 1c and f). However, under the experimental conditions studied, Elliot Lake humic was clearly poorly soluble at pH 10, forming a black suspension when added, and these results suggest that it was unable to act as a solid state electron shuttle in contrast to recent work on neutral pH systems (39). Further investigations used Aldrich humic acid which was soluble and showed a notable difference in both the rate and extent of Fe(III)-reduction (see Fig. S2 in the supplemental material), suggesting that soluble humics may have an influence if they are found within the GDF environment.

Mineralogical characterization. (i) XRD. To analyze the mineralogical changes associated with microbial Fe(III) reduction, at the end of the experiment, samples of the sediment slurry were analyzed by X-ray diffraction (XRD). Analysis of Buxton sediment with or without ferrihydrite amendment, prior to incubation, showed an XRD spectrum dominated by calcite, presumably as a weathered mineral produced from carbonation of CaO from the lime workings, with minor quartz and ankerite [$Ca(Fe, Mg, Mn)(CO_3)_2$] similar to other studies at this site (40). Furthermore, 0.5 N HCl extraction with hydroxylamine of the sediments not amended with ferrihydrite indicated that a small but significant proportion of the sediment was present as "bioavailable" Fe(III)

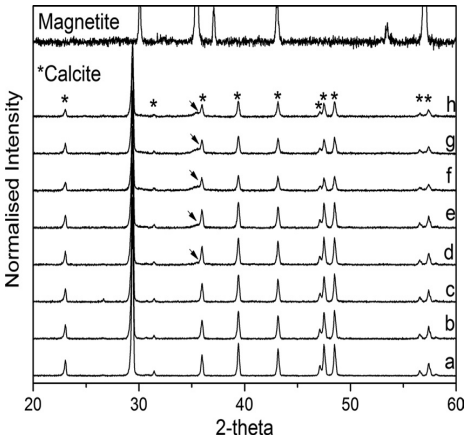

FIG 2 XRD analysis of microcosms containing Buxton sediments incubated under a range of biogeochemical regimes: unamended Buxton sediment (a); Buxton sediment with ferrihydrite amendment (b); oxic control (c); anoxic, no electron donor (d); anoxic, electron donor (e); anoxic AQDS (f); anoxic riboflavin (g); and anoxic ELHA (h). Arrows are used to indicate the broad-shoulder feature characteristic of magnetite in samples d to h. The XRD of magnetite has also been given as a reference (top).

(0.3 mg g^{-1}). In the no-electron-donor sediments incubated for 28 days, a broad magnetite peak was present (Fig. 2d), suggesting that this system can support low levels of microbially mediated Fe(III) reduction and forms detectable quantities of magnetite. Indeed, in all end member anoxic systems there was a clear magnetite signal, confirming that microbial processes lead to extensive magnetite biomineralization in these experiments (Fig. 2d to h).

(ii) TEM/SAED. To further characterize the postreduction Fe mineralogy in these experiments, TEM with EDX and SAED was used on the anoxic microcosms amended with added electron donor, both with and without AQDS, at time zero and 28 days. High-resolution TEM images of samples from the ferrihydrite amended oxic sediments showed an iron coating on the calcite-dominated sediments prior to reduction (Fig. 3b). For the bioreduced systems, after 28 days of incubation, individual spherical nanocrystallites in the range of 2 to 10 nm that showed enrichment in Fe and O via EDX and characteristic of biomagnetite were identified (Fig. 3e) (41). Further analysis of the nano crystallites via SAED confirmed the presence of magnetite in the bioreduced system (Fig. 3d) (42).

(iii) XAS/XMCD. Bioreduced minerals were also characterized using Fe $L_{2,3}$ edge spectroscopy to gain a greater understanding of the redox chemistry and potential reactivity of the newly formed iron mineral phase. Magnetite (Fe_3O_4) has a crystal structure consisting of Fe(II) and Fe(III) in octahedral and tetrahedral coordination with a stoichiometric ratio of 1:1:1 [$Fe(II)O_h$-$Fe(III)T_d$-$Fe(III)O_h$], i.e., one-third Fe(II). Prior to incubation, a dried ferrihydrite-amended Buxton sediment sample was analyzed, and the pronounced shoulder feature at 707.5 eV seen in the $L_{2,3}$ edge XAS in the starting material is characteristic of an Fe(III) mineral (Fig. 4, line a) (43). This characteristic Fe(III)-like feature became less prominent in samples taken from the system with electron donor added after the 28-day incubation (Fig. 4, line b) and from the system with an electron donor and AQDS (Fig. 4, line c), which is indicative of an increase in the amount of Fe(II) present. Both end member spectra are characteristic of a biogenic magnetite-like iron mineral phase (43, 44).

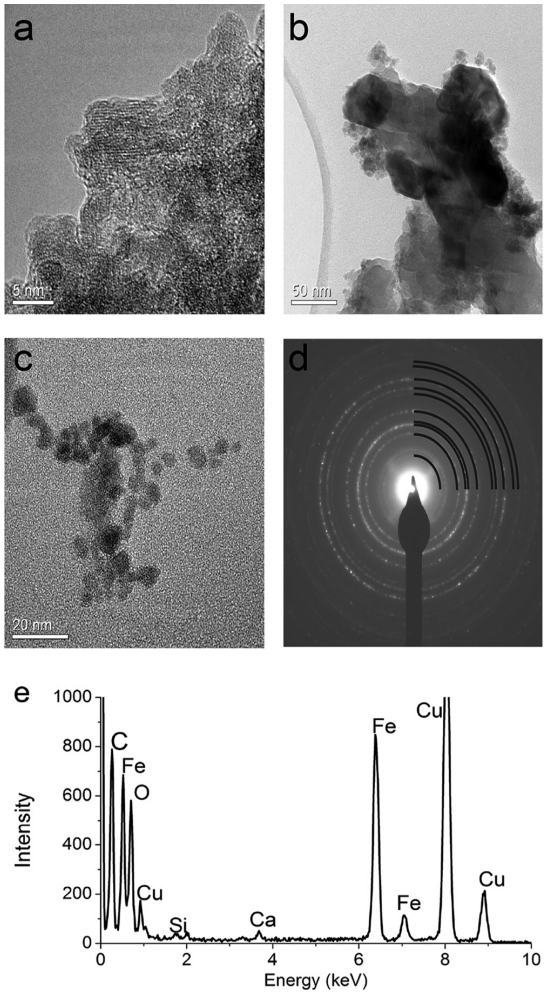

FIG 3 High-resolution TEM images of ferrihydrite prepared from anhydrous $FeCl_3$ (a), calcite within the Buxton sediment (b), and biogenic magnetite (c) in anoxic electron donor systems after 28 days of incubation, with the corresponding SAED pattern (d) and its energy dispersive X-ray analysis (e) on an individual crystallite. The SAED pattern has been overlaid with the standard pattern of magnetite, confirming its identity (42).

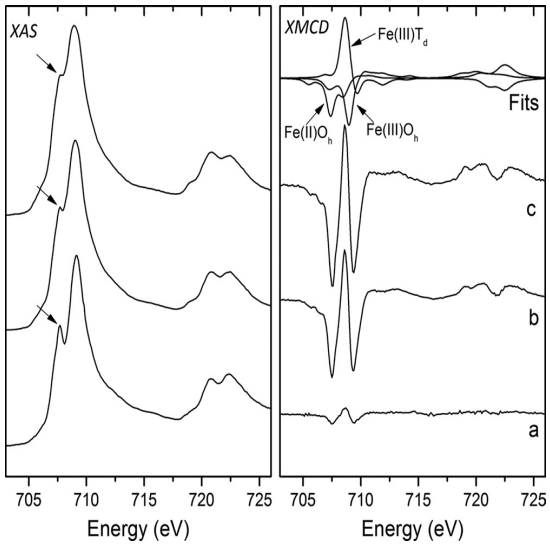

FIG 4 X-ray absorption spectra (XAS) and X-ray magnetic circular dichroism (XMCD) analyses of microcosms containing Buxton sediments incubated under a range of biogeochemical regimes: ferrihydrite-amended oxic sediment (line a); an anoxic, electron donor system after a 28-day incubation (line b); and an anoxic AQDS system after a 28-day incubation (line c). Arrows indicate shoulder features characteristic of an Fe(III)-rich compound, and the three main theoretical components of magnetite have been indicated on the XMCD spectrum (Fits). The intensities of the first three peaks at the L_3 edge XMCD are related to the relative amounts of Fe(III) d^6 O_h (negative), Fe(III) d^5 T_d (positive), and Fe(III) d^5 O_h (negative) present in the sample (43, 54).

The XMCD spectra obtained (Fig. 4) display the characteristic peaks corresponding to Fe(II)O_h, Fe(III)T_d, and Fe(III)O_h expected for magnetite at both the L_2 and the L_3 edges (43). The significant increase in amplitude of the XMCD signal observed for samples that were incubated with an electron donor corresponds to an increase in the magnetization of the sample, which is another confirmation that a magnetic material is produced by the microbial Fe(III) reduction. The XMCD were fitted to calculated spectra corresponding to Fe(II)O_h, Fe(III)T_d, and Fe(III)O_h to determine the stoichiometry of the materials (see Fig. S3 in the supplemental material). The results show that the magnetite produced in the absence of an electron shuttle is nonstoichiometric and contains less Fe(II) than expected (0.79:0.99:1.22); however, the magnetite produced with an electron shuttle (AQDS) is much closer to stoichiometry (0.96:0.95:1.08). In comparison, reference biogenic magnetite made using a pure culture of *Geobacter sulfurreducens* and exhibiting a particle size similar to those reported and produced under optimal conditions usually contains a very slight excess of Fe(II) (1.02:0.96:1.01) (45) with respect to the other cations in the crystal structure.

Microbial communities associated with Fe(III) reduction. A 16S rRNA gene clone library prepared from the nonincubated Buxton sediment (Fig. 5, column a) revealed a diverse community comprising of 40 different phylotypes from 80 sequences, dominated by two bacterial types from the phylogenetic group *Bacteroidetes*: designated CVCloAm3P11 (27.8%) and CVCloAm3Ph31 (12.5% of the clone library), both of which have been reported previously in Cabeço de Vide, a serpentinization-driven subterrestrial alka-

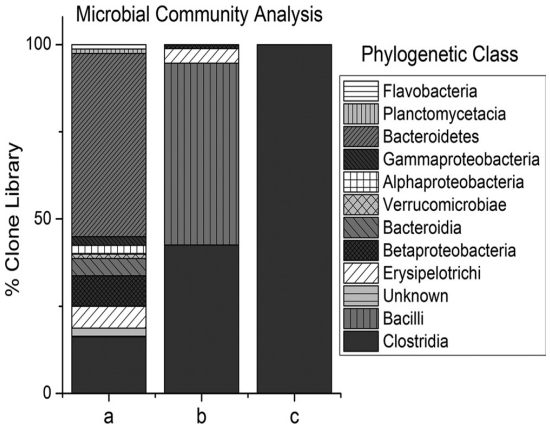

FIG 5 16S rRNA gene clone libraries of raw, nonincubated Buxton sediment (column a), sediment pellet taken from a progressive 28-day anoxic incubation (anoxic, electron donor system) (column b), and sediment pellet taken after a seventh progressive enrichment in defined medium containing 10 mM sodium lactate, 1 g of yeast extract $liter^{-1}$, and 50 mM ferrihydrite (column c).

line aquifer in Portugal (46). After the 28-day incubation in the anoxic system, a far less diverse community was seen, with nine distinct phylotypes from 94 sequences analyzed, primarily comprising organisms most closely related to *Enterococcus saccharolyticus* (97.2% sequence similarity, 48.9% of the clone library), *Clostridium ruminantium* (100% sequence similarity, 25.5% of the clone library), and *Clostridium* sp. strain 9B4 (99.6% sequence similarity, 16% of the clone library) (Fig. 5, column b). The dominance of clostridia in these systems may account for the production of propionic and butyric acids during incubation (see Fig. S1 in the supplemental material). Further enrichments in a defined medium adapted from (29), supplemented with ferrihydrite as the electron acceptor, and sodium lactate as the electron donor, simplified the community (Fig. 5, column c, and see Fig. S4 in the supplemental material), with close relatives to the following detected: *Alkaliphilus oremlandii* (47) (100% sequence similarity, 30.1% of the clone library), *Clostridium* sp. strain 9B4 (99.2% sequence similarity, 60.2% of the clone library), *Clostridium mangenotii* (99.4% sequence similarity, 8.6% of the clone library), and an uncultured bacterium (96% match, 1% of the clone library).

Interestingly, these organisms are Gram-positive bacteria, whom, unlike well-characterized Gram-negative Fe(III)-reducing bacteria (e.g., *Geobacter* and *Shewanella* species) (7, 48), lack an outer membrane that contains abundant *c*-type cytochromes, thought to play a pivotal role in Fe(III) reduction at ambient pH by allowing direct contact with Fe(III) oxides. Little is known about the mechanism of electron transfer to extracellular minerals in Gram-positive bacteria, although recent studies suggest this to be via a direct reductive mechanism governed by surface-localized multi-heme cytochromes (49, 50). Further work to gain an insight into these processes will be the focus of future studies, including exploring the potential of electron transfer between the cell-mineral interface, enhanced by humic materials which can act as electron shuttles.

Conclusions. Here, we show for the first time that indigenous microbial populations present in sediments from a high-pH legacy lime works have the ability to reduce solid-phase ferrihydrite to magnetite as the exclusive postreduction iron mineral phase, where the elevated pH in these systems appears to stabilize the biogenic magnetite formed, in agreement with reported pH/Eh stability field calculations (51). The role of organics has also been investigated and is required to stimulate maximal rates of Fe(III) reduction. Within geological disposal environments, organic carbon would be provided from chemical and biological degradation of cellulose materials common in the ILW. Microbial Fe(III) reduction could prove important in utilizing, as electron donors, compounds such as isosaccharinic acid that are formed chemically by alkali hydrolysis and can form strong mobile complexes with radionuclides. Fe(III) reducers could also potentially use hydrogen formed from steel corrosion as an electron donor, and these organisms could therefore act as a sink for reducing equivalents that could otherwise be destined for methanogenesis (4). Thus, microbial Fe(III) reduction, along with a cascade of other redox processes, has the potential to reduce gas production, which would lead to overpressurization and the loss of structural integrity of the emplaced multibarrier system. Since this could promote radionuclide releases, it is a major concern in long-term GDF operation. Interestingly, magnetite is a potent reductant of radionuclides with U(VI) (52), Tc(VII) (53), and Np(V) (23)—all potentially reactive to the biomineral at ambient pH. The findings presented here therefore have clear implications for the safety case that will have to be prepared to underpin the development of any potential GDF designs prior to regulator acceptance.

ACKNOWLEDGMENTS

We thank Thanos Rizoulis for help with data acquisition, Alastair Bewsher and Paul Lythgoe for ion analyses, and John Waters for XRD analysis (University of Manchester). We thank Mike Ward (University of Leeds) for TEM support. We also thank Elke Arenholz and Vicky Coker for XAS/XMCD data acquisition and analysis.

This study was supported by the BIGRAD consortium under the United Kingdom Natural Environmental Research Council (NE/H007768/1). J.R.L. acknowledges support from the Royal Society. The Advanced Light Source is supported by the Director, Office of Science, Office of Basic Energy Sciences, of the U.S. Department of Energy under contract DE-AC02-05CH11231.

REFERENCES

1. **Department for Environment Fisheries and Rural Affairs, Department for Business Enterprise and Regulatory Reform and Regulatory Reform, Welsh Assembly Government and Department of the Environment, Northern Ireland.** 2008. Managing radioactive waste safely: a framework for implementing geological disposal. DEFRA, London, United Kingdom.
2. **Rizoulis A, Steele HM, Morris K, Lloyd JR.** 2012. The potential impact of anaerobic microbial metabolism during the geological disposal of intermediate-level waste. Mineral. Mag. **76**:3261–3270.
3. **Glaus MA, Van Loon LR.** 2008. Degradation of cellulose under alkaline conditions: new insights from a 12-year degradation study. Environ. Sci. Technol. **42**:2906–2911.
4. **Libert M, Bildstein O, Esnault L, Jullien M, Sellier R.** 2011. Molecular hydrogen: an abundant energy source for bacterial activity in nuclear waste repositories. Phys. Chem. Earth A/B/C **36**:1616–1623.
5. **Lloyd JR.** 2003. Microbial reduction of metals and radionuclides. FEMS Microbiol. Rev. **27**:411–425.
6. **Lovley DR, Holmes DE, Nevin KP.** 2004. Dissimilatory Fe(III) and Mn(IV) reduction. Adv. Microb. Physiol. **49**:219–286.
7. **Lovley DR, Stolz JF, Nord GL, Phillips EJP.** 1987. Anaerobic production of magnetite by a dissimilatory iron-reducing microorganism. Nature **330**:252–254.
8. **Myers CR, Nealson KH.** 1988. Bacterial manganese reduction and growth with manganese oxide as the sole electron acceptor. Science **240**:1319–1321.
9. **Grant WD, Mwatha WE, Jones BE.** 1990. Alkaliphiles: ecology, diversity and applications. FEMS Microbiol. Lett. **75**:255–269.
10. **Gorlenko V, Tsapin A, Namsaraev Z, Teal T, Tourova T, Engler D, Mielke R, Nealson K.** 2004. *Anaerobranca californiensis* sp. nov., an anaerobic, alkalithermophilic, fermentative bacterium isolated from a hot spring on Mono Lake. Int. J. Syst. Evol. Microbiol. **54**:739–743.
11. **Pedersen K, Nilsson E, Arlinger J, Hallbeck L, O'Neill A.** 2004. Distribution, diversity, and activity of microorganisms in the hyper-alkaline spring waters of Maqarin in Jordan. Extremophiles **8**:151–164.
12. **Pollock J, Weber K, Lack J, Achenbach L, Mormile M, Coates J.** 2007. Alkaline iron(III) reduction by a novel alkaliphilic, halotolerant, *Bacillus* sp. isolated from salt flat sediments of Soap Lake. Appl. Microbiol. Biotechnol. **77**:927–934.
13. **Zavarzina D, Kolganova T, Boulygina E, Kostrikina N, Tourova T, Zavarzin G.** 2006. *Geoalkalibacter ferrihydriticus* gen. nov. sp. nov., the first alkaliphilic representative of the family *Geobacteraceae*, isolated from a soda lake. Microbiology **75**:673–682.
14. **Roh Y, Chon C-M, Moon J-W.** 2007. Metal reduction and biomineralization by an alkaliphilic metal-reducing bacterium, *Alkaliphilus metalliredigens* (QYMF). Geosci. J. **11**:415–423.
15. **Ye Q, Roh Y, Carroll SL, Blair B, Zhou J, Zhang CL, Fields MW.** 2004. Alkaline anaerobic respiration: isolation and characterization of a novel alkaliphilic and metal-reducing bacterium. Appl. Environ. Microbiol. **70**:5595–5602.
16. **Jones MN, Bryan ND.** 1998. Colloidal properties of humic substances. Adv. Colloid Interface Sci. **78**:1–48.

17. **Moulin V, Moulin C.** 1995. Fate of actinides in the presence of humic substances under conditions relevant to nuclear waste disposal. Appl. Geochem. **10**:573–580.
18. **Lovley DR, Coates JD, Blunt-Harris EL, Phillips EJP, Woodward JC.** 1996. Humic substances as electron acceptors for microbial respiration. Nature **382**:445–448.
19. **Scott DT, McKnight DM, Blunt-Harris EL, Kolesar SE, Lovley DR.** 1998. Quinone moieties act as electron acceptors in the reduction of humic substances by humics-reducing microorganisms. Environ. Sci. Technol. **32**:2984–2989.
20. **von Canstein H, Ogawa J, Shimizu S, Lloyd JR.** 2008. Secretion of flavins by *Shewanella* species and their role in extracellular electron transfer. Appl. Environ. Microbiol. **74**:615–623.
21. **Law GTW, Geissler A, Burke IT, Livens FR, Lloyd JR, McBeth JM, Morris K.** 2011. Uranium redox cycling in sediment and biomineral systems. Geomicrobiol. J. **28**:497–506.
22. **Geissler A, Law GTW, Boothman C, Morris K, Burke IT, Livens FR, Lloyd JR.** 2011. Microbial communities associated with the oxidation of iron and technetium in bioreduced sediments. Geomicrobiol. J. **28**:507–518.
23. **Law GTW, Geissler A, Lloyd JR, Livens FR, Boothman C, Begg JDC, Denecke A, Rothe M, Jr, Dardenne K, Burke IT, Charnock JM, Morris K.** 2010. Geomicrobiological redox cycling of the transuranic element neptunium. Environ. Sci. Technol. **44**:8924–8929.
24. **Lloyd JR, Sole VA, Van Praagh CVG, Lovley DR.** 2000. Direct and Fe(II)-mediated reduction of technetium by Fe(III)-reducing bacteria. Appl. Environ. Microbiol. **66**:3743–3749.
25. **Lloyd JR, Yong P, Macaskie LE.** 2000. Biological reduction and removal of Np(V) by two microorganisms. Environ. Sci. Technol. **34**:1297–1301.
26. **Morris K, Livens FR, Charnock JM, Burke IT, McBeth JM, Begg JDC, Boothman C, Lloyd JR.** 2008. An X-ray absorption study of the fate of technetium in reduced and reoxidized sediments and mineral phases. Appl. Geochem. **23**:603–617.
27. **Cornell RM, Schwertmann U.** 2003. The iron oxides: structure, properties, reactions, occurrences and uses, 2nd ed. Wiley-VCH, London, United Kingdom.
28. **Schwertmann U, Cornell RM.** 2000. General preparative techniques: iron oxides in the laboratory. Wiley-VCH Verlag GmbH, Berlin, Germany.
29. **Lovley DR, Phillips EJP.** 1988. Novel mode of microbial energy metabolism: organic carbon oxidation coupled to dissimilatory reduction of iron or manganese. Appl. Environ. Microbiol. **54**:1472–1480.
30. **van der Laan G, Kirkman IW.** 1992. The 2p absorption spectra of 3d transition metal compounds in tetrahedral and octahedral symmetry. J. Phys. Condens. Matter **4**:4189.
31. **Patterson AL.** 1939. The Scherrer formula for X-ray particle size determination. Phys. Rev. **56**:978–982.
32. **van der Laan G, Thole BT.** 1991. Strong magnetic X-ray dichroism in 2p absorption spectra of 3d transition-metal ions. Phys. Rev. B **43**:13401.
33. **Cardinale M, Brusetti L, Quatrini P, Borin S, Puglia AM, Rizzi A, Zanardini E, Sorlini C, Corselli C, Daffonchio D.** 2004. Comparison of different primer sets for use in automated ribosomal intergenic spacer analysis of complex bacterial communities. Appl. Environ. Microbiol. **70**:6147–6156.
34. **Lane DJ, Pace B, Olsen GJ, Stahl DA, Sogin ML, Pace NR.** 1985. Rapid determination of 16S rRNA sequences for phylogenetic analyses. Proc. Natl. Acad. Sci. U. S. A. **82**:6955–6959.
35. **Ashelford KE, Chuzhanova NA, Fry JC, Jones AJ, Weightman AJ.** 2006. New screening software shows that most recent large 16S rRNA gene clone libraries contain chimeras. Appl. Environ. Microbiol. **72**:5734–5741.
36. **Schloss PD, Westcott SL, Ryabin T, Hall JR, Hartmann M, Hollister EB, Lesniewski RA, Oakley BB, Parks DH, Robinson CJ, Sahl JW, Stres B, Thallinger GG, Van Horn DJ, Weber CF.** 2009. Introducing mothur: open-source, platform-independent, community-supported software for describing and comparing microbial communities. Appl. Environ. Microbiol. **75**:7537–7541.
37. **Cole JR, Wang Q, Cardenas E, Fish J, Chai B, Farris RJ, Kulam-Syed-Mohideen AS, McGarrell DM, Marsh T, Garrity GM, Tiedje JM.** 2009. The Ribosomal Database Project: improved alignments and new tools for rRNA analysis. Nucleic Acids Res. **37**:D141–D145.
38. **Van Loon GW, Duffy SJ.** 2000. Environmental chemistry, p 430–485. Oxford University Press, Oxford, England.
39. **Roden EE, Kappler A, Bauer I, Jiang J, Paul A, Stoesser R, Konishi H, Xu H.** 2010. Extracellular electron transfer through microbial reduction of solid-phase humic substances. Nat. Geosci. **3**:417–421.
40. **Burke IT, Mortimer RJG, Palaniyandi S, Whittleston RA, Lockwood CL, Ashley DJ, Stewart DI.** 2012. Biogeochemical reduction processes in a hyper-alkaline leachate affected soil profile. Geomicrobiol. J. **29**:769–779.
41. **Cutting RS, Coker VS, Fellowes JW, Lloyd JR, Vaughan DJ.** 2009. Mineralogical and morphological constraints on the reduction of Fe(III) minerals by *Geobacter sulfurreducens*. Geochim. Cosmochim. Acta **73**:4004–4022.
42. **Wechsler BA, Lindsley DH, Prewitt CT.** 1984. Crystal structure and cation distribution in titanomagnetites ($Fe_{3-x}Ti_xO_4$). Am. Mineral. **69**:754–770.
43. **Pattrick RAD, van der Laan G, Henderson CMB, Kuiper P, Dudzik E, Vaughan DJ.** 2002. Cation site occupancy in spinel ferrites studied by X-ray magnetic circular dichroism: developing a method for mineralogists. Eur. J. Mineral. **14**:1095–1102.
44. **Coker VS, Gault AG, Pearce CI, van der Laan G, Telling ND, Charnock JM, Polya DA, Lloyd JR.** 2006. XAS and XMCD evidence for species-dependent partitioning of arsenic during microbial reduction of ferrihydrite to magnetite. Environ. Sci. Technol. **40**:7745–7750.
45. **Byrne JM, Telling ND, Coker VS, Pattrick RAD, van der Laan G, Arenholz E, Tuna F, Lloyd JR.** 2011. Control of nanoparticle size, reactivity, and magnetic properties during the bioproduction of magnetite by *Geobacter sulfurreducens*. Nanotechnology **22**:455709.
46. **Tiago I, Veríssimo A.** 29 November 2012. Microbial and functional diversity of a subterrestrial high pH groundwater associated with serpentinization. Environ. Microbiol. doi:10.1111/1462-2920.12034.
47. **Fisher E, Dawson AM, Polshyna G, Lisak J, Crable B, Perera E, Ranganathan M, Thangavelu M, Basu P, Stolz JF.** 2008. Transformation of inorganic and organic arsenic by *Alkaliphilus oremlandii* sp. nov. strain OhILAs. Ann. N. Y. Acad. Sci. **1125**:230–241.
48. **Nealson KH, Myers CR.** 1992. Microbial reduction of manganese and iron: new approaches to carbon cycling. Appl. Environ. Microbiol. **58**:439–443.
49. **Carlson HK, Iavarone AT, Gorur A, Yeo BS, Tran R, Melnyk RA, Mathies RA, Auer M, Coates JD.** 2012. Surface multiheme *c*-type cytochromes from *Thermincola potens* and implications for respiratory metal reduction by Gram-positive bacteria. Proc. Natl. Acad. Sci. U. S. A. **109**:1702–1707.
50. **Wrighton KC, Thrash JC, Melnyk RA, Bigi JP, Byrne-Bailey KG, Remis JP, Schichnes D, Auer M, Chang CJ, Coates JD.** 2011. Evidence for direct electron transfer by a Gram-positive bacterium isolated from a microbial fuel cell. Appl. Environ. Microbiol. **77**:7633–7639.
51. **Mills AL, Bell PE, Herman JS.** 1987. Biogeochemical conditions favoring magnetite formation during anaerobic iron reduction. Appl. Environ. Microbiol. **53**:2610–2616.
52. **Latta DE, Gorski CA, Boyanov MI, O'Loughlin EJ, Kemner KM, Scherer MM.** 2011. Influence of magnetite stoichiometry on U(VI) reduction. Environ. Sci. Technol. **46**:778–786.
53. **McBeth JM, Lloyd JR, Law GTW, Livens FR, Burke IT, Morris K.** 2011. Redox interactions of technetium with iron-bearing minerals. Mineral. Mag. **75**:2419–2430.
54. **Coker VS, Pearce CI, Lang C, van der Laan G, Pattrick RAD, Telling ND, Schuler D, Arenholz E, Lloyd JR.** 2007. Cation site occupancy of biogenic magnetite compared to polygenic ferrite spinels determined by X-ray magnetic circular dichroism. Eur. J. Mineral. **19**:707–716.

Supporting Information

Microbial reduction of Fe(III) under alkaline conditions relevant to geological disposal

Adam J. Williamson, Katherine Morris, Sam Shaw, James M. Byrne[*], Christopher Boothman[1] and Jonathan R. Lloyd*[#]

Research Centre for Radwaste and Decommissioning and Williamson Research Centre for Molecular Environmental Science, School of Earth, Atmospheric and Environmental Sciences. The University of Manchester, Manchester, M13 9PL, U.K.

*Current address: Zentrum für Angewandte Geowissenschaften, Geomikrobiologie, Universität Tübingen, Sigwartstrasse 10, 72076, Tübingen

#Corresponding author email: jon.lloyd@manchester.ac.uk.

Time(days)	0	3	7	14	28
Average lactate conc (mM)	10.35	9.96	5.83	0.83	0.00
Average acetic acid conc (mM)	0.00	3.77	19.37	26.87	30.53
Average formic acid conc (mM)	0.00	1.81	3.19	1.09	0.00
Average propionic acid conc (mM)	0.00	0.58	4.86	8.05	8.95
Average n-butyric acid conc (mM)	0.00	0.76	3.06	2.27	2.35

Supplementary Figure S1: Ion chromatographic analysis of organic acids of supernatant samples taken from the electron donor amended system over the 28 day incubation period.

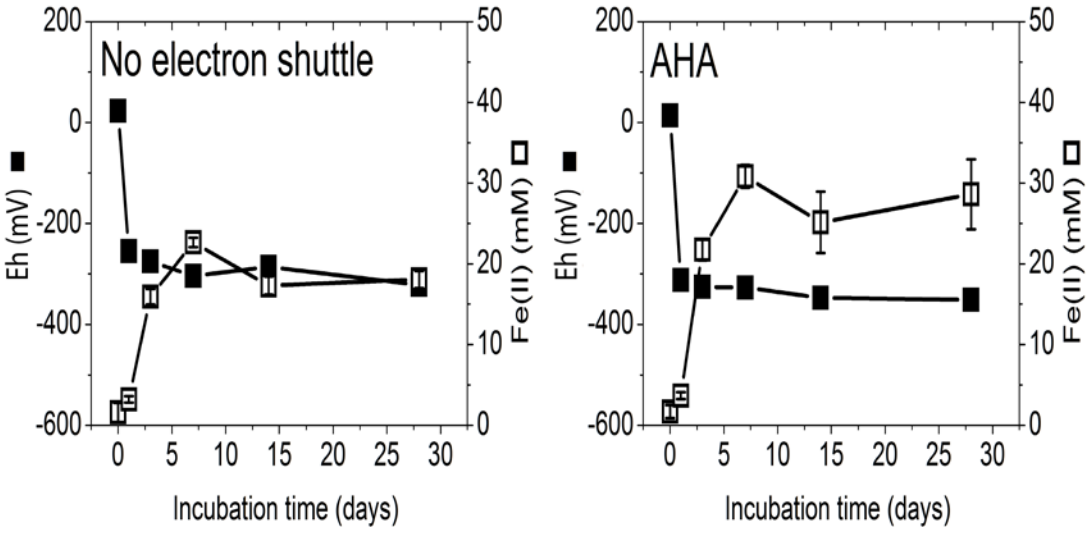

Supplementary Figure S2: 0.5 N HCl extractable Fe(II) concentration (Fe(II); ▫) and reduction potential (Eh; ▪) in microcosms containing Buxton sediments supplemented with 120 mM ferrihydrite incubated without electron shuttle (left) and with Aldrich humic acid (AHA) (right).

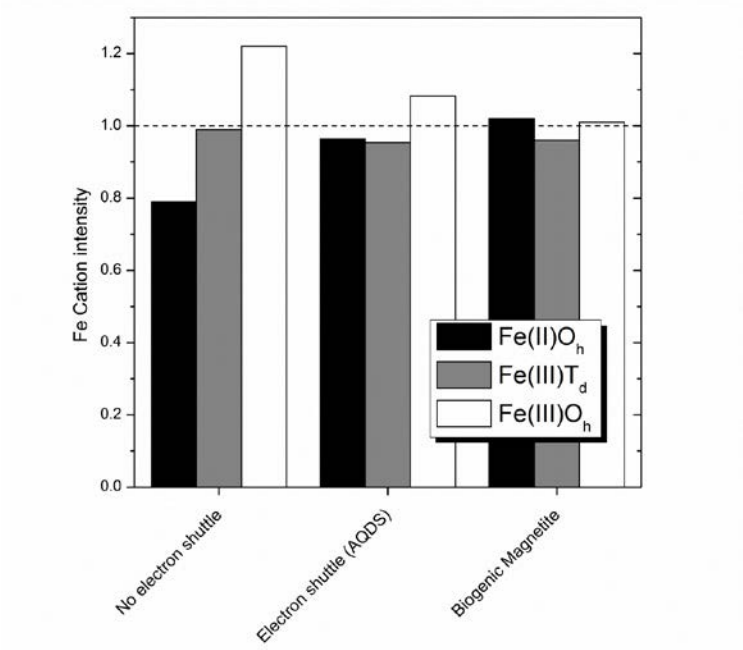

Supplementary Figure S3: Fe(II) and Fe(III) cation occupancies in O_h and T_d sites were determined using by fitting XMCD spectra to atomic multiplet calculations (1, 2, 3) for incubations with electron donor (lactate) but without electron shuttle and incubations with electron donor (lactate) and electron shuttle (AQDS). Samples are compared to the cation occupancy of biogenic magnetite of similar particle size produced under optimum conditions. The dashed line indicates stoichiometric magnetite with a cation site occupancy of (1:1:1 Fe(II)O_h:Fe(III)T_d:Fe(III)O_h).

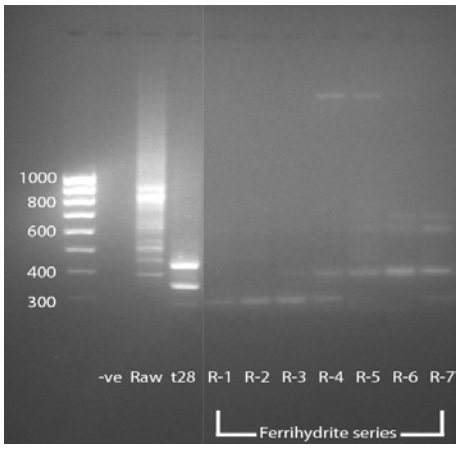

Supplementary Figure S4: Ribosomal Intergenic Spacer Analysis of raw, non-incubated Buxton sediment (Raw), following a 28 day incubation (t28) and consecutive enrichments in defined medium with 50 mM ferrihydrite as a source of electron acceptor (R-1 to R-7).

1. **van der Laan G, Kirkman IW.** 1992. The 2p absorption spectra of 3d transition metal compounds in tetrahedral and octahedral symmetry. Journal of Physics: Condensed Matter **4:**4189.

2. **Patterson AL.** 1939. The Scherrer Formula for X-Ray Particle Size Determination. Phys. Rev. **56:**978-982.

3. **van der Laan G, Thole BT.** 1991. Strong magnetic X-ray dichroism in 2p absorption spectra of 3d transition-metal ions. Physical Review B **43:**13401.

5

Microbial Reduction of U(VI) under Alkaline Conditions; Implications for Radioactive Waste Geodisposal

Paper currently in review in Environmental Science and Technology

5. Microbial Reduction of U(VI) under Alkaline Conditions; Implications for Radioactive Waste Geodisposal

*Adam J. Williamson,[†] Katherine Morris,[†] John Charnock, [†] Gareth T.W. Law,[‡] Athanasios Rizoulis[†] and Jonathan R. Lloyd [† *]*

† Research Centre for Radwaste Disposal and Williamson Research Centre for Molecular Environmental Science, School of Earth, Atmospheric and Environmental Sciences, The University of Manchester, Manchester, M13 9PL, UK.

‡ Centre for Radiochemistry Research and Research Centre for Radwaste Disposal, School of Chemistry, The University of Manchester, Manchester, M13 9PL, UK.

* email: jon.lloyd@manchester.ac.uk

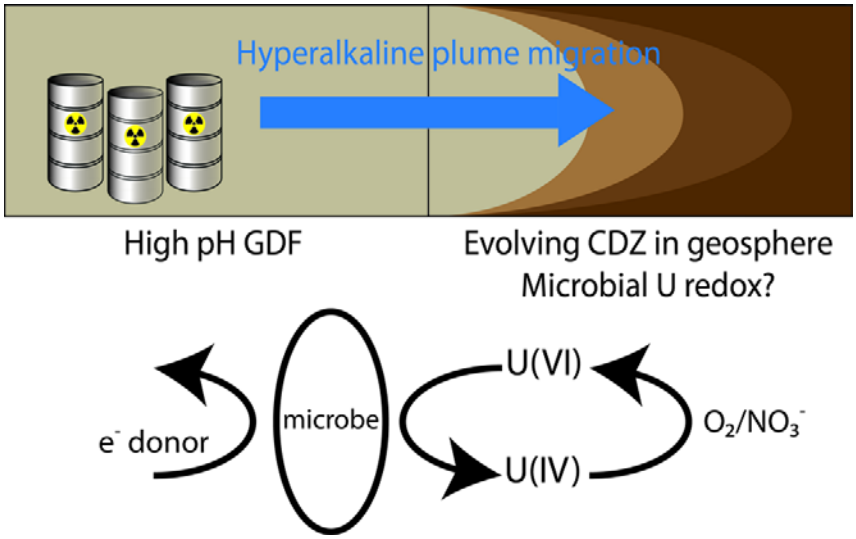

5.1. Abstract

Although there is consensus that microorganisms significantly influence uranium speciation and mobility in the subsurface under circumneutral conditions, no work has yet explored microbiologically-mediated U(VI) redox cycling under alkaline conditions relevant to the geological disposal of cementitious intermediate level radioactive waste. Here, we describe microcosm experiments that explore U(VI) biogeochemistry at pH 10 using sediments from a legacy lime working site, stimulated with an added electron donor, and incubated in the presence and absence of added Fe(III) as ferrihydrite. In systems without added Fe(III), partial U(VI) reduction occurred, forming a U(IV)-bearing non-uraninite phase which underwent reoxidation in the presence of air (O_2) and nitrate. By contrast, in the presence of added Fe(III), U(VI) was first removed from solution by sorption to the Fe(III) mineral, followed by bioreduction to a uraninite like phase, which also underwent air (O_2) and nitrate reoxidation. To explore further the mechanisms of reduction, anthraquinone-2,6-disulphonate (AQDS), an extracellular electron shuttle, was added to selected experiments. XAS and geochemical analyses suggested that AQDS enhanced U(VI) reduction. Microbial ecology analysis by 16S rRNA gene amplicon pyrosequencing showed that Gram-positive bacteria belonging to Firmicutes and Bacteroidetes phyla dominated in the post-reduction sediments. These data provide the first insights into uranium biogeochemistry at high pH and have significant implications for the long-term fate of uranium in geological disposal scenarios.

Keywords: Uranium, metal reduction, alkaliphiles, radioactive waste, geodisposal

5.2. Introduction

Over the last 50+ years, civilian and military nuclear programmes have led to a substantial legacy of intermediate level radioactive wastes, which contain uranium as the most significant radionuclide by mass. In the UK, Government policy is that these materials will be disposed of in a deep geological disposal facility, and this position is echoed in many other countries [1]. The environmental behaviour of uranium is controlled by a combination of complexation, precipitation, redox and adsorption processes. Under oxidising conditions, U(VI) predominates as the uranyl ion (UO_2^{2+}), which is relatively soluble as anionic U(VI) carbonate species (e.g. $[UO_2(CO_3)_2]^{2-}$ (aq)) [2]. It is important to note that U(VI) is also able to interact with sediments and minerals such as ferrihydrite *via* sorption and/or incorporation, controlled by groundwater chemistry and sediment mineralogy. Under reducing conditions, poorly soluble U(IV) species dominate. The

differences in solubility between relatively soluble U(VI) and poorly soluble U(IV) have led to a substantial body of work examining the behaviour of U(VI) when microbially mediated reduction is promoted using biostimulation approaches [3–5] . Biostimulation involves the addition of an electron donor such as acetate to the sub-surface, which promotes the development of anoxia and precipitation of U(IV). Under biostimulation conditions at neutral pH, both microbially-mediated and abiotic U(VI) reduction mechanisms are reported [6–8]. Here, the development of metal- and sulphate-reducing conditions is important, with enzymatic reduction of U(VI) likely to dominate, and both soluble and sorbed U(VI) susceptible to bioreduction [3,5]. Most studies have focussed on systems where U(IV) forms uraninite-like phases [4,5], although more recent work suggests that "non-uraninite" U(IV) bioreduction end products can also accumulate in selected pure culture experiments, and natural and engineered sediment systems [8,9]. The non-uraninite U(IV) is thought to be polymeric and coordinated to carboxyl and/or phosphoryl groups on biomass [8]. The reoxidation behaviour of U(IV) species has also been reasonably well studied under circumneutral conditions, with microcosm experiments showing fast reoxidation, but with column and field observations suggesting slower reoxidation rates [10,11]. Ca^{2+} and Mn^{2+} are also thought to influence long term stability of U(IV) [12,13].

Understanding the biogeochemical cycling of uranium is key to predicting its speciation and fate in the shallow subsurface; however, there have been few studies focussed on radionuclide biogeochemistry under alkaline conditions relevant to geological disposal where cementitious materials will be used. For example, in many geodisposal concepts, intermediate level wastes (ILW) will be grouted in steel drums and cement will be used for engineering or backfill purposes [1,14]. After ILW disposal, groundwater ingress through the engineered facility is expected, resulting in a hyperalkaline plume from the cementitious materials into the surrounding host rock. This will form a persistent, high pH, chemically disturbed zone over timescales of 10^5 - 10^6 years that will evolve from pH >13 to pH 10 over time [15]. The potential for microbial processes stimulated by electron donors (e.g. organics from the degradation of cellulose in the ILW) released into the deep subsurface from the Geological Disposal Facility (GDF), and associated metal reduction processes, is being increasingly recognized [16–19]. This work addresses the paucity of data surrounding such potential processes, focusing on uranium redox cycling in a high pH, biogeochemically active system. We have used model sediments from an alkaline legacy lime workings site in Buxton, UK, to characterise the impact of microbial processes on the biogeochemistry of uranium and associated mineralogical

phases at pH 10. Two model systems have been used. In the first, a waste-margin sediment was used to explore the biogeochemical fate of U(VI) in carbonate dominated, alkaline systems. In the second, the same sediment was enriched with Fe(III) (as ferrihydrite) to address the impact of stimulated microbial Fe(III) reduction on the behaviour of uranium. This is important, as iron will be a significant component of ILW and the wider GDF environment, and Fe(III) reduction is a potential control on uranium solubility. Anthraquinone-2,6- disulphonate (AQDS), an extracellular electron shuttle and humic analogue, was also added to key bioreduction experiments to further explore the mechanisms of U(VI)- and Fe(III)-reduction in these high pH systems where metal solubility is expected to be low. Subsequent experiments examined reoxidation scenarios to assess the potential impact of reaction with oxidants such as nitrate [20] in the waste forms, and the potential for ingress of oxygenated groundwater [21].

5.3. Materials and methods

5.3.1. Sediment collection and storage

Near surface sediment (~ 10 cm depth) was collected at the waste margins of the legacy lime workings ponds of an old lime working site in Buxton, UK [17]. This is an alkaline impacted site where CaO has been weathered over several decades, so that the indigenous microbial population is well developed [17]. Sediments and surface waters were transferred into sterile containers and stored at 4 °C in darkness prior to use. Experiments were started within one month of sampling.

5.3.2. Uranium bioreduction microcosm experiments.

To determine the fate of U(VI) under anoxic, alkaline conditions, microcosms were prepared in triplicate; sediments were slurried with pH 11.8 surface waters, the initial pH adjusted to 10 with 1 M HCl and the sediment: solution ratio was set at 1:10. Anaerobic microbial processes were stimulated with the addition of 10 mM sodium lactate and 1 g L^{-1} yeast extract similar to recent work [17]. Two systems were established: a Buxton sediment and surface water incubation with *no added Fe(III)*, and a *with added Fe(III)* system where 30 mM ferrihydrite was added. Two additional experiments were established with a soluble electron shuttle added to explore the role of extracellular Fe(III) and U(VI) bioreduction. Here, 100 µM of AQDS was added to microcosms with and without added Fe(III). Uranium as U(VI) (UO_2Cl_2 (aq)) was then added to all microcosms and experimental controls to a final concentration of 420 µM. The bottles were then crimp sealed with thick butyl rubber stoppers and incubated at 20 °C in the dark. Sample manipulations were performed using aseptic technique under anoxic

conditions as appropriate. During incubation, the pH of the microcosms dropped during the first fortnight of the experiment, and the pH adjusted to pH 10 using deoxygenated, sterile 2 M NaOH as necessary. Bioreduction experiments were sampled periodically to monitor for biogeochemical changes, and after 210 days samples were removed and stored under anoxic conditions at –80 °C for microbiological (DNA) and X-ray Absorption Spectroscopy (XAS) analysis.

5.3.3. Uranium reoxidation experiments.

For air reoxidation experiments, microbially reduced sediments were transferred into sterile, conical flasks (solid:solution ratio of 1:10) on an orbital shaker at 125 rpm at 20 °C. For nitrate reoxidation experiments, microbially reduced sediment microcosms were amended with $NaNO_3$ to a final concentration of 30 mM NO_3^-. Reoxidation experiments were sampled periodically to monitor for biogeochemical changes, and after 14 days samples were removed and stored under anoxic conditions at –80 °C for microbiological (DNA) and XAS analysis.

5.3.4. Geochemical analyses.

Sample slurries were analysed for pH and Eh using a calibrated Denver Instrument Digital Meter and electrodes. To assess the bulk Fe-content of the sediment, aqua-regia digests were performed. Biogenic Fe(II) and total bioavailable Fe were assessed by 0.5 N HCl extraction *via* the ferrozine colorimetric assay on a sub-sample of sediment slurry [22]. Samples were then centrifuged (5 minutes at 10,500 *g*) and the supernatant was analysed for total U using an ICP-MS (Agilent 7500cx). In addition, in selected samples, a colorimetric assay for U(VI) was used to assess U speciation in solution [23,24]. Inorganic anions (NO_3^-, NO_2^- and SO_4^{2-}) were analysed using a Dionex ICS5000 ion chromatograph. Colorimetric assays were performed on a Jenway 6715 spectrometer and typically, calibrations had $R^2 > 0.99$.

5.3.5. Uranium L_{III}-edge XAS analysis.

At the end of the bioreduction and reoxidation experiments, moist sediment pellets were obtained by centrifugation for XAS analysis. The resulting wet pastes (typically 0.5 g of sediment with < 50% water content) were individually mounted under appropriate atmospheric conditions in airtight XAS sample cells. The samples were then stored under Ar at - 80 °C until XAS analysis which was conducted at the Diamond Light Source, Didcot, Oxford, UK. Here, U L_{III}-edge spectra were collected at room temperature on beamline B18 in fluorescence mode using a 9-element Ge detector [25].

Standard spectra were also collected in transmission mode for U(VI) (as schoepite) and U(IV) (as uraninite). XANES spectra from all samples were calibrated with Y foil, background subtracted, and normalised for drift to a standardised E_0 position. Initially, linear combination fitting between an oxic U(VI) bearing sample (the *oxic with added Fe(III)* XANES spectrum) and a reduced U(IV) bearing sample (the *with added Fe(III) + AQDS* reduced XANES spectrum) was undertaken to gain insight into the relative extent of reduction of U(VI) to U(IV) using ATHENA [26,27]. Latterly, background subtraction, data normalisation, and fitting of the EXAFS spectra were performed using Pyspline [28] and DLEXCURV using full curve wave theory [29]. Shells were only included in the final fit if they improved the fit by > 5 % and were statistically significant as shown by the reduced X^2 test.

5.3.6. 16S rRNA gene amplicon pyrosequencing and data analysis.

Bacterial community structure was examined in the bulk Buxton sediment and also in the *no added Fe(III)*, and *with added Fe(III)* microcosms at incubation end points. Samples from the subsequent nitrate reoxidation experiments were also characterised after 14 days of reoxidation. DNA was isolated from ~ 0.2 g of sediment using the MoBio PowerSoil™ DNA Isolation Kit (MoBio Laboratories, Inc., Carlsbad, CA, USA). PCR for amplicon pyrosequencing was performed using tagged fusion bacterial primers 27F [30] and 338R [31], targeting the V1-V2 hypervariable region of the bacterial 16S rRNA gene (see Supporting Information). The pyrosequencing run was performed at The University of Manchester sequencing facility, using a Roche 454 Life Sciences GS Junior system. The 454 pyrosequencing reads were analysed using Qiime 1.6.0 release [32], and de-noising and chimera removal was performed in Qiime during OTU picking (at 97% sequence similarity) with usearch [33]. Taxonomic classification of all reads was performed in Qiime using the Ribosomal Database Project (RDP) at 80 % confidence threshold [34], while the closest GenBank match for the OTUs that contained the highest number of reads (the representative sequence for each OTU was used) was identified by Blastn nucleotide search. In addition, rarefaction curves were computed by Qiime. The raw 38,623 pyrosequencing reads of this study have been deposited in the NCBI Sequence Read Archive (SRA) under accession number SRP036830 (BioProject ID: PRJNA236650).

5.4. Results and discussion

5.4.1. Sediment bioreduction experiments.

To explore the biogeochemistry of uranium under anoxic conditions at pH 10, microcosms were constructed using calcite dominated sediments and groundwaters from a high pH lime workings site in the UK [17] (Supporting Information Table 1). There was a progression of microbial redox processes in both the *no added Fe(III)* and *with added Fe(III)* microcosms which were maintained at pH 10 (Figure 1A and B)). For the *no added Fe(III)* system, nitrate concentrations dropped rapidly after incubation, and were below the limit of detection from 3 days. This was followed by the subsequent ingrowth of 0.5 N HCl extractable Fe(II) from day 3 onwards due to microbially mediated Fe(III) reduction. In addition, the Eh fell from +69 ± 10 mV at the start of the experiment, to -310 ± 10 mV after 28 days (Figure 1A). Over longer-term 210 day incubations, the sulfate concentration remained constant (74 ± 1 µM), confirming that microbial sulfate reduction did not occur at pH 10, similar to observations in other alkaline, anoxic experiments [16,17]. In the *with added Fe(III)* experiments, rapid development of reducing conditions also occurred, with nitrate removal and Fe(II) ingrowth occurring by day 3 and a drop in Eh from +60 ± 6 mV at t=0 to -345 ± 17 mV by 28 days accompanied by significant levels of Fe(III) reduction with 0.5 N HCl extractable Fe(II) at 7.3 ± 1.2 mM (Figure 1B). At 210 days, there was a decrease in 0.5 N extractable Fe(II), consistent with the formation of (bio)magnetite under high pH conditions [17]. Again, sulfate concentrations remained constant throughout incubation, confirming that no sulfate reduction occurred at high pH. In the *no added Fe(III) + AQDS* experiment, AQDS addition had little overall impact on the rate of Fe(III)-reduction (Figure 1C) whilst for the *with added Fe(III) + AQDS* experiment, there was an increased rate and extent of Fe(III)-reduction compared to the system without the electron shuttle (Figure 1D) [17].

5.4.2. Uranium fate during bioreduction – *no added Fe(III).*

To investigate uranium behaviour in the Buxton sediment microcosms, U(VI) was incubated with a range of sediment treatments and controls. In the *no added Fe(III)* microcosms, 45.5 ± 2.8 % of the initial U-spike remained in solution after 1 hour (Figure 1A). The concentration of uranium in solution then fluctuated over the first fortnight and thereafter trended downwards to a final value of 35.1 ± 1.3 % of the original spike by day 210 (Figure 1A). In addition, a spectrophotometric U(VI) assay was run on early-, mid- and end- time point samples and this confirmed that soluble uranium in these experiments was U(VI). In order to explore the solid-phase speciation and behaviour of uranium further in these heterogeneous systems, uranium L_{III}-edge

XANES and EXAFS spectra were collected on selected samples. The *no added Fe(III)* sample at 210 days showed a XANES spectrum intermediate between the oxic and reduced end-members which suggested that partial reduction of sediment-associated U(VI) had occurred (Supporting Information Figure 1). Linear combination fitting of the XANES spectra between the oxic and reduced end-members suggested an approximately 50 : 50 % contribution from oxic and reduced end-member spectra respectively (Supporting Information Table 2). The corresponding EXAFS spectra were consistent with this interpretation and could best be fitted with an approximate 60 : 40 % mixture of U(VI) (first shell of 2 axial O (O_{ax}) at 1.80 Å) and U(IV) (first shell of 8 equatorial O (O_{eq}) at 2.4 Å), with a best fit of 1.3 O_{ax} at 1.79 Å and 6 O_{eq} at 2.41 Å. Interestingly, addition of a shell of 1.7 C backscatterers at 2.9 Å significantly improved the fit and this is consistent with the U(VI) being partially speciated as a U(VI)-carbonate sorbate in this carbonate dominated system (Figure 2; Supporting Information Table 3). In the *no added Fe(III) + AQDS* system, U(VI) removal from solution was broadly similar to the experiment without AQDS, but with only 16.4 ± 1.3 % remaining in solution at 210 days, modestly lower than in the parallel experiment without an electron shuttle (Figure 1C). Linear combination fitting of the XANES spectra with the oxic and reduced end members suggested an approximate 25 % U(VI) : 75 % U(IV) mix in the sample (Supporting Information Table 2). Again, the EXAFS data were consistent with this interpretation, and the spectra could be modelled with a best fit of approximately 45 % U(VI) and 55 % U(IV) (0.9 O_{ax} at 1.8 Å and 4 O_{eq} at 2.38 Å; Figure 2, Supporting Information Table 3). Interestingly, in both the *no added Fe(III),* and *no added Fe(III) + AQDS* experiments, the U(IV) component of the spectrum did not display the characteristic uraninite, U-O-U backscatterer at 3.8 Å (Figure 2 B and C). The absence of this distinctive feature suggests that a non-uraninite U(IV) phase may dominate in this high carbonate, high pH system.

5.4.3. Uranium fate during bioreduction – *with added Fe(III).*

In the microbially active *with added Fe(III)* microcosms, almost complete sorption of U(VI) occurred by 1 hour with 95.1 ± 0.2 % removal to sediments. Thereafter, during bioreduction the uranium concentrations were variable for the first fortnight and then remained low over the remainder of the experiment, with the biogeochemical changes in the system having little effect on the U-solubility (Figure 1B). Initial sorption at pH 10 was enhanced compared to the *no added Fe(III)* system and was likely dominated by reaction of U(VI) with ferrihydrite [35]. In the *with added Fe(III) + AQDS* system, the

addition of the soluble electron shuttle had little effect on uranium solubility which showed strong sorption to ferrihydrite in the first hour (Figure 1D). Again, solid phase U-speciation was examined using XAS on select samples. In the *with added Fe(III)* system at 210 days, the XANES spectra showed reduction to U(IV) (Supporting Information Figure 1). Further linear combination fitting of the XANES for this sample, using the oxic and reduced end members, suggested U(IV) was predominantly present in the sample (approximately 85 % U(IV); Supporting Information Table 2). The corresponding EXAFS spectrum was consistent with this, and could best be modelled with a modest contribution from U(VI) of approximately 10 % but dominated by a U(IV) like coordination environment. For the U(IV) EXAFS modelling, the modelled U(IV)-O coordination number was below the stoichiometric UO_2 value of 8 O_{eq} at 2.37 Å [36] and the best fit was 3.8 O_{eq} at 2.38 Å suggesting undercoordination and/or artefacts associated with self-absorption of the sample during data acquisition. In addition, fitting of an additional shell of 1.1 U backscatters at 3.87 Å (characteristic of the U-O-U coordination of 12 U at 3.87 Å seen in nano-particulate uraninite) significantly improved the fit and suggested a uraninite like contribution to the spectrum ([35]; Figure 2; Supporting Information Table 3). In the *with added Fe(III) + AQDS* system the XANES spectrum again showed significant reduction to U(IV) and this sample was used as the reduced end member for linear combination fitting. Interestingly, the EXAFS spectrum could again be best fitted with only a modest U(VI) contribution of ~ 10 %, with the U(IV) fitted as an under-coordinated uraninite like phase (Supporting Information Table 3). Finally, a sterilized (autoclaved) *with added Fe(III)* sediment which had previously undergone significant Fe(III)-reduction to bio-magnetite as the dominant end product, was reacted with U(VI) for 7 days to examine pathways for abiotic versus enzymatic reduction. Here, the sterile, reduced sediment showed only modest reactivity to U(VI) with 24 ± 2 % of U(VI) removed to the solid phase. Analysis of a XANES spectrum for this sample showed a U(VI) like coordination environment and linear combination fitting between U(VI) and U(IV) standards showed, within error, that all sorbed uranium was present as U(VI) (Supporting Information Table 2). This confirmed that pathways for abiotic reduction of U(VI) in these high pH, calcium carbonate / magnetite dominated systems were minimal.

5.4.4. Reoxidation experiments.

A range of nitrate and air reoxidation experiments were performed to investigate the stability of uranium in the bioreduced sediments. Air reoxidation of the *no added*

Fe(III) experiment showed significant reoxidation of Fe(II) to Fe(III) by 14 days with complete remobilisation of uranium to solution as U(VI) (Figure 1A). Interestingly, the reoxidised sediment showed less affinity for U(VI) than the original material. This is presumably because of gross changes in solution chemistry and mineralogy brought on by bioreduction similar to previous observations [10,37,38]. For the air reoxidation of the *with added Fe(III)* sediments, again there was significant Fe(II) reoxidation and complete U(VI) remobilisation by 14 days, with the reoxidised sediment showing little affinity for U(VI) in stark contrast to the original experiment where >95 % removal was seen by 1 hour. For these samples, oxidative remobilisation was essentially complete such that XAS was not possible on the reoxidised sediments.

With nitrate reoxidation, the *no added Fe(III)* system showed significant denitrification at 14 days. At this point, complete Fe(II) oxidation had occurred, the Eh had risen from - 94 mV to + 10 mV and soluble U(VI) increased from 151 μM at the start of the reoxidation to 270 μM at the end point (Figure 1E). In the *with added Fe(III)* experiment significant (93 %) denitrification of the 30 mM nitrate occurred coupled to a rise in Eh to - 70 mV. Complete reoxidation of Fe(II) had occurred at 14 days. Remobilisation of uranium to solution was significant with ~50 % present in solution as U(VI) at 14 days, and again highlighting that the reoxidised sediment had a significantly lower affinity for U(VI) than the original material. Interestingly, the nitrate reoxidation experiments showed less remobilisation of uranium to solution compared to the parallel air reoxidation experiments, and XAS analysis on the sediments was possible at these higher uranium loadings. In the *no added Fe(III)* nitrate reoxidised system, the XANES showed essentially complete reoxidation to U(VI) (Supporting Information Table 2) and the EXAFS data could be modelled as U(VI) carbonate with 2 O_{ax} at 1.80 Å, 5.6 O_{eq} at 2.43 Å and 2.1 C at 3.00 Å, confirming complete reoxidation of the sample (Figure 2; Supporting Information Table 3). In the *with added Fe(III) system*, the nitrate reoxidation XANES spectrum was intermediate between U(VI) and U(IV) and linear combination fitting suggested approximately 50% U(IV) remained at the experiment end point, despite essentially complete Fe(III)-reoxidation (Supporting Information Figure 2). The *with added Fe(III)* nitrate reoxidised EXAFS spectrum was complex, requiring several shells of backscatterers to achieve a good fit. These consisted of 0.5 O_{ax} at 1.73, 2 short O_{eq} at 2.21 and 2 O_{eq} at 2.43 Å, and with the axial oxygen occupancy implying an approximate 25% U(VI) contribution (Figure 2). The strong signal in the EXAFS at 3.24 Å could be fitted with 1 Fe backscatterer, which

significantly improved the fit and may suggest that the uranium was in an iron rich environment in the reoxidised sediment.

5.4.5. Bacterial diversity assessed by 16S rRNA gene amplicon pyrosequencing.

Pyrosequencing of the bulk Buxton sediment revealed a diverse community with 10028 reads (after de-noising and removal of short chimeric reads) grouped to 768 operational taxonomic units (OTUs at 97 % sequence ID similarity) affiliated to 21 bacterial phyla. These were dominated by Bacteroidetes (44.2 %), β-Proteobacteria (25.5 %) and Firmicutes (16.6 %) (Figure 3; Supporting Information Table 4). After 210 days incubation of the *no added Fe(III)* sediment, a far less diverse community was seen with 6358 reads and 239 OTUs (Supporting Information Table 4). This interpretation was supported by rarefaction curves (Supporting Information Figure 3). Sequence analyses showed that there was a clear enrichment in Firmicutes (47.1 %) and Bacteriodetes (41.3 %) (Figure 3). A similar streamlining of diversity was observed in the *with added Fe(III)* system after 210 days incubation, with 7504 reads and 217 OTUs, again with Firmicutes (48.8 %) and Bacteriodetes (34.2 %) dominating (Figure 3; Supporting Information Table 4). These community shifts may indicate that alkaline metal reduction is driven by these Gram-positive Firmicutes and Bacteroidetes bacteria. Interestingly, to date all anoxic cultures of bacteria that have been reported to reduce Fe(III) at alkaline pH also belong to the Gram-positive Firmicutes phylum and more specifically the Bacilli [39,40] and Clostridia classes [41–45]. Nevertheless, many of the dominant identified OTUs of this study were not closely affiliated to any cultured microorganisms (showing less than 90 % ID similarity), but in most cases they were related closely to environmental sequences previously found in highly alkaline environments (Supporting Information Table 5). Moreover, 2 % to 10.8 % of the sequences in these three bacterial communities were closely related (99 % ID similarity) to not only sequences previously detected in samples from the same site [17], but also to uncultured bacterium clone D0488D12 (Accession number GU559506) from a uranium contaminated aquifer ([46]; Supporting Information Table 5).

Following the 14 day reoxidation incubation with nitrate, the microbial community of the *no added Fe(III)* treatment was further enriched in Firmicutes-related sequences. Further community analysis revealed that 17.6 % of the reads were affiliated (100 % ID similarity) to an uncultured Erysipelotrichaceae bacterium clone 8GT0-42 (JX417293), previously detected in the same experimental site [17], and 16.1 % of the reads had 94 %

sequence similarity to an alkaliphilic nitrate-reducing *Bacillus* sp. JAEA No. 3-2 (AB437410) (Supporting Information Table 5). In contrast, the microbial community of the *with added Fe(III)* nitrate reoxidised sediment appeared to favour the dominance (66.1 % of the population) of reads that were closely related (98 % ID similarity) to *Pseudomonas peli* strain: R-20805 [47] (NR_042451) (Supporting Information Table 5), consistent with the ability to respire nitrate.

5.5. Significance

In this study, we demonstrate for the first time that an indigenous microbial community can mediate significant U(VI) reduction at pH 10 in sediments from a lime workings site. The U(IV) which formed on bioreduction showed differences in its speciation: the *no added Fe(III)* EXAFS spectra were indicative of a non-uraninite U(IV) phase whilst in ferrihydrite amended systems, the U(IV) was speciated as uraninite. Interestingly, pyrosequencing revealed that the microbial ecology of the bioreducing systems was dominated by Gram-positive species, in contrast to studies examining U(VI) reduction at neutral pH where Gram-negative species often dominate [5]. Furthermore, when U(VI) was exposed to a pre-reduced Fe(III)-reducing sediment that had been sterilised under anoxic conditions, there was low uranium sorption and XAS confirmed that only U(VI) was present in the sediment. This suggests that enzymatic pathways for U(VI) reduction are dominant in these sediments and it is noteworthy that the mechanisms of Fe(III)- and U(VI)-reduction are poorly constrained in Gram-positive species that lack an outer membrane with *c*-type cytochromes that are implicated in Fe(III) and U(VI) reduction in Gram-negative cells e.g. *Geobacter* and *Shewanella* species [48]. Experiments with the addition of AQDS as an extra-cellular electron shuttle showed enhanced Fe(III) reduction in systems *with added Fe(III)* and enhanced U(VI)-reduction in both *no added Fe(III)* and *with added Fe(III)* experiments, again suggesting a role for extracellular electron transport in metal reduction at high pH. Sediment reoxidation experiments showed essentially complete U(VI) remobilisation after 14 days of air reoxidation. In the nitrate reoxidation experiments, less remobilisation was observed with residual U(IV) present in the *with added Fe(III)* system. Clearly, the role of abiotic U(IV) oxidation with nitrite in these systems warrants further work. In conclusion, these data highlight the importance of biogeochemical processes in controlling the long term fate of uranium in conditions directly relevant to the geological disposal of intermediate level radioactive wastes.

5.6. Supporting information available

Details of sediment and surface water composition, linear combination fitting analysis, XAS modelling, design of tagged fusion primers and PCR amplifications, U L_{III} edge XANES spectra from all bioreduced (Supporting Information Figure 1) and nitrate reoxidised samples (Supporting Information Figure 2), rarefaction curves (Supporting Information Figure 3), Buxton surface water composition (Supporting Information Table 1), linear combination fitting estimates (Supporting Information Table 2), EXAFS fitting results (Supporting Information Table 3), pyrosequencing data processing (Supporting Information Table 4) and phylogenetic affiliations of the most abundant bacterial OTUs identified (Supporting Information Table 5). This material is available free of charge *via* the internet at http://pubs.acs.org.

5.7. Acknowledgments

This work has been funded as part of the NERC BIGRAD consortium through UK Natural Environment Research Council consortium grant NE/H007768/1. Beamtime at Diamond station B18 was funded by grants SP7367 and SP7593 from the Diamond Light Source. We thank Dr Steve Parry and Prof. J.W. Fred Mosselmans for assistance at Diamond. We also thank Nick Masters-Waage for help with geochemical data acquisition, Sam Shaw and Tim Marshall for assistance with EXAFS modelling, Christopher Boothman for pyrosequencing sample preparation and Alistair Bewsher and Paul Lythgoe for analytical support.

5.8. References

(1) Morris, K.; Law, G. T. W.; Bryan, N. D. Chapter 6 Geodisposal of Higher Activity Wastes. In *Nuclear Power and the Environment*; Harrison, R., Ed. The Royal Society of Chemistry, 2011; pp. 129–151.

(2) Clark, D. L.; Hobart, D. E.; Neu, M. P. Actinide carbonte complexes and their importance in actinide environmental chemistry. *Chem. Rev.* **1995**, *95* (1), 25–48.

(3) Newsome, L.; Morris, K.; Lloyd, J. R. The biogeochemistry and bioremediation of uranium and other priority radionuclides. *Chem. Geol.* **2014**, *363*, 164–184.

(4) Lovley, D. R.; Phillips, E. J. P. Bioremediation of uranium contamination with enzymatic uranium reduction. *Environ. Sci. Technol.* **1992**, *26* (11), 2228–2234.

(5) Williams, K. H.; Bargar, J. R.; Lloyd, J. R.; Lovley, D. R. Bioremediation of uranium-contaminated groundwater: a systems approach to subsurface biogeochemistry. *Curr. Opin. Biotechnol.* **2013**, *24* (3), 489–497.

(6) Anderson, R. T.; Vrionis, H. A.; Ortiz-Bernad, I.; Resch, C. T.; Long, P. E.; Dayvault, R.; Karp, K.; Marutzky, S.; Metzler, D. R.; Peacock, A.; et al. Stimulating the *in situ* activity of *Geobacter* species to remove uranium from the groundwater of a uranium-contaminated aquifer. *Appl. Environ. Microbiol.* **2003**, *69* (10), 5884–5891.

(7) N'Guessan, A. L.; Vrionis, H. A.; Resch, C. T.; Long, P. E.; Lovley, D. R. Sustained removal of uranium from contaminated groundwater following stimulation of dissimilatory metal reduction. *Environ. Sci. Technol.* **2008**, *42* (8), 2999–3004.

(8) Bargar, J. R.; Williams, K. H.; Campbell, K. M.; Long, P. E.; Stubbs, J. E.; Suvorova, E. I.; Lezama-Pacheco, J. S.; Alessi, D. S.; Stylo, M.; Webb, S. M.; et al. Uranium redox transition pathways in acetate-amended sediments. *Proc. Natl. Acad. Sci.* **2013**, *110* (12) , 4506–4511.

(9) Bernier-Latmani, R.; Veeramani, H.; Vecchia, E. D.; Junier, P.; Lezama-Pacheco, J. S.; Suvorova, E. I.; Sharp, J. O.; Wigginton, N. S.; Bargar, J. R. Non-uraninite products of microbial U(VI) reduction. *Environ. Sci. Technol.* **2010**, *44* (24), 9456–9462.

(10) Law, G. T. W.; Geissler, A.; Burke, I. T.; Livens, F. R.; Lloyd, J. R.; McBeth, J. M.; Morris, K. Uranium redox cycling in sediment and biomineral systems. *Geomicrobiol. J.* **2011**, *28* (5-6), 497–506.

(11) Campbell, K. M.; Veeramani, H.; Ulrich, K.-U.; Blue, L. Y.; Giammar, D. E.; Bernier-Latmani, R.; Stubbs, J. E.; Suvorova, E.; Yabusaki, S.; Lezama-Pacheco, J. S.; et al. Oxidative dissolution of biogenic uraninite in groundwater at Old Rifle, CO. *Environ. Sci. Technol.* **2011**, *45* (20), 8748–8754.

(12) Cerrato, J. M.; Barrows, C. J.; Blue, L. Y.; Lezama-Pacheco, J. S.; Bargar, J. R.; Giammar, D. E. Effect of Ca^{2+} and Zn^{2+} on UO_2 Dissolution Rates. *Environ. Sci. Technol.* **2012**, *46* (5), 2731–2737.

(13) Veeramani, H.; Schofield, E. J.; Sharp, J. O.; Suvorova, E. I.; Ulrich, K.-U.; Mehta, A.; Giammar, D. E.; Bargar, J. R. Effect of Mn(II) on the structure and reactivity of biogenic uraninite. *Environ. Sci. Technol.* **2009**, *43* (17), 6541–6547.

(14) Wieland, E.; Dähn, R.; Gaona, X.; Macé, N.; Tits, J. Micro- and macroscopic investigations of actinide binding in cementitious materials. In *Cement-Based Materials for Nuclear Waste Storage*; Bart, F.; Cau-di-Coumes, C.; Frizon, F.; Lorente, S., Eds.; Springer New York, **2013**; pp. 93–101.

(15) Marty, N. C. M.; Fritz, B.; Clément, A.; Michau, N. Modelling the long term alteration of the engineered bentonite barrier in an underground radioactive waste repository. *Appl. Clay Sci.* **2010**, *47* (1-2), 82–90.

(16) Rizoulis, A.; Steele, H. M.; Morris, K.; Lloyd, J. R. The potential impact of anaerobic microbial metabolism during the geological disposal of intermediate-level waste. *Mineral. Mag.* **2012**, *76* (8), 3261–3270.

(17) Williamson, A. J.; Morris, K.; Shaw, S.; Byrne, J. M.; Boothman, C.; Lloyd, J. R. Microbial reduction of Fe(III) under alkaline conditions relevant to geological disposal. *Appl. Environ. Microbiol.* **2013**, *79* (11), 3320–3326.

(18) Anderson, C.; Johnsson, A.; Moll, H.; Pedersen, K. Radionuclide geomicrobiology of the deep biosphere. *Geomicrobiol. J.* **2011**, *28* (5-6), 540–561.

(19) Behrends, T.; Krawczyk-Bärsch, E.; Arnold, T. Implementation of microbial processes in the performance assessment of spent nuclear fuel repositories. *Appl. Geochemistry* **2012**, *27* (2), 453–462.

(20) Jacquot, F.; Libert, M. F.; Romero, M. A.; Besnainou, B. *In vitro* evaluation of microbial effects on bitumen waste form. In Microbial Degradation Processes in Radioactive Waste Repository and in Nuclear Fuel Storage Areas; Wolfram, J. H., Rogers, R. D., Gazso, L. G., Eds. Springer: Netherlands, 1997; Vol 11, pp. 275–283.

(21) Riekkola, R.; Sievänen, U.; Vieno, T. Controlling of disturbances due to groundwater inflow into ONKALO and the deep repository. *Work. Rep.* **2003**, *46*.

(22) Lovley, D. R.; Phillips, E. J. Rapid assay for microbially reducible ferric iron in aquatic sediments. *Appl Env. Microbiol.* **1987**, *53* (7), 1536–1540.

(23) Johnson, D. A.; Florence, T. M. Spectrophotometric determination of uranium(VI) with 2-(5-bromo-2-pyridylazo)-5-diethylaminophenol. *Anal. Chim. Acta* **1971**, *53* (1), 73–79.

(24) Wielinga, B.; Bostick, B.; Hansel, C. M.; Rosenzweig, R. F.; Fendorf, S. Inhibition of bacterially promoted uranium reduction: ferric (hydr)oxides as competitive electron Acceptors. *Environ. Sci. Technol.* **2000**, *34* (11), 2190–2195.

(25) Dent, A. J.; Cibin, G.; Ramos, S.; Smith, A. D.; Scott, S. M.; Varandas, L.; Pearson, M. R.; Krumpa, N. A.; Jones, C. P.; Robbins, P. E., B18: A core XAS spectroscopy beamline for Diamond. *J. Phys.: Conf. Ser.* ***2009***, *190*, 012039.

(26) Ravel, B.; Newville, M. ATHENA, ARTEMIS, HEPHAESTUS: data analysis for X-ray absorption spectroscopy using IFEFFIT. *J. Synchrotron Radiat.* **2005**, *12* (4), 537–541.

(27) Law, G. T. W.; Geissler, A.; Lloyd, J. R.; Livens, F. R.; Boothman, C.; Begg, J. D. C.; Denecke, M. A.; Rothe, J.; Dardenne, K.; Burke, I. T.; et al. Geomicrobiological redox cycling of the transuranic element neptunium. *Environ. Sci. Technol.* **2010**, *44* (23), 8924–8929.

(28) Tenderholt, A.; Hedman, B.; Hodgson, K. O., PySpline: A modern, cross-platform program for the processing of raw averaged XAS edge and EXAFS data. In *X-Ray Absorption Fine Structure-XAFS13*, Hedman, B.; Painetta, P., Eds. Amer Inst Physics: Melville, 2007; Vol. 882, pp. 105-107.

(29) Tomic, S.; Searle, B. G.; Wander, A.; Harrison, N. M.; Dent, A.; Inglesfield, J. The DL EXCURV package, 2005.

(30) Lane, D. J. 16S/23S rRNA sequencing. In *Nucleic Acid Techniques in Bacterial Systematic*, Stackebrandt, E., Goodfellow, M.,. John Wiley and Sons: New York, 1991, pp. 115-175.

(31) Hamady, M.; Walker, J. J.; Harris, J. K.; Gold, N. J.; Knight, R. Error-correcting barcoded primers for pyrosequencing hundreds of samples in multiplex. *Nat. Methods* **2008**, *5* (3), 235–237.

(32) Caporaso, J. G.; Kuczynski, J.; Stombaugh, J.; Bittinger, K.; Bushman, F. D.; Costello, E. K.; Fierer, N.; Pena, A. G.; Goodrich, J. K.; Gordon, J. I. QIIME allows analysis of high-throughput community sequencing data. *Nat. Methods* **2010**, *7* (5), 335–336.

(33) Edgar, R. C. Search and clustering orders of magnitude faster than BLAST. *Bioinformatics* **2010**, *26* (19), 2460–2461.

(34) Cole, J. R.; Wang, Q.; Cardenas, E.; Fish, J.; Chai, B.; Farris, R. J.; Kulam-Syed-Mohideen, A. S.; McGarrell, D. M.; Marsh, T.; Garrity, G. M.; et al. The Ribosomal Database Project: improved alignments and new tools for rRNA analysis. *Nucleic Acids Res.* **2009**, *37* (suppl 1), 141–145.

(35) Waite, T. D.; Davis, J. A.; Payne, T. E.; Waychunas, G. A.; Xu, N. Uranium(VI) adsorption to ferrihydrite: application of a surface complexation model. *Geochim. Cosmochim. Acta* **1994**, *58* (24), 5465–5478.

(36) Schofield, E. J.; Veeramani, H.; Sharp, J. O.; Suvorova, E.; Bernier-Latmani, R.; Mehta, A.; Stahlman, J.; Webb, S. M.; Clark, D. L.; Conradson, S. D.; et al. Structure of biogenic uraninite produced by *Shewanella oneidensis* strain MR-1. *Environ. Sci. Technol.* **2008**, *42* (21), 7898–7904.

(37) Moon, H. S.; Komlos, J.; Jaffé, P. R. Biogenic U(IV) oxidation by dissolved oxygen and nitrate in sediment after prolonged U(VI)/Fe(III)/SO_4^{2-} reduction. *J. Contam. Hydrol.* **2009**, *105* (1-2), 18–27.

(38) Begg, J. D. C.; Burke, I. T.; Lloyd, J. R.; Boothman, C.; Shaw, S.; Charnock, J. M.; Morris, K. Bioreduction behavior of U(VI) sorbed to sediments. *Geomicrobiol. J.* **2011**, *28* (2), 160–171.

(39) Ma, C.; Zhuang, L.; Zhou, S. G.; Yang, G. Q.; Yuan, Y.; Xu, R. X. Alkaline extracellular reduction: isolation and characterization of an alkaliphilic and halotolerant bacterium, *Bacillus pseudofirmus* MC02. *J. Appl. Microbiol.* **2012**, *112* (5), 883–891.

(40) Pollock, J.; Weber, K.; Lack, J.; Achenbach, L.; Mormile, M.; Coates, J. Alkaline iron(III) reduction by a novel alkaliphilic, halotolerant, *Bacillus* sp. isolated from salt flat sediments of Soap Lake. *Appl. Microbiol. Biotechnol.* **2007**, *77* (4), 927–934.

(41) Ye, Q.; Roh, Y.; Carroll, S. L.; Blair, B.; Zhou, J.; Zhang, C. L.; Fields, M. W. Alkaline anaerobic respiration: isolation and characterization of a novel alkaliphilic and metal-reducing bacterium. *Appl. Environ. Microbiol.* **2004**, *70* (9), 5595–5602.

(42) Roh, Y.; Chon, C.-M.; Moon, J.-W. Metal reduction and biomineralization by an alkaliphilic metal-reducing bacterium, *Alkaliphilus metalliredigens* (QYMF). *Geosci. J.* **2007**, *11* (4), 415–423.

(43) Zhilina, T. N.; Zavarzina, D. G.; Osipov, G. A.; Kostrikina, N. A.; Tourova, T. P. *Natronincola ferrireducens* sp. nov., and *Natronincola peptidovorans* sp. nov., new anaerobic alkaliphilic peptolytic iron-reducing bacteria isolated from soda lakes. *Microbiology* **2009**, *78* (4), 455–467.

(44) Zhilina, T.; Zavarzina, D.; Kolganova, T.; Lysenko, A.; Tourova, T. *Alkaliphilus peptidofermentans*; sp. nov., a new alkaliphilic bacterial soda lake isolate capable of peptide fermentation and Fe(III) reduction. *Microbiology* **2009**, *78 (4)*, 445–454.

(45) Gorlenko, V.; Tsapin, A.; Namsaraev, Z.; Teal, T.; Tourova, T.; Engler, D.; Mielke, R.; Nealson, K. *Anaerobranca californiensis* sp. nov., an anaerobic, alkalithermophilic, fermentative bacterium isolated from a hot spring on Mono Lake. *Int. J. Syst. Evol. Microbiol.* **2004**, *54* (3), 739–743.

(46) Elifantz, H.; N'Guessan, L. A.; Mouser, P. J.; Williams, K. H.; Wilkins, M. J.; Risso, C.; Holmes, D. E.; Long, P. E.; Lovley, D. R. Expression of acetate

permease-like (apl) genes in subsurface communities of *Geobacter* species under fluctuating acetate concentrations. *FEMS Microbiol. Ecol.* **2010**, *73* (3), 441–449.

(47) Vanparys, B.; Heylen, K.; Lebbe, L.; De Vos, P. *Pseudomonas peli* sp. nov. and *Pseudomonas borbori* sp. nov., isolated from a nitrifying inoculum. *Int. J. Syst. Evol. Microbiol.* **2006**, *56* (8), 1875–1881.

(48) Lloyd, J. R. Microbial reduction of metals and radionuclides. *FEMS Microbiol. Rev.* **2003**, *27* (2-3), 411–425.

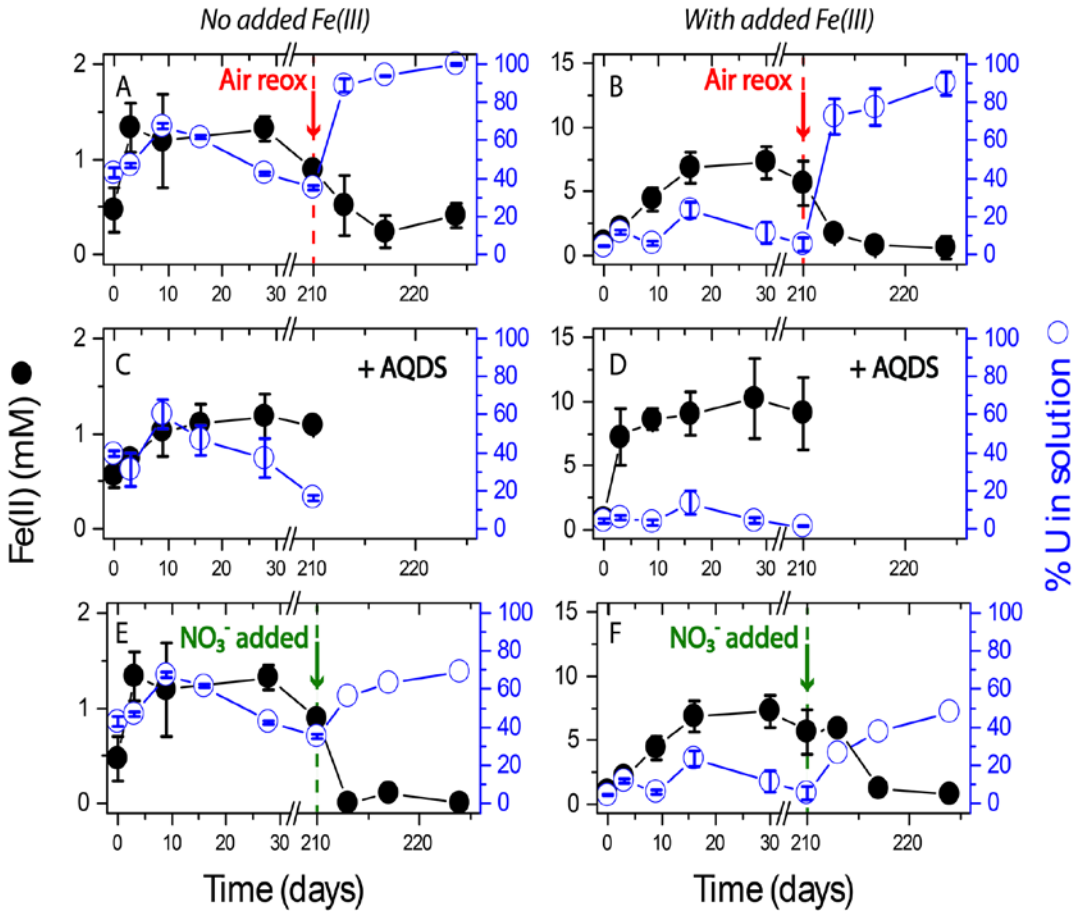

Figure 1: Biocycling of U in Buxton sediments showing 0.5 N HCl extractable Fe(II) concentration (mM) (●) and total $U_{(aq)}$ (expressed as % of the added U(VI)) (○). Systems: (A) no added Fe(III) reduction with air reoxidation from 210 days; (B) with added Fe(III) reduction and air reoxidation from 210 days; (C) no added Fe(III) reduction + AQDS; (D) with added Fe(III) reduction + AQDS; (E) with added Fe(III) reduction and nitrate reoxidation from 210 days; (F) with added Fe(III) reduction and air reoxidation from 210 days. Error bars are 1σ of triplicate results (where not shown, errors are within the size of the symbol). Dashed lines indicate the start of reoxidation experiments; red for air and green for nitrate treatments (nitrate reoxidations were run as single experiments).

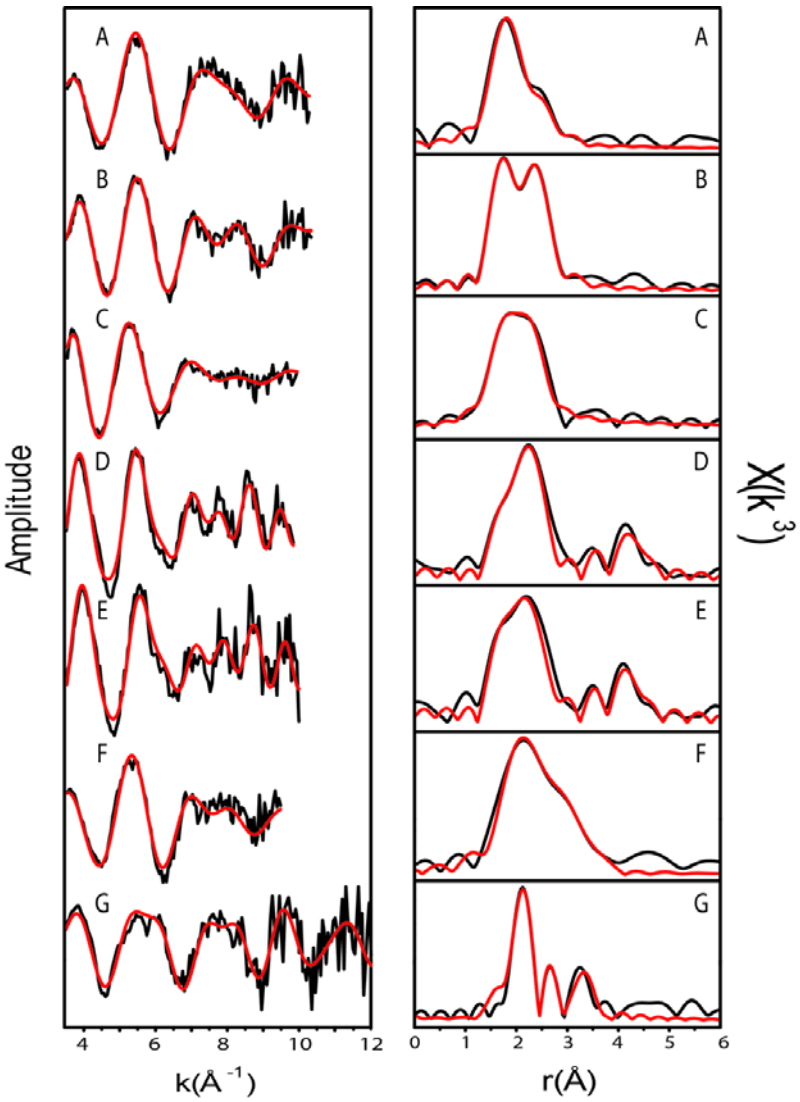

Figure 2: k^3 weighted ^{238}U $L_{(III)}$ edge EXAFS spectra (left) and Fourier transform (right) for bioreduction systems at experimental end-points: (A) no added Fe(III) oxic sediment; (B) no added Fe(III) reduction; (C) no added Fe(III) + AQDS reduction; (D) with added Fe(III) reduction; (E) with added Fe(III) reduction + AQDS; (F) no added Fe(III) and subsequent nitrate reoxidation; and (G) with added Fe(III) and subsequent nitrate reoxidation. Black lines are the experimental data and red lines are the best-fit models (SI Table 3).

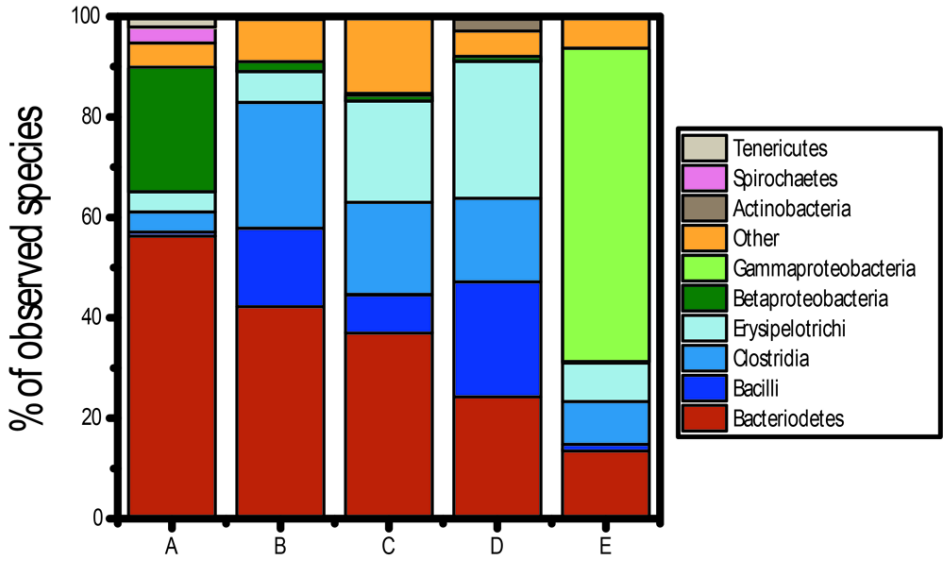

Figure 3: Bacterial phylogenetic diversity at the Phylum level for (A) bulk unamended sediment; (B) no added Fe(III) reduction; (C) with added Fe(III) reduction; (D) no added Fe(III) and subsequent nitrate reoxidation (E) with added Fe(III) and subsequent nitrate reoxidation. Only the phyla with more than 1% of the total number of reads are shown. Abundance at the class level is shown for Firmicutes (blue hues) and Proteobacteria (green hues).

5.9. Supporting information

5.9.1. Sediment and surface water characteristics

Full characteristics of the sediments used in this study have been reported previously [1] with composition dominated by calcite, and minor quartz and ankerite. The elemental composition, as determined by XRF, was dominated by Ca (51.2 wt %), with significant concentrations of Si (1.1 wt %), Al (0.5 wt %) and Fe (0.17 wt %). The bulk extractable iron in the sample was estimated by using aqua regia digestion and ICP-OES analysis which showed 0.92 g kg^{-1} Fe (16 mM kg^{-1} Fe). Additionally, throughout the experiment, the bio-available Fe was estimated by ferrozine assay after 0.5 N HCl extraction [2] and here, 4.6 mM kg^{-1} Fe was extracted indicating ~ 1/3 of the bulk Fe was bioavailable.

5.9.2. Linear combination fitting analysis

Selected XANES spectra from end member oxic and reduced sediments *oxic with added Fe(III)* and reduced *with added Fe(III) + AQDS* samples were compared to the schoepite and uraninite standard spectra. Within the expected spectral differences apparent between non-matrix matched samples, the *oxic with added Fe(III)* sample displayed U(VI)-like XANES spectral features and the *with added Fe(III) + AQDS* system displayed U(IV)-like XANES spectral features. Fitting is therefore shown between the oxic and reduced sediments as schoepite and uraninite were clearly not matched to these sediments. The fitting for schoepite and uraninite was broadly similar to the data from the sediment oxic and reduced end-members and thus we have confidence that this approach gave appropriate trends for U(VI) and U(IV) components.

5.9.3. XAS modeling

Phase shifts were determined by ab initio calculations using the Hedin Lundqvist and von Barth ground states [3]. For the majority of samples, data acquisition allowed us to fit a k range between 3 and 10 $Å^{-1}$. For the nitrate reoxidised with added iron sample, we were able to collect data for an extended time period and here, fitting was possible between 3 – 12 $Å^{-1}$. The data were fitted in k^3 space. For modelling purposes, it was assumed that all U was either as U(VI) bound to 2 axial oxygens at ~1.8 Å and 4 equatorial oxygens at ~2.4 Å or as U(IV) bound to 8 oxygens at ~2.4 Å. The initial fits was made based on the relative contributions of U(VI) and U(IV) from the linear combination fitting and then refined. For the *no added Fe(III)* sediments, U(VI) carbonate phases were modelled using literature values for U(VI) carbonate [4]. In the with added Fe(III) nitrate reoxidised system there was a strong signal at 3.2 Å and the

fit was only significantly improved by adding a shell of Fe. Shells of backscattering atoms were added around a central U atom and the least squares residual (R factor [3]) was minimised by refining the energy correction E_f (Fermi energy), the absorber/scatter distance (r), the Debye Waller factor (a) and the number of atoms (n) in each shell. Shells were only included in the model fit if the overall R-factor was improved by >5 % and satisfied the reduced X^2 test.

5.9.4. Design of tagged fusion primers and PCR amplifications

PCR of the V1-V2 hypervariable region of the bacterial 16S rRNA gene was performed using tagged fusion universal bacterial primers 27F [5] and 338R [6], synthesised by IDTdna (Integrated DNA Technologies, BVBA, Leuven, Belgium). The fusion forward primer (5'-CCATCTCATCCCTGCGTGTCTCCGACTCAGNNNNNNNNNNAGAGTTTGATGMTGGCTCAG-3') contained the 454 Life Sciences "Lib-L Primer A", a 4 base "key" sequence (TCAG), a unique ten-base pair multiplex identifier (MID) sequence for each sample, and bacterial primer 27F. Roche's MID-1 barcode (ACGAGTGCGT) was used for the *no added Fe(III)* reduction 210 days, MID-2 (ACGCTCGACA) for the *with added Fe(III)* 210 days, MID-3 (AGACGCACTC) *no added Fe(III)* and subsequent nitrate reoxidation 14 days, MID04 (AGCACTGTAG)) *with added Fe(III)* and subsequent nitrate reoxidation 14 days, and MID05 (ATCAGACAC) for the bulk Buxton sediment. The reverse fusion primer (5'-CCTATCCCCTGTGTGCCTTGGCAGTCTCAGTGCTGCCTCCCGTAGGAGT-3') contained the 454 Life Sciences "Lib-L Primer B", a 4 base "key" sequence (TCAG), and bacterial primer 338R.

The PCR amplification was performed in 50 μl volume reactions using 0.5 μl (2.5 units) FastStart High Fidelity DNA polymerase (Roche Diagnostics GmbH, Mannheim, Germany), 1.8 mM $MgCl_2$, 200 μM of each dNTP, 0.4 μM of each forward and reverse fusion primers. The PCR conditions included an initial denaturing step at 95°C for 2 min, followed by 35 cycles of 95°C for 30 sec, 55°C for 30 sec, 72°C for 45 sec, and a final elongation step at 72°C for 5 min. PCR products were loaded onto an agarose gel, and following gel electrophoresis, bands of the correct fragment size (approximately 410 bp) were excised, purified using a QIAquick gel extraction kit (QIAGEN, GmBH, Hilden, Germany), and eluted in 30 μl of DNAse free H_2O. The purified PCR products were quantified using an Agilent 2100 Bioanalyzer (Agilent Technologies, Inc., Santa Clara, CA, USA), and pooled so that the mixture contained equal amounts of DNA from

each sample. The emulsion PCR and the pyrosequencing run were performed at the University of Manchester sequencing facility, using a Roche 454 Life Sciences GS Junior system.

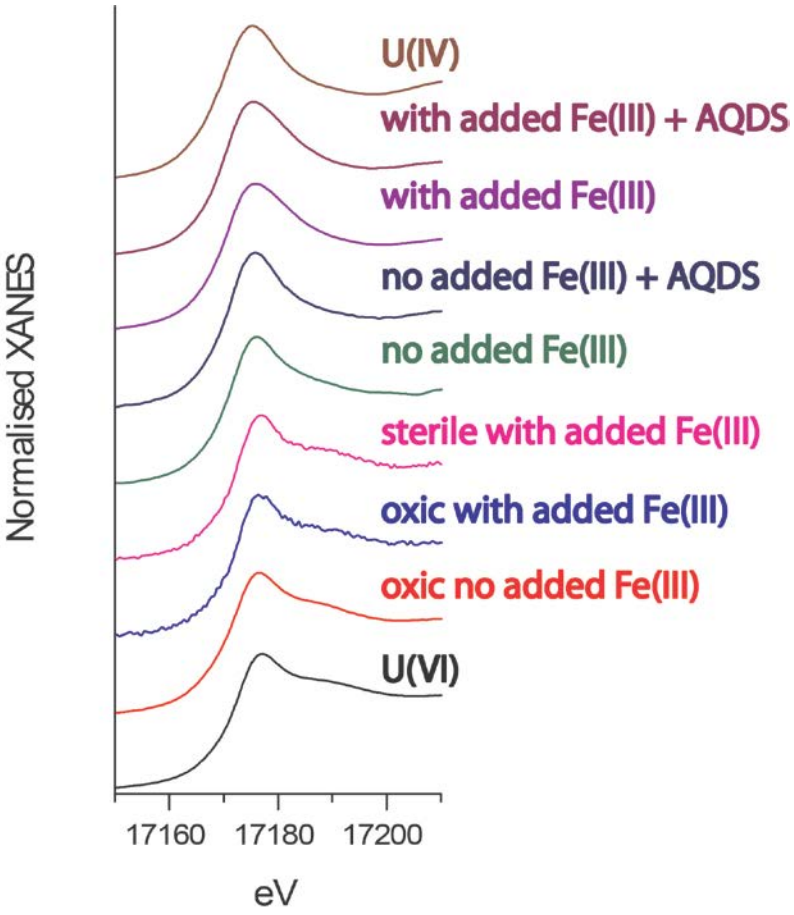

SI Figure 1: U $L_{(III)}$-edge normalised XANES spectra for all sediment bioreducing treatments with schoepite (U(VI)) and uraninite (U(IV)) reference spectra.

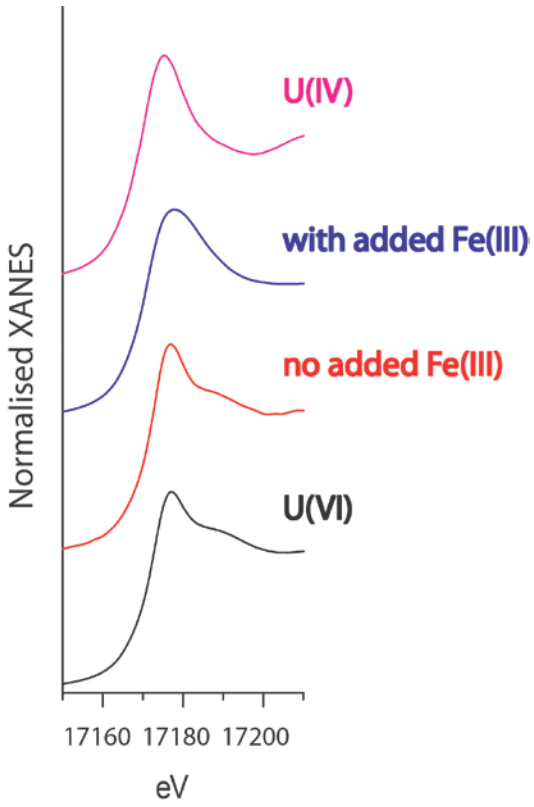

SI Figure 2: U $L_{(III)}$-edge normalised XANES spectra for nitrate reoxidised sediments, no added Fe(III) and with added Fe(III) with schoepite (U(VI)) and uraninite (U(IV)) reference spectra.

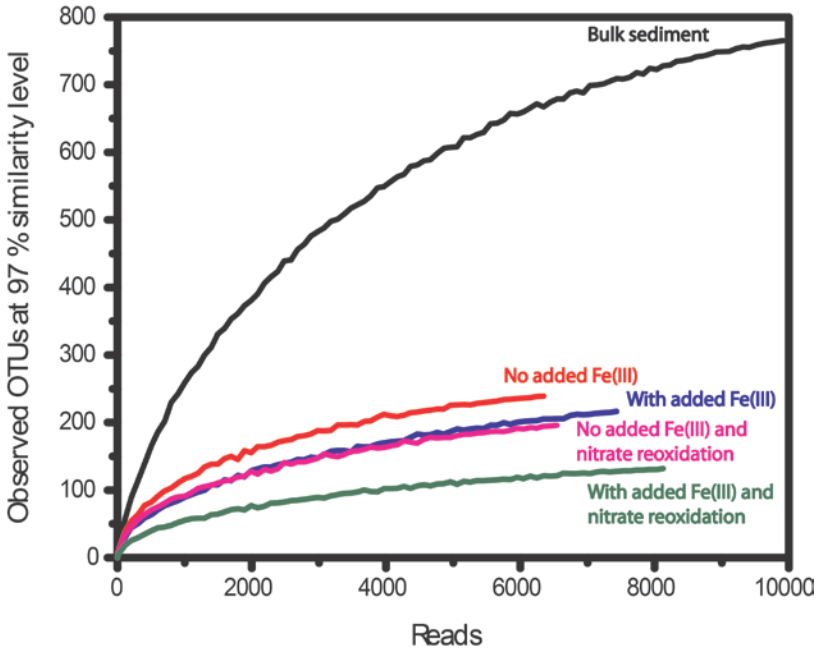

SI Figure 3: Rarefaction curves showing the number of observed operational taxonomic units (OTUs) at 97 % ID similarity per sample, after 16S rRNA gene amplicon pyrosequencing.

SI Table 1: Buxton Harpur Hill lime workings surface water major anions and cations. Note, on equilibration of surface waters with sediment and electron donor, SO_4^{2-} concentration at t=0 was 7.12 ppm.

Cations	**Na^+**	**Ca^{2+}**	**Si^{4+}**	**K^+**	**Sr^{2+}**	**Ba^{2+}**
Concentration (mg l^{-1})	38.7	270	10.4	58.2	1.01	0.633

Anions	**Cl^-**	**NO_3^-**	**NO_2^-**	**SO_4^{2-}**
Concentration (mg l^{-1})	60.8	30.5	0	0.5

SI Table 2: Linear combination fitting percentage estimates (± ~ 20 %) for U XANES modelling with U(VI) bearing oxic end member with added Fe(III) and U(IV) bearing reduced with added Fe(III) + AQDS end member spectra. N/A indicates not applicable as the sample was used as an end member spectrum for linear combination modelling.

Treatment	**U(VI) (%)**	**U(IV) (%)**
Oxic no added Fe(III)	80	20
Oxic with added Fe(III)*	N/A (100%)	N/A (0%)
Sterile with added Fe(III)	91	9
No added Fe(III)	52	48
No added Fe(III) + AQDS	23	77
With added Fe(III)	14	86
With added Fe(III) + AQDS*	N/A (0%)	N/A (100%)
No added Fe(III) and subsequent nitrate reoxidation	96	4
With added Fe(III) and subsequent nitrate reoxidation	57	43

SI Table 3: EXAFS fitting results from bioreduction microcosm experiments: no added Fe(III), no added Fe(III) + AQDS, with added Fe(III), with added Fe(III) + AQDS; and subsequent nitrate reoxidation experiments: no added Fe(III) and with added Fe(III). N is coordination number, r is interatomic distance (Å) and σ^2 is Debye Waller factor (Å^2). Errors on are r ± 0.02 Å (first shell), 0.05 Å (outer shells) and $2\sigma^2$ are ± 25 %; N ± 25 %. R (least squares residual) is a measure of the overall goodness of fit.

Sample	Shell	N	Atom	r	$2\sigma^2$	R
No added Fe(III) oxic sediment	1	1.8	O	1.82	0.012	28
	2	3.7	O	2.42	0020	
	3	1.5	C	2.88	0.002	
No added Fe(III)	1	1.3	O	1.79	0.005	29
	2	6.0	O	2.41	0.020	
No added Fe(III) + AQDS	1	0.9	O	1.8	0.008	20
	2	4	O	2.38	0.013	
With added Fe(III)	1	0.2	O	1.74	0.006	25
	2	3.8	O	2.38	0.029	
	3	1.1	U	3.87	0.006	
With added Fe(III) + AQDS	1	0.2	O	1.74	0.012	29
	2	4.9	O	2.35	0.030	
	3	0.9	U	3.86	0.002	
No added Fe(III) nitrate and subsequent nitrate reoxidation	1	2	O	1.80	0.009	32
	2	5.6	O	2.43	0.021	
	3	2.1	C	3.00	0.005	
With added Fe(III) and subsequent nitrate reoxidation	1	0.5	O	1.75	0.010	32
	2	2	O	2.19	0.006	
	3	2	O	2.42	0.015	
	4	1	Fe	3.23	0.015	

SI Table 4: Number of pyrosequencing reads obtained for (A) bulk unamended sediment; (B) no added Fe(III) reduction 210 days; (C) with added Fe(III) reduction 210 days; (D) no added Fe(III) and subsequent nitrate reoxidation 14 days and (E) with added Fe(III) and subsequent nitrate reoxidation 14 days, number of reads after denoising and removal of short and chimeric sequences, and the number of observed operational taxonomic units (OTUs) at 97 % ID similarity.

Sample	**Number of reads**	**Number of reads after chimera check & denoising**	**Observed OTU's**
(A) Bulk unamended sediment	11553	10028	768
(B) No added Fe(III)	7090	6358	239
(C) With added Fe(III)	8208	7504	217
(D) No added Fe(III) and subsequent nitrate reoxidation	7423	6566	196
(E) With added Fe(III) and subsequent nitrate reoxidation	8888	8167	132

SI Table 5: Phylogenetic affiliations of the most abundant bacterial OTUs identified in samples from (A) bulk unamended sediment, (B) no added Fe(III) reduction 210 days, (C) with added Fe(III) reduction 210 days, (D) no added Fe(III) and subsequent nitrate reoxidation 14 days and (E) with added Fe(III) and subsequent nitrate reoxidation 14 days.

	% of total population								
(A) Bulk unamended sediment	**(B) No added Fe(III)**	**(C) With added Fe(III)**	**(D) No added Fe(III) and subsequent nitrate reoxidation**	**(E) With added Fe(III) and subsequent nitrate reoxidation**	**Phylogenetic affiliation**	**Closest phylogenetic relative**	**ID % similarity**	**Environment (reference)**	**Accession number**
		0.3		**61.1**	Proteobacteria; γ-proteobacteria	*Pseudomonas guineae* strain : LMG 24016	99	Psychrotolerant bacterium from an Antarctic environment [7]	NR_042607
						Pseudomonas peli strain : R-20805	98	Nitrifying inoculums [8]	NR_042451
3.4	**13.7**	**9.0**	**9.2**	4.6	Bacteroidetes	Uncultured bacterium clone bur-54	100	Buxton [1]	JX417334
15.6	3.3	**9.4**	1.1	3.0	Bacteroidetes	Uncultured bacterium clone bur-93	100	Buxton [1]	JX417368
0.1	**6.6**	**13.4**	4.2	5.9	Actinobacteria	Uncultured actinobacterium clone 009T7	90	Iron redox cycling bacteria from Talladega freshwater sediments [9]	DQ110023
0.2	**7.4**	**10.5**	3.6	4.4	Bacteroidetes	Uncultured Bacteroidetes bacterium clone BHL3-310I-57	97	Chromate reduction in Fe(II) containing soil affected hyperalkaline leachate [10]	FR695957
						Iron-reducing enrichment clone Cl-A4 clone Cl-A4	96	Fe(III) reduction in polluted Scheldt estuary sediments, NW Europe [11]	DQ676996
0.5	**13.4**	**6.9**	5.1	1.3	Firmicutes; Bacilli	*Trichococcus pasteurii* strain KoTa2 complete sequence	99	Gram positive lactic acid/pyruvate producing fermenting bacteria [12]	NR_036793

2.0	2.4	**10.8**	1.4	3.1	Firmicutes; Erysipelotrichaceae	Uncultured bacterium clone D0488D12	99	U contaminated aquifers [13]	GU559506
						Uncultured bacterium clone bur-71	99	Buxton [1]	JX417349
	1.8	1.1	**17.6**	1.5	Firmicutes; Erysipelotrichaceae	Uncultured bacterium clone 8GT0-42	100	Buxton [1]	JX417293
			16.1		Firmicutes; Bacillus	*Bacillus* sp. JAEA No. 3-2	94	Alkaliphilic nitrate-reducing from soil (Murakami and Honda, unpublished)	AB437410
	8.3	0.9	3.0	0.1	Firmicutes; Clostridia	*Clostridium sticklandii* str. DSM 519	100	Able to use amino acids as carbon and energy sources [14]	FP565809
0.2	1.0	**5.5**	0.7	2.4	Firmicutes; Erysipelotrichaceae	Uncultured bacterium clone SYMH02_C3-07B-077	99	Anaerobic sulfate reduction and methanogenesis in a terrestrial mud volcano [15]	JQ245691
5.0	0.3	0.1	0.2		Bacteriodetes	Uncultured bacterium clone bur-13	97	Buxton [1]	JX417302
5.1	0.1				Proteobacteria; β-proteobacteria	*Quatrionicoccus australiensis* strain Ben 117	95	From activated sludge biomass [16]	NR_029035

5.10. References

(1) Williamson, A. J.; Morris, K.; Shaw, S.; Byrne, J. M.; Boothman, C.; Lloyd, J. R. Microbial reduction of Fe(III) under alkaline conditions relevant to geological disposal. *Appl. Environ. Microbiol.* **2013**, *79* (11), 3320–3326.

(2) Lovley, D. R.; Phillips, E. J. Rapid assay for microbially reducible ferric iron in aquatic sediments. *Appl Env. Microbiol.* **1987**, *53* (7), 1536–1540.

(3) Tomic, S.; Searle, B. G.; Wander, A.; Harrison, N. M.; Dent, A.; Inglesfield, J. The DL EXCURV package, 2005.

(4) Bernhard, G.; Geipel, G.; Reich, T.; Brendler, V.; Amayri, S.; Nitsche, H. Uranyl(VI) carbonate complex formation: Validation of the $Ca_2UO_2(CO_3)_3$ (aq.) species. *Radiochim. Acta.* **2001**, *89*, 511-518

(5) L Lane, D. J. 16S/23S rRNA sequencing. In *Nucleic Acid Techniques in Bacterial Systematic*, Stackebrandt, E., Goodfellow, M.,. John Wiley and Sons: New York, 1991 pp 115-175.

(6) Hamady, M.; Walker, J. J.; Harris, J. K.; Gold, N. J.; Knight, R. Error-correcting barcoded primers for pyrosequencing hundreds of samples in multiplex. *Nat. Methods* **2008**, *5* (3), 235–237.

(7) Bozal, N.; Montes, M. J.; Mercadé, E. *Pseudomonas guineae sp.* nov., a novel psychrotolerant bacterium from an Antarctic environment. *Int. J. Syst. Evol. Microbiol.* **2007**, *57*, 2609–2612.

(8) Vanparys, B.; Heylen, K.; Lebbe, L.; De Vos, P. *Pseudomonas peli sp.* nov. and *Pseudomonas borbori sp.* nov., isolated from a nitrifying inoculum. *Int. J. Syst. Evol. Microbiol.* **2006**, *56*, 1875–1881.

(9) Weber, K. A.; Urrutia, M. M.; Churchill, P. F.; Kukkadapu, R. K.; Roden, E. E. Anaerobic redox cycling of iron by freshwater sediment microorganisms. *Environ. Microbiol.* **2006**, *8*, 100–113.

(10) Whittleston, R. A.; Stewart, D. I.; Mortimer, R. J. G.; Tilt, Z. C.; Brown, A. P.; Geraki, K.; Burke, I. T. Chromate reduction in Fe(II)-containing soil affected by hyperalkaline leachate from chromite ore processing residue. *J. Hazard. Mater.* **2011**, *194*, 15–23.

(11) Lin, B.; Hyacinthe, C.; Bonneville, S.; Braster, M.; Van Cappellen, P.; Röling, W. F. M. Phylogenetic and physiological diversity of dissimilatory ferric iron reducers in sediments of the polluted Scheldt estuary, Northwest Europe. *Environ. Microbiol.* **2007**, *9*, 1956–1968.

(12) Janssen, P. H.; Evers, S.; Rainey, F. A.; Weiss, N.; Ludwig, W.; Harfoot, C. G.; Schink, B. *Lactosphaera* gen. nov., a new genus of lactic acid bacteria, and transfer of *Ruminococcus pasteurii* Schink 1984 to *Lactosphaera pasteurii* comb. nov. *Int. J. Syst. Bacteriol.* **1995**, *45*, 565–571.

(13) Elifantz, H.; N'Guessan, L. A.; Mouser, P. J.; Williams, K. H.; Wilkins, M. J.; Risso, C.; Holmes, D. E.; Long, P. E.; Lovley, D. R. Expression of acetate permease-like (apl) genes in subsurface communities of *Geobacter* species under fluctuating acetate concentrations. *FEMS Microbiol. Ecol.* **2010**, *73*, 441–449.

(14) Fonknechten, N.; Chaussonnerie, S.; Tricot, S.; Lajus, A.; Andreesen, J.; Perchat, N.; Pelletier, E.; Gouyvenoux, M.; Barbe, V.; Salanoubat, M. *Clostridium*

sticklandii, a specialist in amino acid degradation: revisiting its metabolism through its genome sequence. *BMC Genomics* **2010**, *11*, 555.

(15) Cheng, T.-W.; Chang, Y.-H.; Tang, S.-L.; Tseng, C.-H.; Chiang, P.-W.; Chang, K.-T.; Sun, C.-H.; Chen, Y.-G.; Kuo, H.-C.; Wang, C.-H.; et al. Metabolic stratification driven by surface and subsurface interactions in a terrestrial mud volcano. *ISME J.* **2012**, *6*, 2280–2290.

(16) Maszenan, A. M.; Seviour, R. J.; Patel, B.; Schumann, P. *Quadricoccus australiensis* gen. nov., sp. nov., a beta-proteobacterium from activated sludge biomass. *Int. J. Syst. Evol. Microbiol.* **2002**, *52*, 223–228.

6

Biogeochemical Cycling of ^{99}Tc in Alkaline Sediments

Paper in preparation for Environmental Science and Technology

6. Biogeochemical Cycling of ^{99}Tc in Alkaline Sediments

Adam J. Williamson,[†] Jonathan R. Lloyd,[†] Christopher Boothman,[†] Gareth T.W. Law,[‡] Joe S. Small,[‖] Heather A. Williams, [§] and Katherine Morris[† *]

† Research Centre for Radwaste Disposal and Williamson Research Centre for Molecular Environmental Science, School of Earth, Atmospheric and Environmental Sciences, The University of Manchester, Manchester, M13 9PL, UK.

‡ Centre for Radiochemistry Research and Research Centre for Radwaste Disposal, School of Chemistry, The University of Manchester, Manchester, M13 9PL, UK.

§ Department of Nuclear Medicine, Manchester Royal Infirmary, Oxford Road, M13 9WL, UK.

‖ National Nuclear Laboratory, Risley, Warrington, Cheshire, WA3 6AS, UK.

*email katherine.morris@manchester.ac.uk

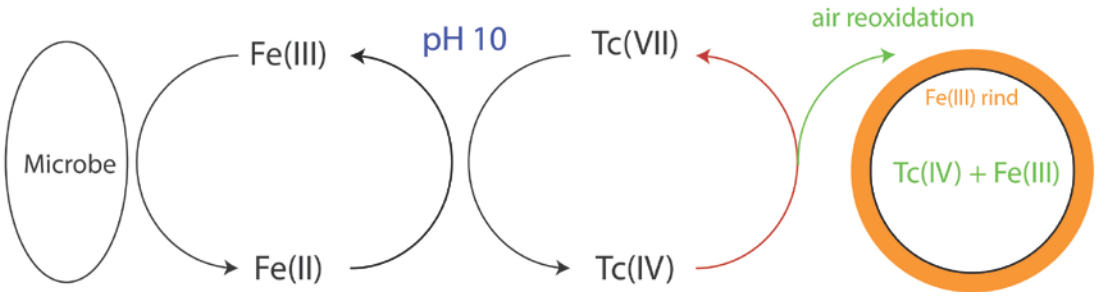

6.1. Abstract

^{99}Tc will be present in significant quantities in intermediate level nuclear wastes (ILW) and due to its longevity ($t_{1/2}$ 2.13 x 10^5 years) and high mobility in oxic environments it is considered a problematic radionuclide. The current concept for disposing of ILW in many nations is via geological disposal in a cementitious environment. Understanding the biogeochemistry of Tc in such high pH environments is important for any disposal safety case. Here, microcosm experiments have been established using alkaline sediments from the vicinity of a legacy lime workings site. To further probe the potential coupling between Tc(VII) and Fe(III) biogeochemistry, systems were also run with additional Fe(III) as an electron acceptor as ferrihydrite. Experiments were run at trace level (100 Bq ml^{-1}) to track biogeochemical changes, whilst parallel higher concentrations (56 KBq ml^{-1}) were used to assess Tc speciation and coordination environment using XAS. In addition, a few targeted experiments were also conducted using ultra-trace concentrations of ^{99m}Tc, to explore interactions at very low (10^{-12} M) levels. A cascade of microbial redox processes occurred at pH 10 – 10.5 in all microbially active systems. In systems without added Fe(III), significant (~ 35%) removal of Tc(VII) occurred and solvent extractions with TPAC suggested that residual aqueous Tc was predominantly Tc(IV). In ferrihydrite enriched systems, reactive Fe(II) dominated and complete Tc removal from solution occurred. Pre-reduced Fe(II)-bearing sediments were also reacted with Tc(VII) to probe for coupling between these two redox active metals; collectively these data suggest Tc(VII) reduction was predominantly abiotic, mediated via biogenic Fe(II). On bioreduction, the solid phase associated Tc(IV) that was formed exhibited a hydrous TcO_2 like phase. Air reoxidation experiments were also conducted to explore the long term stability of Tc(IV), and here moderate Fe(II) reoxidation and significant Tc remobilisation occurred in both no added Fe(III) and with added Fe(III) systems. There was also evidence for a change in Tc-speciation on reoxidation with the potential for Tc(IV) incorporation into the reoxidised, Fe rich system. In nitrate reoxidation experiments, significant Fe(II) reoxidation occurred, however no significant Tc remobilisation was observed. These data provide the first insights into technetium biogeochemistry in high pH sediments and have significant implications for the long-term fate of technetium in geological disposal scenarios.

6.2. Introduction

^{99}Tc is a long lived ($t_{1/2}$ 2.13 x 10^5 years), high yield (6.14 %) fission product of ^{235}U and will be present in appreciable quantities in radioactive wastes. It exists predominantly as the pertechnetate species (TcO_4^-) in oxic environments, which is highly mobile. Under circumneutral conditions, microbial reduction to Tc(IV) can occur by direct enzymatic pathways (Lloyd et al. 1997; Wildung et al. 2000) or indirectly mediated by Fe(II) biominerals such as magnetite (Lloyd et al. 2000; Fredrickson et al. 2004). Sediment associated Fe(II) has also been found to reduce Tc(VII) (Wildung et al. 2004; Begg et al. 2007; Begg et al. 2008), with the rate of reduction kinetically influenced by Fe speciation and concentration (Fredrickson et al. 2004; Fredrickson et al. 2009; Jaisi et al. 2009;). Tc(IV) predominantly exists as poorly soluble hydrous TcO_2 like phases (Lloyd et al. 2000; Lukens et al. 2002; Wildung et al. 2004; Morris et al. 2008;) or at ultra-dilute concentrations ($<10^{-12}$ mol l^{-1}, below the solubility threshold for TcO_2 precipitation) presumably as Tc(IV) sorbed to sediments (Burke et al. 2010; Lear et al. 2010; Corkhill et al. 2013). Interestingly, Tc(IV) solubility reportedly increases with humic content, high carbonate and chloride in waters (Sekine et al. 1993; Geraedts et al. 2002; Hess et al. 2004; Maes et al. 2004; Zachara et al. 2007; Boggs et al. 2011).

There is increasing international consensus for the management of radioactive waste via geological disposal into the deep subsurface. It is clear that any engineering program of this type will require the use of cement. In addition, many wastes destined for deep disposal are grouted and some concepts consider extensive use of cement as a backfill material. The potential for microbial processes affecting metal transport in the deep subsurface associated with disposal environments is being increasingly recognised (Anderson et al. 2011; Behrends et al. 2012) and a few studies have explored alkaline conditions relevant to geodisposal (for example Rizoulis et al. 2012; Williamson et al. 2013; Williamson et al. in review) and one study exploring pH 10 Tc(VII) reduction with a haloalkaliphilic microorganism (Khijniak et al. 2003). Tc(IV) has been reported to be resistant to reoxidation by air (Burke et al. 2006; Joyce M McBeth et al. 2007; Begg et al. 2008). In some cases, reoxidation of Tc(IV) may be limited by oxygen diffusion into the mineral that Tc has become associated with, such as phyllosilicates (Fredrickson et al. 2009). Tc has also been widely reported to be recalcitrant to reoxidation by nitrate (Begg et al. 2008; Geissler et al. 2011) which will be present in many intermediate level wastes (Albrecht 2013).

The focus of this study is, therefore, to gain a better understanding of Tc biogeochemistry at high pH (10-10.5), using microbiologically active alkaline sediments collected from a legacy lime workings in Buxton, UK. To track biogeochemical transformations, sediment microcosms were spiked with 100 Bq ml^{-1} (1.6 μM) TcO_4^- with and without added ferrihydrite and sealed to allow anoxic conditions to develop, facilitating the microbial reduction of Fe(III) and other potential electron acceptors. Pre-reduced sediments containing biogenic Fe(II) were also reacted with Tc(VII) to probe for abiotic coupling between these two redox active metals. Selected experiments were also run at higher radionuclide concentrations (56 kBq ml^{-1}, 0.9 mM) ^{99}Tc to allow analysis using XAS techniques. Additionally, a set of pre-reduced sediments was prepared with using ^{99m}Tc at ~ 10^{-12} M to quantify radionuclide behaviour in reduced systems at very low concentrations using gamma camera imaging (Lear et al. 2010). Finally, a series of reoxidation experiments on pre-reduced sediments were also conducted to assess the behaviour of Tc after reaction with air and nitrate.

6.3. Materials and methods

6.3.1. Sample collection

Sediments were collected at the margins of a legacy lime workings area at Harpur Hill Buxton, Derbyshire (Rizoulis et al. 2012; Williamson et al. 2013; Williamson et al. in review). Sediments and surface waters were transferred into sterile containers and stored at 4°C in darkness prior to use. The elemental composition of the sediment was determined by X-ray fluorescence (Axios sequential XRF). Full sediment characteristics have been reported previously (Williamson et al. 2013) with materials dominated by calcite, with minor quartz and ankerite

6.3.2. Bioreduction microcosm construction

To investigate Tc(VII) behaviour under anoxic, pH 10 conditions, microcosms were prepared in sterile serum bottles in triplicate with sediments slurried with pH 11.8 surface waters (sediment: solution ratio of 1:10). All systems had 10 mM sodium lactate and 1 g L^{-1} yeast extract added as carbon sources and potential electron donors to stimulate microbial activity, and the pH was adjusted to pH 10 with 1 M HCl before incubation. To explore technetium solubility and its coupling to biogeochemical processes at pH 10, a Buxton sediment and surface water incubation with *no added Fe*(III) and a *with added Fe(III)* system (where 30 mM ferrihydrite was added) were prepared (Williamson et al. 2013). To explore further the mechanisms of radionuclide biocycling under alkaline anoxic conditions, incubations with *no added Fe(III)* and *with*

added Fe(III) were allowed to progress through to Fe(III) reduction for 28 days and then spiked with Tc(VII) as pertechnetate (100 Bq ml^{-1} (1.6 μM)). The headspace of bottles was flushed with argon and the bottles were crimp sealed with thick butyl rubber stoppers, then incubated at 20 °C in the dark. Sample manipulations were performed under anaerobic conditions as appropriate and using aseptic technique. During incubations, the pH of the microcosms dropped, particularly in the first week of the experiment, so during this time, daily pH adjustment to pH 10 was undertaken using 2 M NaOH.

6.3.3. Reoxidation experiments

For air reoxidation experiments, microbially reduced sediments (25 ml) with and without added Fe(III), were transferred into sterile, 250 ml conical flasks sealed with a foam plug and swirled daily. For nitrate reoxidation experiments, bioreduced sediments with and without added ferrihydrite were amended with $NaNO_3$ to a final concentration of 30 mM. Reoxidation experiments were run for 2 months and sampled periodically to monitor for biogeochemical transformations.

6.3.4. Geochemical analyses

Sample slurries were analysed for pH and Eh using a calibrated Denver Instrument Digital Meter and probes. To assess non-detrital Fe, aqua regia digests were run (Chen & Ma 2001), followed by ICP-AES on filtered supernatant (Perkin Elmer Optima 5300 dual view ICP-AES). Biogenic Fe(II) and total bioavailable Fe were assessed by 0.5 N HCl extraction via the ferrozine colorimetric assay on a sub-sample of sediment slurry (Lovley & Phillips 1987). Colorimetric assays were performed on a Jenway 6715 spectrometer and typically, calibration regressions had $R^2 > 0.99$. Samples were then centrifuged (5 mins with a relative centrifugal force of 15,800 *g*) and the supernatant was analysed for NO_2^-, NO_3^- and organic acids (lactic, acetic, formic, propionoic and butyric) using a Dionex DXICS5000 ion chromatograph. Technetium concentrations were measured using liquid scintillation counting (Tri-Carb 1900 TR Scintillation Counter, Packard; Optiphase HiSafe3 Liquid Scintillant, Perkin Elmer) for 10 mins with a detection limit of 30 cpm (ca. 0.5 Bq). Additionally, the speciation of aqueous Tc was assessed at select points using extraction with tetraphenylarsoniumchloride (TPAC) (Wildung et al. 2000).

6.3.5. X-ray absorption spectroscopy (XAS)

To determine the fate of Tc in microcosms, ~ 0.9 mM ^{99}Tc was injected into a range of sediment treatments. An air reoxidation sample from the *with added Fe(III)* progressive anoxia system was prepared by agitation on an orbital shaker under a CO_2 controlled atmosphere for 7 days. Solid samples for analysis were obtained by centrifugation of the suspension and removal of the supernatant. The resulting wet paste was mounted onto an airtight XAS sample cell, which was double sealed with Kapton film and heat sealed into a vacuum bag in an anaerobic glove box (Coy Laboratory Products, MI) and stored in an argon filled Kilner jar at -80 °C prior to analysis at the Diamond Light Source, Didcot, Oxford, UK. Tc K edge spectra were collected at room temperature on beamline B18 in fluorescence mode using a 9-element Ge detector (Dent et al. 2009). Spectra from a Tc(VII) standard (TcO_4^-) was collected in transmission mode and a Tc(IV) standard was taken from the literature (Hess et al., 2004). Multiple scans were collected for each system and scans were averaged to improve the signal to noise ratio. The merged XANES spectra were obtained following background subtraction and normalisation, and linear combination fitting (LCF) between end member spectra was performed using ATHENA (Ravel & Newville 2005). EXAFS fitting was in k^3 space typically between 3 and 13 $Å^{-1}$ and using ARTEMIS (Ravel & Newville 2005). Shells were included in the fit only if the overall R-factor was improved by >5 % and the new fit satisfied the reduced X^2 test.

6.3.6. 16S rRNA gene amplicon pyrosequencing and data analysis

Bacterial community structure was examined in the bulk Buxton sediment and in microcosms supplemented with low (100 Bq ml^{-1}) and high (56 kBq ml^{-1}) Tc with *no added Fe(III),* and *with added Fe(III)* at incubation end points. DNA was isolated from ~ 0.2 g of sediment using the MoBioPowerSoil™ DNA Isolation Kit (MoBio Laboratories, Inc., Carlsbad, CA, USA). PCR for amplicon pyrosequencing was performed using tagged fusion bacterial primers 27F (Lane 1991) and 338R (Hamady et al. 2008), targeting the V1-V2 hypervariable region of the bacterial 16S rRNA gene, targeting the V1-V2 hypervariable region of the bacterial 16S rRNA gene. Details of the PCR procedure have been previously reported (Williamson et al. in review). The fusion forward primer (5'-CCATCTCATCCCTGCGTGTCTCCGACTCAGNNNNNNNNNNAGAGTTTGATC MTGGCTCAG-3'contained the 454 Life Sciences "Lib-L Primer A", a 4 base "key" sequence (TCAG), a unique ten-base barcode "MID" sequence for each sample, and bacterial primer 27F. The series of N`s in the primer denotes the MID and is different

for each specific sample as follows. Roche's MID4 barcode (AGCACTGTAG) was used for the bulk Buxton sediment, for the low Tc experiments, MID5 (ATCAGACACG) for 28 day *no added Fe(III)* sample, MID6 (ATATCGCGAG) for 28 day *with added Fe(III)* and for the 60 day high Tc experiments, MID7 (CGTGTCTCTA) for *no added Fe(III)*, and MID8 (CTCGCGTGTC) for *high Tc with added Fe(III)*. The reverse fusion primer (5'-CCTATCCCCTGTGTGCCTTGGCAGTCTCAGTGCTGCCTCCCGTAGGAGT-3') contained the 454 Life Sciences "Lib-L Primer B", a 4 base "key" sequence (TCAG), and bacterial primer 338R. The pyrosequencing run was performed at The University of Manchester sequencing facility, using a Roche 454 Life Sciences GS Junior system. The 454 pyrosequencing reads were analysed using Qiime 1.6.0 release (Caporaso et al. 2010), and de-noising and chimera removal was performed in Qiime during OTU picking (at 97% sequence similarity) with usearch (Edgar 2010). Taxonomic classification of all reads was performed in Qiime using the Ribosomal Database Project (RDP) at 80 % confidence threshold (Cole et al. 2009), while the closest GenBank match for the OTUs that contained the highest number of reads (the representative sequence for each OTU was used) was identified by Blastn nucleotide search. In addition, Qiime was used to show the rarefaction curves.

6.3.7. Geochemical modelling

Geochemical modelling was used to assist the interpretation of the Tc concentration data obtained during bioreduction. The PHREEQC (version 2) geochemical speciation and reaction computer program (Parkhurst & Appelo 1999) was used to calculate the solubility of reduced Tc(IV) phases under the measured solution pH (9.76) and Eh (-369 mV) conditions including the effect of carbonate and acetate. The solubility of the phase $TcO_2.1.6H_2O$ was calculated using thermodynamic data for Tc reviewed by the NEA Thermodynamic Database Project (Guillaumont & Mompean 2003) and which includes Tc(IV) carbonate and acetate complexes. In addition, the solubility of an amorphous phase $TcO_{2(am)}$ was calculated which is defined by the HATCHES thermodynamic database, which uses the NEA Tc(IV) aqueous speciation model (Bond et al. 1997). This more soluble phase is based on solubility measurements undertaken by UK Nirex Ltd. The potential effect of carbonate complexation on Tc solubility was examined by modelling Tc solubility at maximum representative concentrations of carbonate measured in the bioreduction experiments (20 mM) and with no carbonate. A

concentration of 5 mM acetate was included in both speciation calculations to represent volatile fatty acids present.

6.3.8. Gamma imaging of ^{99m}Tc associated activity

Microcosms were transported to the Manchester Royal Infirmary (UK) for ^{99m}Tc imaging with a dual-headed Siemens Symbia T6 gamma camera (Siemens healthcare Erlangen, Germany) with a high resolution general purpose collimator (2 mm holes, 0.5 cm accuracy). Pre-reduced sediments with *no added Fe(III)* and *with added Fe(III)* and a biogenic magnetite control at pH 7 (synthesized using *Geobacter sulfurreducens* (Byrne et al. 2011) and containing ~30 mM Fe(II)) were spiked with ca 18-22 MBq of ^{99m}Tc activity as pertechnetate (final concentration ~ 20 x 10^{-12} M ^{99m}Tc). After injection of the ^{99m}Tc, samples were placed between the two planar detector heads of the gamma camera, orientated vertically, and images of the ^{99m}Tc distribution acquired. The initial series of images comprised 48 sequential 15 minute images for the first 12 hours, followed by a further 15 minute image at 26 hours post-injection. After imaging was complete, samples were stored at ambient temperature for 7 days to allow ^{99m}Tc to decay to background levels. The images from both detector heads were analysed by defining two background regions, and regions over the areas of the image representing the sediment, suspension and remainder of the container for each sample at each time-point. The proportion of ^{99m}Tc that had settled with the sediment, and that in the remainder of the aqueous fraction were calculated using the geometric mean of background-corrected total counts per second for each sample region, corrected for radioactive decay. Image analysis and export of images from gamma-camera data acquisition were conducted using Xeleris workstation imaging software (GE Medical Systems, Milwaukee, WI).

6.4. **Results and discussion**

6.4.1. Sediment and surface water characteristics

Sediment elemental composition, as determined by XRF, was dominated by Ca (51.2 wt %), with significant concentrations of Si (1.1 wt %), Al (0.5 wt %) and Fe (0.17 wt %). The total iron in the sample was assessed by aqua regia digestion and ICP-AES analysis with 1.03 g kg^{-1} (18.4 mM kg^{-1}) Fe. Additionally, the bioavailable Fe was estimated by ferrozine assay after 0.5 N HCl extraction (Lovley and Phillips, 1988) and here, 8.95 mM kg^{-1} Fe was extracted indicating ~ 50 % of the total Fe was “bioavailable”.

6.4.2. Biogeochemistry in sediment microcosms

To explore the biogeochemistry of technetium under anoxic conditions at pH 10, microcosms were constructed using calcite dominated sediments and surface waters from a high pH lime workings site in the UK (Williamson et al. 2013; Williamson et al. in review) **(**Supporting Information Table 1). Bioreduction progressed through a cascade of terminal electron acceptors in both the *no added Fe(III)* and *with added Fe(III)* experiments (Figure 1A and B). For the *no added Fe(III)* experiment, nitrate removal to below detection limit and significant Fe(II) ingrowth (0.95± 0.21 mmol L^{-1} of slurry) from Fe(III) reduction had occurred by day 3, indicating anaerobic processes were established quickly (Supporting Information Figure 1). In the systems *with added Fe(III)*, again complete nitrate removal had occurred by day 3 (Supporting Information Figure 1), Fe(II) ingrowth to sediments occurred from 3 days and by day 28 had stabilised at 4.82 ± 0.55 mmol L^{-1} of slurry (Figure 1B).

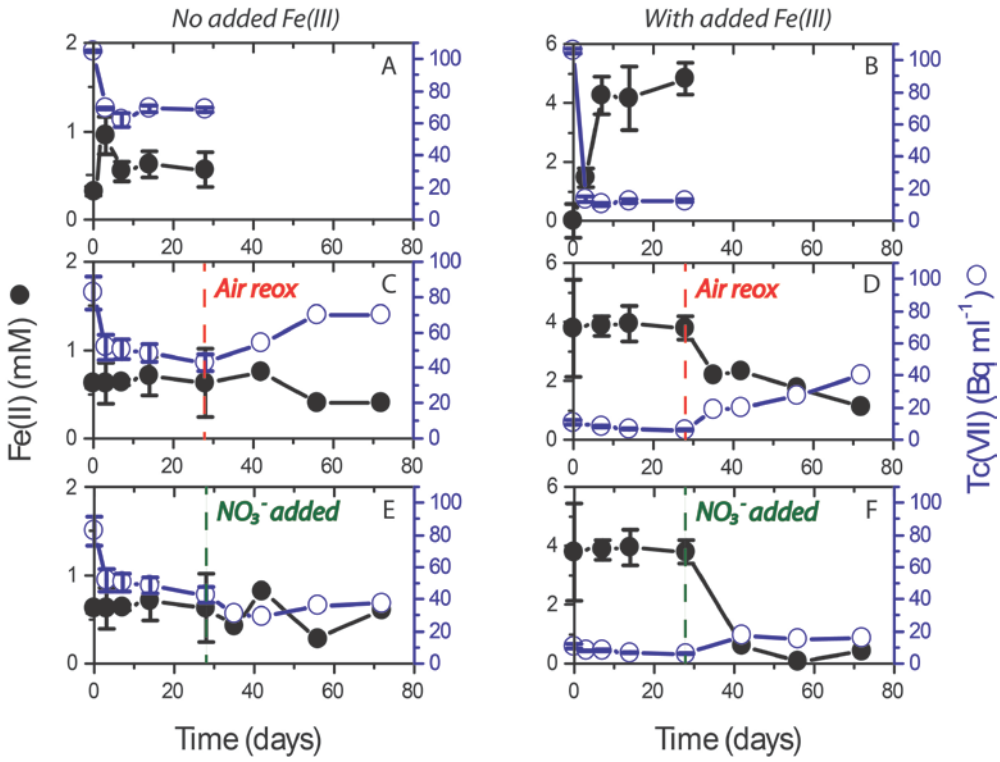

Figure 1: Redox cycling on Fe and technetium in high pH sediments showing 0.5 N HCl extractable Fe(II) concentration (●) and % Tc(VII) in solution (O) in progressive anoxia experiments with: (A) no added Fe(III); (B) with added Fe(III), and pre-reduced sediments with no added Fe(III) (C+E), and with added Fe(III) (D+F). Error bars are 1σ of triplicate results (where not shown, errors are within the size of the symbol). Dashed lines indicate the start of reoxidation experiments; red for air and green for nitrate (reoxidation were run as single experiments).

6.4.3. Technetium fate during bioreduction- *no added Fe(III)* systems

To investigate Tc behaviour in the Buxton sediment microcosms, Tc(VII) was spiked into range of sediment treatments and monitored with time. In the *no added Fe(III)* system, the initial time point at 1 hour showed no removal of Tc(VII) had occurred as expected, however by day 3, 30% removal of Tc had occurred, presumably via reductive sorption to sediments as Tc(IV). Interestingly, TPAC analysis on the < 0.2 µm filtered aqueous phase at day 3 suggested that a significant fraction of the filterable Tc was speciated as Tc(IV) in the extraction. This suggests a soluble or colloidal Tc(IV) phase may exist in these carbonate dominated systems (Wildung et al. 2000). This was supported by γ-imaging experiments with 20 pM ^{99m}Tc, which indicated that up to ~40 % was present in the aqueous suspension after 26 hours of settling in contrast to the with added Fe(III) and magnetite ^{99m}Tc experiments, where clear partitioning was seen at 26 hours (Figure 2). Together these data suggest that strong partitioning to the bulk sediment was not occurring at between 10^{-6} and 10^{-12} M Tc concentrations in the *no added Fe(III)* experiments.

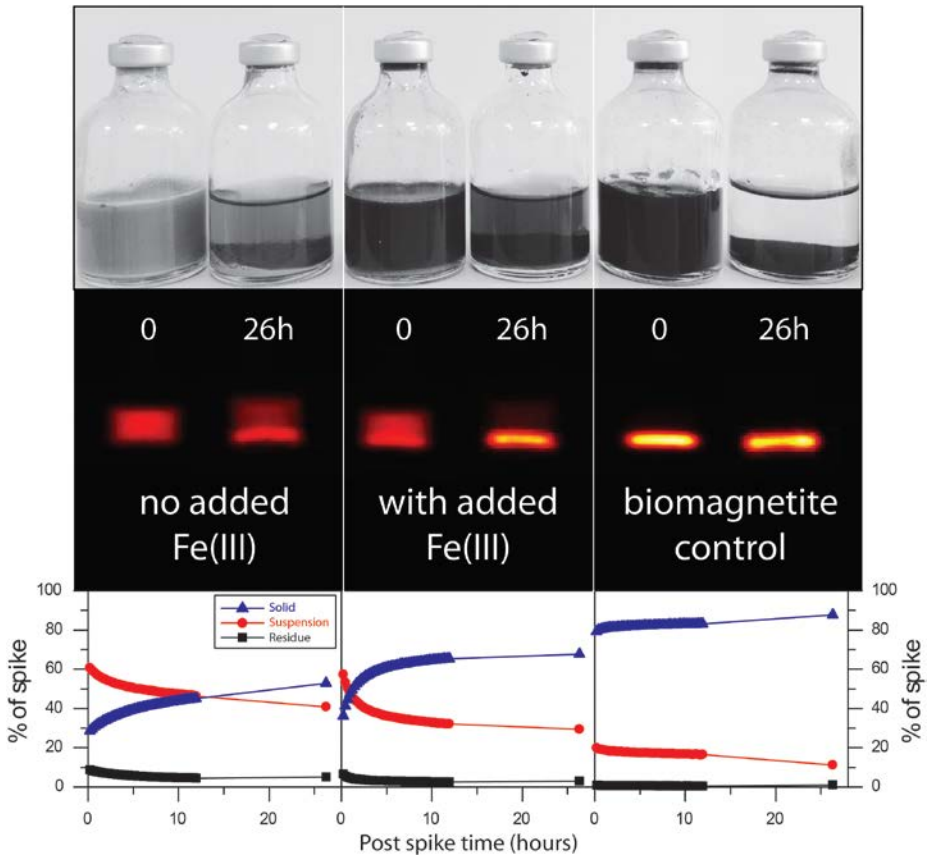

Figure 2: Start and end point γ-camera images for microcosm experiments with no added Fe(III), with added Fe(III) and biomagnetite (reducing control). Images were taken approximately 5 min after injection of ~ 20 pM ^{99m}Tc (0) or following 26 h incubation.

Geochemical modelling calculated that the phase $TcO_{2(am)}$ has a theoretical solubility of 4.51×10^{-8} M under the experimental conditions in the presence of 20 mM of carbonate. In the absence of carbonate, $TcO_{2(am)}$ was decreased by a small amount to 4.29×10^{-8} M. Tc-acetate complexes included in the speciation model had a very low concentration (2.5×10^{-12} M) and do not affect the solubility. The phase $TcO_2.1.6H_2O$ defined by (Guillaumont & Mompean 2003) is less soluble (4.51×10^{-9} M and 4.29×10^{-9} M) in the presence and absence of carbonate respectively. These calculations indicate that under the experimental conditions used, carbonate complexation had only a minor effect on Tc solubility. Significantly, the measured activity of Tc after bioreduction of the 100 Bq ml^{-1} spiked experiments was 68 Bq ml^{-1}, 1×10^{-6} M, more than one order of magnitude above the modelled solubility of $TcO_{2(am)}$. This suggests that Tc may be associated with colloidal material present in the supernatant in these oversaturation experiments. The modelled solubility of $TcO_{2(am)}$ and $TcO_2.1.6H_2O$ under the experimental conditions is around 200 times higher than the concentration of the 20 pM ^{99m}Tc experiments, where Tc(IV) is more likely to be sorbed to the reduced mineral phases. Given that the supernatant of these experiments was cloudy even at 26 hours (Figure 2), it is possible that Tc(IV) is associated with unsettled fines and/or is in true solution as a species which is not within the database. Interestingly, several studies have observed incomplete removal of Tc to solids in μM concentration ranges (< 0.22 μm filtered) (Wildung et al. 2000; Geraedts et al. Maes et al. 2004; Wildung et al. 2004; Law et al. 2010) and at elevated pH (Thorpe et al. 2014) and these observations clearly warrant further work.

In order to explore further the speciation of solid phase associated Tc, Tc K-edge XANES and EXAFS spectra were collected on sediment experiments at higher Tc concentrations (56 kBq ml^{-1}). We note that, due to the elevated levels of ^{99}Tc in these samples, pH amendment was not performed and that at the end of the experiments the following pH values were recorded; 8.2 in the *no added Fe(III)* system and 8.8 in the *with added Fe(III)* system. In the *no added Fe(III)* system, after 60 days of incubation, removal of Tc in the XAS sample was consistent with the lower level experiments. The XANES spectrum of the solids showed a Tc(IV) like signature confirming reductive precipitation to Tc(IV). Linear combination fitting between end members comprising a Tc(VII) standard (pertechnetate) and a Tc(IV) standard (crystalline TcO_2) showed a 100 % contribution from the Tc(IV) spectrum. The Tc EXAFS data could be fitted with a short chain hydrous TcO_2 model (Lukens, J. I. Bucher, et al. 2002; Peretyazhko et al.

2012; Peretyazhko et al. 2008) using 6 O at 2.02 Å and 2 Tc at 2.56 Å (Figure 4A; Supporting Information Table 2). When Tc was added to pre-reduced sediments with *no added Fe(III)*, approximately 50 % of the Tc(VII) was removed to the solid phase by day 28 and the XANES and EXAFS were consistent with the presence of Tc(IV) species. This suggested a relatively low reactivity for the solid phase but that an abiotic, Fe(II)–mediated reduction pathway for Tc(VII) was possible in these low Fe systems at elevated pH (Figure 1,3 4; Supporting Information Table 2).

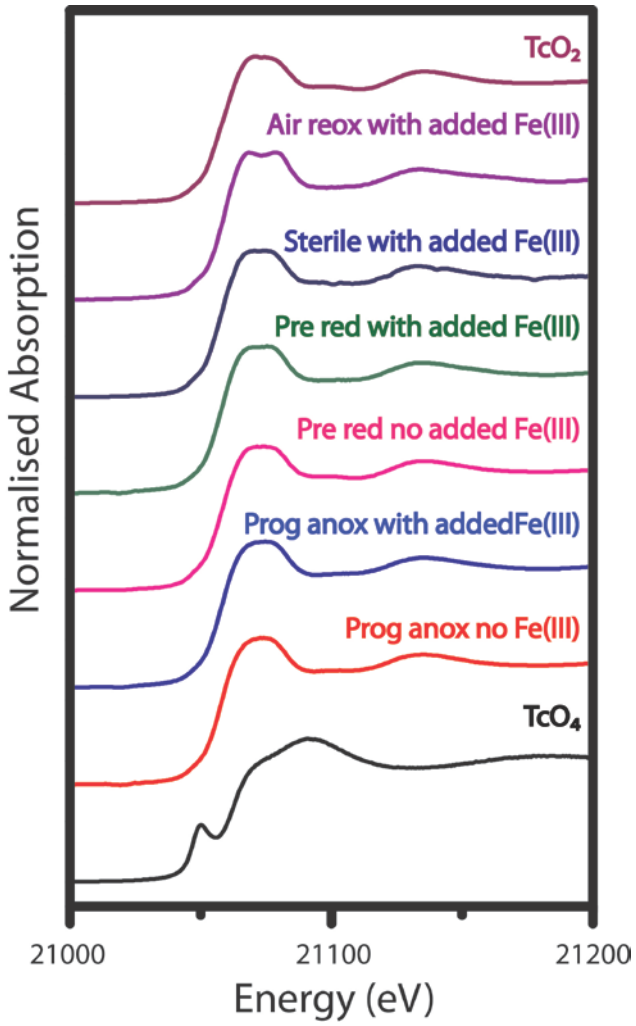

Figure 3: ^{99}Tc K edge XANES stack plot of all bioreducing, sterile and reoxidation treatments with Tc(VII)O_4^- and Tc(IV)O_2 reference spectra (Hess et al. 2004).

6.4.4. Technetium fate during bioreduction- *with added Fe(III)* systems

In the *with added Fe(III)* microcosms, Tc was soluble at the first time point, as expected, indicating no reductive removal in the initial incubation. However, near complete removal of Tc occurred by day 3, with 0.22 ± 0.03 µM (approximately 10 % of the initial spike) remaining in solution, which is around 4 times the modelled solubility of $TcO_{2(am)}$. These observations were consistent with γ-imaging experiments

with 20 x 10^{-12} M ^{99m}Tc, where 60 % was removed to solids by one day, again showing a greater reactivity of the Fe(II) biominerals to Tc(VII) in this system. Interestingly, for the ultra-dilute imaging experiments, ^{99m}Tc(VII) removal in this system was at a lower rate and extent than the biomagnetite control. This may be a result of a lower reactivity in these pH 10 systems compared to biomagnetite at pH 7, or it may reflect varying effects of Tc(IV) associated with suspended material present in the gamma study microcosm experiments (Figure 2).

The development of Fe(III)-reducing conditions was also robust in the parallel XAS experiments run at 56 kBq ml^{-1}. In both microbially active progressive experiments (with Tc added prior to incubation of the microcosms) and "pre-reduced" high activity samples (that had been incubated for 60 days prior to Tc addition), significant Fe(III) reduction had occurred (~50 % of the bioavailable Fe(III) fraction), similar to the low level Tc system although the end point pH here was 8.8. Both XANES and LCF analyses confirmed complete reductive removal of Tc(IV) had occurred (Figure 3). The EXAFS spectrum could be fitted with a similar model to the *no added Fe(III)* system, with 6 O at 2.01 Å, and 2 Tc at 2.51 Å, consistent with a hydrous TcO_2 like phase (Figure 4B; Supporting Information Table 2). Interestingly, Fe(III) reduction was visually slower than in the low level experiment, which may suggest that Tc had a radiotoxic effect on the microbial community, previously observed in a haloalkaliphilic community at pH 10 (Khijniak et al. 2003).

Tc was also spiked into microbially active and autoclaved pre-reduced pH 10 sediments *with added Fe(III)*, where significant Fe reduction had occurred forming magnetite (Williamson et al., 2013). Complete removal occurred at the first time point in the ^{99}Tc low level experiments, suggesting a high reactivity of Fe(II) in this system to Tc(VII); magnetite has been showed to be a potent Tc(VII) reductant at circumneutral pH (Lloyd et al. 2000; Fredrickson et al. 2004; Fredrickson et al. 2009). In the parallel high activity sample, XANES and LCF analyses confirmed complete reductive precipitation to Tc(IV) and the microbially active EXAFS spectrum could be fitted with a hydrous Tc like spectrum (Figure 3; Figure 4D; Supporting Information Table 2). The addition of a further shell of 1 Fe at 3.53 Å also significantly improved the fit, suggesting that the reduced Tc(IV) phase has an association with the Fe(II)-bearing minerals in this magnetite dominated system (Williamson et al. 2013).

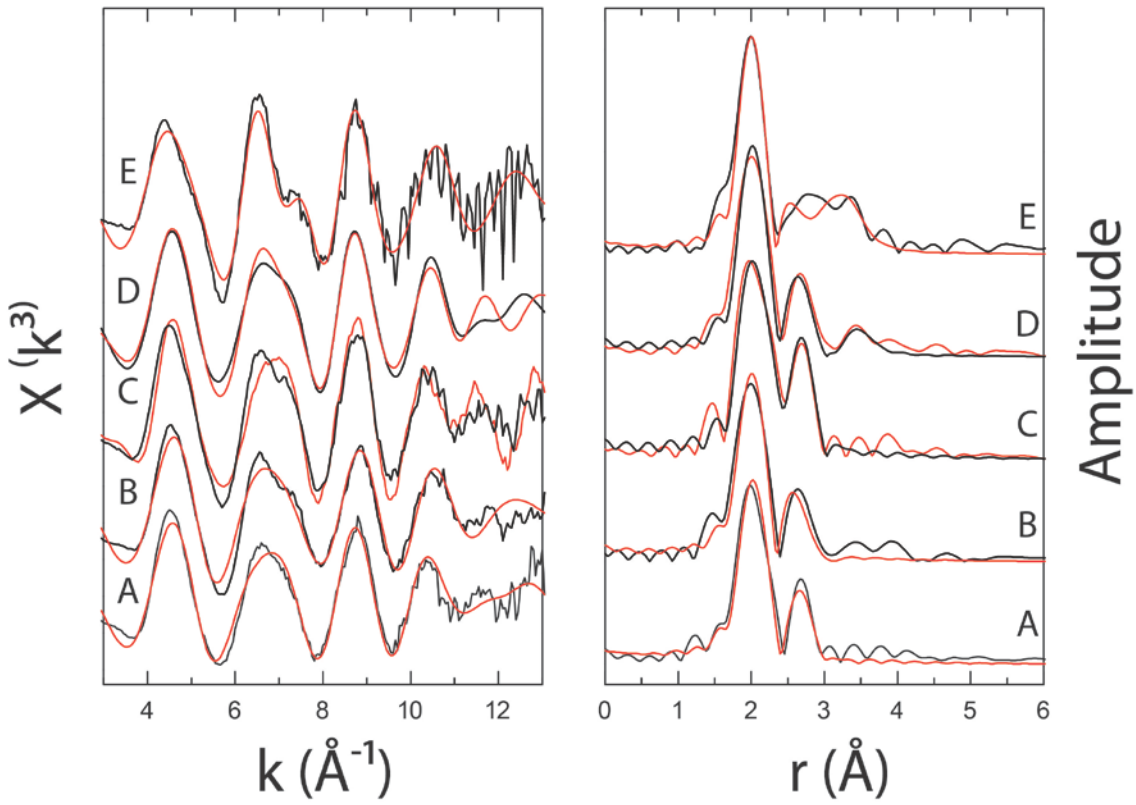

Figure 4: k^3 weighted ^{99}Tc K edge EXAFS spectra (left) and Fourier transform (right) for progressive anoxia experiments; (A) no added Fe(III); (B) with added Fe(III), and pre-reduced experiments with (C) no added Fe(III); (D) with added Fe(III) and (E) air reoxidised pre-reduced sediments with added Fe(III). The Fourier Transform is plotted with a phase correction calculated from the first shell of oxygen backscatterers. Black lines are the experimental data and red lines are the best-fit models (SI Table 2).

6.4.5. Air reoxidation experiments

During the geological disposal of radioactive waste, reoxidation may occur via ingress of oxygenated groundwaters (Riekkola et al. 2003). When the *no added Fe(III)* sediments were exposed to air, oxidising conditions re-established by day 1 and significant (approximately 30 %) Fe(II) reoxidation occurred by 1 month, and the Eh had risen to + 100 mV after 2 months. Significant Tc(VII) remobilisation was apparent after 2 months of reoxidation, with 70 % of the initial spike in solution, and similar to past work (Burke et al. 2006; Begg et al. 2007; McBeth et al. 2007; Geissler et al. 2011).

When pre-reduced sediments *with added Fe(III)* were reoxidised with air, the Eh rose to +127 mV, and significant Fe(II) reoxidation (~75 %) and Tc remobilisation (~ 40 % of

the initial spike) occurred over 2 months. XAS analysis was possible on the parallel high level sample and the XANES showed a Tc(IV) like spectrum. Interestingly there was a double peak in the near edge of this spectrum (Figure 3), which has been previously attributed to Tc-Fe bonding (Heald et al. 2012). The EXAFS spectrum did not fit well with the hydrous TcO_2 like structure used for the reduced samples (Supporting Information Table 2). A much better fit was obtained assuming Tc substitution into the octahedral site of partially reoxidised magnetite as recently observed in mineralogical experiments (Marshall et al. in review) (Figure 4E; Supporting Information Table 2).

6.4.6. Nitrate reoxidation experiments

Reoxidation may also occur during geological disposal by reaction with oxidants such as nitrate present in the wasteform (Jacquot et al. 1997; Albrecht 2013). When pre-reduced sediments with *no added Fe(III)* sediments were reoxidised by the addition of 30 mM nitrate, complete removal of NO_3^- occurred by 14 days, however only minor transient NO_2^- (~ 0.5 mM) formed. Moderate Fe(II) reoxidation also occurred, however, no significant Tc(VII) remobilisation was noted (< 5 %) in these systems after 2 months, consistent with past work (McBeth et al. 2007; Begg et al. 2008; Morris et al. 2008; Geissler et al. 2011). In the *with added Fe(III)* system, the Eh rose to +41.2 mV and complete reduction of the added nitrate to nitrite occurred by day 14, however no further denitrification was observed. Essentially complete Fe(II) reoxidation occurred by day 28, however no significant Tc remobilisation (< 10 %) was observed after 2 months.

6.4.7. Bacterial diversity assessed by 16S rRNA gene amplicon pyrosequencing

Pyrosequencing of the bulk Buxton sediment revealed a diverse community with 4383 reads (after de-noising and removal of short chimeric reads) grouped to 193 operational taxonomic units (OTUs at 97 % sequence ID similarity) affiliated to 32 bacterial phyla. These were dominated by Firmicutes (31.3 %), Proteobacteria (25.2 %) and Bacteroidetes (24.5 %), (Figure 5; Supporting Information Table 3). After 28 days of incubation of the *no added Fe(III)* sediment, with low concentrations of Tc, a far less diverse community was seen with 4527 reads and 81 OTUs (Supporting Information Table 3). This interpretation was supported by rarefaction curves (Supporting Information Figure 2). Sequence analyses showed that there was a clear enrichment in organisms affiliated with Firmicutes (76.6 %) (Figure 5). A similar streamlining of

diversity was observed in the *with added Fe(III)* low Tc concentration system after 28 days incubation, with 5196 reads and 73 OTUs, again with Firmicutes (67.3 %) dominating (Figure 5; Supporting Information Table 3). These community shifts may indicate that alkaline metal reduction is driven by Gram-positive Firmicutes, implicated in previous work on samples from this site (Williamson et al. 2013; Williamson et al. in review).

In all incubations, there was also enrichment in sequences affiliated with Bacilli, with 16.7-26.4% most closely related to *Trichoccocus* sp. N1 (Accession number JN688044) capable of cellulose degradation (Gao et al. 2014) (Supporting Information Table 4). Additionally, in systems with low levels of Tc, there was a significant increase in sequences previously detected in samples from the same site, designated bur-71 (JX417349), closely affiliated to the Erysipelotrichi class of the Firmicutes (100 % similarity, 9.5-11.8 % of the pyrosequencing reads) (Williamson et al. 2013) and a close relative (96 % similarity (9.2-14.5 %) to *Proteocatella sphenisci* strain PPP2, a pyschrotolerant, spore forming fermentative anaerobe (Pikuta et al. 2009) (Supporting Information Table 4). Interestingly, in the *with added Fe(III)* sample, there was a close match (99 % similarity, 8.5 % of sequences) to an uncultured *Alkaliphilus* sp. (KF954221), previously noted in a hyperalkaline site in Allas Springs, Cyprus (Rizoulis personal communication) (Supporting Information Table 4).

In the *no added Fe(III)* system augmented with higher concentrations of Tc for XAS, the microbial community was enriched in γ-Proteobacteria related sequences after 56 days of incubation. Further community analysis revealed that 41.9 % of the reads were affiliated (100 % sequence similarity) to *Pseudomonas* sp. D65lp (JN228318), (Jutkina et al. 2011) (Supporting Information Table 4). In the XAS sample *with added Fe(III)*, a lower abundance of γ-Proteobacteria was observed and the community was dominated by a β-Proteobacterium, designated clone 9GQ-39 (JN133830), and affiliated to *Rhodoferax* (Muruganandam et al. unpublished) (100% sequence match, 10.1 of sequences) and a close match to *Pelosinus* sp.UFO1 (DQ295866) (97 % sequence similarity, 6.84 % of sequences) (Ray et al. 2010) belonging to the Clostridia class, which have been found in Fe(III)-reducing enrichments obtained from various environments (Supporting Information Table 4). The presence of Gram-negative bacteria in these high level Tc systems, especially in the *no added Fe(III)* system, may be linked to the drop in pH observed by the end of the incubation as pH amendment was not possible in these higher activity experiments.

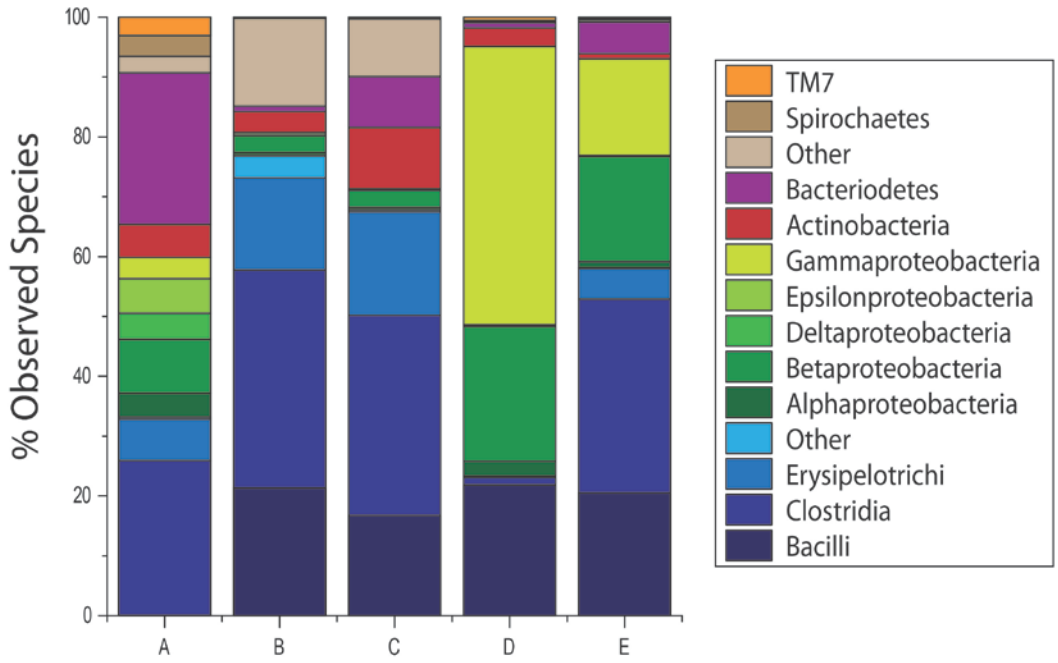

Figure 5: Bacterial phylogenetic diversity at the Phylum level for (A) bulk unamended sediment; low level Tc bioreduction experiments (B) no added Fe(III); (C) with added Fe(III) and high level Tc bioreduction experiments (D) no added Fe(III); (E) with added Fe(III). Only the phyla with more than 1% of the total number of reads are shown. Abundance at the class level is shown for Firmicutes (blue hues) and Proteobacteria (green hues).

6.5. Conclusions and geochemical significance

We show, for the first time, that an indigenous microbial community can mediate Tc(VII) reduction under alkaline conditions. In systems without added Fe(III), Tc(IV) removal occurred; although at a relatively low reactivity (~ 40 % removal). In the parallel high level experiments, solid associated Tc was determined by XAS to be hydrous TcO_2 like phases. Modelling of the system suggested that Tc was present in the aqueous phase, above the modelled solubility of amorphous or hydrated TcO_2 and including carbonate complexation effects. This points to the association of Tc with colloids, which clearly warrants further study, to fully understand the impact of microbial processes on Tc fate and mobility in high pH reduced systems. Nevertheless, this first observation of bioreduction of Tc under alkaline conditions, relevant to the geological disposal of ILW, is significant in underpinning current assumptions made in the safety case for geological disposal that Tc(IV) will be the dominate species. The observation that bioreduction occurs at very low (2×10^{-11} M) concentrations below the predicted TcO_2 solubility indicates that such bioreduction processes will also be of significance in more distal regions away from the waste source where sorption

processes become more significant. In systems *with added Fe(III)*, the resultant Fe(II) bearing magnetite dominated sediments showed enhanced reductive removal of Tc(IV) compared to the *no added Fe(III)* systems. Additionally, when these systems were exposed to air, there was a suggestion that Tc(IV) incorporation into the reoxidised Fe(III) mineral may be possible. The high stability of these reduced Tc(IV) bearing phases to oxygenated water ingress and potential oxidants in the ILW wasteform such as nitrate also has implications in the safe long-term sequestration of technetium.

6.6. Acknowledgements

This work has been funded as part of the NERC BIGRAD consortium through UK Natural Environment Research Council consortium grant NE/H007768/1. JRL acknowledges financial support from the Royal Society. Beamtime at beamline B18 was funded by grants SP7367 and SP7593 from the Diamond Light Source. We thank Prof. Fred Mosselmans and Dr. Steve Parry for assistance at Diamond and Carolyn Pearce for helpful discussions. We also thank Alistair Bewsher and Paul Lythgoe for analytical geochemistry support.

6.7. Supporting information

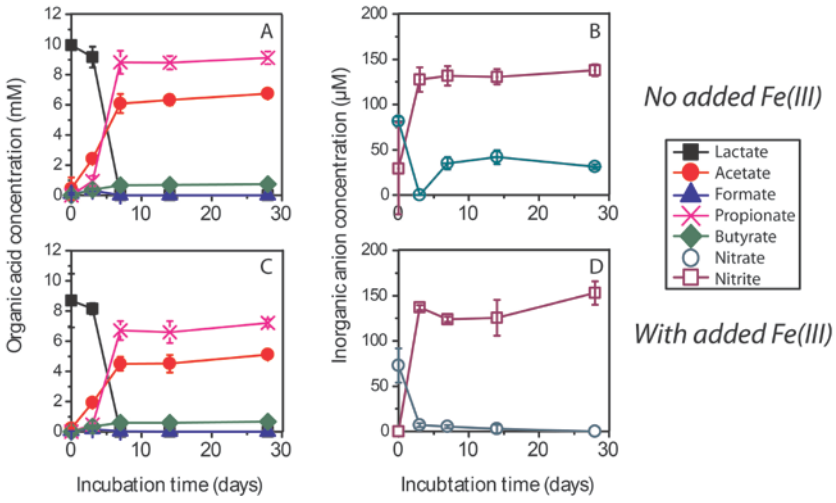

SI Figure 1: Ion chromatographic analysis of organic acids and inorganic anions in supernatant samples taken from the progressive anoxia systems with no added Fe(III) (A+B) and with added Fe(III) (C+D) over a 28 day incubation period.

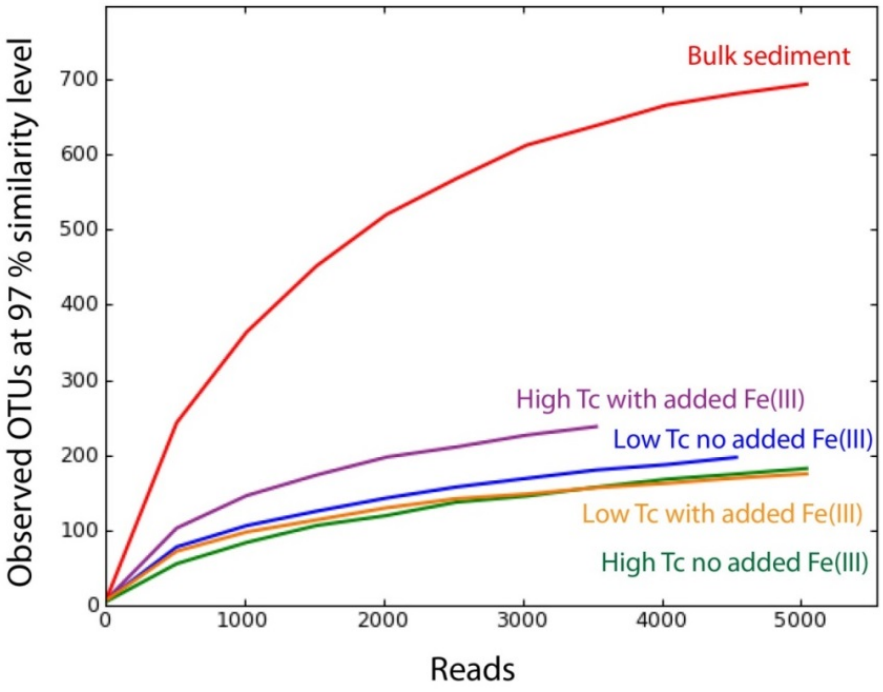

SI Figure 2: Rarefaction curves showing the number of observed operational taxonomic units (OTUs) at 97 % ID similarity per sample, after 16S rRNA gene amplicon pyrosequencing.

SI Table 1: Buxton Harpur Hill lime workings groundwater major anions and cations.

Cations	**Na^{+}**	**Al^{3+}**	**Si^{4+}**	**K^{+}**	**Ca^{2+}**	**Sr^{2+}**	**Ba^{2+}**
Concentration (mg/l)	36.4	0	0.004	5.24	75.8	0.17	0

Anions	**Cl^{-}**	**NO_3^{-}**	**NO_2^{-}**	**SO_4^{2-}**	**PO_4^{3-}**
Concentration (mg/l)	58.3	33.5	0	7.7	0

SI Table 2: EXAFS fitting results from progressive anoxia experiments: (A) no added Fe(III); (B) with added Fe(III); pre-reduced sediments with (C) no added Fe(III); (D) with added Fe(III) and (E) air reoxidised pre reduced sediments with added Fe(III). CN denotes coordination number, r is interatomic distance (Å) and σ^2 is Debye Waller factor ($Å^2$). ΔE_0 represents the shift in energy from the calculated Fermi level (eV) and $S0^2$ denotes the amplitude factor which was constrained between 0.85 and 1.05. R is the goodness of the fit and χ_v^2 is the reduced χ^2 value. Numbers in parentheses are the standard deviation on the last decimal place.

Sample	% Tc (s)	Shell	Path	CN	r (Å)	$2\sigma^2$ ($Å^2$)	ΔE_0 (eV)	$S0^2$	R	χ_v^2
A	51	1	O	6	2.02 (1)	0.011 (3)	-0.55 ±1.88	0.85 (8)	**0.043**	627
Hydrous TcO_2		2	Tc	2	2.56 (2)	0.017 (4)				
B	98.5	1	O	6	2.01 (1)	0.011 (4)	-2.36 ±2.42	0.88 (12)	**0.044**	1304
Hydrous TcO_2		2	Tc	2	2.51 (2)	0.020 (5)				
B	98.5	1	O	6	2.01 (2)	0.011 (4)	-1.04 ±2.14	0.89 (13)	0.037	1333
Sorbed fit		2	Tc	2	2.51 (2)	0.020 (5)				
		3	Fe	1	3.51 (7)	0.014 (16)				
C	70	1	O	6	2.01 (1)	0.010 (3)	-0.55 ±1.88	0.85 (11)	**0.043**	627
Hydrous TcO_2		2	Tc	2	2.57 (2)	0.017 (4)				
D	99	1	O	6	2.01 (1)	0.009 (4)	-1.23 ±2.08	0.89 (13)	0.050	1418
Hydrous TcO_2		2	Tc	2	2.54 (2)	0.016 (4)				
D	99	1	O	6	2.01 (1)	0.010 (3	-1.17 ±2.01	0.90 (13)	**0.038**	1361
Sorbed fit		2	Tc	2	2.54 (2)	0.017 (4)				
		3	Fe	1	3.53 (6)	0.010 (13)				
D	99	1	O	6	2.01 (2)	0.009 (4)	-0.83 ±2.38	0.87 (14)	0.030	1830
Incorporated fit		2	Tc	1	2.54 (2)	0.008 (4)				
		3	Fe	1	3.10 (11)	0.022 (28)				
		4	Fe	1	3.53 (9)	0.013 (20)				
E	50	1	O	6	2.00 (2)	0.008 (2)	-4.27 ±3.16	0.85 (5)	0.124	181
Hydrous TcO_2		2	Tc	2	2.45 (5)	0.028 (14)				
E	50	1	O	6	2.00 (2)	0.008 (2)	-4.82 ±2.45	0.85 (5)	0.091	145
Sorbed fit		2	Tc	2	2.45 (4)	0.026 (11)				
		3	Fe	2	3.50 (4)	0.010 (8)				
E	50	1	O	6	2.01 (2)	0.010 (2)	-3.45 ±2.46	0.85 (3)	**0.047**	131
Incorporated fit		2	Tc	0.8	2.50 (3)	0.012 (8)				
		3	Fe	3	3.08 (5)	0.024 (13)				
		4	Fe	3	3.49 (4)	0.023 (10)				

SI Table 3: Number of pyrosequencing reads obtained for (A) bulk unamended sediment; the low Tc experiments (B) no added Fe(III) reduction 28 days; (C) with added Fe(III) reduction 28 days; and the high Tc experiments (D) no added Fe(III) reduction 56 days and (E) with added Fe(III) reduction 56 days, number of reads after denoising and removal of short and chimeric sequences, and the number of observed operational taxonomic units (OTUs) at 97 % ID similarity.

Sample	**Number of reads**	**Number of reads after chimera check & denoising**	**Observed OTU's**
(A) Bulk unamended sediment	6812	4383	193
(B) Low Tc no added Fe(III)	5325	4527	81
(C) Low Tc with added Fe(III)	6044	5196	73
(D) High Tc no added Fe(III)	5674	4947	97
(E) High Tc with added Fe(III)	4273	3527	110

SI Table 4: Phylogenetic affiliations of the most abundant bacterial OTUs identified in samples from (A) bulk unamended sediment; the low Tc experiments (B) no added Fe(III) reduction 28 days; (C) with added Fe(III) reduction 28 days; and the high Tc experiments (D) no added Fe(III) reduction 56 days and (E) with added Fe(III) reduction 56 days.

% of total population									
(A) Bulk unamended sediment	(B) Low Tc No added Fe(III)	(C) Low Tc With added Fe(III)	(D) High Tc No added Fe(III)	(E) High Tc With added Fe(III)	**Phylogenetic affiliation**	**Closest phylogenetic relative**	**ID % similarity (Identities)**	**Environment (reference)**	**Accession number**
0.1	**20.8**	**16.7**	**21.61**	**19.49**	Firmicutes; Bacilli	*Trichococcus* sp. N1	99 (100)	Cellulolytic (Gao et al. 2014)	JN688044
	14.52	**9.19**			Bacteria	Uncultured bacterium clone BJ	99 (100)	Activated sludge (Xiao et al. unpublished)	NR_041885
						Proteocatella sphenisci strain PPP2	96 (100)	Psychrotolerant spore forming anaerobe (Pikuta et al. 2009)	KC551725
5.02	**11.79**	**9.5**	0.12	1.24	Firmicutes; Erysipelotrichi	Uncultured bacterium clone bur-71	100 (87)	Alkaline Fe(III)-reducing consortium (Williamson et al. 2013)	JX417349
0.21	**7.25**	**4.48**		2.33	Firmicutes; Clostridia	*Proteiniclasticum* sp.	99 (100)	Cellulolytic (Gao et al. 2014)	JN688045
						Uncultured bacterium clone a82	99 (100)	Cr (VI) resistant and reducing bacteria (Chen et al. unpublished)	HM468016
1.46	2.16	**9.15**		0.06	Bacteria	Uncultured bacterium clone C7	91 (99)	Homo-acetogenic consortium (Parameswaran et al. 2011)	GU595095
		8.5			Firmicutes; Clostridia	*Alkaliphilus* sp.	99 (82)	Hyperalkaline Allas Spring (Rizoulis et al. unpublished)	KF954221
			41.9	0.26	Proteobacteria; Gammaproteobacteria	*Pseudomonas sp. D65lp*	100 (100)	Aromatic Degrading (Jutkina et al. 2011)	JN228318
0.64	0.2	0.58	**7.44**	1.58	Proteobacteria; Betaproteobacteria	*Hydrogenophaga* sp. KAs3-R15	100 (100)	Arsenic transforming bacteria from arsenic contaminated groundwater (Sarkar and Sar. unpublished)	JX110543

		0.02	**6**	0.23	Proteobacteria; Betaproteobacteria	*Methylibium* sp. W125	99 (100)	Oligotrophic denitrifying bacteria (Hashimoto et al. 2005)	AB162105
				10.58	Proteobacteria; Gammaproteobacteria	*Yersinia enterocolitica*	98 (98)	Gut pathogen (Reuter et al. unpublished)	JN688044
1.19	0.04	0.1	0.59	**10.12**	Proteobacteria; Betaproteobacteria	Uncultured bacterium clone 9GQ-39	100 (100)	Iron reduction in biostimualted sediments (Muruganandam et al. unpublished)	JQ086988
						Uncultured bacterium clone D0488F04	99 (100)	Uranium contaminated aquifer (Elifantz et al. 2010)	HQ660787
0.02	0.02	**0.04**		**6.84**	Firmicutes; Clostridia	*Pelosinus* sp. UFO1	97 (100)	Closely matched to various Fe(III), AQDS and U(VI) reducing consortia (Ray et al. 2010)	DQ295866
7	0.4	0.12	0.12		Proteobacteria; Epsilonproteobacteria	Uncultured bacterium clone BG2M07A02	100 (100)	Biological Ammonium Removal from Coal Combustion Wastewaters (Vishnivetskaya unpublished)	JX995633
6.33		1.72	0.24		Bacteriodetes	Uncultured bacterium clone bur-71	100 (87)	Fe(III) reducing consortium (Williamson et al. 2013)	JX417343
						Uncultured soil bacterium clone T68AC-18	99 (100)	Hyperalkaline, chromite ore processing residue (Whittleston et al. unpublished)	FN706497

6.8. References

Albrecht, A., 2013. Les réactions redox dans les barrières ouvragées en béton, leur catalyse microbienne et l'impact sur la spéciation des radionucléides: Introduction et état de l'art. *Revue Générale Nucléaire*, 4, 70–83.

Anderson, C., Johnsson, A., Moll, H. & Pedersen, K., 2011. Radionuclide geomicrobiology of the deep biosphere. *Geomicrobiology Journal*, 28 (5-6), 540–561.

Begg, J.D.C., Burke, I.T., Charnock, J.M. & Morris, K., 2008. Technetium reduction and reoxidation behaviour in Dounreay soils. *Radiochimica Acta*, 96 (9-11), 631–636.

Begg, J.D.C., Burke, I.T. & Morris, K., 2007. The behaviour of technetium during microbial reduction in amended soils from Dounreay, UK. *Science of The Total Environment*, 373 (1), 297–304.

Behrends, T., Krawczyk-Bärsch, E. & Arnold, T., 2012. Implementation of microbial processes in the performance assessment of spent nuclear fuel repositories. *Applied Geochemistry*, 27 (2), 453–462.

Bond, K. A, Heath, T. G. and Tweed, C. J. (1997). HATCHES: A Referenced Thermodynamic Database for Chemical Equilibrium Studies. Nirex Report NSS/R379.

Boggs, M.A., Minton, T., Dong, W., Lomasney, S., Islam, M.R., Gu, B. & Wall, N.A., 2011. Interactions of Tc(IV) with humic substances. *Environmental Science & Technology*, 45 (7), 2718–2724.

Burke, I.T., Boothman, C., Lloyd, J.R., Livens, F.R., Charnock, J.M., McBeth, J.M., Mortimer, R.J.G. & Morris, K., 2006. Reoxidation behavior of technetium, iron, and sulfur in estuarine sediments. *Environmental Science & Technology*, 40 (11), 3529–35.

Burke, I.T., Livens, F.R., Lloyd, J.R., Brown, A.P., Law, G.T.W., McBeth, J.M., Ellis, B.L., Lawson, R.S. & Morris, K., 2010. The fate of technetium in reduced estuarine sediments: combining direct and indirect analyses. *Applied Geochemistry*, 25 (2), 233–241.

Caporaso, J.G., Kuczynski, J., Stombaugh, J., Bittinger, K., Bushman, F.D., Costello, E.K., Fierer, N., Pena, A.G., Goodrich, J.K. & Gordon, J.I., 2010. QIIME allows analysis of high-throughput community sequencing data. *Nature Methods*, 7 (5), 335–336.

Chen, M. & Ma, L.Q., 2001. Comparison of three aqua regia digestion methods for twenty florida soils. *Soil Science Society of America Journal*, 65 (2), 491–499.

Cole, J.R., Wang, Q., Cardenas, E., Fish, J., Chai, B., Farris, R.J., Kulam-Syed-Mohideen, A.S., McGarrell, D.M., Marsh, T., Garrity, G.M. & Tiedje, J.M., 2009. The Ribosomal Database Project: improved alignments and new tools for rRNA analysis. *Nucleic Acids Research*, 37 (suppl 1), 141–145.

Corkhill, C.L., Bridge, J.W., Chen, X.C., Hillel, P., Thornton, S.F., Romero-Gonzalez, M.E., Banwart, S.A. & Hyatt, N.C., 2013. Real-time gamma imaging of technetium transport through natural and engineered porous materials for radioactive waste disposal. *Environmental Science & Technology*, 47 (23), 13857–13864.

Dent, A.J., Cibin, G., Ramos, S., Smith, A.D., Scott, S.M., Varandas, L., Pearson, M.R., Krumpa, N.A., Jones, C.P. & Robbins, P.E., 2009. B18: A core XAS spectroscopy beamline for Diamond. *Journal of Physics: Conference Series*, 190 (1), 12039.

Edgar, R.C., 2010. Search and clustering orders of magnitude faster than BLAST. *Bioinformatics*, 26 (19), 2460–2461.

Elifantz, H., N'Guessan, L.A., Mouser, P.J., Williams, K.H., Wilkins, M.J., Risso, C., Holmes, D.E., Long, P.E. & Lovley, D.R., 2010. Expression of acetate permease-like (apl) genes in subsurface communities of *Geobacter* species under fluctuating acetate concentrations. *FEMS Microbiology Ecology*, 73 (3), 441–449.

Fredrickson, J.K., Zachara, J.M., Kennedy, D.W., Kukkadapu, R.K., McKinley, J.P., Heald, S.M., Liu, C. & Plymale, A.E., 2004. Reduction of TcO_4^- by sediment-associated biogenic Fe(II). *Geochimica et Cosmochimica Acta*, 68 (15), 3171–3187.

Fredrickson, J.K., Zachara, J.M., Plymale, A.E., Heald, S.M., McKinley, J.P., Kennedy, D.W., Liu, C. & Nachimuthu, P., 2009. Oxidative dissolution potential of biogenic and abiogenic TcO_2 in subsurface sediments. *Geochimica et Cosmochimica Acta*, 73 (8), 2299–2313.

Gao, Z.M., Xu, X. & Ruan, L.W., 2014. Enrichment and characterization of an anaerobic cellulolytic microbial consortium SQD-1.1 from mangrove soil. *Applied Microbiology and Biotechnology*, 98 (1), 465–74.

Geissler, A., Law, G.T.W., Boothman, C., Morris, K., Burke, I.T., Livens, F.R. & Lloyd, J.R., 2011. Microbial communities associated with the oxidation of iron and technetium in bioreduced sediments. *Geomicrobiology Journal*, 28 (5-6), 507–518.

Geraedts, K, Bruggeman, C, Maes, A, Van, L., L, R., Rossberg, Reich & T, 2002. Evidence for the existence of Tc(IV)-humic substance species by X-ray absorption near-edge spectroscopy. *Radiochimica Acta*, 90 (12), 879-884.

Guillaumont, R., Fanghänel, T., Fuger J., Grenthe, I., Neck V., Palmer, D.A., and Rand, M.H., (2003) Chemical Thermodynamics 5. In F. J. Mompean, C. Domenech-Orti, K. Ben-Said, and M. Illemassène, eds, *Update on the chemical thermodynamics of uranium, neptunium, plutonium, americium and technetium*, Elsevier, NEA-OECD, p. 970.

Hamady, M., Walker, J.J., Harris, J.K., Gold, N.J. & Knight, R., 2008. Error-correcting barcoded primers for pyrosequencing hundreds of samples in multiplex. *Nature Methods*, 5 (3), 235–237.

Hashimoto, T., Whang, K.-S. & Nagaoka, K., 2005. A quantitative evaluation and phylogenetic characterization of oligotrophic denitrifying bacteria harbored in subsurface upland soil using improved culturability. *Biology and Fertility of Soils*, 42 (3), 179–185.

Heald, S.M., Krupka, K.M. & Brown, C.F., 2012. Incorporation of pertechnetate and perrhenate into corroded steel surfaces studied by X-ray absorption fine structure spectroscopy. *Radiochimica Acta International Journal for Chemical Aspects of Nuclear Science and Technology*, 100 (4), 243–253.

Hess, N.J., Xia, Y., Rai, D. & Conradson, S.D., 2004. Thermodynamic model for the solubility of $TcO_2 \cdot xH_2O$ (am) in the Aqueous Tc (IV)–Na^+–Cl^-–H^+–OH^-–H_2O system. *Journal of Solution Chemistry*, 33 (2), 199–226.

Icenhower, J.P., Qafoku, N.P., Zachara, J.M. & Martin, W.J., 2010. The biogeochemistry of technetium: A review of the behavior of an artificial element in the natural environment. *American Journal of Science*, 310 (8), 721–752.

Jacquot, F., Libert, M.F., Romero, M.A. & Besnainou, B., 1997. In vitro evaluation of microbial effects on bitumen waste form. In J. H. Wolfram, R. D. Rogers, & L. G.

Gazso, eds, *Microbial Degradation Processes in Radioactive Waste Repository and in Nuclear Fuel Storage Areas*. Springer Netherlands, pp. 275–283.

Jaisi, D.P., Dong, H., Plymale, A.E., Fredrickson, J.K., Zachara, J.M., Heald, S. & Liu, C., 2009. Reduction and long-term immobilization of technetium by Fe(II) associated with clay mineral nontronite. *Chemical Geology*, 264 (1-4), 127–138.

Jutkina, J., Heinaru, E., Vedler, E., Juhanson, J. & Heinaru, A., 2011. Occurrence of plasmids in the aromatic degrading bacterioplankton of the baltic sea. *Genes*, 2 (4), 853–68.

Khijniak, T. V, Medvedeva-Lyalikova, N.N. & Simonoff, M., 2003. Reduction of pertechnetate by haloalkaliphilic strains of *Halomonas*. *FEMS microbiology ecology*, 44 (1), 109–15.

Lane, D.J., 1991. 16S/23S rRNA sequencing. In E. Stackebrandt & M. Goodfellow, eds, *Nucleic Acid Techniques in Bacterial Systematics*. New York: John Wiley & Sons, pp. 115-175.

Lear, G., McBeth, J.M., Boothman, C., Gunning, D.J., Ellis, B.L., Lawson, R.S., Morris, K., Burke, I.T., Bryan, N.D., Brown, A.P., Livens, F.R. & Lloyd, J.R., 2010. Probing the biogeochemical behavior of technetium using a novel nuclear imaging approach. *Environmental Science & Technology*, 44 (1), 156–62.

Lloyd, J., Cole, J. & Macaskie, L., 1997. Reduction and removal of heptavalent technetium from solution by *Escherichia coli*. *Journal of Bacteriology*, 179 (6), 2014–2021.

Lloyd, J.R., Sole, V.A., Van Praagh, C.V.G. & Lovley, D.R., 2000. Direct and Fe(II)-mediated reduction of technetium by Fe(III)-reducing bacteria. *Applied and Environmental Microbiology*, 66 (9), 3743–3749.

Lovley, D.R. & Phillips, E.J., 1987. Rapid assay for microbially reducible ferric iron in aquatic sediments. *Applied Environmental Microbiology*, 53 (7), 1536–1540.

Lukens, W.W., Bucher, J.I., Edelstein, N.M. & Shuh, D.K., 2002. Products of pertechnetate radiolysis in highly alkaline solution: structure of $TcO_2.xH_2O$. *Environmental Science & Technology*, 36 (5), 1124–1119.

Maes A., Geraedts, K, Bruggeman, C, , Vancluysen J., Rossberg, A Reich & T, 2004. Evidence for the interaction of technetium colloids with humic substances by X-ray absorption spectroscopy. *Envrionmental Science & Technology*, 38 (7), 2044-2051.

Marshall, T.A., Morris, K., Law, G.T.W., Livens, F.R., Mosselmans, J.F.W., Bots, P. & Shaw, S., in review. Incorporation of 99- technetium(IV) into magnetite. *Environmental Science & Technology*.

McBeth, J., Lloyd, J.R., Law, G. T. W., Livens, F. R., Burke, I. T., & Morris, K., 2011. Redox interactions of technetium with iron-bearing minerals. *Mineralogical Magazine*, 75 (4), 2419–2430.

McBeth, J.M., Lear, G., Lloyd, J.R., Livens, F.R., Morris, K. & Burke, I.T., 2007. Technetium Reduction and Reoxidation in Aquifer Sediments. *Geomicrobiology Journal*, 24 (3-4), 189–197.

Morris, K., Livens, F.R., Charnock, J.M., Burke, I.T., McBeth, J.M., Begg, J.D.C., Boothman, C. & Lloyd, J.R., 2008. An X-ray absorption study of the fate of technetium in reduced and reoxidised sediments and mineral phases. *Applied Geochemistry*, 23 (4), 603–617.

Parameswaran, P., Torres, C.I., Lee, H.-S., Rittmann, B.E. & Krajmalnik-Brown, R., 2011. Hydrogen consumption in microbial electrochemical systems (MXCs): the role of homo-acetogenic bacteria. *Bioresource Technology*, 102 (1), 263–71.

Parkhurst, D.J., and Appelo, C.A.J., 1999. User's guide to PHREEQC (Version 2)- A computer program for speciation, batch-reaction, one-dimensional transport, and inverse geochemical calculations. *U.S. Geological Survey Water-Resources Investigations Report*, 4199-4259.

Peretyazhko, T., Zachara, J.M., Heald, S.M., Jeon, B.-H., Kukkadapu, R.K., Liu, C., Moore, D. & Resch, C.T., 2008. Heterogeneous reduction of Tc(VII) by Fe(II) at the solid–water interface. *Geochimica et Cosmochimica Acta*, 72 (6), 1521–1539.

Peretyazhko, T.S., Zachara, J.M., Kukkadapu, R.K., Heald, S.M., Kutnyakov, I. V, Resch, C.T., Arey, B.W., Wang, C.M., Kovarik, L., Phillips, J.L. & Moore, D.A., 2012. Pertechnetate (TcO_4^-) reduction by reactive ferrous iron forms in naturally anoxic, redox transition zone sediments from the Hanford Site, USA. *Geochimica et Cosmochimica Acta*, 92 (0), 48–66.

Pikuta, E. V, Hoover, R.B., Marsic, D., Whitman, W.B., Lupa, B., Tang, J. & Krader, P., 2009. *Proteocatella sphenisci* gen. nov., sp. nov., a psychrotolerant, spore-forming anaerobe isolated from penguin guano. *International Journal of Systematic and Evolutionary Microbiology*, 59 (Pt 9), 2302–2307.

Ravel, B. & Newville, M., 2005. ATHENA, ARTEMIS, HEPHAESTUS: data analysis for X-ray absorption spectroscopy using IFEFFIT. *Journal of Synchrotron Radiation*, 12 (4), 537–541.

Ray, A.E., Connon, S.A., Sheridan, P.P., Gilbreath, J., Shields, M., Newby, D.T., Fujita, Y. & Magnuson, T.S., 2010. Intragenomic heterogeneity of the 16S rRNA gene in strain UFO1 caused by a 100-bp insertion in helix 6. *FEMS Microbiology Ecology*, 72 (3), 343–53.

Riekkola, R., Sievänen, U. & Vieno, T., 2003. Controlling of disturbances due to groundwater inflow into ONKALO and the deep repository. *Working Report*, 46.

Rizoulis, A., Steele, H.M., Morris, K. & Lloyd, J.R., 2012. The potential impact of anaerobic microbial metabolism during the geological disposal of intermediate-level waste. *Mineralogical Magazine*, 76 (8), 3261–3270.

Sekine, T., Watanabe, A., Yoshihara, K. & Kim, J., 1993. Complexation of technetium with humic acid. *Radiochimica Acta*, 63, 87-90.

Thorpe, C.L., Boothman, C., Lloyd, J.R., Law, G.T.W., Bryan, N.D., Atherton, N., Livens, F.R. & Morris, K., 2014. The interactions of strontium and technetium with Fe(II) bearing biominerals: implications for bioremediation of radioactively contaminated land. *Applied Geochemistry*, 40, 135–143.

Wildung, R.E., Gorby, Y.A., Krupka, K.M., Hess, N.J., Li, S.W., Plymale, A.E., McKinley, J.P. & Fredrickson, J.K., 2000. Effect of electron donor and solution chemistry on products of dissimilatory reduction of technetium by *Shewanella putrefaciens*. *Applied and Envionmental Microbiology*, 66 (6), 2451-2460.

Wildung, R.E., Li, S.W., Murray, C.J., Krupka, K.M., Xie, Y., Hess, N.J. & Roden, E.E., 2004. Technetium reduction in sediments of a shallow aquifer exhibiting dissimilatory iron reduction potential. *FEMS Microbiology Ecology*, 49 (1), 151–162.

Williamson, A.J., Morris, K., Charnock, J.M., Law, G.T.W., Rizouliz, A. & Lloyd, John, R., in review. Microbial reduction of U(VI) under alkaline conditions; implications for radioactive watse disposal. *Environmental Science & Technology*.

Williamson, A.J., Morris, K., Shaw, S., Byrne, J.M., Boothman, C. & Lloyd, J.R., 2013. Microbial reduction of Fe(III) under alkaline conditions relevant to geological disposal. *Applied and Environmental Microbiology*, 79 (11), 3320–3326.

Zachara, J.M., Heald, S.M., Jeon, B.-H., Kukkadapu, R.K., Liu, C., McKinley, J.P., Dohnalkova, A.C. & Moore, D.A., 2007. Reduction of pertechnetate [Tc(VII)] by aqueous Fe(II) and the nature of solid phase redox products. *Geochimica et Cosmochimica Acta*, 71 (9), 2137–2157.

7

Microbial Reduction of Np(V) under Alkaline Conditions

Paper in preparation for Mineralogical Magazine (special edition for IGDTP 2014 conference)

7. Microbial Reduction of Np(V) under Alkaline Conditions

Adam J. Williamson,[†] Katherine Morris,[†] Gareth T.W. Law,[‡] and Jonathan R. Lloyd [†*]

† Research Centre for Radwaste Disposal and Williamson Research Centre for Molecular Environmental Science, School of Earth, Atmospheric and Environmental Sciences, The University of Manchester, Manchester, M13 9PL, UK.

‡ Centre for Radiochemistry Research and Research Centre for Radwaste Disposal, School of Chemistry, The University of Manchester, Manchester, M13 9PL, UK.

*email jon.lloyd@manchester.ac.uk

7.1. Abstract

^{237}Np will be present in significant quantities in radioactive wastes and due to its long half-life (2.13 x 10^6 years) and potential mobility as Np(V) in oxic environments, understanding its behaviour during radioactive waste disposal scenarios is of particular importance. Here, microcosm experiments have been established using sediments from the vicinity of a legacy lime workings to reflect the higher pH conditions expected during disposal of concrete-based intermediate level wastes. To further probe the influence of Fe(III) biogeochemistry on Np(V) under these higher pH conditions, systems were run with additional Fe(III) added as ferrihydrite. Biogeochemical changes were tracked in experiments run at low levels of Np(V) (20 Bq ml^{-1}; 3.3 μM), whilst parallel higher concentrations (2.5 KBq ml^{-1}; 414 μM) were used to assess Np speciation and coordination environment using X-ray absorption spectroscopy (XAS). As expected, a cascade of microbial reduction processes occurred in all microbially active systems poised at an initial of pH 10. In systems without added Fe(III), significant (90 %) sorption of Np(V) occurred at the first time point (1 hour) and residual aqueous Np was removed by day 1 in microbially active sediments. In the ferrihydrite enriched systems, complete Np removal from solution occurred at the first time point (1 hour), suggesting enhanced sorption of Np(V) to the added Fe(III). For higher activity sediments, XAS confirmed that reduction from Np(V) to Np(IV) had occurred. To further explore the mechanisms of neptunium removal, pre-reduced, Fe(III)-reducing sediments at pH 10 were spiked with Np(V) and XAS analysis showed reduction to Np(IV) suggesting an indirect Fe(II)-mediated pathway for reduction at high pH.

7.2. Introduction.

^{237}Np(V) is a long-lived (2.13 x 10^6 years) transuranic alpha emitter with high radiotoxicity and the UK higher activity wastes have ca. 440 kg^{-1} of ^{237}Np present with ca 70% of the ^{237}Np partitioned to the intermediate level waste fraction (NDA 2014). In addition, as a long lived daughter decay product of ^{241}Am and grand-daughter of ^{241}Pu, it is expected to become the dominant transuranic in radioactive wastes between 10^4 and 10^7 years (Lloyd & Renshaw 2005). In oxic environments at all but extreme pH values, Np(V) exists predominantly as the pentavalent neptunyl ($Np(V)O_2^+$) species which has the lowest affinity for surface sorption of all the transuranic elements (Kaszuba & Runde 1999; Lloyd & Renshaw 2005). Under reducing conditions, Np(IV) forms which is prone to hydrolysis and sorption reactions (Kaszuba & Runde 1999). Microbial

interactions with Np have been reported with immobilisation by biosorption of Np(V) (Songkasiri et al. 2002; Gorman-Lewis et al. 2013), reductive immobilisation to Np(IV) by pure cultures of the Fe(III)-reducing bacterium *Shewanella putrefaciens* (now *Shewanella oneidensis*) (Lloyd et al. 2000) and sediment consortia (Rittmann et al. 2002; Law et al. 2010), all reported in the literature. Enzymatic Np(V) reduction was not observed by *Geobacter sulfurreducens* however, suggesting that not all Fe(III)-reducing bacteria are capable of direct Np(V) reduction, despite being thermodynamically favourable at circumneutral pH (Renshaw et al. 2005). As little is known about the biogeochemistry of Np(V) at higher pH (pH 10) conditions relevant to the disposal of cementitious intermediate level wastes, the focus of this work was to study the fate of Np(V) in microbially active high pH sediments collected from a legacy lime workings in Buxton, UK (Rizoulis et al. 2012; Williamson et al. 2013). Two sets of experiments were set up and analysed. Background biogeochemical transformations, that could potentially control Np(V) fate, were studied in sediment microcosms that were spiked with low "tracer" concentrations of Np(V) (20 Bq ml^{-1}; 3.3 μM), with and without added Fe(III) as ferrihydrite. The microcosms were sealed to allow anoxic conditions to develop, and samples were removed periodically to monitor a range of (bio)geochemical markers. Additionally, pre-reduced Fe(II)-rich sediments were incubated at 5 °C to suppress microbial activity and also reacted with Np(V) to probe for abiotic reduction of Np(V). Selected experiments were also run at higher Np(V) concentrations (2.5 kBq ml^{-1}; 414 μM) to allow XAS characterisation, including neptunium speciation, in these experiments.

7.3. Materials and methods

7.3.1. Safety

^{237}Np is a radioactive alpha emitter with beta/gamma emitting daughter isotopes. Following a suitable risk assessment, work with radioisotopes should only be handled by qualified workers in a specialist radiochemistry laboratory. The possession and use of radioactive materials is subject to statuary controls.

7.3.2. Sample collection

Sediments were collected at the margins of a legacy lime workings area at Harpur Hill Buxton, Derbyshire (Williamson et al. 2013; Rizoulis et al. 2012). Sediments and surface waters were transferred into sterile containers and stored at 4°C in darkness prior to use. The elemental composition of the sediment was determined by X-ray fluorescence (Axios Sequential XRF).

7.3.3. Bioreduction microcosm construction

To investigate Np(V) behaviour under anoxic conditions, microcosms were prepared in sterile serum bottles in triplicate with sediments slurried with pH 11.8 surface waters at a sediment: solution ratio of 1:10. All systems had 10 mM sodium lactate and 1 g l^{-1} yeast extract added as carbon sources and potential electron donors to stimulate microbial activity, and the pH was adjusted to pH 10 with 1 M HCl before incubation. To explore neptunium solubility and its coupling to biogeochemical processes at pH 10, Buxton sediment and surface water incubations with *no added Fe* (III) and *with added Fe(III)* (where 30 mM ferrihydrite was added) were prepared (Williamson et al. 2013; Williamson et al. in review). The headspaces of bottles were flushed with argon and the bottles were crimp sealed with thick butyl rubber stoppers, then incubated at 20 °C in the dark. To explore further the mechanisms of radionuclide transformations under alkaline anoxic conditions, incubations with *no added Fe(III)* and *with added Fe(III)* were allowed to progress through to Fe(III) reduction for 28 days and then spiked with Np(V) (20 Bq ml^{-1}; 3.31 μM). The preparation of Np(V) has been outlined by previous co-workers (Law et al. 2010). Sample manipulations were performed under anaerobic conditions as appropriate and using aseptic technique. During incubations, the pH of the microcosms dropped to range of 7- 8, as the pH was unamended throughout the experiments due to radiological safety considerations.

7.3.4. Geochemical analyses-low level experiments

Sample slurries were analysed for pH and Eh using a calibrated Denver Instrument Digital Meter and probes. To assess non-detrital Fe, aqua-regia digests were run, (Chen & Ma 2001), followed by ICP-AES on filtered supernatant (Perkin Elmer Optima 5300 dual view ICP-AES). Biogenic Fe(II) and total bioavailable Fe were assessed extraction into 0.5 N HCl and quantification using the ferrozine colorimetric assay on a sub-sample of sediment slurry (Lovley & Phillips 1987). Colorimetric assays were performed on a Jenway 6715 spectrometer and typically, calibration regressions had R^2 > 0.99. Samples were then centrifuged (5 mins with a relative centrifugal force (RCF) of 15,800 *g*) and the supernatant was analysed for NO_2^- , NO_3^-, SO_4^{2-} and organic acids (lactic, acetic, formic, propionoic and butyric) using a Dionex ICS5000 ion chromatograph. Samples were then centrifuged (5 mins, RCF 15,800 *g*) and the supernatant was analysed for total Np using ICP-MS (Agilent 7500cx).

7.3.5. X-ray absorption spectroscopy (XAS)-high level experiments

To identify the fate of Np(V), a select set of higher activity experiments were prepared for XAS analyses. Here, 2.5 kBq ml^{-1} (414 μM) Np (V) was injected into oxic, progressive anoxia and pre-reduced sediments. The geochemistry of these systems was tracked only at experimental end points as dictated by a radiological risk assessment, and the pH and concentration of soluble Np by ICP-MS were measured. After reaction (1 h for oxic sediments and 2 months for progressive and pre-reduced systems) a wet paste (typically 0.5 g of sediment with < 50% water content) was transferred to a cryogenic XAS sample vial in an argon filled glove bag, packed with compressed parafilm and centrifuged (5 mins, RCF 15,800 *g*) to remove the residual supernatant. The pellet was then packed with cotton wool and double sealed with Kapton film and stored in an argon filled Kilner jar at -80 °C prior to analysis. XAS measurements were conducted at the INE Beamline for actinide research at the ANKA synchrotron light source, Germany (Rothe et al. 2012). Neptunium L_{III} edge spectra (17.610 keV) were collected in fluorescence mode by a 5 pixel solid-state detector (LEGe Canberra) using Ge(422) monochromator crystals at 77 K using a cryostat. Energy calibration was completed by parallel measurement of a Y foil. A total of 7-10 spectra were collected per sample and scans were averaged to improve the signal to noise ratio. XANES spectra were collected for all samples, and where possible, EXAFS data were also collected. The ionization energy (E_0) was set to the position of the Np L_{III} white-line maximum (17.610 keV) for background subtraction. XANES spectra were obtained following background subtraction and data normalisation. The EXAFS spectra were obtained following background subtraction using ATHENA (Ravel & Newville 2005) and were modelled to provide an estimate of the average Np oxidation state using linear combination fitting function of ATHENA (Ravel & Newville 2005). End member spectra used in linear combination modelling were Np(V) and Np(IV) standards (Rossberg et al. 2014; Hennig 2007). The data were fit in k^3 space between 3 and 8 $Å^{-1}$ and shells were only included in the model fit if the overall R-factor was improved by > 5 % and satisfied the reduced X^2 test.

7.4. Results and Discussion

7.4.1. Sediment and surface water characteristics

The sediment consisted of calcite, with minor quartz and ankerite (Williamson et al. 2013; Williamson et al. in review). The elemental composition, as determined by XRF, was dominated by Ca (52.8 wt %), with significant concentrations of Si (1.1 wt %), Al (0.51 wt %) and Fe (0.15 wt %). The total iron in the sample was determined at 0.51 g

kg^{-1} (9.1 mM kg^{-1}) and the bioavailable Fe was estimated at 0.27 g kg^{-1} (4.78 mM kg^{-1}), indicating ~ 50 % of the total Fe was bioavailable.

7.4.2. Biogeochemistry in sediment microcosms

To explore the biogeochemistry of neptunium under anoxic conditions at pH 10, microcosms were constructed using calcite dominated sediments and surface waters from a high pH lime workings site in the UK (Williamson et al. 2013) **(**Table 1).

Table 1: Buxton Harpur Hill lime workings surface water major anions and cations.

Cations	**Na^+**	**Ca^{2+}**	**Al^{3+}**	**Si^{4+}**	**K^+**	**Sr^{2+}**	**Ba^{2+}**
Concentration (mg l^{-1})	41.0	194	0.18	2.33	79.2	1.26	0.73

Anions	**Cl^-**	**NO_3^-**	**NO_2^-**	**SO_4^{2-}**	**PO_4^{3-}**
Concentration (mg l^{-1})	62.5	31.9	0.7	2.4	0

These sediments have been used in other studies from our group (Rizoulis et al. 2012; Williamson et al. 2013; Williamson et al. in review; Williamson et al. in prep), focusing on the biogeochemistry of Fe(III), Tc(VII) and U(VI) under carefully controlled high pH conditions, maintained by the regular addition of base. In these experiments, we made no attempt to control the pH of the microcosms. The higher activities of our Np experiments made such manipulations impractical, and we therefore monitored the pH as anoxia developed and a range of anaerobic biogeochemical processes developed (including microbial Fe(III) reduction) (Figure 1). During this incubation period the pH of the microcosms dropped to circumneutral (pH 7- 8) values in both the *no added Fe(III)* and *with added Fe(III)* experiments. This is likely due to a range of biogeochemical processes, including the production of organic acids (predominantly acetic and butyric acids), during microbial metabolism (Figure 2).

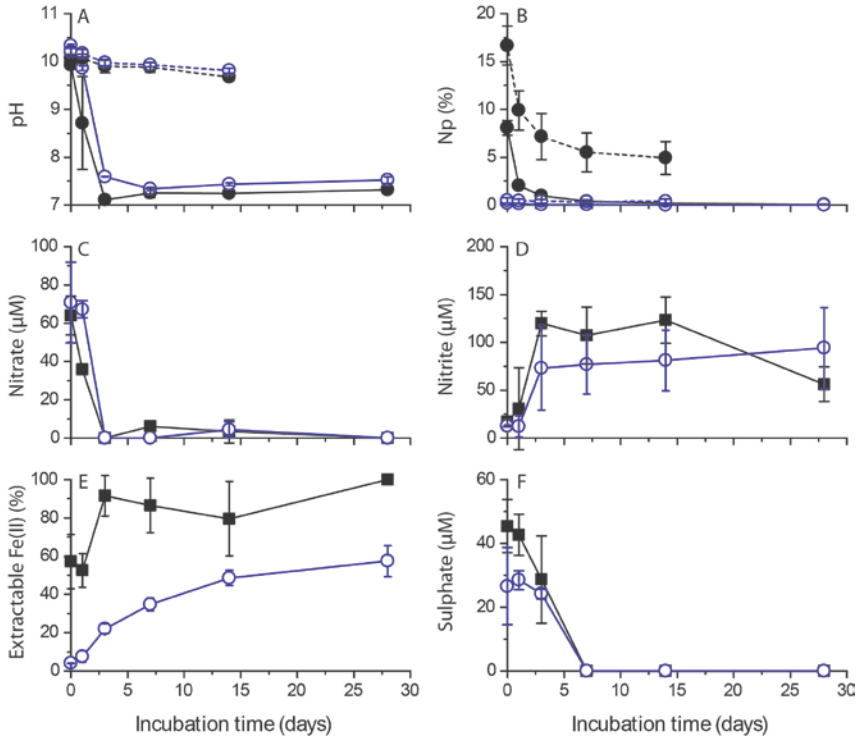

Figure 1: Bioreduction of Buxton sediments with no added Fe(III) (●) and with added Fe(III) (O) showing (A) pH; (B) % Np in solution; (C) NO_3^-; (D) NO_2^-; (E) 0.5 N HCl extractable sediment Fe as Fe(II) (%) and (F) SO_4^{2-}. Dashed lines in A and B represent pre-reduced controls. Error bars are 1 σ of triplicate results (where not shown, errors are within the symbol size).

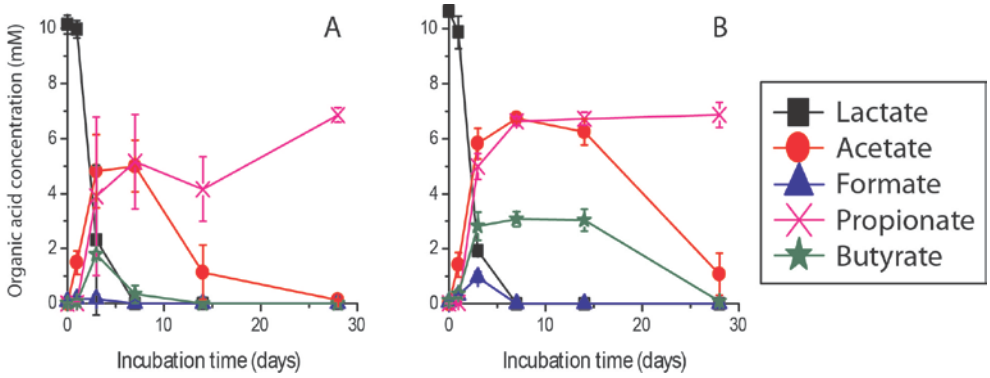

Figure 2: Ion chromatographic analysis of organic acids in supernatant samples taken from the progressive anoxia systems with (A) no added Fe(III) and (B) with added Fe(III) over the 28 day incubation period.

For the *no added Fe(III)* experiment, as expected there was complete nitrate removal by day 1, followed by complete Fe(III) reduction by day 3, similar to previous experiments (Williamson et al. in review). The Eh also fell from +179 ± 1 mV at the start of the experiment, to -82.0 ± 12 mV by day 14 (Figure 1). Complete sulphate removal was

also observed by day 7 (Figure 1), which is in contrast to sediment microcosms maintained at pH 10, where sulphate reduction is energetically unfavourable (Rizoulis et al. 2012; Williamson et al. 2013; Williamson et al. in review). In the systems *with added Fe(III)*, complete nitrate removal occurred by day 3, with concomitant nitrite production. However no significant further denitirification was observed throughout the experiment (Figure 1). 0.5 N HCl extractable Fe(II) concentration reached 8.84 ± 0.54 mM L^{-1} of slurry (~50 % of total bioavailable Fe(III)) and complete removal of 27 uM sulphate had occurred by day 14, implying the presence of an active sulphate-reducing community (Figure 1). This was supported further by a drop in the reduction potential from +164 ± 2 mV at the first time point to -246 ± 5 mV by 14 days (Figure 1). The excess of reduced Fe(II), compared to the levels of sulphate reduced, suggests direct enzymatic reduction of Fe(III) rather than a sulphide-mediated reaction mechanism.

7.4.3. Neptunium fate during bioreduction- *no added Fe(III)* systems

To investigate the environmental behaviour of neptunium in these high pH environments, tracer concentrations of Np(V) (20 Bq ml^{-1};3.3 μM) was added to sterilized oxic surface water samples, microbially-active sediment slurry microcosms as well as a chilled (5 °C) pre-reduced Fe(II) bearing sediments at 0.57 ± 0.09 mM L^{-1} of slurry. The lower incubation temperature was used to suppress microbial activity. In experiments with sterile, 0.2 μm filtered surface water equilibrated with Np(V) for 3 days prior to analysis, the solubility of Np(V) was initially high, with 84 % of the spike remaining in solution. In oxic sediment microcosms, significant Np sorption occurred to sediments after 1 hour (~ 95 % removed) suggesting significant uptake of Np(V) to these sediments at pH 10. In microbially active *no added Fe(III)* microcosms, again, significant Np sorption occurred after 1 hour, however, after a further 7 days of incubation, additional Np removal was recorded and by day 14 essentially complete removal of the radionuclide was observed (Figure 1). In pre-reduced, Fe(II)-bearing sediments incubated at 5°C, substantial Np(V) removal occurred over 2 weeks, yet these systems were not as effective in removing Np(V) from solution as the microbially active experiments (Figure 1). In order to further explore the speciation of solid phase associated Np in these experimental systems, Np L_{III} -edge XANES and where possible EXAFS spectra were collected on parallel experiments at higher (2.5 kBq ml^{-1}, 414 μM) concentrations. The oxic sediment showed a Np(V) like spectrum confirming a significant interaction of Np(V) with the sediment from the lime-working site. By contrast, the bioreduced *no added Fe(III)* sample showed a Np(IV)-like XANES

spectrum after 60 days incubation, with a loss of the near edge multiple scattering resonance, from the neptunyl moiety, confirming reductive scavenging of Np(IV) to solids (Figure 3). To further quantify the extent of Np(V) reduction, linear combination fitting of the end-member XANES spectra from the *no added Fe(III)* samples were performed, using data from Np(V) and Np(IV) standards, and could be fitted with a 84 % contribution from the Np(IV) spectrum. The Np EXAFS data could be fitted to a k range of 8, and here a fit of one shell of oxygen backscatterers indicative of Np(IV) using 8 O at 2.34 Å was possible. There was no evidence of a short dioxygenyl interaction in the EXAFS, again confirming reduction in these initially alkaline sediments (Figure 4; Table 2). When Np was added to pre-reduced sediments with *no added Fe(III)* incubated at 5°C, the XANES looked similar to data collected from the progressive anoxia system, and linear combination fitting confirmed that significant (~ 75 %) Np(V) reduction to Np(IV) had occurred (Figure 3). This would suggest that Np(V) reduction in these systems is most likely mediated abiotically, presumably via interactions with biogenic Fe(II) (or potentially Mn(II)) in the sediments (Law et al. 2010).

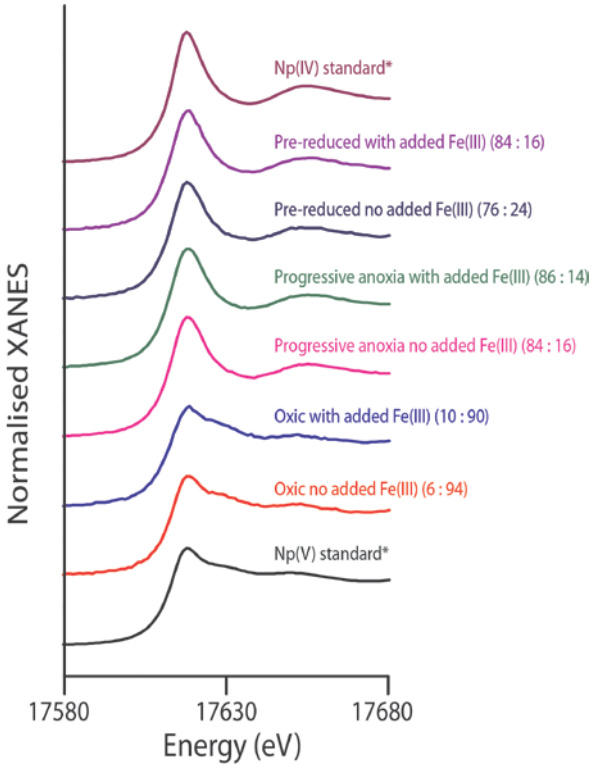

Figure 3: ^{237}Np L_{III} edge XANES stack plot of all oxic, bioreducing systems and pre-reduced sediments incubated at 5 °C with $Np(V)O_2^+$ and $Np(IV)O_2$ reference spectra. Values in brackets are estimated Np(IV):Np(V) ratio determined by linear combination modelling between Np(IV) and Np(V) standards (Rossberg et al. 2014; Hennig 2007).

7.4.4. Neptunium fate during bioreduction- *with added Fe(III)* systems

In all oxic, progressive anoxia and pre-reduced sediments *with added Fe(III)*, complete Np(V) sorption had occurred by the initial time point, suggesting that enhanced sorption to the added ferrihydrite had occurred compared to the no added Fe(III) systems, and in line with predicted Np(V) ferrihydrite interactions (Girvin et al. 1991) (Figure 1). The EXAFS data could be fitted with 2 axial oxygen backscatterers at 1.91 Å, indicative of Np(V). Again, the XANES data from these experiments showed a clear progression from Np(V) in oxic sediments to Np(IV) in progressive and pre-reduced sediments. Linear combination fitting incorporating Np(V) and Np(IV) standards confirmed, within error, that 100 % Np(IV) was present on the solid phase (Figure 3). The EXAFS analyses supported these observations, with a model of 8 oxygen backscatterers at 2.41 Å, typical of Np(IV) coordination (Figure 4; Table 2). Interestingly, the addition of two Fe backscatterers at 3.44 Å improved the fit and satisfied the reduced χ^2 test. This suggests an Fe interaction in these systems, and is similar to the postulated Np(IV) interactions in Fe(III)-reducing iron rich sediments at circumneutral pH (Law et al. 2010).

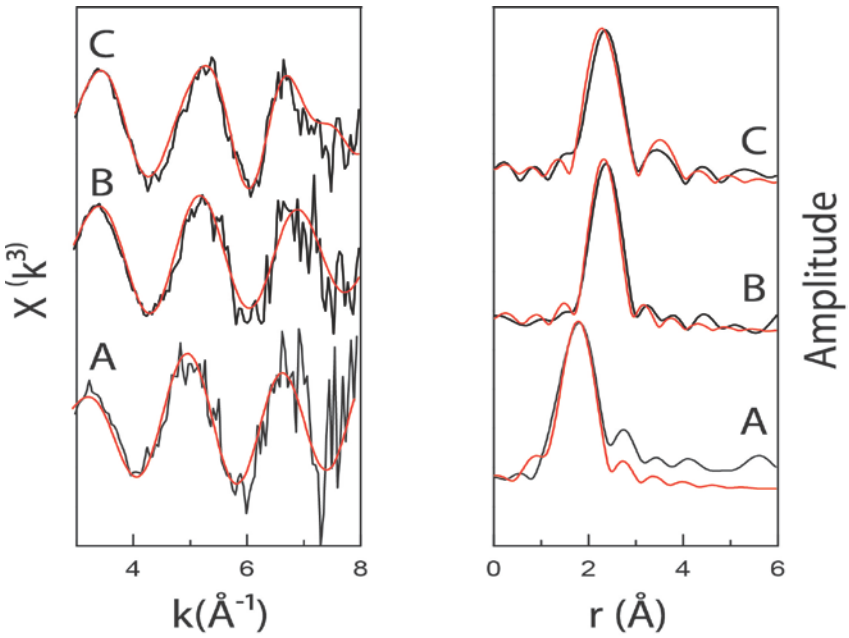

Figure 4: k^3 weighted ^{237}Np L_{III} edge EXAFS spectra (left) and Fourier transform (right) for (A) oxic sediments with no added Fe(III) and progressive anoxia experiments with (B) no added Fe(III) and (C) with added Fe(III). The Fourier Transform is plotted with a phase correction calculated from the first shell of oxygen backscatterers. Black lines are the experimental data and red lines are the best-fit models (Table 2).

Table 2: EXAFS fitting results from oxic with added Fe(III) sediments and progressive anoxia experiments: no added Fe and with added Fe. CN denotes coordination number, r is interatomic distance (Å) and σ^2 is Debye Waller factor ($Å^2$). ΔE_0 represents the shift in energy from the calculated Fermi level. $S0^2$ denotes the amplitude factor which was constrained between 0.85 and 1.05 in reduced samples and set to 1 in the oxic sample. R is the goodness of the fit and χ_v^2 is the reduced χ^2 value. Numbers in parentheses are the standard deviation on the last decimal place.

Sample	Shell	Path	CN	r (Å)	$2\sigma^2$ ($Å^2$)	ΔE_0 (eV)	S_0^2	R	χ_v^2
Oxic no added Fe(III)	1	O_{ax}	2	1.91 (4)	0.036 (2)	8.69 ±3.62	1	**0.024**	8.4
	2	O_{eq}	6	2.39 (3)	0.008 (4)				
No added Fe(III)	1	O_{eq}	8	2.33 (2)	0.015 (6)	5.71 ±1.78	0.92 ±0.16	**0.029**	20
With added Fe(III)	1	O_{eq}	8	2.34 (3)	0.026 (5)	4.21 ±1.55	1.05 ±0.22	**0.056**	50.3
With added Fe(III)	1	O_{eq}	8	2.34 (2)	0.022 (4)	6.94 ±1.88	1.05 ±0.23	**0.025**	35.0
	2	Fe	2	3.44 (5)	0.030 (7)				

7.5. Conclusions and geochemical significance.

For the first time, we show that an indigenous microbial community can mediate Np(V) reduction in a sediment system initially prepared at pH 10. Significant Np(V) sorption to oxic sediments was apparent in these high pH, carbonate rich sediments. Microbially-mediated reduction of both the sorbed and soluble Np(V) in these systems suggests a potential controlling influence of Np mobility in high pH environments representative of conditions that will develop around cementitious ILW radwaste in a geodisposal facility. The precise mechanism of Np(V) reduction requires further investigation and could be catalysed enzymatically (Lloyd et al. 2000), or more likely via biogenic Fe(II), as proposed for Tc(VII) reduction in neutral (Lloyd et al. 2000) and high systems (Williamson et al. in prep). This work also highlights the impact of microbial metabolism on the pH of alkali environments representative of ILW. In this study microbial activity, for example organic acid production, was able to decrease the pH of the system from pH 10 to pH 7-8. The hydrolysis of cellulose (by abiotic or microbial mechanisms) within ILW wasteform, followed by fermentation of the breakdown products to form organic acids, may help form localised pH neutral microniches within the waste, which may in turn support enhanced microbial activities, in these “extreme” environments. The rate and extent of such processes clearly requires further

investigation, alongside their impact on radionuclide speciation and mobility, including further studies on Np.

7.6. Acknowledgements.

This work has been funded as part of the NERC BIGRAD consortium through UK Natural Environment Research Council consortium grant NE/H007768/1. JRL acknowledges financial support from the Royal Society. Beamtime at beamline INE for actinide research at the ANKA synchrotron light source, Germany was funded by Actinet Awards C3-15 and C5-06. We thank Dr. Jörg Rothe and Dr. Kathy Dardenne for assistance at ANKA and Alistair Bewsher and Paul Lythgoe for analytical geochemistry support.

7.7. References.

Chen, M. & Ma, L.Q., 2001. Comparison of three aqua regia digestion methods for twenty florida soils. *Soil Science Society of America Journal*, 65 (2), 491–499.

Girvin, D.C., Ames, L.L., Schwab, A.P. & McGarrah, J.E., 1991. Neptunium adsorption on synthetic amorphous iron oxyhydroxide. *Journal of Colloid and Interface Science*, 141 (1), 67–78.

Gorman-Lewis, D., Jensen, M.P., Harrold, Z.R. & Hertel, M.R., 2013. Complexation of neptunium(V) with *Bacillus subtilis* endospore surfaces and their exudates. *Chemical Geology*, 341, 75–83.

Hennig, C. (2007). Evidence for double-electron excitations in the L_3-edge X-ray absorption spectra of actinides. *Physical Review B*, *75* (035120), 1–7.

Kaszuba, J.P. & Runde, W.H., 1999. The aqueous geochemistry of neptunium: dynamic control of soluble concentrations with applications to nuclear waste disposal. *Environmental Science & Technology*, 33(24), 4427–4433.

Law, G.T.W., Geissler, A., Lloyd, J.R., Livens, F.R., Boothman, C., Begg, J.D.C., Denecke, M.A., Rothe, J., Dardenne, K., Burke, I.T., Charnock, J.M. & Morris, K., 2010. Geomicrobiological redox cycling of the transuranic element neptunium. *Environmental Science & Technology*, 44 (23), 8924–8929.

Lloyd, J.R., Sole, V.A., Van Praagh, C.V.G. & Lovley, D.R., 2000a. Direct and Fe(II)-mediated reduction of technetium by Fe(III)-reducing bacteria. *Applied and Environmental Microbiology*, 66 (9), 3743–3749.

Lloyd, J.R. & Renshaw, J., 2005. Microbial transformations of radionuclides: fundamental mechanisms and biogeochemical implications. In A. Siegal & R. K. O. Siegal, eds. *Metal Ions in Biological Systems*. New York: M. Dekker, pp. 205–240.

Lloyd, J.R., Yong, P. & Macaskie, L.E., 2000. Biological reduction and removal of Np(V) by two microorganisms. *Environmental Science & Technology*, 34 (7), 1297–1301.

Lovley, D.R. & Phillips, E.J., 1987. Rapid assay for microbially reducible ferric iron in aquatic sediments. *Applied and Environmental Microbiology*, 53 (7), 1536–1540.

NDA, 2014. *The 2013 UK Radioactive Waste and Materials Inventory: Waste Quantities from all Sources*, NDA, Cumbria, p. 17.

Ravel, B. & Newville, M., 2005. ATHENA, ARTEMIS, HEPHAESTUS: data analysis for X-ray absorption spectroscopy using IFEFFIT. *Journal of Synchrotron Radiation*, 12 (4), 537–541.

Renshaw, J.C., Butchins, L.J.C., Livens, F.R., May, I., Charnock, J.M. & Lloyd, J.R., 2005. Bioreduction of uranium: environmental implications of a pentavalent intermediate. *Environmental Science & Technology*, 39 (15), 5657–5660.

Rittmann, B.E., Banaszak, J.E. & Reed, D.T., 2002. Reduction of Np(V) and precipitation of Np(IV) by an anaerobic microbial consortium. *Biodegradation*, 13 (5), 329–342.

Rossberg A., Scheinost A.C., Schmeisser N., Rothe J., Kaden P., Schild D., Wiss T., Daehn R. (2014). AcReDaS, an Actinide Reference Database for XAS, EELS, IR, Raman and NMR Spectroscopy, https://www.hzdr.de/acredas.

Rothe, J., Butorin, S., Dardenne, K., Denecke, M.A., Kienzler, B., Löble, M., Metz, V., Seibert, A., Steppert, M., Vitova, T., Walther, C. & Geckeis, H., 2012. The INE-Beamline for actinide science at ANKA. *The Review of scientific instruments*, 83 (4) 043105.1-043105.13

Songkasiri, W., Reed, D.T. & Rittmann, B.E., 2002. Bio-sorption of neptunium (V) by *Pseudomonas fluorescens*. *Radiochimica Acta*, 90 (9/11), 785–789.

Williamson, A. J., Lloyd, J. R., Boothman, C., Law, G. T. W., Small, J. S., Williams, H. A., & Morris, K. in preparation. Biogeochemical cycling of ^{99}Tc in alkaline sediments. *Environmental Science & Technology*.

Williamson, A.J., Morris, K., Charnock, J.M., Law, G.T.W., Rizouliz, A. & Lloyd, John, R., in review. Microbial reduction of U(VI) under alkaline conditions; implications for radioactive watse disposal. *Environmental Science & Technology*.

Williamson, A.J., Morris, K., Shaw, S., Byrne, J.M., Boothman, C. & Lloyd, J.R., 2013. Microbial reduction of Fe(III) under alkaline conditions relevant to geological disposal. *Applied and Environmental Microbiology*, 79 (11), 3320–3326.

8

Summary, Conclusions and Future Directions

8. Summary, Conclusions and Future Directions

8.1. Summary and conclusions

This project focuses on understanding microbial processes that may impact on the disposal of radioactive wastes and in particular the biogeochemistry of metals under alkaline conditions representative of the evolved CDZ of a GDF. Using controlled microcosm experiments with sediments from a legacy lime working in Buxton, UK, the primary goal of this study was to investigate biogeochemical transformations at pH 10 and assess the impact of these processes on the behaviour of priority radionuclides.

The focus of Chapter 4 was to quantify the rate and extent of microbial Fe(III) reduction under alkaline (pH 10) conditions, and identify any Fe(II)-bearing end products that may interact with U(VI), Tc(VII), Np(V) or other priority radionuclides. Here, sediment and surface waters were mixed, adjusted to pH 10 and supplied with excess Fe(III) as ferrihydrite (120 mM). In these Fe(III) enriched systems, Fe(III) reduction occurred in anaerobic samples and magnetite was characterised as the exclusive post reduction mineral phase formed. The subsequent addition of the electron donors sodium lactate and yeast extract and soluble electron shuttles (AQDS, riboflavin and humics) all enhanced Fe(III) reduction, as hypothesised in these systems where Fe(III) solubility was low. These systems were dominated by a Gram-positive community and further enrichments in defined media (Lovley & Phillips 1988) identified close relatives of *Clostridium* sp. 9B4 (99 %) and *Alkaliphilus oremlandii* (100 %) from the Firmicutes phylum as culturable members of this Fe(III)-reducing community.

Chapter 5 focussed on the biogeochemistry of uranium at pH 10. Experiments were conducted with and without added Fe(III) as ferrihydrite to identify potential coupling between the microbial iron cycle and uranium speciation at high pH. The U(IV) which formed during bioreduction showed differences in its speciation: the “no added Fe(III)” EXAFS spectra were indicative of a poorly ordered non-uraninite U(IV) phase whilst in the “with added Fe(III)” system, the U(IV) was identified as uraninite. The addition of AQDS also increased the extent of microbial U(VI) reduction in these systems. Both U(IV) products were susceptible to air (O_2) reoxidation, however the uraninite product showed a greater stability to nitrate reoxidation, with evidence to suggest that uranium was associated with the reoxidised Fe (III) mineral. When U(VI) was added to heat killed pre-reduced sediment containing magnetite, no U(VI) reduction occurred, suggesting that U(VI) reduction in these systems was predominantly enzymatic.

Pyrosequencing was used in these experiments and showed the dominance of a Gram-positive community, implicating them in the direct enzymatic reduction of U(VI).

In Chapter 6, microcosm experiments were established with added Tc(VII) to explore ^{99}Tc behaviour in alkaline Buxton sediments, again with and without added Fe(III). In both systems, Tc(VII) reduction occurred, resulting in the formation of a short chain polymeric hydrous TcO_2 like structure. In the "no added Fe(III)" system however, only partial removal of Tc(IV) to sediments was observed and solvent extraction with TPAC suggested that residual aqueous Tc was predominantly Tc(IV). This was supported by geochemical modelling and suggests an association of Tc with colloids. Heat killed pre-reduced, magnetite-bearing sediments were exposed to Tc(VII) and results indicated that Tc(VII) reduction in these systems was likely dominated by indirect Fe(II)-mediated mechanisms. Partial Tc(IV) reoxidation and remobilisation occurred during air reoxidation experiments, with evidence to suggest Tc incorporation into the reoxidised Fe mineral. No Tc(IV) reoxidation was observed when sediments were exposed to 30 mM nitrate however, despite essentially complete nitrate removal and Fe(III) reoxidation.

Chapter 7 investigated the biogeochemical behaviour of neptunium under alkaline conditions. Due to radiological safety considerations, the pH in these systems was not amended and here, the pH dropped from 10 to 7-8. Significant Np sorption to sediments was apparent at the initial time point, and residual soluble Np was removed in all anaerobic incubations after 1 day of incubation, indicating that Np(V) reduction occurred during early stages of metal reduction, corroborating previous observations (Law et al. 2010). XAS confirmed complete Np(V) reduction had occurred in microbially active progressive anoxia systems and pre-reduced Fe(II)-bearing sediments incubated at 5 °C, suggesting that Np(V) reduction was likely dominated by an abiotic (Fe(II)-mediated) mechanism.

In summary, these studies show that biogeochemical processes of relevance to the evolution of a GDF biosphere can occur at pH 10 in alkaline impacted sediments, mediated by an indigenous microbial community present in the Harpur Hill lime workings site in Buxton, UK. Furthermore, evidence for significant Fe(III) reduction and reductive immobilisation of radionuclides (U, Tc and Np) has been shown, with data suggesting direct enzymatic reduction of Fe(III) and U(VI), and indirect (Fe(II)-mediated) mechanisms suggested for Tc(VII) and Np(V) reduction. This has implications for radioactive waste disposal, where indigenous microorganisms will be

most likely present in the wasteform, but also introduced from repository construction, GDF operations and from groundwater ingress, post closure. A water activity of > 0.6 is required for life, however microorganisms may survive as spores under stressful conditions and remain dormant over prolonged periods of time (McCabe 1990). In this context, it is interesting that Gram-positive spore-forming bacteria dominated in several of my experiments. ILW will also contain a high abundance of bioavailable organic material, which may serve as electron donors for heterotrophic microorganisms and promote radionuclide immobilisation in the deep subsurface. The microbial metabolism of organics in the ILW may also produce significant quantities of gas, predominantly, CO_2, CH_4 and H_2. This may cause a build-up in pressure, which may result in the loss of waste packaging integrity and also promote radionuclide transport in groundwater, including radioactive C-14 gases. Gas generation could also be a significant mechanism for direct release of ^{3}H ($t_{1/2}$ 12.3 y) and ^{14}C ($t_{1/2}$ 5700 y) from the repository. ^{3}H will have decayed before reaching the biosphere (Walke et al. 2012), but hydrogen may serve as a potent electron donor for metal/radionuclide-reducing microorganisms, which may help reduce repository over-pressurisation. These microbial metal reduction processes may also help poise the system above methanogenesis, limiting the amount of $^{14}CH_4$ produced (alongside other repository processes such as sulphate reduction).

This study highlights the impact of microbes on chemical behaviour (pH, Eh and organic metabolites) under conditions relevant to ILW disposal. This has significant beneficial implications for the safety case of a GDF, as these may affect radionuclide speciation, solubility and sorption processes, in many cases limiting radionuclide mobility. Furthermore, microbes may also form biofilms which may impact on physical properties, such as decreasing mineral porosity (Wragg et al. 2012). Changes in pH may also promote the formation of localised microniches, which may comprise of a significantly different environment, maintained under optimum conditions by the microbial colony. Overall, this work demonstrates the potential for microbial processes in alkaline conditions relevant to radioactive waste geodisposal. This work has implications for biogeochemical evolution, wasteform integrity and radionuclide behaviour in a geodisposal environment. Moreover, it highlights key microbial processes that should be considered when developing a long-term post closure performance assessment for an ILW GDF.

8.2. Future directions

i) Biogeochemical transformations under alkaline conditions in flow through systems

Due to the heterogeneity of natural systems, microcosm experiments are advantageous as they allow simplified, controlled experiments to characterise fundamental biogeochemical processes. The closed nature of microcosms however limits their similarity to natural systems. Flow-through column experiments may further the understanding of alkaline biogeochemistry in these systems and assess radionuclide mobility in flow through systems at deep subsurface temperatures (~10 °C) or those relevant to deep geodisposal of ILW. This would also combat the acidification of the microcosm experiments which was observed from organic acid fermentation and would help naturally buffer the system at pH 10. The use of carbonate as a biological buffer has been used in recent studies at high pH (Fuller et al. 2014), but can affect radionuclide speciation (e.g. formation of soluble carbonate complexes which hinder U(VI) reduction (Zheng et al. 2003) and microbial activity (Brooks et al. 2003). High concentrations of sodium may be toxic to non-halophilic microorganisms.

ii) Mechanisms of alkaline Gram-positive metal reduction

To date, there is a paucity of studies which have explored mechanisms of metal reduction by Gram-positive bacteria (Desvaux et al. 2006; Ehrlich 2008; Wrighton et al. 2011; Carlson et al. 2012; Gavrilov et al. 2012). Furthermore, no studies to date have investigated Gram-positive metal reduction at alkaline pH and this clearly warrants further work. From this study, close relatives of *Proteiniclasticum* sp. (99 %) and *Alkaliphilus oremlandii* (98 %) from the Firmicutes phylum were isolated and capable of solid phase Fe(III) reduction at pH 10. Additionally, A*lkaliphilus oremlandii* has its full genome sequenced (Fisher et al. 2008) and so would be a good model organism to use in in conjunction with characterised Fe mineral phases and uranium to understand direct metal reduction under alkaline conditions.

The use of functional genomics (proteomics, metabolomics, transcriptomics) may also help to develop an understanding of alkaliphilic Gram-positive cell processes. Recent work has suggested the significance of riboflavin in extracellular alkaline Gram-positive Fe(III) reduction (Fuller et al. 2014). Pure culture work with other electron shuttling compounds and humic acids may also give an insight into the mechanisms of Gram-positive metal reduction under alkaline conditions, where metal solubility is low. Evidence for direct enzymatic U(VI) reduction was also observed using a Gram-positive dominated community, so further characterising the mechanisms of U(VI) reduction using enrichment/pure cultures in these systems would be of great interest.

iii) Products of U(VI) reduction under alkaline conditions

In uranium microcosm experiments with no added Fe(III), partial reductive removal of U(VI) was observed and EXAFS modelling suggested the formation of a non-uraninite phase. Often described as mononuclear U(VI), these poorly ordered polymers of U(VI) coordinated to carboxyl and/or phosphoryl groups on biomass, have been the focus of several recent studies (Bernier-Latmani et al. 2010; Bargar et al. 2013). No work to date has focussed on these products forming under alkaline conditions, and using nanoscale imaging techniques such as cryo-TEM and scanning transmission X-ray microscopy (STXM), in conjunction with X-ray micro-characterisation techniques (μXRD, μXRF, μXAS can focus on a 10 x 10 μM spot size (0.5 x ~1 mm for regular XAS)) may also give a better insight into these uranium biominerals at the microbe-mineral interface.

iv) Tc(IV) geochemistry under alkaline conditions

In technetium microcosm experiments with no added Fe(III), solvent extractions on < 0.22 μm filtered samples with TPAC suggested that soluble or colloidal Tc(IV) species may be present. The oxidation state of Tc in these ultra-dilute aqueous samples may be resolved by using XAS on pore water samples from a sediment incubation (56 kBq ml^{-1} Tc(VII) spike), for example on the I20 Beamline at Diamond.

v) Np(IV) stability to oxidative perturbations under alkaline conditions

Only one study to date has explored Np(IV) reoxidation. This was done at circumneutral pH, and the Np(IV) was resistant to complete reoxidation, with 50 % converted to Np(V) after 40 days of treatment with air (O_2) or nitrate (Law et al. 2010). Complete Np reduction was observed in the microcosm experiments detailed in this study, similar to (Law et al. 2010), but the susceptibility to reoxidation of these minerals at pH 10 are currently unknown. Exposing Np(IV) in pre-reduced sediments with and without added Fe(III) to air (O_2) and nitrate (30 mM) at pH 10 would assess Np(IV) stability under alkaline conditions, using low (20 Bq ml^{-1}) and high (2.5 KBq ml^{-1}) Np concentrations for geochemical (Fe(II)/Fe(III) by UV-vis and Np by ICP-MS) and mineralogical analyses (XAS) respectively.

vi) Alkaline Pu biogeochemistry

^{239}Pu is a long lived ($t_{1/2}$ 2.41 x 10^5) fission product of ^{235}U and will also be present in significant quantities in UK radioactive waste inventory, with ~97 % partitioned to the ILW fraction (NDA 2014). Under circumneutral conditions it predominantly exists as Pu(IV) (Lloyd 2003) and forms insoluble complexes in soils and sediments which limits environmental mobility and bioavailability. Under alkaline conditions, Pu(V)

dominates, but disproportionates to Pu(IV) and Pu(VI) (Choppin et al. 1997). Pu(VI) is generally not considered in the environment, however it can persist at higher radionuclide concentrations in marine and saline conditions (Choppin et al. 1997). Microbially mediated reductive solubilisation of Pu(IV) to Pu(III) has also been reported, especially in the presence of complexing ligands (EDTA) and electron shuttles (AQDS) (Rusin et al. 1994; Plymale et al. 2012). Additionally, in high carbonate, basic solutions, soluble Pu(VII) species have been observed (Morss et al. 2007). To investigate alkaline Pu biogeochemistry, a series of progressive anoxia and pre-reduced microcosm experiments could be established to track Pu geochemistry (ICP-MS), with select XAS and pyrosequencing sampling to characterise mineralogical transformations and microbial community shifts respectively.

vii) The bioavailability of GDF representative electron donor and acceptors

The current UK concept for disposing of radioactive wastes includes grouting in stainless steel drums. Although this study has focussed on ferrihydrite as the Fe(III) electron acceptor, it is unknown whether the products of stainless steel corrosion will be bioavailable under alkaline conditions. Long-term corrosion tests have shown to produce a range of iron oxides and hydroxides including α, β and γ-FeOOH, γ-Fe_2O_3 and Fe_3O_4 (Vértes & Czakó-Nagy 1989). Characterising long-term corrosion products experiments using mineralogical techniques (XRD, TEM, XAS) before and after microbially active incubations may give an insight into iron oxide bioavailability under alkaline conditions. UK ILW is heterogeneous and will comprise of organics (such as isosaccharinic acid (ISA)), produced through alkaline degradation of cellulose for example, which will be present in contaminated clothing and tissues for example (Glaus & Van Loon 2008). ISA can form soluble complexes with radionuclides (Gaona et al. 2008), but serving as an electron donor in biogeochemical processes may limit its negative impact on radionuclide transport .

8.3. References

Bargar, J.R., Williams, K.H., Campbell, K.M., Long, P.E., Stubbs, J.E., Suvorova, E.I., Lezama-Pacheco, J.S., Alessi, D.S., Stylo, M., Webb, S.M., Davis, J.A., Giammar, D.E., Blue, L.Y. & Bernier-Latmani, R., 2013. Uranium redox transition pathways in acetate-amended sediments. *Proceedings of the National Academy of Sciences of the United States of America*, 110 (12), 4506–4511.

Bernier-Latmani, R., Veeramani, H., Vecchia, E.D., Junier, P., Lezama-Pacheco, J.S., Suvorova, E.I., Sharp, J.O., Wigginton, N.S. & Bargar, J.R., 2010. Non-uraninite products of microbial U(VI) reduction. *Environmental Science & Technology*, 44 (24), 9456–9462.

Brooks, S.C., Fredrickson, J.K., Carroll, S.L., Kennedy, D.W., Zachara, J.M., Plymale, A.E., Kelly, S.D., Kemner, K.M. & Fendorf, S., 2003. Inhibition of bacterial U(VI) reduction by calcium. *Environmental Science & Technology*, 37 (9), 1850–1858.

Carlson, H.K., Iavarone, A.T., Gorur, A., Yeo, B.S., Tran, R., Melnyk, R.A., Mathies, R.A., Auer, M. & Coates, J.D., 2012. Surface multiheme c-type cytochromes from *Thermincola potens* and implications for respiratory metal reduction by Gram-positive bacteria. *Proceedings of the National Academy of Sciences of the United States of America*, 109 (5), 1702–1707.

Choppin, G.R., Bond, A.H. & Hromadka, P.M., 1997. Redox speciation of plutonium. *Journal of Radioanalytical and Nuclear Chemistry*, 219 (2), 203–210.

Desvaux, M., Dumas, E., Chafsey, I. & Hebraud, M., 2006. Protein cell surface display in Gram-positive bacteria: from single protein to macromolecular protein structure. *FEMS Microbiology Letters*, 256 (1), 1–15.

Ehrlich, H.L., 2008. Are Gram-positive bacteria capable of electron transfer across their cell wall without an externally available electron shuttle? *Geobiology*, 6 (3), 220–224.

Fisher, E., Dawson, A.M., Polshyna, G., Lisak, J., Crable, B., Perera, E., Ranganathan, M., Thangavelu, M., Basu, P. & Stolz, J.F., 2008. Transformation of inorganic and organic arsenic by *Alkaliphilus oremlandii* sp. nov. strain OhILAs. *Annals of the New York Academy of Sciences*, 1125 (1), 230–241.

Fuller, S.J., McMillan, D.G.G., Renz, M.B., Schmidt, M., Burke, I.T. & Stewart, D.I., 2013. Extracellular electron transport mediated Fe(III) reduction by a community of alkaliphilic bacteria that use flavins as electron shuttles. *Applied and Environmental Microbiology*, 80 (1), 128-137.

Gaona, X., Montoya, V., Colàs, E., Grivé, M. & Duro, L., 2008. Review of the complexation of tetravalent actinides by ISA and gluconate under alkaline to hyperalkaline conditions. *Journal of Contaminant Hydrology*, 102 (3-4), 217–227.

Gavrilov, S.N., Lloyd, J.R., Kostrikina, N.A. & Slobodkin, A.I., 2012. Fe(III) oxide reduction by a Gram-positive thermophile: physiological mechanisms for dissimilatory reduction of poorly crystalline Fe(III) oxide by a thermophilic Gram-positive bacterium *Carboxydothermus ferrireducens*. *Geomicrobiology Journal*, 29 (9), 804–819.

Glaus, M.A. & Van Loon, L.R., 2008. Degradation of cellulose under alkaline conditions: new insights from a 12 years degradation study. *Environmental Science & Technology*, 42 (8), 2906–2911.

Law, G.T.W., Geissler, A., Lloyd, J.R., Livens, F.R., Boothman, C., Begg, J.D.C., Denecke, M.A., Rothe, J., Dardenne, K., Burke, I.T., Charnock, J.M. & Morris, K., 2010. Geomicrobiological redox cycling of the transuranic element neptunium. *Environmental Science & Technology*, 44 (23), 8924–8929.

Lloyd, J.R., 2003. Microbial reduction of metals and radionuclides. *FEMS Microbiology Reviews*, 27 (2-3), 411–425.

Lovley, D.R. & Phillips, E.J.P., 1988. Novel mode of microbial energy metabolism: organic carbon oxidation coupled to dissimilatory reduction of iron or manganese. *Applied and Environvironmental Microbiology*, 54 (6), 1472–1480.

McCabe, A., 1990. The potential significance of microbial activity in radioactive waste disposal. *Experientia*, 46 (8), 779–787.

Morss, L., Edelstein, N., Fuger, J. & Katz, J., 2007. *The Chemistry of the Actinide and Transactinide Elements*, 4th ed, New York: Springer, p. 4188.

NDA, 2014. *The 2013 UK Radioactive Waste and Materials Inventory: Waste Quantities from all Sources*, NDA, Cumbria, p. 17.

Plymale, A.E., Bailey, V.L., Fredrickson, J.K., Heald, S.M., Buck, E.C., Shi, L., Wang, Z., Resch, C.T., Moore, D.A. & Bolton, H., 2012. Biotic and abiotic reduction and solubilization of $Pu(IV)O_2.xH_2O(am)$ as affected by anthraquinone-2,6-disulfonate (AQDS) and ethylenediaminetetraacetate (EDTA). *Environmental Science & Technology*, 46 (4), 2132-2140.

Rusin, P.A., Quintana, L., Brainard, J.R., Strietelmeier, B.A., Tait, C.D., Ekberg, S.A., Palmer, P.D., Newton, T.W. & Clark, D.L., 1994. Solubilization of plutonium hydrous oxide by iron-reducing bacteria. *Environmental Science & Technology*, 28 (9), 1686–1690.

Vértes, A. & Czakó-Nagy, I., 1989. Mössbauer spectroscopy and its application to corrosion studies. *Electrochimica Acta*, 34 (6), 721–758.

Walke, R.C., Thorne, M.C. & Norris, S., 2012. Biosphere studies supporting the disposal system safety case in the UK. *Mineralogical Magazine*, 76 (8), 3225–3232.

Wragg, J., Harrison, H., West, J.M. & Yoshikawa, H., 2012. Comparison of microbiological influences on the transport properties of intact mudstone and sandstone and its relevance to the geological disposal of radioactive waste. *Mineralogical Magazine*, 76 (8), 3251–3259.

Wrighton, K.C., Thrash, J.C., Melnyk, R.A., Bigi, J.P., Byrne-Bailey, K.G., Remis, J.P., Schichnes, D., Auer, M., Chang, C.J. & Coates, J.D., 2011. Evidence for direct electron transfer by a Gram-positive bacterium isolated from a microbial fuel cell. *Applied and Environmental Microbiology*, 77 (21), 7633–7639.

Zheng, Z., Tokunaga, T.K. & Wan, J., 2003. Influence of calcium carbonate on U(VI) sorption to soils. *Environmental Science & Technology*, 37 (24), 5603–5608.

Appendix

Conference Presentations

Appendix. Conference Presentations

A.1. Oral presentations

3rd Annual BIGRAD conference, University of Sheffield, UK ..... **20-21 June 2013**

Iron biogeochemistry - from molecular processes to global cycles, FIMIN, Monte Verità, Ascona, Switzerland ..... **03-08 March 2013**

2nd Annual BIGRAD conference, British Geological Survey (BGS), Nottingham, UK ..... **12-13 July 2012**

22nd V.M. Goldschmidt conference, Montreal, Canada..... **24-29 June 2012**

Environmental Mineralogy Groups' research in progress meeting, University of Reading, UK ..... **28th May 2012**

A.2. Poster presentations

Implementing Geological Disposal- Technology Platform (IGD-TP) conference, The University of Manchester, UK ..... **24-26 June 2014**

14th International conference on the chemistry and migration behaviour of actinides and fission products in the geosphere, Brighton, UK ..... **08-13 Sept 2013**

Postgraduate research conference, The University of Manchester, UK ..... **1st Dec 2012**

Research frontiers in radioactive waste management, a one day research symposium, University of Sheffield, UK..... **10th Oct 2012**

Geomicrobiology and its significance for biosphere processes, a Mineralogical Society conference, The University of Manchester, UK ..... **19-20 April 2012**

Electron transfer at the microbe-mineral interface, a Biochemical Society conference, University of East Anglia, UK ..... **02-04 April 2012**

Postgraduate research conference, The University of Manchester, UK ..... **14th Dec 2011**

Geological disposal of radioactive waste: underpinning science and technology, Loughborough University, UK. ..... **18-20 Oct 2011**

Coordinating Group on Environmental Radioactivity (COGER), University of Sterling, UK ..... **04-06 July 2011**

*****1st Annual BIGRAD conference, University of Leeds, UK..... **27-28 June 2011**

*****prepared by A. J Williamson presented by J. R Lloyd